Durham E-Theses

Modelling of some semiconductor devices with large signal excitation

Visuwan, Sansern

How to cite:

Visuwan, Sansern (1979) *Modelling of some semiconductor devices with large signal excitation*, Durham theses, Durham University. Available at Durham E-Theses Online: http://etheses.dur.ac.uk/8431/

MODELLING OF SOME SEMICONDUCTOR DEVICES

WITH LARGE SIGNAL EXCITATION.

SANSERN   VISUWAN.

B.Sc (Chulalongkorn Univ.)

M.Sc (Dunelm)

Department of Applied Physics and Electronics.

University of Durham.

September 1979

A thesis submitted for the degree of

Doctor of Philosophy of the University of Durham.

ABSTRACT.

Under large signal conditions, the inherent nonlinearity of semiconductor devices is relatively strong, and numerical methods for the solutions of the system equations seem to be inevitable. In this work, numerical algorithms for time-independent and time-dependent modelling of bipolar devices have been developed and used to study both the internal and terminal characteristics of some n^+-p and n^+-p-p^+ diodes over a wide range of operation. The effect of minority carrier lifetime on the characteristics of the devices has been investigated, considering the cases of diodes with the same width, diodes with the same recombination criterion, and diodes with the same lifetime but different recombination criteria respectively.

In the frequency domain, we studied the influence of the lifetime in terms of harmonic analysis, by applying the Fast Fourier Transform directly to the solutions. The quasi-static spectra obtained from the exact, and approximated diode characteristics, together with the dynamic spectrum, are shown and considered.

Acknowledgement.

I wish to express my gratitude to my supervisor, Dr. B J Stanier, for his encouragement, kindly help and invaluable advice. I should also like to give my thanks to Dr. M J Morant for the useful discussions and suggestions.

Dr. D M Greig kindly helped me with the mathematical problems and the invaluable discussions, to her I would like to express my sincerest thanks.

I am also indebted to all the duty advisors in the Computer Unit, in particularly Mr. M Monro and Mr. R Gawley, for their generously help, useful information in the programming and thesis preparation. To them I would like to give my deepest thanks.

Mr and Mrs. C B Rowcroft who have made me and my family feel so welcome and helped us so much in every aspect during the past years. To them I would like to express my sincerest thanks.

This work would not have been completed without the constantly encouragement and patience from my wife, Molvipa, to whom this thesis is dedicated.

To my wife, Molvipa.

CONTENTS.

Chapter 1

Introduction

During the past few years, advances in digital computers and digital computation techniques have led to considerable development in the field of computer-aided design. The computer is used extensively to develop and design semiconductor devices. The work is centered on development of models which will predict device performance over a wide range of operation. The models should also be accurate, and give detailed and extensive information about the internal behaviour of the device.

The inherent nature of nonlinearity and also the strong coupling between the physical parameters of the device make the modelling technique complicated. However, these techniques have been remarkably developed in both the time and frequency domains, and they can be classified into 2 types; the analytical approach, and the numerical approach.

1.1 The analytical approach

The analytical approach has been developed widely and was used in the early analyses of semiconductor devices. The methods are based on certain approximations and assumptions which are used to simplify the mathematical description of the physics of the device. The development began with Schockly's classical theory of depletion approximation <1> which assumes that there are no mobile

carriers existing in the space-charge region. By using Boltzmann statistics, the concept of quasi-equilibrium, and by neglecting the drift current components, the behaviour of the devices can be predicted. The depletion model has been used successfully and is widely accepted, particularly with alloyed junction devices under low-level injection conditions. For diffusion devices under high-level injection conditions however, departures from this model were found and ascribed to the presence of mobile carriers in the space-charge region. For a high-level injection model, Cornu <2> proposed an assumption that the space-charge densities on each side of the junction decrease exponentially, rather than being constant as in the case of the depletion model. The Cornu model provides very good agreement with the exact numerical solutions. However, the model can be analyzed only in the limiting case when the potential barrier becomes small compared to the thermal voltage (kT/q).

A later model proposed by Choo <3> assumed that the contribution of the ionized impurities to the space-charge on the lightly doped side of the junction could be neglected under high-level injection conditions. The use of this model together with the quasi-equilibrium and quasi-neutrality assumptions gives results closer to the exact numerical solutions at any injected level. However, the solutions can only be obtained by solving the implicit equations.

In general computer aided circuit analysis and design requires that the solutions obtained from the above models

be formulated so that the device can be represented by discrete circuit elements. A valid representation should contain both static and dynamic descriptions of the device. Linvill's classical multiple-lump model <4> represents the recombination and charge storage terms in the continuity equations by two new circuit elements called combinance and storance respectively. The neutral regions are then represented by a series of parallel pairs of combinance and storance, while the space-charge region is represented by a capacitor. This model can represent a p-n junction diode exactly if the number of sections approaches infinity. A counterpart of the Linvill model is the Wang-Branin model <6> where the unfamiliar circuit elements used in the Linvill model are replaced by conventional circuit elements. A simpler model was proposed by Barna and Horelick <5> which accounted for conductivity modulation. The model is based on the study of bulk resistance during transient behaviour as suggested by Ko <7><8>. It consists of a finite number of conventional circuit elements. The model was shown to give satisfactory results at any injection level. Recently, Chua and Tseng<9> attempting to achieve greater simplicity, have presented yet another model called the memristive diode model. This model contains only four conventional circuit elements, including a nonlinear charge controlled resistor called a memristor. The model proved capable of predicting diode behaviour under forward, reverse, and sinusoidal operation modes, and at the same time allowing for second order effects due to conductivity modulation.

The analytical approach has the advantage of providing analytically tractable solutions supporting quantitative explanation of the device behaviour. However, the approximations and assumptions which are necessary to achieve analytical solution inhibit the models ability to provide complete and exact descriptions of the device properties. In addition, the method is only valid for some ideally-geometry devices, e.g. those having abrupt step impurity profile.

1.2 The numerical approach.

The numerical approach is essentially based on using successive approximation techniques to solve the nonlinear equations in the physics of the device. The results obtained using this approach can therefore be highly accurate in predicting the behaviour of the device at any injection level. They are often referred to as the exact solutions although they depend on the model used. Many algorithms which use numerical analysis have been proposed. The main problem has been the development of computational methods. which ensure convergence or stability of the solutions.

In one-dimensional analysis, the development of dc-steady state modelling began with the self-consistent scheme of Gummel <10> applied to a junction transistor. His iterative scheme starts with an estimate at the value of the electrostatic potential, from which the quasi-Fermi potentials, carrier densities and linearized Poisson equation, are calculated. The algorithm is computationally

simple, but convergence can only be obtained under low and moderate injection levels.

De Mari <11> has extended the basic Gummel algorithm, and applied it to single-junction devices. By treating the current density equations as two independent first order linear differential equations, the analytical system equations can be reformulated. When damping factors were introduced in various regions, the algorithm was shown to give higher accuracy than the Gummel method and applied to a wider range of injection-level conditions. The algorithm is however limited to cases involving slight or moderate recombination. Arandjelovic <12> applied the De Mari algorithm to a junction diode but included the recombination processes and nonconstant mobilities. Later work by Calzolari, et.al, <13> presented a more numerical approach using the finite difference approximation to transform the nonlinear differential equations into nonlinear algebraic equations. The Picard and Newton iteration were subsequently employed for the solutions. Seidmann and Choo <14> also derived an algorithm using the same principle as Calzolari, however, in the iteration loop, instead of treating the generation recombination term explicity in the continuity equations, the term was placed implicitly in its partial linearization. Both the Calzolari and Siedman and Choo methods were shown to give solutions at any injection level as well as allowing for strong recombination.

In the field of dynamic modelling, De Mari <15> began by extending his static algorithm to include the partial

derivative terms, using the generalized implicit scheme in the discretization procedure. The switching behaviour of a diode was studied intensively. Later Scharfetter and Gummel <16> used De Mari's analytical procedure when dealing with the current densities, and proposed a special stable difference approximation scheme to overcome the stability problem encountered at particularly high injection levels. Caughey <17> developed a direct numerical algorithm using the Newton method to linearized the equations in which the perturbation terms are evaluated simultaneously in the iterative loop. Peterson <18> modified the Scharfetter algorithm using the so-called "quasi-linearization" techniques, (which are essentially generalized R-dimensional Newton's methods), to study the transient phenomena in a p-i-n diode. At the same time Hachtel et al. <19> proposed a more general algorithm. By reformulating the equations, his iteration scheme was required only to calculate p and E, and the use of sparse matrix computation made the algorithm more efficient in terms of time and storage. Later work by Collin and Churchill <20> dealt with MOS devices in which the stability problem is less severe than in junction devices. This allows the current density terms to be substituted into the continuity equations directly. However, an extra check when solving for the potential was introduced to prevent inconsistency. Recently, Fortino and Nadan <21> applied shooting techniques used in the solution of initial value problems to model MOS devices under small signal a.c. excitation. The method however requires a reconditioning

procedure which makes it less attractive than other methods.

For the general use of computer aided circuit analysis, optimization techniques <22> can be applied to the numerical results as obtained above to produce a representation of the device in terms of conventional circuit elements.

The numerical approach is generally superior to the analytical approach if exact solutions are desired. It is valid for most types of device at any injection level whilst allowing for strong recombination. However, it cannot express the closed form relationships between the parameters which are apparent in the analytical approach.

1.3 Harmonic analysis.

The study of harmonic generation and distortion in the frequency domain can be done in a similar manner to that used in time domain analysis, i.e, either by analytical methods or by numerical methods. The analytical methods basically rely on fast convergence series representations. Following the work by George <24> on higher dimension transform theory, Narayanan <23> used a generalization of the power series called the Volterra series representation to develop an a.c. model of a transistor from the approximation solution. The method derives the closed form relationships of the harmonic components in terms of the device parameters. The method is however restricted to small signal a.c. analysis. Kulesza and Katib <25> used power series to study the harmonic generation in a Schottky

barrier diode where only resistive components were considered in the models.

In comparison with the above methods, a numerical approach provides more general solutions. Albrecht and Jansen <26> used the Volterra series representation when solving the system equations directly. The method requires no approximation and hence provides more accurate solutions. The harmonic distortion and cross modulation in p-i-n diode were obtained successfully, but the method is again limited to small signal a.c conditions. Later work by Doi <27> considered the large signal cases where nonlinearities were strong. By using Newton's method to obtain solutions, and by employing modified Bessel functions together with nodal analysis to derive the harmonic components, the complete behaviour of diodes and transistors in the frequency domain can be obtained. However the method is still dependent on the approximated characteristics of the devices.

Another approach to the solution of these problems involves the use of time domain steady-state analysis, followed by Fourier Transformation. This direct transformation is relatively simple due to the full development of the Fast Fourier Transform. The accuracy of the frequency domain solutions is determined by the accuracy in the time domain, and hence nearly exact frequency domain solutions may be obtained.

1.4 Motivation and aim of the study.

Investigation of semiconductor device performance is one of the prime interests in the Department of Applied Physics and Electronics. Different materials have been studied intensively for use in preparing semiconductor devices, and many experimental techniques are employed to evaluate their characteristics and physical parameters. Recently this work has been extended into frequency domain analysis <25>, but only simple analytical models have yet been considered.

The purpose of the work described in this thesis was initially to develop a microprocessor based system capable of simulating both the time and frequency domain properties of some simple semiconductor devices. However, it was found that this system would be too expensive at present, and hence only simulation on a main frame computer has been used in the work. One-dimensional modelling of some p-n junction diodes has been studied intensively for both static and dynamic behaviours including harmonic analysis in the frequency domain. Emphasis was placed on the terminal current-voltage characteristics of the devices, and their relation with the minority carrier lifetimes.

1.5 Organization of the thesis.

In this chapter, both analytical and numerical modelling techniques for semiconductor devices have been reviewed, including also a mention of some work in the frequency domain.

Chapter 2 is devoted to one-dimensional mathematical

models of semiconductor devices. The problems involved in the modelling are discussed, and some auxiliary equations are given to denote the relation between the physical parameters of the devices. The boundary conditions necessary to obtain solution of the problems are also provided.

In chapter 3, the generalized numerical procedure of solving nonlinear boundary-value problems is discussed leading to development of the algorithms for the solutions. The use of the procedure is demonstrated by analysing Schottky barrier diodes under reverse biased conditions.

In chapter 4, a numerical algorithm for d-c steady-state modelling is developed and used to investigate the static behaviour of some diodes. Both internal and terminal characteristics are considered under forward and reverse bias. The main emphasis is on the effect of the minority carrier lifetimes on the device properties. Low frequency responses to sinusoidal excitation are also included in order to provide static harmonic analysis for comparison with the corresponding dynamic case.

In chapter 5, the dynamic behaviours of diodes is considered. A fast algorithm for this purpose is developed and used to study the transients resulting from step excitation at various injection levels. The effect on the response to sinusoidal excitation of the minority carrier lifetimes is comprehensively studied.

In chapter 6, harmonic generation within the frequency domain is studied utilizing the Fast Fourier Transformation applied to the steady-state solotion obtained previously in

chapters 4 and 5. These results will be referred to as the static and dynamic spectra respectively. From these spectra, the effects on the harmonic components caused by the minority carrier lifetime of the device involved are investigated.

Chapter 7 concludes with a summary of the algorithms used and the results obtained in both the time and frequency domains together with a consideration of possible future work.

Appendix A gives a method for inversion of the tridiagonal matrix system which is the basis of the algorithms used throughout this work.

Appendix B is provided to introduce a cubic spline interpolation required in the determination of the responses to sinusoidal excitation from the diode characteristic curves.

Appendix C gives the computer subroutines used in both static and dynamic analyses.

Chapter 2

Mathematical Modelling of p-n Junction Devices

In this chapter some basic equations and important parameters to be used in the analysis will be derived and discussed to provide a mathematical model for the behaviour of p-n junction devices.

The problem contains a set of simultaneous nonlinear differential equations which will be referred to as the system equations and some auxiliary equations. In order to obtain an efficient computer solution, some boundary conditions and normalized forms of the equations will be prepared.

2.1 Basic equations for semiconductor devices

2.1.1 Current density equations.

In a junction device, the difference in the concentrations of carriers of the same type in each region causes the flow of charged particles in such a direction as to even out the concentration gradients existence between the two regions. If we define the number of carriers passing through unit area in unit time as flux, this is referred to as the Diffusion Flux. In addition, the existing of electric field, either resulting from the diffusion flow or from external excitation, results in another flow of the charged particles in a direction determined by the field. This flux is referred to as the Drift Flux.

Therefore, the net flux densities of holes and

electrons are given by

$$F_p = -D_p\frac{\partial p}{\partial x} + \mu_p.p.E$$

(2.1)

$$F_n = -D_n\frac{\partial n}{\partial x} - \mu_n.n.E$$

(2.2)

The current crossing a unit area (the current density) is then the particle flux density multiplied by the charge of the carrier. i.e,

$$J_p = F_p \ q \qquad , \text{ and}$$

$$J_n = F_n \ (-q)$$

Thus, in terms of the current densities, equations 2.1 and 2.2 become

$$J_p = q \ \mu_p \ p \ E - q \ D_p \ \frac{\partial p}{\partial x}$$

(2.3)

$$J_n = q \ \mu_n \ n \ E + q \ D_n \ \frac{\partial n}{\partial x}$$

(2.4)

In equilibrium conditions, the diffusion and drift currents of holes and electrons are equal but in opposite directions, resulting in no net current flowing in the device. On the other hand, in non-equilibrium conditions, the current densities of holes and electrons are determined by the difference of two current components, and the total conduction current density is the sum of the contributions due to holes and electrons.

$$J_{cond} = J_p + J_n$$

(2.5)

2.1.2 The Continuity equations.

Most semiconductor devices operate under
non-equilibrium conditions, in which the carrier
concentration product p.n differs from its equilibrium
value n_i^2. Their performance can be determined by the
process of returning to equilibrium. In the case of
injection ($np>n_i^2$) and extraction ($np<n_i^2$) of excess
carriers the return of equilibrium is through recombination
and generation of electron-hole pairs respectively. At a
particular time, the carrier distributions can be described
by the solutions of the transport equations.

$$\frac{\partial p}{\partial t} = -U_p - \frac{\partial F_p}{\partial x}$$

and

$$\frac{\partial n}{\partial t} = -U_n - \frac{\partial F_n}{\partial x}$$

or, in terms of the current densities, we obtain

$$\frac{\partial p}{\partial t} = -U_p - \frac{1}{q}\frac{\partial J_p}{\partial x}$$

$$\frac{\partial n}{\partial t} = -U_n + \frac{1}{q}\frac{\partial J_n}{\partial x}$$

2.1.3 Maxwell's equations.

Maxwell's equations state that;

$$\nabla \times H = J + \frac{\partial D}{\partial t} \tag{2.8}$$

$$\nabla \times E = -\frac{\partial B}{\partial t} \tag{2.9}$$

$$\nabla . D = \rho \tag{2.10}$$

$$\nabla \cdot B = 0 \tag{2.11}$$

Where

H is the magnetic intensity (amps/m)

J is the current density (amps/m^2)

D is the electric displacement (coulombs/m^2)

E is the electric field (volts/m)

B is the magnetic induction (webers/m), and

ρ is the volume charge density (coulombs/m^3)

From Maxwell's equations the relation between the electrostatic potential, V, and the continuity equations can be determined, using auxiliary formulae, namely

$$B = \mu H$$

$$B = \nabla \times A$$

where A is the vector potential (weber/m^2) and a relation from the vector analysis that

$$\nabla \times (\nabla \times Z) = \nabla (\nabla \cdot Z) - \nabla^2 Z$$

It can be readily shown that

$$E = -\nabla V - \frac{\partial A}{\partial t}$$

or

$$\left(\nabla^2 - \mu \epsilon \frac{\partial^2}{\partial t^2}\right) V = -\frac{\rho}{\epsilon} \tag{2.12}$$

But, after a time greater than the propagation time for the electric field to travel from the contact to one edge of the device, we can approximate

$$\left(\nabla^2 - \mu \epsilon \frac{\partial^2}{\partial t^2}\right) V \implies \nabla^2 V$$

and then we obtain the well-known Poisson equation

$$E = -\nabla^2 V = \rho/\epsilon$$

In the one-dimentional case, we obtain

$$\frac{\partial E}{\partial x} = \frac{\rho}{\epsilon} \qquad\qquad\qquad (2.13)$$

or

$$\frac{\partial^2 V}{\partial x^2} = -\frac{\rho}{\epsilon}$$

For a p-n junction device, we can state that

$$\rho = q\,(p - n + N)$$

where

$$N = N_D - N_A$$

= Net ionized densities of donors over acceptors, and

ϵ = dielectric constant of material

It should be noted here that during a very short time interval, in the range of the dielectric relaxation times of some semiconductor devices, the Poisson equation can not be assumed.

In a p-n junction device, the space-charge region may be treated as a parallel plate capacitor of area A. When a current I flows into one of the plates, the charge q on this plate must be accumulating at a rate $(dq/dt) = I$, and equally, there must be a negative charge -q on the other plate which is changing at the same rate. The current in is equal to the current out. Gauss's theorem shows that the electric field between the plates is

$$E = q/(\epsilon A)$$

Therefore $\quad I_D = \epsilon A \dfrac{\partial E}{\partial t}$

or $\quad\quad J_p = \epsilon \dfrac{\partial E}{\partial t}$ $\quad\quad\quad\quad$ (2.14)

The time-varying field thus induces charges on the opposite plate so as to keep the current flow continuous. This may be treated as contributing a current called the Displacement Current J_D. Just as the movement of charge creates a conduction current J_C, the time varying field creates a displacement current.

Therefore, the total current J_T can be given as

$$J_T = J_C + J_D \quad\quad\quad\quad (2.15)$$

Or $\quad \epsilon \dfrac{\partial E}{\partial t} = J_T + J_p + J_n$ $\quad\quad\quad$ (2.16)

In the steady-state case where there is no dependence of the field on time, the displacement current is obviously zero.

2.1.4 Shockley Read Hall (SRH) - recombination - generation model.

The recombination and generation of electrons and holes in semiconductors may take place at some type of recombination - generation centers or traps. Under steady state conditions, a single energy level recombination center is characterized by its capture cross section for holes and electrons and the energy involved in these transitions. The capture cross sections are inversely proportional to the lifetimes of holes and electrons respectively, and the transition energy may be measured from the appropriate edge of the energy gap of the semiconductor.

There are four basic processes involved in the carriers generation and recombination through traps. These are electron capture, electron emission, hole capture and hole emission. Assuming that the semiconductor is non-degenerate, the net capture rate for electrons by the traps under non-equilibrium condition is given by

$$U_{cn} = (n.f_{tp} - n_1.f_t)/T_{no}$$

Similarly, for holes we can write

$$U_{cp} = (p.f_t - p_1.f_{tp})/T_{po}$$

where

$$f_t = (1 + exp(E_t-F_t)/kT)^{-1}$$

f_{tp} is the fraction of traps occupied by holes

f_t is the fraction of traps occupied by electrons

$$= 1 - f_{tp}$$

T_{no}, T_{po} are the minority carrier lifetimes in highly extrinsic material

E_t is the energy level of the recombination – generation centers or traps.

For non-equilibrium but steady-state conditions, the rate of recombination can be obtained by requiring that the net rate of capture of electrons be equal to that of holes. This implies that

$$U = U_{cn} = U_{cp}$$

$$= \frac{(pn - n_i^2)}{(T_{po}(n+n_1) + T_{no}(p+p_1))} \tag{2.17}$$

Where

$$n_1 = n_i exp(E_t-E_i)/kT$$

$$P_1 = n_i \exp(E_i - E_t)/kT$$

n_1 is the density of electrons in the conduction band when the Fermi level at E_t.

P_1 is the density of holes in the valence band when the Fermi level falls at E_t.

For the most effective generation and recombination, let us assume that the single level , uniformly distributed traps are located at the intrinsic Fermi level. Thus $P_1 = n_1 = n_i$ and equation 2.17 becomes

$$U = \frac{(pn - n_i^2)}{(T_{po}(n+n_i) + T_{no}(p+n_i))} \qquad (2.18)$$

2.1.5 Mobility equations.

In a vacuum, the carrier motions are influenced only by the electric field whereas in a solid, carriers interact repeatedly with the surrounding lattice and hence their motion will be dependent upon the impurity density.

Theoretically, the mobility is approximated by <16>

$$\left[\frac{\mu_o}{\mu}\right]^2 = 1 + \frac{N}{N/S + N_o} + \frac{(E/A)^2}{E/A + F} + (E/B)^2 \qquad (2.19)$$

where the constants are given in table 2.1 for silicon
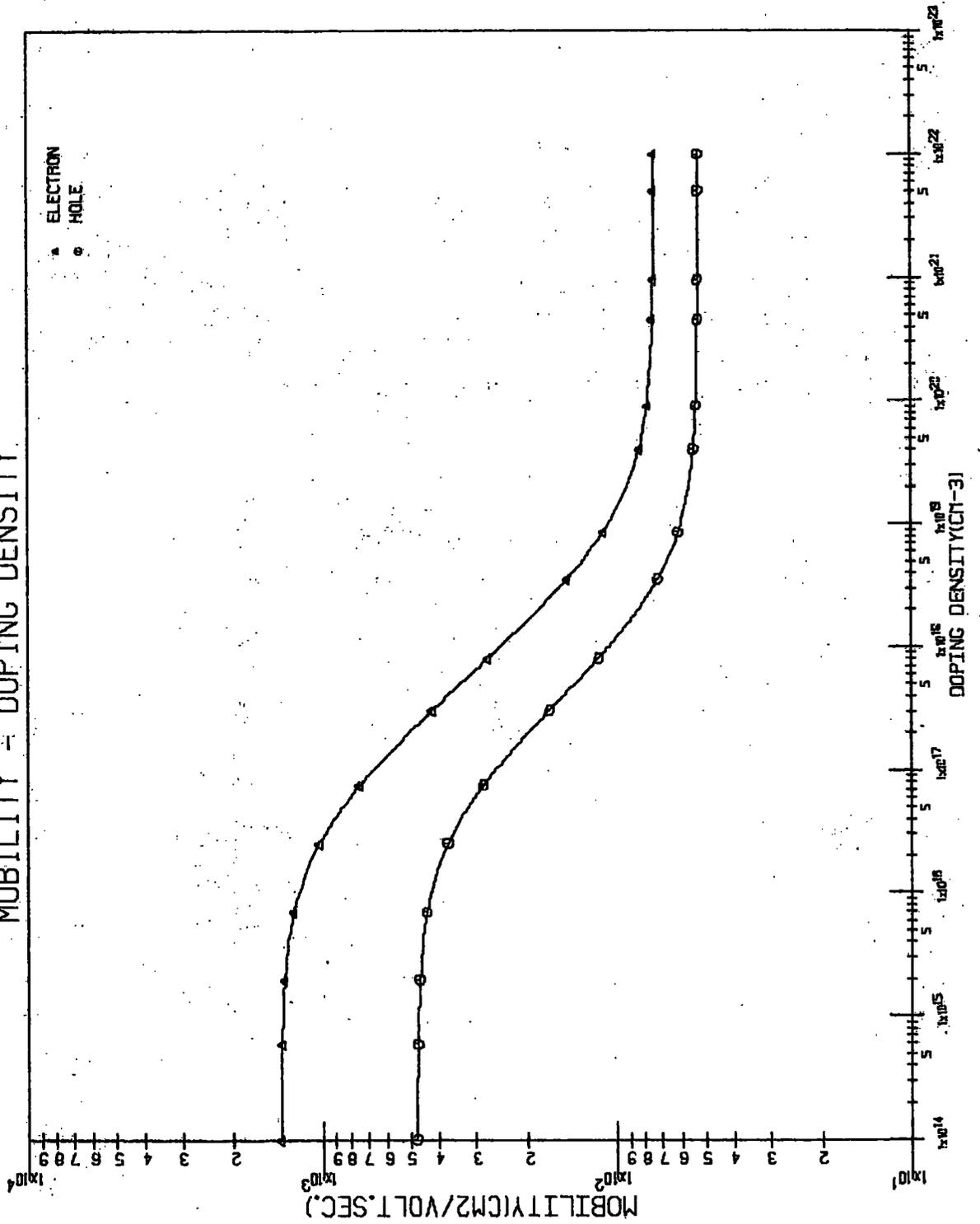
FIGURE (2.1)

TABLE 2.1 VALUES OF THE CONSTANTS IN EQUATION 2.19

	μ_o	N_o	S	A	F	B
HOLE	480	4×10^{16}	81	6.1×10^3	1.6	2.5×10^4
ELECTRON	1400	3×10^{16}	350	3.5×10^3	8.8	7.4×10^3

For simplicity, due to small influence of the field-dependent terms, we will neglect these terms in the analysis. The mobility may therefore be approximated by

$$\left[\frac{\mu_o}{\mu}\right]^2 = 1 + \frac{N}{N/S + N_o} \qquad (2.20)$$

and is shown in Fig. 2.1 , for silicon,

The relation between the carrier mobilities and the carrier diffusion constants can be obtained from the Einstein relations,

$$\mu_p = (q/KT)D_p \quad \text{for holes, and}$$

$$\mu_n = (q/KT)D_n \quad \text{for electrons}$$

$$(2.21)$$

The Einstein relations also show that the carrier diffusion constant are nonlinear, monotonically increasing functions of the carrier densities.

2.1.6 Diffusion lengths.

When a p-n junction device is connected to an external source, injection of excess carriers takes place and as a

result the carrier density in the device will become greater than it was in thermal equilibrium. Therefore recombination is necessary for a return to equilibrium . The process has little effect in the region where the injected excess carriers are minority. The decay of the excess minority carrier density is shown to be governed by the diffusion equation and the density falls off as $\exp(-x/L_{pn})$

where $L_p = (D_p.T_p)^{1/2}$

$$L_n = (D_n.T_n)^{1/2} \qquad (2.22)$$

L_p and L_n are the diffusion lengths of holes and electrons respectively. By using the Einstein relations and the mobility equations, the relations between the diffusion length and lifetimes can be derived. An example for the case of silicon is shown in Fig. 2.2

The relation between diffusion length and width of a region is often used as a measure of the effectiveness of the recombination process. If the width to diffusion length ratio is very large compared to unity, then we have strong recombination. But if it is comparable to unity or less than unity, we have moderate recombination and slight recombination respectively.

2.2 Boundary conditions.

In order to solve the system equations, which are nonlinear differential equations, some boundary conditions must be provided. They may be obtained through some assumptions and from the physical properties of the
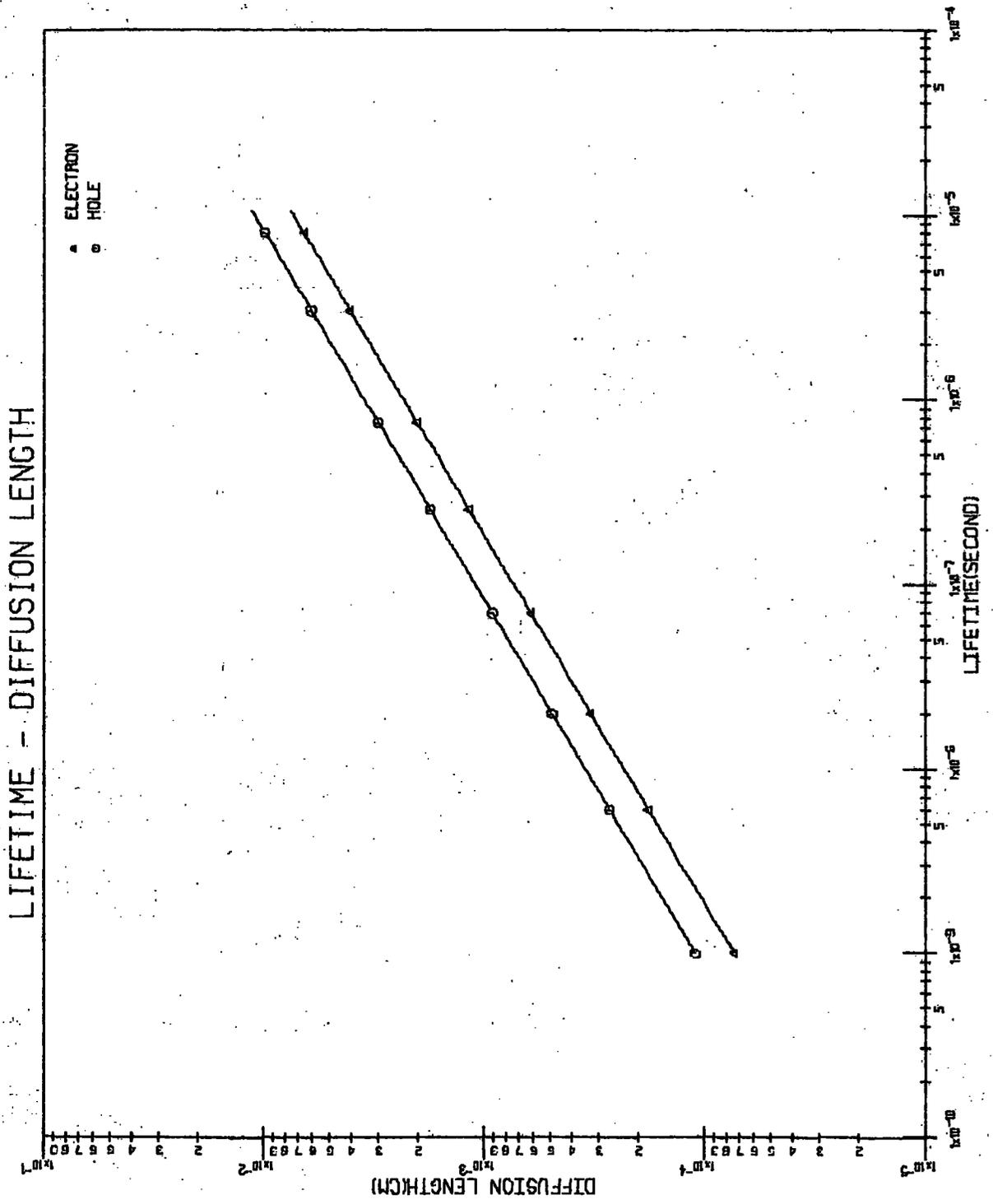
FIGURE (2.2)

devices.

2.2.1 Boundary conditions based on ohmic contacts assumption.

For a device with the so-called ohmic contacts or "perfectly absorbing" contacts, we mean that an infinite recombination velocity s_R is assumed. Therefore finite hole and electron current densities at the contacts require

$$(p - p_o)\Big|_{\text{ohmic contact}} = \lim_{S_{RP} \to \infty} (J_p/S_{Rp}) = 0$$

$$(n - n_o)\Big|_{\text{ohmic contact}} = \lim_{S_{Rn} \to \infty} (J_n/S_{Rn}) = 0$$

Thus give

$$p = p_o$$

$$n = n_o$$

or equivalently $\phi_p = \phi_n$ at both ohmic contacts

Where subscript o means their values at the thermal equilibrium and ϕ_p , ϕ_n are hole and electron quasi-fermi potentials respectively.

2.2.2 Boundary conditions based on the space-charge neutrality assumption.

A semiconductor in which the impurities are completely ionized and uniformly distributed will normally obey the condition of space-charge neutrality at the ohmic contact. Hence the net charge density ρ at the ohmic contacts of the semiconductor will be zero . Thus gives

$$\rho = q.(p - n + N_D - N_A) = 0$$

and implies that E = 0

2.2.3 Boundary conditions under current injection.

When a p-n junction device is connected to an external source carriers are injected uniformly over the cross section of the device. Using the fact that total current density injected through the device, J_T, is always constant at a particular time, we have, for the device shown in Fig. 2.3 ,

$$J_n(o,t) = J_T(t)$$

$$J_p(L,t) = J_T(t)$$
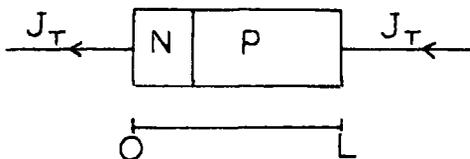
Figure 2.3

2.3 Normalization of the equations.

In order to reduce unnecessary computations of some constant quantities, the equations should be normalized into their dimensionless forms. For example, consider the hole current density equation.

$$J_p = q\mu_p pE - q\frac{(KT)}{q}\mu_p\frac{\partial p}{\partial x} \tag{2.23}$$

Let starred variables represent the normalized values, and define some normalizing factors such as <11>

$$\mu_p^* = \mu_p/(D_o/V_o)$$

$$p^* = p/n_i$$

$$E^* = E/(V_o/L_D)$$

$$x^* = x/L_D$$

where

$V_o = kT/q$, and the Debye length is given by

$$L_D = (\epsilon V_o/(qn_i))^{1/2}$$

Equation 2.23   becomes

$$J_p = (qD_o n_i/L_D) \, \mu_p^*(p^* E^* - \frac{\partial p^*}{3x^*})$$

Let $J_p^* = J_p/(qD_o n_i/L_D)$

we finally have

$$J_p^* = \mu_p^*(p^* E^* - \frac{\partial p^*}{\partial x^*})$$

For convenience, we remove all the stars and use the same symbols for the normalized variables, thus the normalized equation of the hole current density is

$$J_p = \mu_p(p \, E - \frac{\partial p}{\partial x})$$

Similarly, by using the normalizing factors shown in table 2.2 , the normalized system equations including the auxiliary equations can be written as following

$$J_n = \mu_n(n \, E + \frac{\partial n}{\partial x})$$

$$\frac{\partial p}{\partial t} = -U_p - \frac{\partial J_p}{\partial x}$$

$$\frac{\partial n}{\partial t} = -U_n + \frac{\partial J_n}{\partial x}$$

$$\frac{\partial E}{\partial t} = J_T - J_p - J_n$$

$$\frac{\partial E}{\partial x} = p - n + N$$

$$\frac{\partial^2 V}{\partial x^2} = -(p - n + N)$$

$$U = \frac{p\,n - 1}{(T_{po}(n + 1) + T_{no}(p + 1))} \qquad (2.18)$$

TABLE 2.2 LIST OF THE NORMALIZING FACTORS.

VARIABLE	NORMALIZED QUANTITY	NORMALIZING FACTOR	UNIT
Position coordinate	x	$L_D = \sqrt{\epsilon V_0 / (q n_i)}$	m.
Time coordinate	t	L_D / D_0	sec.
Voltage	V	$V_0 = kT/q$	volt.
Electric field	E	V_0 / L_D	volt/m.
Charge density	p, n, N	n_i	m^{-3}
Current density	J_T, J_p, J_n, J_D	$q D_0 n_i / L_D$	amp/m^2
Recombination – generation rate	U	$D_0 n_i / L_D^2$	$m^{-3}.sec^{-1}$
Mobility coefficient	μ_p, μ_n	D_0 / V_0	$m^2/v.sec.$
Diffusion coefficient	D_0	1	$m^2/sec.$

Chapter 3

Numerical Solution of Nonlinear Boundary-Value Problems.

Differential equations can normally be classified into two types, depending on the prescribed conditions. If the conditions are given at one point in the range of the independent variable, the differential system is known as an initial-value problem. When the conditions are given at two or more distinct points, the system is known as a boundary-value problem. For our nonlinear problems, the system conditions are of the latter type, and we have nonlinear boundary-value problems.

3.1 Existing algorithms for the solutions.

The common techniques for solving boundary - value problems can be classified as

1) Shooting technique

2) Finite difference techniques.

The shooting method basically reduces the boundary-value problem to an initial-value problem, where estimations are made at one boundary to complete the necessary initial values. An attempt is then made to integrate the variables to the other boundary. If this can be accomplished, corrections are made to the initial estimation and then the process is repeated until convergence is achieved. Thus the shooting method is obviously based on integration methods which have been well developed and are easily accessible. There exist several efficient schemes ranging from the relatively simple to the

quite sophisticated, for example Runge - Kutta, Adams - Moulton, Gear's methods etc., <29><30>, most of which have automatic error controls with a variable step-size to minimize truncation and round off errors.

Although the shooting method is simple to use, in many practical problems the differential equations are so unstable that they blow up before the integration can be completed. This can occur even in the case of extremely accurate initial estimate and therefore the shooting method is unsuitable for certain problems.

In order to improve stability but at the same time preserve the advantages of the shooting method, a "multiple shooting method" has been proposed by Morrison et al. <32>. This replaces the original two - point boundary-value problem with a k-point boundary-value problem, which splits the integration interval into k-1 equal subintervals, for each of which the original shooting method is applied. By using a reasonable number of k boundary conditions, i.e shortening the subinterval, the integration should end before any stability can occur. For more difficult problems however, the multiple shooting method has always proved inadequate.

For these more complicated cases, a finite difference method <33><34> does offer a solution for it establishes firm overall control on the entire solution. The stability problem is less severe for this method than for the shooting methods, and it is sometimes preferred for this reason, especially for nonlinear problems.

Unlike the shooting methods, there is no standard form

of the finite difference technique , so each problem must be solved individually. The procedure begins with replacing the original differential equations by a linear algebraic system of equations (AX = b). This is done by subdividing the interval into k-1 subintervals (not necessarily equal) and by replacing the derivatives of the original differential equations with approximate finite difference equations. This is often referred to as the discretization procedure. If the problem is nonlinear, the nonlinear terms must be linearized in some fashion, and initial estimate must be made for all variables at all subintervals. Finally, the linear algebraic system of equations is formed as a matrix and solved by any of the methods of solving linear simultaneous equations. <29> <39> For nonlinear cases, an initial estimate and a successive approximation method must be used. The matrix A must be formed during each iteration and the process is continued until the solution converges to an acceptable accuracy.

To summarise, the method for solving a nonlinear boundary-value problem is as follows: <33>

1) Subdivide the interval into k-1 subintervals.

2) Discretize the differential equation into finite difference equation.

3) Linearize the equation.

4) Make the initial estimations.

5) Using the estimations, generate the elements of the linearized algebraic equations

A X = b

6) Solve the linear system of equations.

7) Modify the solution with the previous solution to obtain better estimates.

8) Return to step 5) until convergence is achieved.

It can be seen from the above that the two main problems met in the solution are discretization and linearization, so some basic procedures involving these will be set out in order to develop algorithms for our problems.

3.2 Finite difference approximations for derivatives.

The purpose of discretization is to transform a differential equation into a difference equation which can be arranged as a system of algebraic equations suitable for digital computer solution. The basic approximation involves the replacement of a continuous domain by a mesh or grid of discrete points within the domain, and the replacement of derivatives by finite difference approximations.

In solving the two-dimensional boundary-value problem <35>

$$L U = f(u) \; ; \; u = u(x,y) \tag{3.1}$$

in a domain D as shown in Fig. 3.1 subject to domain boundary conditions.

Taylor's series for $u(x \pm \Delta x, y)$ about (x,y) gives

$$u(x \pm \Delta x, y) = u(x,y) \pm \Delta x \frac{\partial u(x,y)}{\partial x} + (\Delta x)^2 \frac{\partial^2 u(x,y)}{2 \; \partial x^2}$$

$$\pm (\Delta x)^3 \frac{\partial^3 u(x,y)}{6 \; \partial x^3} + O[(\Delta x)^4] \tag{3.2}$$
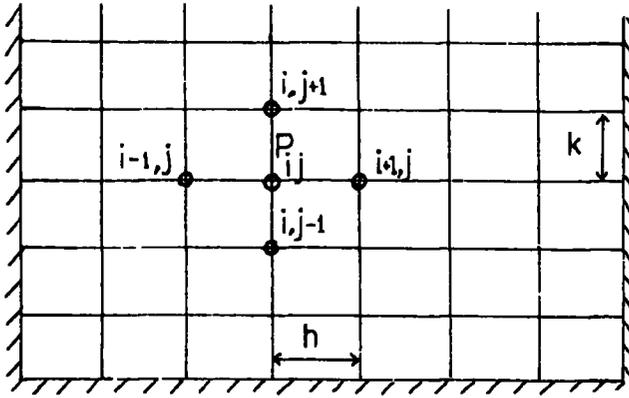
Figure 3.1

Let the points P_{ij} form a discrete approximation for D, and evaluate the derivative at point (x,y) where

$$x_i = ih \ , \ y_j = jk$$

Further $u_{ij} = u(x_i \ , \ y_j)$ will ultimately be employed for the exact solution.

Equation 3.2 can be written, as

$$u(x+\Delta x,y) - u(x,y) = \Delta x \ \frac{\partial u(x,y)}{\partial x} + O[(\Delta x^2)]$$

which, upon division by Δx, results in the relationship

$$\frac{\partial u}{\partial x}\bigg|_{ij} = \frac{1}{h}(u_{i+1,j}-u_{ij}) -\frac{h^2}{2} \frac{\partial^2 u}{\partial x^2}\bigg|_{ij} + O(h^2) \qquad (3.3)$$

Similarly, for $u(x- \Delta x,y)$, equation 3.2 may be expressed as

$$\frac{\partial u}{\partial x}\bigg|_{ij} = \frac{1}{h}(u_{ij}-u_{i-1,j}) +\frac{h^2}{2} \frac{\partial^2 u}{\partial x^2}\bigg|_{ij} + O(h^2) \qquad (3.4)$$

If only first order approximation is considered, equation 3.3 results in the forward difference approximation,

$$\frac{\partial u}{\partial x}\bigg|_{ij} = \frac{1}{h}(u_{i+1,j}-u_{ij}) + O(h) \qquad (3.5)$$

with equation 3.4 providing the backward difference approximation

$$\frac{\partial u}{\partial x}\bigg|_{ij} = \frac{1}{h}(u_{ij}-u_{i-1,j}) + O(h) \qquad (3.6)$$

For a second order approximation, adding equations 3.3 and 3.4 , results in the central difference approximation.

$$\frac{\partial u}{\partial x}\bigg|_{ij} = \frac{1}{2h}(u_{i+1,j}-u_{i-1,j}) + O(h^2)$$

Adding the two possible forms of the original expansion equation 3.2 , we find

$$u(x+\Delta x,y)+u(x-\Delta x,y) = 2u(x,y)+(\Delta x)^2\frac{\partial^2 u}{\partial x^2} + O(h^4)$$

or

$$\frac{\partial^2 u}{\partial x^2}\bigg|_{ij} = \frac{1}{h^2}(u_{i-1,j}-2u_{ij}+u_{i+1,j}) + O(h^4) \qquad (3.7)$$

3.2.1 Higher - order approximation

In some problems, higher accuracy of the approximation for the second derivative may be required. An alternative approach is to use the fourth order Cowell's method [36] suggested by Klopfenstein and Wu [37]. In the approximation of

$$L^2 u = f(u)$$

$$u = u(x,y)$$

we obtain

$$\frac{u_{i-1,j} - 2u_{ij} + u_{i+1,j}}{h^2} = B_0 f_{i-1,j} + B_1 f_{ij} + B_2 f_{i+1,j}$$

$$i = 1, 2, \ldots \ldots \ldots N$$

When $B_0 = 1/12$, $B_1 = 10/12$ and $B_2 = 1/12$, the equation then becomes

$$u_{i-1,j} - 2u_{ij} + u_{i+1,j} = (h^2/12) f_{i-1,j} + 10f_{ij} + f_{i+1,j} \tag{3.8}$$

3.2.2 Variable mesh distribution

The discretization stepsize h is one of the important parameters which control the stability and discretization error of the system. In the region where abruptness of the function occurs, a fine mesh distribution is necessary. It seems to be redundant in the region where the function changes slowly. Thus a variable mesh distribution is often desirable.

Consider a variable mesh distribution of Fig. 3.2 with the mesh spacing at point i

$$h_i = x_{i+1} - x_i$$
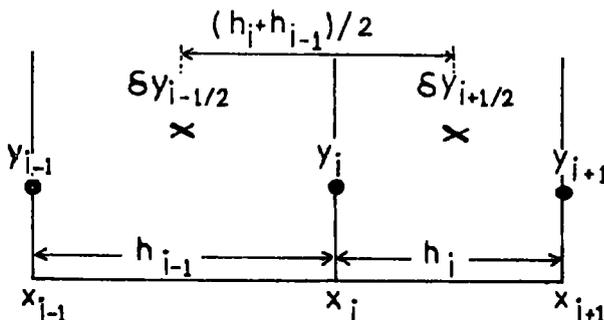
Figure 3.2

By using the central difference approximation with the

central difference operator, δ defined as <35>

$$\delta y_n = y_{n+1/2} - y_{n-1/2}$$

a second derivative of a function $y = f(x)$ can be obtained.
At a mesh point i we have

$$\frac{d^2y}{dx^2}\bigg|_{x=x_i} = \frac{\delta^2 y_i}{(h_i + h_{i-1})/2}$$

$$= \frac{\dfrac{\delta y_{i+1/2}}{h_i} - \dfrac{\delta y_{i-1/2}}{h_{i-1}}}{(h_i + h_{i-1})/2}$$

or

$$\frac{d^2y}{dx^2}\bigg|_{x=x_i} = \frac{a_i y_{i-1} + b_i y_i + c_i y_{i+1}}{(h_i + h_{i-1})/2}$$

where $a_i = 1/(h_{i-1})$

$c_i = 1/h_i$

$b_i = -a_i - c_i$

$\quad = - (h_i + h_{i-1})/(h_i h_{i-1})$

3.3 Picard and Newton linearization.

When solving a system of nonlinear algebraic
equations, it is customary to linearize the equations and
then employ a successive approximation method for solving
simultaneous equations.   As an example, consider a set of
nonlinear algebraic equations.

$$\underset{\sim}{g}(\underset{\sim}{x}) = g_i(\underset{\sim}{x})$$

$$= g_i(x_1, x_2, \ldots, x_R) = 0$$

$$i = 1, 2, \ldots, N \quad R \leq N \tag{3.9}$$

A simple and straight forward method used to linearize the equations is Picard's iteration which introduces a sequence $\left\{ \underset{\sim}{x}^{(k)} \right\}$ such that $\underset{\sim}{g}(\underset{\sim}{x}^{(k)})$ satisfies the same boundary conditions as $\underset{\sim}{f}(\underset{\sim}{x})$, and k is the iterative index. We therefore obtain the linearized form of equation 3.8 as

$$\underset{\sim}{g}(\underset{\sim}{x}^{(k+1)}) - \underset{\sim}{g}(\underset{\sim}{x}^{(k)}) = 0$$

When the sequence $\left\{ x^{(k)} \right\}$ converges, the convergence is linear i.e

$$\underset{\sim}{x}^{(k+1)} - \underset{\sim}{x} = O(\underset{\sim}{x}^{(k)} - \underset{\sim}{x})$$

as $k \longrightarrow \infty$

However if $\underset{\sim}{g}(\underset{\sim}{x})$ is differentiable, i.e, satisfies the Lipschitz's condition, the R-dimensional Newton's method can be used to linearize the equations. This replaces the approximation $\underset{\sim}{x}^{(k)}$ in the solution by the approximation

$$\underset{\sim}{x}^{(k+1)} = \underset{\sim}{x}^{(k)} + \underset{\sim}{\varsigma}^{(k)}$$

$$\tag{3.10}$$

By taking account of the first order terms in the Taylor's series expansion of $g_i(x)$ about $\underset{\sim}{x} = \underset{\sim}{x}^{(k)}$, the linearized system of equation 3.9 becomes <36>

$$g_i(\underset{\sim}{x}^{(k)}) + \sum_{j=1}^{R} \frac{\partial g_i}{\partial x_j^{(k)}} \delta_j^{(k)} = 0$$

$$i = 1,2, \ldots \ldots \quad N$$

or in matrix form

$$\underset{\sim}{g}(\underset{\sim}{x}^{(k)} + \underset{\sim}{G}(\underset{\sim}{x}^{(k)})\underset{\sim}{\delta}^{(k)} = 0 \tag{3.11}$$

Where $\underset{\sim}{G}(\underset{\sim}{x}^{(k)})$ is a diagonal Jacobian matrix, having an element

$$a_{ij}^{(k)} = \frac{\partial g_i}{\partial x_j^{(k)}} \tag{3.12}$$

which may be calculated by direct differentiation of the expressions for g_i . If these are very complicated, it may however be easier to estimate the derivative by calculating <39>

$$h^{-1}\left[g_i(x_1, \ldots, x_{j-1}, x_j+h, x_{j+1}, \ldots, x_R) - g_i(x_1, \ldots, x_R)\right]$$

or

$$\frac{h^{-1}}{2}\left[g_i(x_1, \ldots, x_{j-1}, x_j+h, x_{j+1}, \ldots, x_R)\right.$$

$$\left. g_i(x_1, \ldots, x_{j-1}, x_j-h, x_{j+1}, \ldots, x_R)\right]$$

If $\underset{\sim}{G}$ is singular then $\underset{\sim}{\delta}$ may be infinite, but if $\underset{\sim}{G}$ is non-singular a better approximation for equation 3.10 can be obtained. This results in a sequence $\left\{\underset{\sim}{x}^{(k)}\right\}$ which is usually quadratically convergent, i.e,

$$\underset{\sim}{x}^{(k+1)} - \underset{\sim}{x}^{(k)} = 0((\underset{\sim}{x}^{(k)} - \underset{\sim}{x})^2)$$

$$\text{as } k \longrightarrow \infty \tag{3.13}$$

This method sometimes fails to converge if $\underset{\sim}{x}^{(k)}$ is

not a good approximation for the solution of the system and therefore some modification may be required. A common strategy is to introduce a damping or relaxation factor w, and replace equation 3.10 by

$$\underset{\sim}{x}^{(k+1)} = \underset{\sim}{x}^{(k)} + w^{(k)} \underset{\sim}{\varepsilon}^{(k)}$$

$$(3.14)$$

Where w is calculated to prevent the approximated $\underset{\sim}{x}^{(k+1)}$ from being worse than the approximated $\underset{\sim}{x}^{(k)}$.

The choice between the Picard's and Newton's methods is finally determined by whether one chooses the linearly convergent scheme or the quadratically convergent scheme with extra computation in the evaluation of derivative terms. This comparison has been discussed in references <40> and <41>

3.4 Thermal equilibrium and reverse bias solution.

In order to illustrate the use of the finite difference method for the solution of a nonlinear boundary-value problem, a semiconductor device under thermal equilibrium reverse bias conditions with negligible current flow is investigated. From chapter 2, with these conditions, the system equations reduce to only Poisson equation

$$\frac{d^2 V}{dx^2} = n - p - N$$

$$(3.15)$$

Boltzman relation then gives the normalized carriers densities.

$$N = \exp (v)$$

$$p = \exp (-v)$$

Therefore Poisson equation can also be written as

$$\frac{d^2 V}{dx^2} = 2\sinh V - N \qquad\qquad (3.16)$$

Discretization.

Using the central difference finite approximation, equation 3.16 becomes

$$V_{i+1} - 2V_i + V_{i-1} = C \sinh V_i + D\, N_i \qquad\qquad (3.17)$$

$$i = 1, 2, \ldots\ldots N$$

Where

$$C = 2\, h^2$$

$$D = -\, h^2$$

or, in matrix form

$$\underset{\sim}{A}\ \underset{\sim}{V} = \underset{\sim}{f}\ (\underset{\sim}{V}) + \underset{\sim}{b} \qquad\qquad (3.18)$$

Where

$$
\underset{\sim}{A} =
\begin{vmatrix}
-2 & 1 & & & & & \\
1 & -2 & 1 & & & & \\
& 1 & -2 & 1 & & & \\
& & . & . & . & & \\
& & & . & . & . & \\
& & & & 1 & -2 & 1 \\
& & & & & 1 & -2
\end{vmatrix}
\quad ; \quad
\underset{\sim}{V} =
\begin{vmatrix}
V_1 \\
V_2 \\
V_3 \\
. \\
. \\
V_{N-1} \\
V_N
\end{vmatrix}
$$

$$
\underset{\sim}{f}(\underset{\sim}{V}) =
\begin{vmatrix}
C \sinh V_1 \\
C \sinh V_2 \\
\ldots\ldots \\
\ldots\ldots \\
\ldots\ldots \\
C \sinh V_{N-1} \\
C \sinh V_N
\end{vmatrix}
\quad ; \quad
\underset{\sim}{b} =
\begin{vmatrix}
DN_1 - V_0 \\
DN_2 \\
.. \\
.. \\
.. \\
DN_{N-1} \\
DN_N - V_{N+1}
\end{vmatrix}
$$

If Cowell's method from equation 3.8 is employed, equation 3.17 becomes

$$
\underset{\sim}{A}\,\underset{\sim}{V} = \underset{\sim}{B}.\underset{\sim}{f}(\underset{\sim}{V}) + \underset{\sim}{b}
\qquad\qquad (3.19)
$$

where

$$\underset{\sim}{B} = 1/12 \begin{vmatrix} 10 & 1 & & & & & \\ 1 & 10 & 1 & & & & \\ & 1 & 10 & 1 & & & \\ & & \cdot & \cdot & \cdot & & \\ & & & \cdot & \cdot & \cdot & \\ & & & & 1 & 10 & 1 \\ & & & & & 1 & 10 \end{vmatrix} \quad ; \quad \underset{\sim}{f}(\underset{\sim}{V}) = \begin{vmatrix} C \sinh V_1 + DN_1 \\ C \sinh V_2 + DN_2 \\ C \sinh V + DN \\ \cdots\cdots\cdots\cdots \\ \cdots\cdots\cdots\cdots \\ \cdots\cdots\cdots\cdots \\ C \sinh V_N + DN_N \end{vmatrix}$$

$$\underset{\sim}{b} = \begin{vmatrix} (1/12)(C \sinh V_0 + DN_0) - V_0 \\ 0 \\ 0 \\ \cdot \\ \cdot \\ 0 \\ (1/12)(C \sinh V_{N+1} + DN_{N+1}) - V_{N+1} \end{vmatrix}$$

Linearization.

Applying Newton's method to linearize equation 3.18

Let

$$\underset{\sim}{g}(\underset{\sim}{v}) = \underset{\sim}{A} \underset{\sim}{V} - \underset{\sim}{f}(\underset{\sim}{v}) - \underset{\sim}{b} \tag{3.20}$$

and

$$\underset{\sim}{v}^{(k+1)} = \underset{\sim}{v}^{(k)} + \underset{\sim}{s}^{(k)} \tag{3.21}$$

Linearized equation 3.18 can be written in the form of equation 3.11 as

$$[\underset{\sim}{A}\,\underset{\sim}{v}^{(k)} - \underset{\sim}{f}(\underset{\sim}{v}^{(k)}) - \underset{\sim}{b}] + [\underset{\sim}{A} - \underset{\sim}{F}(\underset{\sim}{v}^{(k)})]\underset{\sim}{s}^{(k)} = 0$$

or

$$[\underset{\sim}{A} - \underset{\sim}{F}(\underset{\sim}{v}^{(k)})]\underset{\sim}{v}^{(k+1)} = \underset{\sim}{f}(\underset{\sim}{v}^{(k)}) + \underset{\sim}{b} - \underset{\sim}{F}(\underset{\sim}{v}^{(k)})\underset{\sim}{v}^{(k)} \qquad (3.22)$$

Where $\underset{\sim}{F}(\underset{\sim}{v})$ is the Jacobian matrix of $\underset{\sim}{f}(\underset{\sim}{v})$

When the modified Newton's method as in equation 3.14 is employed, equation 3.21 can be replaced by

$$\underset{\sim}{v}^{(k+1)} = \underset{\sim}{v}^{(k+1)} + w^{(k)}\underset{\sim}{s}^{(k)} \qquad (3.23)$$

and the linearized equation becomes

$$\frac{1}{w^{(k)}}[\underset{\sim}{A} - \underset{\sim}{F}(\underset{\sim}{v}^{(k)})]\underset{\sim}{v}^{(k+1)} = \underset{\sim}{f}(\underset{\sim}{v}^{(k)}) + \underset{\sim}{b} + \frac{1}{w^{(k)}}\underset{\sim}{F}(\underset{\sim}{v}^{(k)})\underset{\sim}{v}^{(k)} + \left[\frac{1}{w^{(k)}}\underset{\sim}{A} - \underset{\sim}{A}\right]\underset{\sim}{v}^{(k)}$$

Similarly with equation 3.21 the linearized equation 3.19 can be written as

$$[\underset{\sim}{A} - \underset{\sim}{B}\cdot\underset{\sim}{F}(\underset{\sim}{v}^{(k)})]\underset{\sim}{v}^{(k+1)} = \underset{\sim}{B}\,[\underset{\sim}{f}(\underset{\sim}{v}^{(k)}) - \underset{\sim}{F}(\underset{\sim}{v}^{(k)})\underset{\sim}{v}^{(k)}] + \underset{\sim}{b} \qquad (3.25)$$

Finally, it is seen that equations 3.22, 3.24 and 3.25 can be rearranged into the same form as

$$A_{T_i}^{(k)} V_{i-1}^{(k+1)} + B_{T_i}^{(k)} V_i^{(k+1)} + C_{T_i}^{(k)} V_{i+1}^{(k+1)} = D_{T_i}^{(k)} \qquad (3.26)$$

$$i = 1, 2, \ldots \ldots N$$

Where $A^{(k)}$, $B^{(k)}$ and $C^{(k)}$ are determined from the associated matrix equations, and the tridiagonal structure is preserved.

3.4.1 Application to Schottky barriers diodes:

The model used in this example is the Schottky barrier diode shown in Fig. 3.3 . The physical parameters of the diode are as follows:
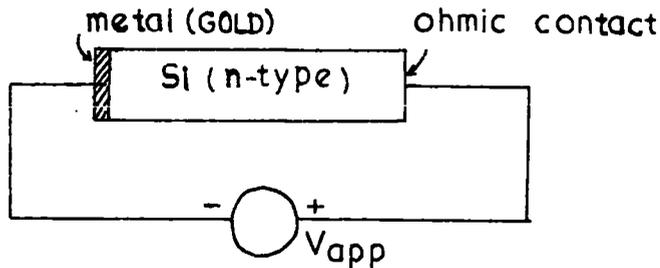
Figure 3.3

Metal : Gold

Semiconductor : n-type silicon

Vacuum work function of metal ϕ_M = 4.70 eV

Vacuum work function of semiconductor ϕ_S = 5.15 eV

Semiconductor band-gap energy Eg = 1.11 eV

Intrinsic carrier density = 10^{10} cm^{-3}

Device length = 1 micron

The boundary condition for equation 3.15 at the metal contact is given by

$$V_o = (\phi_M - \phi_S) + |E_g/2| + V_{app}$$

(3.27)

where V_o is the surface potential at the metal contact.

If ohmic conditions are assumed at the semiconductor contact, the other boundary condition can be determined from its thermal equilibrium potential. By using the electrical neutrality condition, i.e,

$$\frac{d^2V}{dx^2} = e^V - e^{-V} - N = 0$$

we obtain

$$V(x) = \pm \left| \ln\left(\frac{N}{2} + \frac{(N^2+4)^{1/2}}{2}\right) \right| \tag{3.28}$$

Where the plus minus sign refers to n-type and p-type doping respectively. Equation 3.28 provides also an initial approximation for beginning the iteration.

A computer subroutine "COWELL" was written to evaluate equation 3.18 based on the Cowell's method of equation 3.25, which uses the modified Newton's method of equation 3.24 as the prelude for each solution.

The solution at thermal equilibrium and for various values of the reverse bias were obtained successfully. For high reverse bias, the minority carrier density term was neglected to avoid underflow.

For example, consider a constant doping profile diode with $N = 10^{15}$ cm^{-3}. Fig. 3.4 shows the electrostatic potential from the thermal equilibrium condition to -2.0 Volt. reverse bias. The majority carrier distribution can be determined and is depicted in Fig. 3.5. By assuming the validity of the depletion approximation, the barrier potential obtained from Fig. 3.4 is used to calculate the capacitance C. Fig. 3.6 shows a plot of C and $1/C^2$ against bias. It can be seen that the variation of $1/C^2$ is linear and the intercept gives the barrier potential as predicted from simple theory.
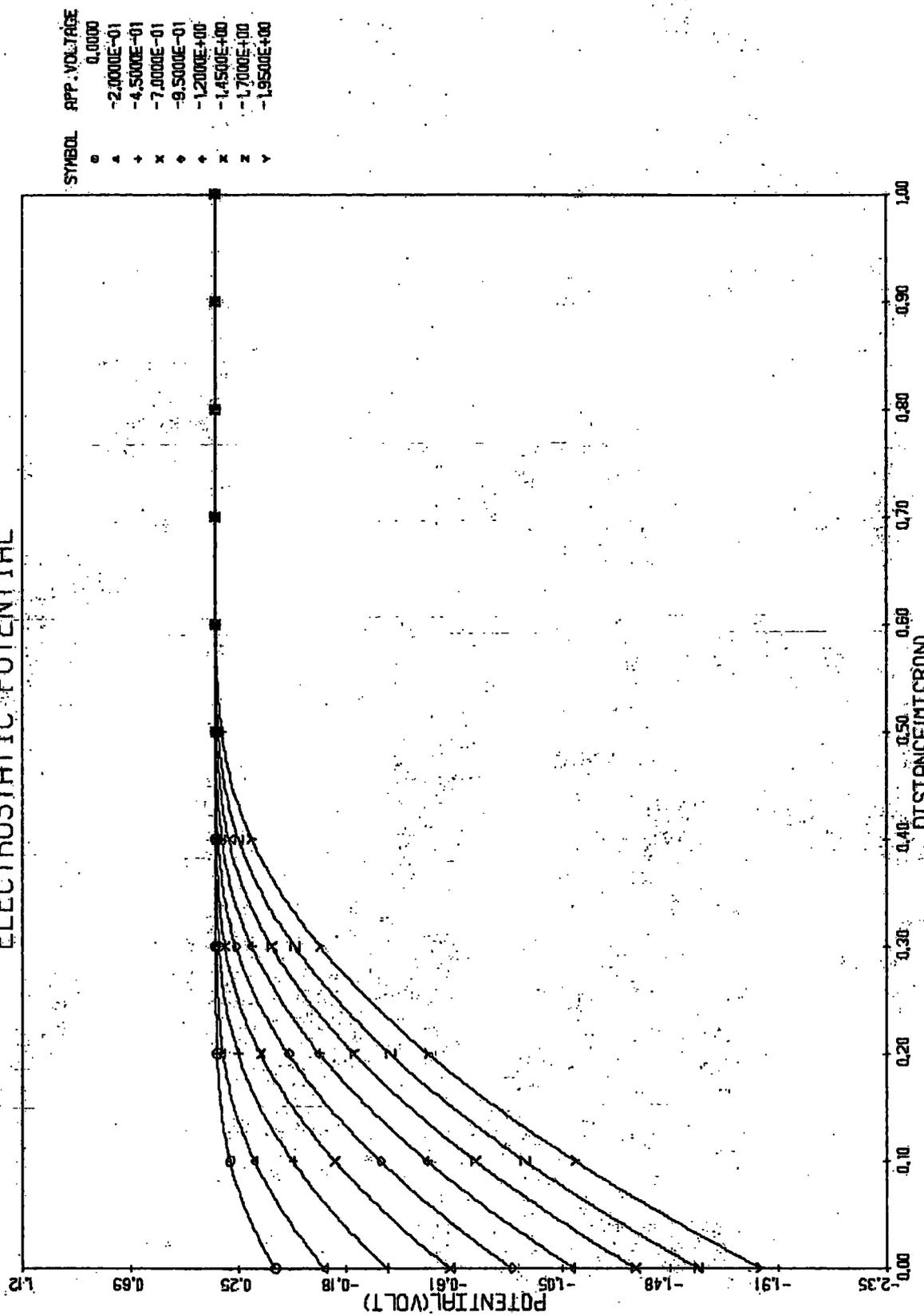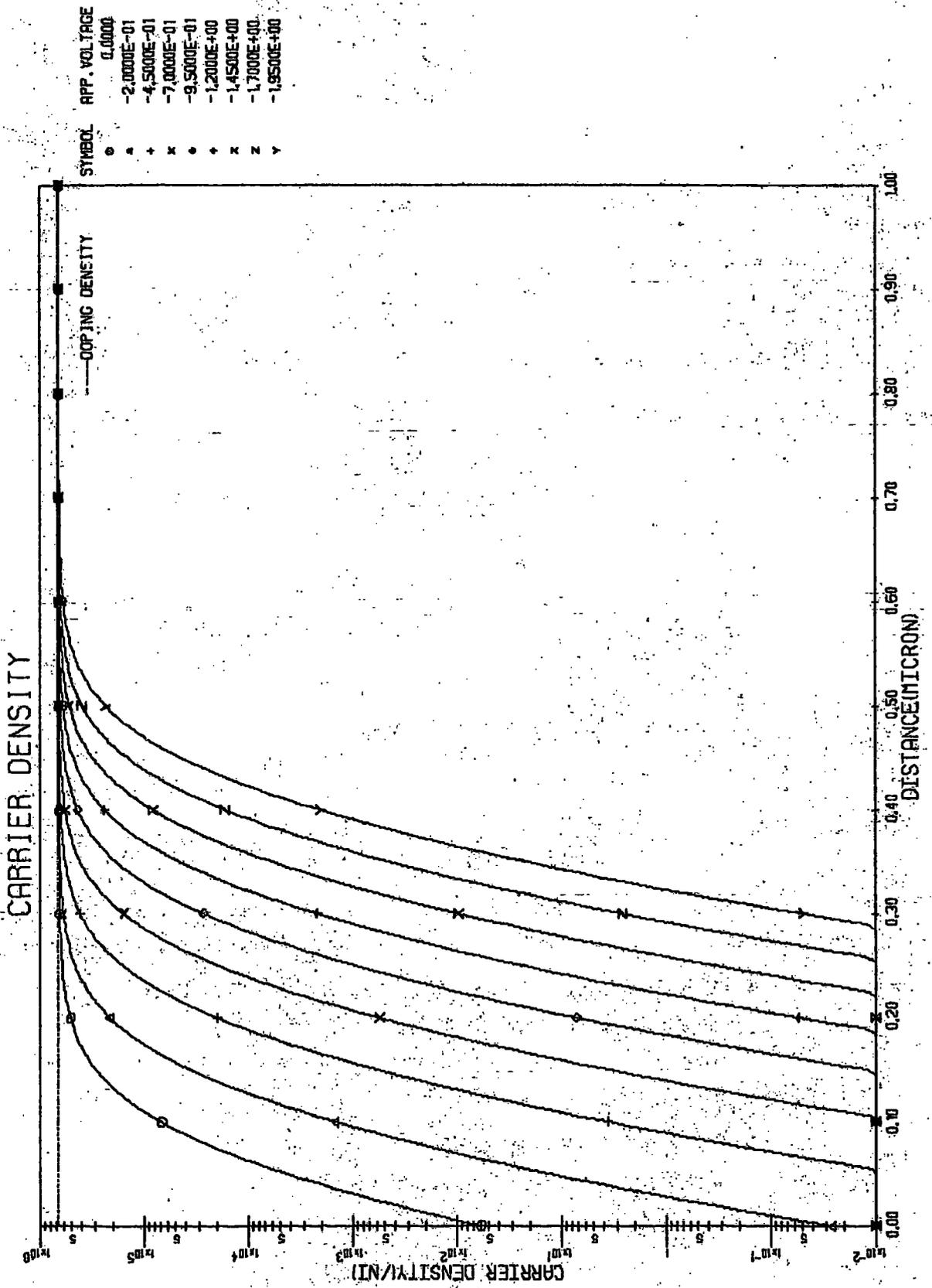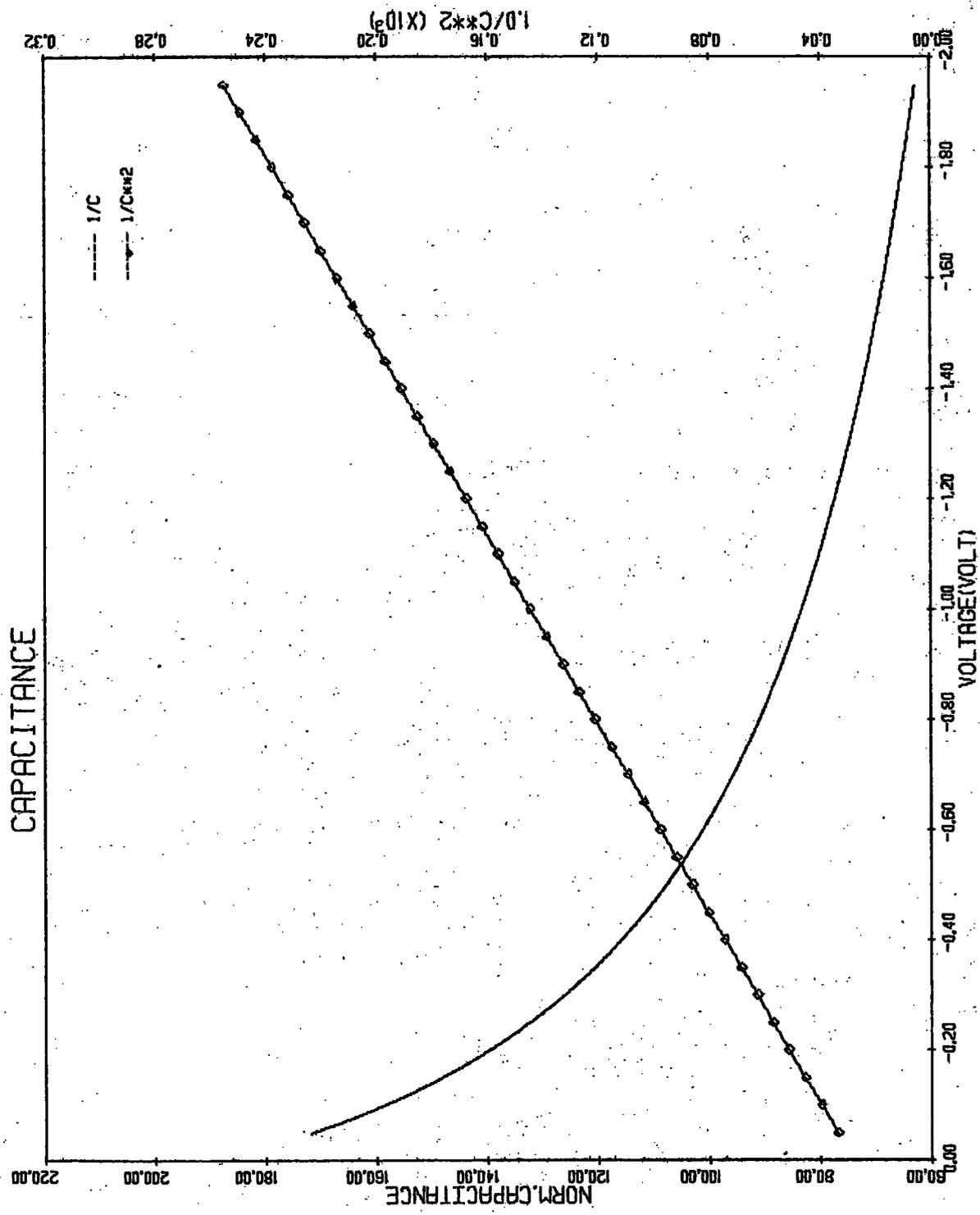
FIGURE (3.4)

FIGURE (3.5)

FIGURE (3.6)

For an arbitrary doping profile diode, with the doping density given by Wu <38>

$$N(x) = 10^{14} + N_{max} \exp\left[-\frac{1}{2}\left[\frac{x-R_p}{\Delta R_p}\right]^2\right]$$

where

$N_{max} = 5.0 \times 10^{16}$ cm^{-3}.

$R_p = 0.25 \times 10^{-4}$ cm.

$\Delta R_p = 0.06 \times 10^{-4}$ cm.

The resulting electrostatic potential and the majority carrier distribution are shown in Figs. 3.7 and 3.8 respectively.

These examples show that the method does not only provide information about the internal behaviour of the diodes, but also allows any arbitrary profile diode to be investigated where the classical analytical methods would become impractical.
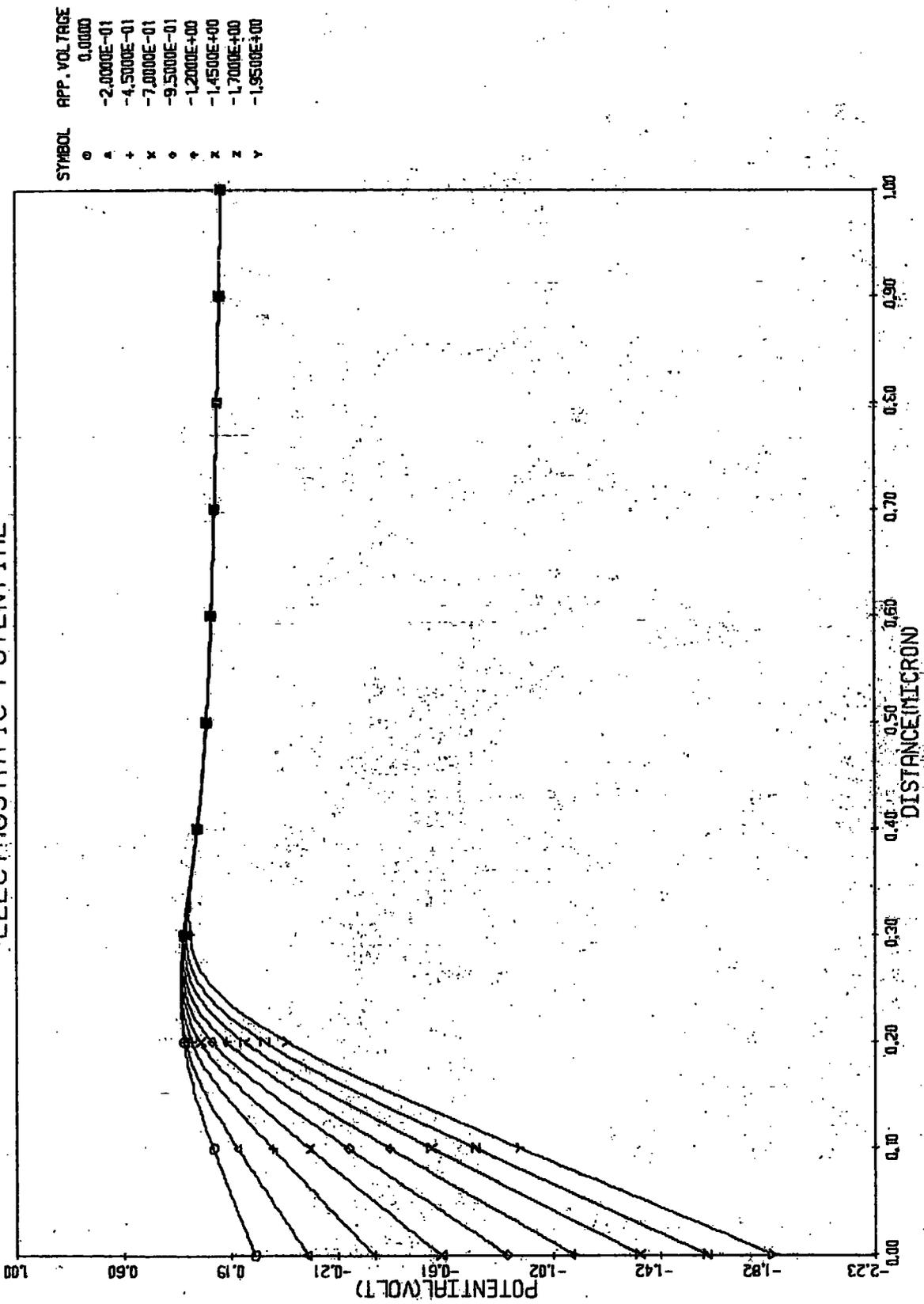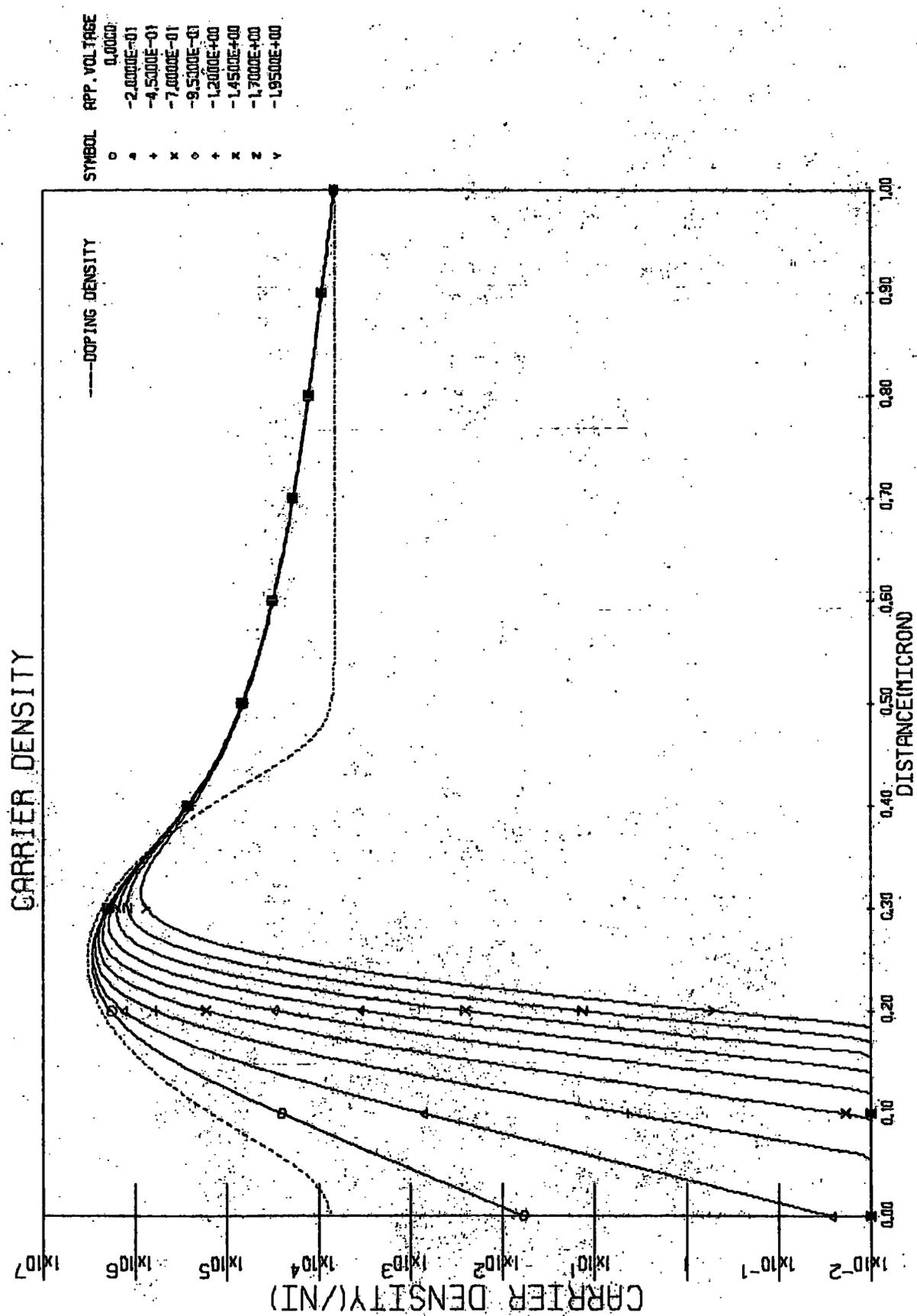
FIGURE (3.7)

FIGURE (3.8)

Chapter 4

Time-Independent Modelling of Junction Devices.

In this chapter, an algorithm for dc-steady state modelling is developed. This will be used to study the static behaviour of p-n junction diodes under both forward and reverse bias. A prime interest is to investigate the effect of the minority carrier lifetime on the diode characteristics. Finally, a method is developed for analysing a simple circuit using the diode under consideration.

The technique initially used was based on Calzolari's algorithm <13>. The scheme employed the Picard iteration with the continuity equations, and calculated the pertubation of the electrostatic potential from the Poisson equation. It was found that the solutions became inconsistent under higher injection level conditions, and therefore an extra test for consistency was required.

An alternative method to overcome this problem can be developed by applying the R-dimentional Newton algorithm (chapter 3) to the Poisson equation. The electrostatic potential is calculated directly rather than its pertubation. This method has advantages not only in terms of stability, but also in terms of simplicity. It can be extended to either a two-dimensional case or to transient analysis, and is economical in the use of computational time.

4.1 Formulation of the system equations.

In dc-steady state analysis, the time dependent terms in the system equations vanish. It is therefore more convenient to rearrange the normalized system equations developed in chapter 2 into the form:

$$J_p = \mu_p \left[p \frac{\partial V}{\partial x} + \frac{\partial p}{\partial x} \right] \qquad (4.1)$$

$$J_n = \mu_n \left[n \frac{\partial V}{\partial x} - \frac{\partial n}{\partial x} \right] \qquad (4.2)$$

$$\frac{\partial J_p}{\partial x} = U_p \qquad (4.3)$$

$$\frac{\partial J_n}{\partial x} = -U_n \qquad (4.4)$$

and

$$\frac{\partial^2 V}{\partial x^2} = n - p - N \qquad (4.5)$$

where , in this case, the normalizing factor for J_p and J_n becomes $(-q\ D_o n_i / L_D)$

For ease of computation, let ϕ_p and ϕ_n to be the hole and electron quasi-Fermi potentials respectively. We can therefore write

$$p = \phi_p\ e^{-V} \qquad (4.6)$$

$$n = \phi_n\ e^{V} \qquad (4.7)$$

Equation 4.6 may be written as

$$\phi_p = p\ e^{V}$$

By differentiation

$$\frac{\partial \phi}{\partial x}p = e^V \frac{\partial p}{\partial x} + p \frac{\partial V}{\partial x} e^V$$

$$= e^V \left[\frac{\partial p}{\partial x} + p \frac{\partial V}{\partial x} \right]$$

or

$$e^{-V} \frac{\partial \phi}{\partial x}p = p \frac{\partial V}{\partial x} + \frac{\partial p}{\partial x}$$

Therefore, equation 4.1 can be written as

$$J_p = \mu_p e^{-V} \frac{\partial \phi}{\partial x}p \qquad\qquad (4.8)$$

Similarly,

$$J_n = -\mu_n e^V \frac{\partial \phi}{\partial x}n \qquad\qquad (4.9)$$

By substituting equations 4.8 and 4.9 into equations 4.3 and 4.4 respectively, and letting $U_p = U_n = U$ we finally obtain

$$\frac{\partial}{\partial x}\left[\mu_p e^{-V} . \frac{\partial \phi}{\partial x}p \right] = U \qquad\qquad (4.10)$$

$$\frac{\partial}{\partial x}\left[\mu_n e^V . \frac{\partial \phi}{\partial x}n \right] = U \qquad\qquad (4.11)$$

4.2 Discretization of the system equations.

a) The Poisson equation

Take the equation

$$\frac{\partial^2 V}{\partial x^2} = n - p - N \qquad\qquad (4.5)$$

By application of the finite difference approximation the

differential equation is discretized into a difference equation. If the variable mesh scheme is chosen, we can write at the mesh point x_i,

$$\frac{a_i V_{i-1} + b_i V_i + c_i V_{i+1}}{(h_i + h_{i-1})/2} = n_i - p_i - N_i$$

or

$$a_i V_{i-1} + b_i V_i + c_i V_{i+1} = \theta_i (n_i - p_i - N_i) \qquad (4.12)$$

$$i = 1, 2, \ldots, N$$

Where

$$a_i = 1/(h_{i-1})$$

$$c_i = 1/h_i$$

$$b_i = -a_i - c_i = -(h_i + h_{i-1})/(h_i h_{i-1})$$

$$\theta_i = (h_i + h_{i-1})/2$$

b) The continuity equations.

From the equation 4.10

$$\frac{\partial}{\partial x}\left[\mu_p e^{-V} \frac{\partial \phi_p}{\partial x}\right] = U \qquad (4.10)$$

which is in the self-adjoint form, the same discretization procedure can also be applied. For convenient, let us write

$$s_p = \mu_p e^{-V}$$

at the mesh point x_i, the approximated equation is obtained as

$$\frac{s_{i+1/2}\left[\dfrac{\phi_{p_{i+1}} - \phi_{p_i}}{h_i}\right] - s_{i-1/2}\left[\dfrac{\phi_{p_i} - \phi_{p_{i-1}}}{h_{i-1}}\right]}{(h_{i-1}+ h_i)/2} = U_i$$

becoming

$$\frac{(s_{i-1/2})\phi_{p_{i-1}}}{h_{i-1}(h_{i-1}+h_i)/2} - \frac{(s_{i+1/2}h_{i-1}+ s_{i-1/2}h_i)\phi_{p_i}}{h_i h_{i-1}(h_{i-1}+h_i)/2} +$$

$$\frac{(s_{i+1/2})\phi_{p_{i+1}}}{h_i(h_{i-1}+h_i)/2} = U_i$$

or

$$a_i\phi_{p_{i-1}} + b_i\phi_{p_i} + c_i\phi_{p_{i+1}} = d_i \qquad\qquad (4.13)$$

where $\quad a_i =(s_{i-1/2})/h_{i-1}$

$$c_i =(s_{i+1/2})/h_i$$

$$b_i = -a_i - c_i$$

$$= -\frac{(s_{i+1/2})h_{i-1}+(s_{i-1/2})h_i}{h_i h_{i-1}}$$

$$d_i = U_i(h_i+h_{i-1})/2$$

Since

$$\mu_{p_{i+1/2}}= (\mu_{p_i}+ \mu_{p_{i+1}})/2$$

and

$$e^{-v_{i+1/2}}= e^{-(v_i+v_{i+1})/2}$$

hence

$$s_{i\pm1/2} = \frac{(\mu_{p_i} + \mu_{p_{i\pm1}})}{2} e^{-(V_i + V_{i\pm1})/2}$$

By using the relation in equation 4.6, equation 4.13 can be written in terms of the vector p as

$$a_i e^{V_{i-1}} p_{i-1} + b_i e^{V_i} p_i + c_i e^{V_{i+1}} p_{i+1} = d_i$$

or, in the form

$$A_{p_i} p_{i-1} + B_{p_i} p_i + C_{p_i} p_{i+1} = D_{p_i} \qquad (4.14)$$

where, in this case

$$A_{p_i} = a_i e^{V_{i-1}}$$

$$= \frac{1}{2h_{i-1}} (\mu_{p_i} + \mu_{p_{i-1}}) e^{(V_{i-1} - V_i)/2}$$

$$C_{p_i} = c_i e^{V_{i+1}}$$

$$= \frac{1}{2h_i} (\mu_{p_i} + \mu_{p_{i+1}}) e^{(V_{i+1} - V_i)/2}$$

$$B_{p_i} = b_i e^{V_i}$$

$$= -\frac{1}{2h_{i-1}} (\mu_{p_i} + \mu_{p_{i-1}}) e^{(V_i - V_{i-1})/2} - \frac{1}{2h_i} (\mu_{p_i} + \mu_{p_{i+1}}) e^{(V_i - V_{i+1})/2}$$

$$D_{p_i} = U_i (h_i + h_{i-1})/2$$

Similarly, the discretized form of equation 4.10 can be derived at the mesh point x_i as

$$A_{n_i} n_{i-1} + B_{n_i} n_i + C_{n_i} n_{i+1} = D_{n_i} \qquad (4.15)$$

where

$$A_{n_i} = \frac{1}{2h_{i-1}} (\mu_{n_i} + \mu_{n_{i-1}}) \ e^{(V_i - V_{i-1})/2}$$

$$C_{n_i} = \frac{1}{2h_i} (\mu_{n_i} + \mu_{n_{i+1}}) \ e^{(V_i - V_{i+1})/2}$$

$$B_{n_i} = -\frac{1}{2h_{i-1}} (\mu_{n_i} + \mu_{n_{i-1}}) \ e^{(V_{i-1} - V_i)/2} - \frac{1}{2h_i} (\mu_{n_i} + \mu_{n_{i+1}}) \ e^{(V_{i+1} - V_i)/2}$$

$$D_{n_i} = U_i (h_i + h_{i-1})/2$$

4.3 Linearization of the system equations.

a) The Poisson equation.

The nonlinear algebraic equation 4.12 can be linearized by using the R-dimentional Newton's method,

$$g_i(\underline{x}^{(k)}) + \sum_{r=1}^{R} \frac{\partial g_i}{\partial x_r^{(k)}} \, \delta_r^{(k)} = 0$$

$$i = 1, 2, \ldots\ldots N$$

where in this case, $\delta_r^{(k)}$ is denoted by

$$V_r^{(k+1)} = V_r^{(k)} + \delta_r^{(k)}$$

and

$$g_i(V_{i-1}, V, V_{i+1}) = a_i V_{i-1} + b_i V_i + c_i V_{i+1} - \theta_i (n_i - p_i - N_i)$$

Therefore, the linearized form of equation 4.3 can be

written as

$$0 = \left[a_i^{(k)} V_{i-1}^{(k)} + b_i^{(k)} V_i^{(k)} + c_i^{(k)} V_{i+1}^{(k)} - \theta_i (n_i^{(k)} - p_i^{(k)} - N_i^{(k)}) \right]$$

$$+ a_i^{(k)} (V_{i-1}^{(k+1)} - V_{i-1}^{(k)}) + \left[b_i^{(k)} - \theta_i (n_i^{(k)} + p_i^{(k)}) \right] (V_i^{(k+1)} - V_i^{(k)})$$

$$+ c_i^{(k)} (V_{i+1}^{(k+1)} - V_{i+1}^{(k)})$$

or

$$a_i^{(k)} V_{i-1}^{(k+1)} + \left[b_i^{(k)} - \theta_i (n_i^{(k)} + p_i^{(k)}) \right] V_i^{(k+1)} + c_i^{(k)} V_{i+1}^{(k+1)}$$

$$= \theta_i (n_i^{(k)} - p_i^{(k)} - N_i^{(k)}) - (n_i^{(k)} + p_i^{(k)}) V_i^{(k)}$$

and finally in the form

$$A_{V_i}^{(k)} V_{i-1}^{(k+1)} + B_{V_i}^{(k)} V_i^{(k+1)} + C_{V_i}^{(k)} V_{i+1}^{(k+1)} = D_{V_i}^{(k)} \qquad (4.16)$$

where

$$A_{V_i}^{(k)} = a_i^{(k)}$$

$$C_{V_i}^{(k)} = c_i^{(k)}$$

$$B_{V_i}^{(k)} = b_i^{(k)} - \theta_i (n_i^{(k)} + p_i^{(k)})$$

$$D_{V_i}^{(k)} = \theta_i \left[(n_i^{(k)} - p_i^{(k)} - N_i^{(k)}) - (n_i^{(k)} + p_i^{(k)}) V_i^{(k)} \right]$$

b) <u>The continuity equations.</u>

For the continuity equations 4.9 and 4.10, the same linearization procedure as in a) could be applied. However this is not necessary. If the Picard-like iteration is employed when dealing with the generation - recombination term U(x), the equations become linear in the context of the iteration loop <13>. The linearized form of equations 4.15 and 4.16 can therefore be written directly as

$$A_{p_i}^{(k)} p_{i-1}^{(k+1)} + B_{p_i}^{(k)} p_i^{(k+1)} + C_{p_i}^{(k)} p_{i+1}^{(k+1)} = D_{p_i}^{(k)} \qquad (4.17)$$

and

$$A_{n_i}^{(k)} n_{i-1}^{(k+1)} + B_{n_i}^{(k)} n_i^{(k+1)} + C_{n_i}^{(k)} n_{i+1}^{(k+1)} = D_{n_i}^{(k)} \qquad (4.18)$$

4.4 <u>Computational algorithm.</u>

4.4.1 <u>Matrix formulation</u>

The system equations are now in the form of sets of linear algebraic equations as in equations 4.16 4.17 and 4.18 and any successive approximation method can be applied to obtain the solutions. The presence of coupling between the parameters requires that these equations must be solved simultaneously at each mesh point. This results in a block matrix of the form

$$\mathcal{A}^{(k)} \mathcal{U}^{(k+1)} = \mathcal{B}^{(k)}$$

$$
\mathcal{A} = \left\|
\begin{array}{ccc|ccc|ccc}
A_p & 0 & 0 & B_p & 0 & 0 & C_p & 0 & 0 \\
0 & A_n & 0 & 0 & B_n & 0 & 0 & C_n & 0 \\
0 & 0 & A_v & 0 & 0 & B_v & 0 & 0 & C_v
\end{array}
\right\|_i
$$

$$
\mathcal{U} = \left\|
\begin{array}{c}
\vdots \\
\begin{array}{c} P \\ N \\ V \end{array}\Big|_{i-1} \\
\begin{array}{c} P \\ N \\ V \end{array}\Big|_{i} \\
\begin{array}{c} P \\ N \\ V \end{array}\Big|_{i+1} \\
\vdots
\end{array}
\right\|
\qquad
\mathcal{B} = \left\|
\begin{array}{c}
\vdots \\
\begin{array}{c} D_p \\ D_n \\ D_v \end{array}\Big|_{i-1} \\
\begin{array}{c} D_p \\ D_n \\ D_v \end{array}\Big|_{i} \\
\begin{array}{c} D_p \\ D_n \\ D_v \end{array}\Big|_{i+1} \\
\vdots
\end{array}
\right\|
$$

However, for convenience, an approximation can be made to permit each set of equations to be solved separately. This requires setting <18>

$$n^{(k+1)} = n^{(k)} \text{ and } V^{(k+1)} = V^{(k)} \text{ in the calculation for } p^{(k+1)}$$

$$V^{(k+1)} = V^{(k)} \text{ and } p^{(k+1)} = p^{(k)} \text{ in the calculation for } n^{(k+1)}$$

$$p^{(k+1)} = p^{(k)} \text{ and } n^{(k+1)} = n^{(k)} \text{ in the calculation for } V^{(k+1)}$$

This method which involves solving the tridiagonal matrix system does not impair the coupling property because the influence of each parameter on the others still exists by way of the previous iteration cycle k. For p, the system is

and similar matrice for n and V.

The tridiagonal matrix can be inverted by the algorithm given in Appendix A, using the following boundary conditions discussed in chapter 2,

$$P_0 = P_{oo} = e^{-Veq(0)}$$

$$P_{N+1} = P_{Lo} = e^{-Veq(L)}$$

$$n_0 = n_{oo} = e^{Veq(0)}$$

$$n_{N+1} = n_{Lo} = e^{Veq(L)}$$

$$V_o = V_{eq}(0) + V_{applied}$$

$$V_{N+1} = V_{eq}(L)$$

where subscript eq denotes the values at thermal equilibrium, and L is the length of device as shown in Fig. 2.3.

4.4.2 The iterative scheme

After the physical parameters of the device have been specified, the iterative scheme for the solutions may begin with the trial approximations for p,n, and v. These quantities can be obtained from the solutions at Thermal equilibrium described in chapter 3. Then the iteration may stated and the cycle followed until the solutions converge to the desired accuracy. The iteration scheme is given as a flow diagram in Fig. 4.1

In order to stop the iteration, a test for convergence must be performed. The solution is acceptable when the condition

$$\max \ | V_i^{(k+1)} - V_i^{(k)} | < \epsilon$$

is satisfied.
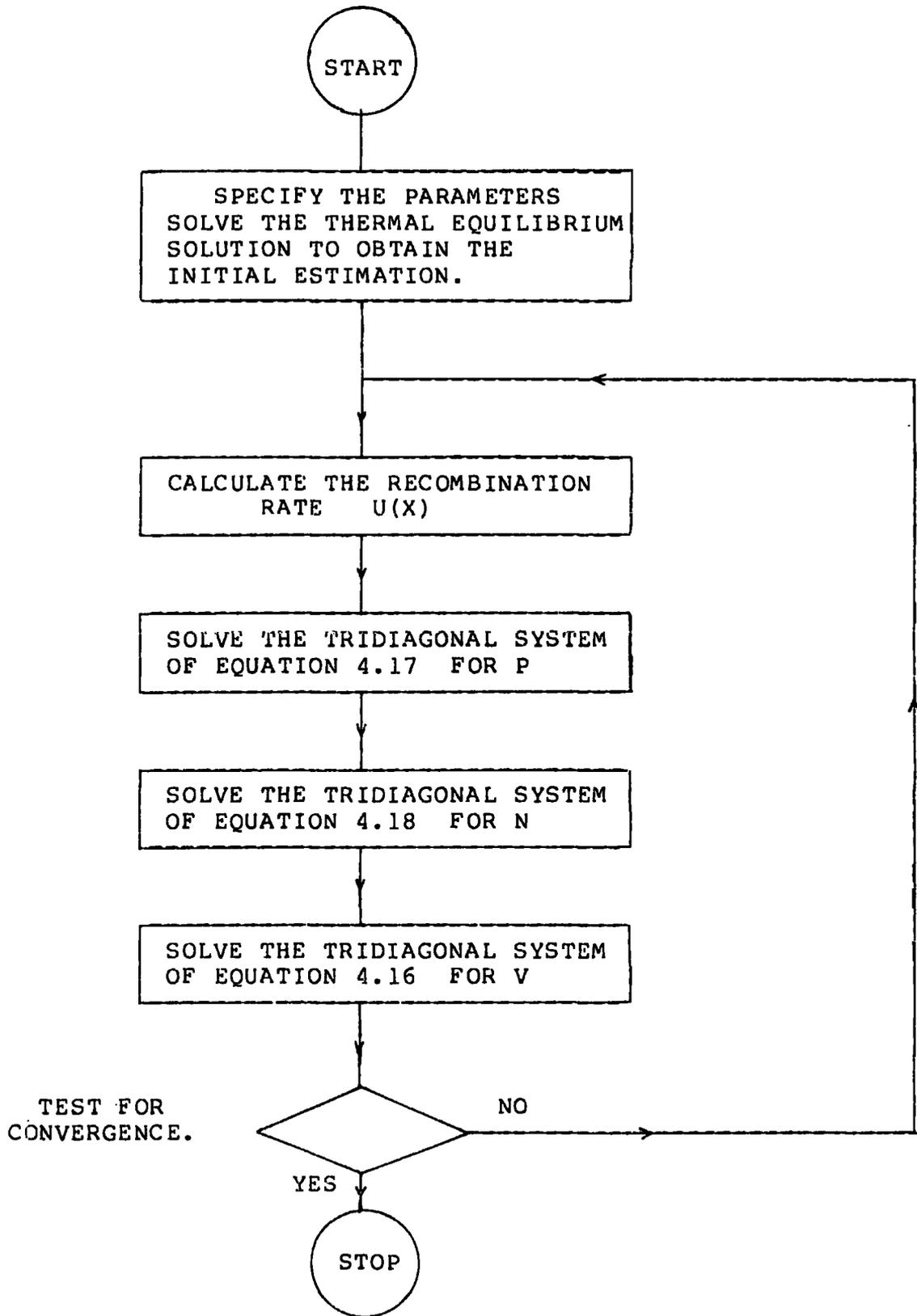
FIGURE 4.1 THE COMPUTATIONAL ALGORITHM.

4.5 Calculation of the current densities

In the calculation of the current densities, a direct method may be used to apply a standard difference approximation to obtain the differentiated terms in the equations 4.1 and 4.2 . The current densities can be determined by using the $v(x)$, $p(x)$ and $n(x)$ obtained from the iteration. However, in our case, this method was not successful because of truncation error in dealing with the two nearly equal but opposite large quantities in the transition region. These correspond to the drift and diffusion current in the simple model of the p-n junction. An alternative method is to employ the De Mari analytical scheme <11>, by treating equations 4.1 and 4.2 as two independent first order linear differential equations in the unknowns $p(x)$ and $n(x)$ respectively.

Thus equation 4.1 may be written as

$$\frac{dp(x)}{dx} + \frac{dV}{dx}.p(x) = \frac{J_p(x)}{\mu_p(x)}$$

Multiplying both sides of the equation by an integrating factor $\exp(\int(dV/dx)\,dx)$ we obtain

$$e^{\int\frac{dV}{dx}.dx} . \left[\frac{dp(x)}{dx} + \frac{dV}{dx}.p(x) \right] = \frac{J_p(x)}{\mu_p(x)} . e^{\int\frac{dV}{dx}.dx}$$

$$\frac{d}{dx}\left[e^{\int\frac{dV}{dx}.dx} . p(x) \right] = \frac{J_p(x)}{\mu_p(x)} . e^{\int\frac{dV}{dx}.dx}$$

Integrating the equation between X and L, we finally have

$$e^{V(x)} \cdot p(x) \bigg|_x^L = \int \frac{J_p(x')}{\mu_p(x')} \cdot e^{V(x')} dx'$$

$$p(x) = e^{-V(x)} \left[-\int \frac{J_p(x')}{\mu_p(x')} e^{V(x')} dx' + p(L) e^{V(L)} \right] \tag{4.19}$$

Similarly, from equation 4.2 we derive

$$n(x) = e^{V(x)} \left[\int \frac{J_n(x')}{\mu_n(x')} e^{-V(x')} dx' + n(L) e^{-V(L)} \right] \tag{4.20}$$

The current densities can now be calculated from the continuity equations 4.3 and 4.4, i.e,

$$J_p(x) = \int_0^x U(x') \, dx' + K_p \tag{4.21}$$

$$J_n(x) = -\int_0^x U(x') \, dx' + K_n \tag{4 22}$$

where the constants K_p and K_n can be obtained by substituting equations 4.21 and 4.22 into equations 4.19 and 4.20 respectively, and evaluating at X = O. We then obtain

$$p(0) = e^{-V(0)} \left\{ -\int_0^L \frac{1}{\mu_p(x)} \left[\int_0^x U(x') \cdot dx' + K_p \right] e^{V(x)} dx + p(L) e^{V(L)} \right\}$$

$$n(0) = e^{V(0)} \left\{ \int_0^L \frac{1}{\mu_n(x)} \left[-\int_0^x U(x') \cdot dx' + K_n \right] e^{-V(x)} dx + n(L) e^{-V(L)} \right\}$$

Therefore

$$K_p = \frac{p(L) e^{V(L)} - p(0) e^{V(0)} - \int_0^L \frac{1}{\mu_p(x)} e^{V(x)} \left[\int_0^x U(x') \, dx' \right] dx}{\int_0^L \frac{1}{\mu_p(x)} e^{V(x)} dx}$$

$$K_n = \frac{n(0)\, e^{-V(L)} - n(L)\, e^{-V(0)} + \int_o^L \frac{1}{\mu_p(x)}\, e^{-V(x)} \left[\int_o^x U(x')\, dx' \right] dx}{\int_o^L \frac{1}{\mu_n(x)}\, e^{V(x)}\, dx}$$

4.6 Numerical results.

We can now able to study the internal and the terminal characteristics of some p-n junction devices, using the current algorithm described in the preceding section, together with the relevant expressions stated in chapter 2. Because we are interested in large signal modeling, we shall carry out investigations in both forward and reverse bias regions, under low-level and high-level injection conditions, and with moderate to strong recombination. Sucessful solutions have been obtained for a variety of different profiles. However, in this section we shall present only a complementary error function profile diode with the n^+-p-p^+ structure. Emphasis is placed on a case of moderate recombination which most power devices satisfy.

A complementary-error function profile diode.

The silicon n^+-p-p^+ diffusion diode under investigation has the impurity profile shown in Fig. 4.2 and the following physical parameters

Temperature 300 K

Dimensions Total length = 13.5   um

   n^+ (erfc diffusion) region = 3 um

p(abrupt) region = 7.43 μm.

Area = 3.48 x 10^{-4} cm?

Lifetimes T_{po}, T_{no} = 1.0 x 10^{-7} sec.

Mobilities see Fig. 2.1 and equation 2.19

IMPURITY PROFILE

IMPURITY DENSITY(/NI)

DISTANCE(MICRON)
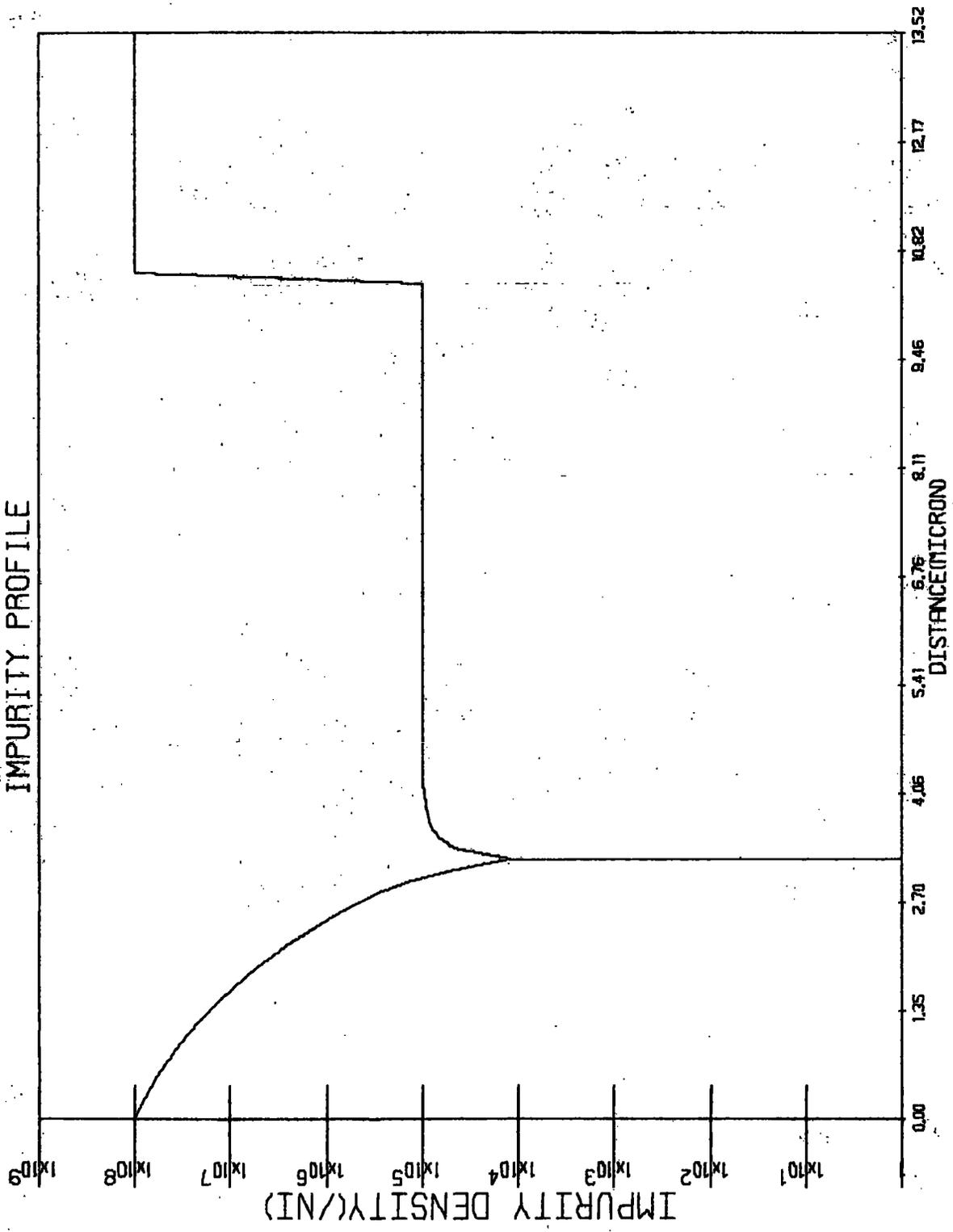
FIGURE (4.2)

4.6.1 Internal characteristics.

4.6.1.1 Forward bias conditions.

The solutions which describe the complete internal characteristics of the diode under various forward bias conditions are shown in Fig. 4.3 to Fig. 4.9 . The space-charge density plotted in Fig. 4.4 shows the failure of the depletion approximation even at moderate injection levels, which supports the Cornu approximation. However, the condition of quasi-equilibrium is seen to be valid for any level, i.e, the electron and hole quasi-Fermi potentials are constant throughout the device except at the ohmic contacts where an infinite recombination velocity is assumed. Under high-level injection conditions Fig. 4.6 shows the existence of a quasi neutrality region where the electron and hole densities are equal and constant. These two conditions are the key on which the analytical model is based to establish the closed form formulae.

The absolute value of recombination rate U(x) is depicted in Fig. 4.7 . Under low-level injection conditions the recombination rate inside the space charge region is relatively higher than outside. This is due to the small amount of excess carriers.

At any bias, the recombination rate reaches its maximum value at the location in the space charge region where the electron density is equal to the hole density. This condition can be verified from the recombination generation model.

We take

$$T_{po} = T_{no} = T$$

Equation 2.18 then becomes

$$U = \frac{p.n - 1}{T(n + p + 2)}$$

Under the condition of constant quasi-Fermi potentials, we have

$$pn = k = constant$$

Thus the recombination rate is

$$U = \frac{k - 1}{T(n + p + 2)}$$

For a given forward bias V, maximum U is obtained when (n+p) is a minimum, i.e,

$$d(p+n) = 0$$

or

$$dp = -dn$$

Since

$$pn = constant$$

by differentiating with respect to p, we have

$$-pdn = ndp$$

$$-dn = \frac{n}{p} dp$$

The minimum condition is therefore satisfied, if

$$dp = -dn = \frac{n}{p} dp$$

or

$$n = p$$

At higher injection levels, injected minority carriers diffuse into the neutral region and are recombined . Therefore the recombination rate outside the space charge region becomes significant.

Under very high injection conditions, where the quasi-neutrality region exists, the recombination rate has a constant maximum value throughout the region. If we take $p = n = n_o$, i.e,

$$p \, n = k = n_o \gg 1$$

we obtain,

$$U_{max} = \frac{n_o^2}{2Tn_o}$$

$$= \frac{n_o}{2T}$$

Fig. 4.8 illustrates the ratio of electron and hole currents to the total current. At very low injection levels, the current in the space charge region is mainly due to recombination. The currents outside the region are obviously due to majority carriers flowing from the contacts to replenish the lost charges. Under higher injection conditions, minority carriers diffuse away from edge of the space charge region and are recombined in the neutral regions. This is responsible for the minority carrier currents in both sides of the device. These minority currents are significantly increased as the injection level becomes very high.

Finally, the forward current can be summarized as shown in Fig. 4.9 . Under low level injection, the injected

minority carrier in both regions is still very low, therefore the space charge recombination current dominates. The gradient plotted on a $\log_e$ scale is seen to be approximatly $0.6(q/kT)$. For medium and high level injection, the injected minority carrier density become comparable with, and then greater than, the doping density respectively. The recombination currents outside the space charge region therefore become dominant and the recombination current inside the space charge region may be neglected. The resulting gradient in this range is approximately $0.9(q/kT)$. At still higher injection levels, the effect of voltage drop in the bulk regions caused by the current flow becomes important and the current increases more slowly with increasing bias. It is seen that the solution shows agreement with the idealized analytical approximation for an abrupt junction diode when the recombination current in the space charge region is included. (see for example, A.T.Sah, et, al <42>)
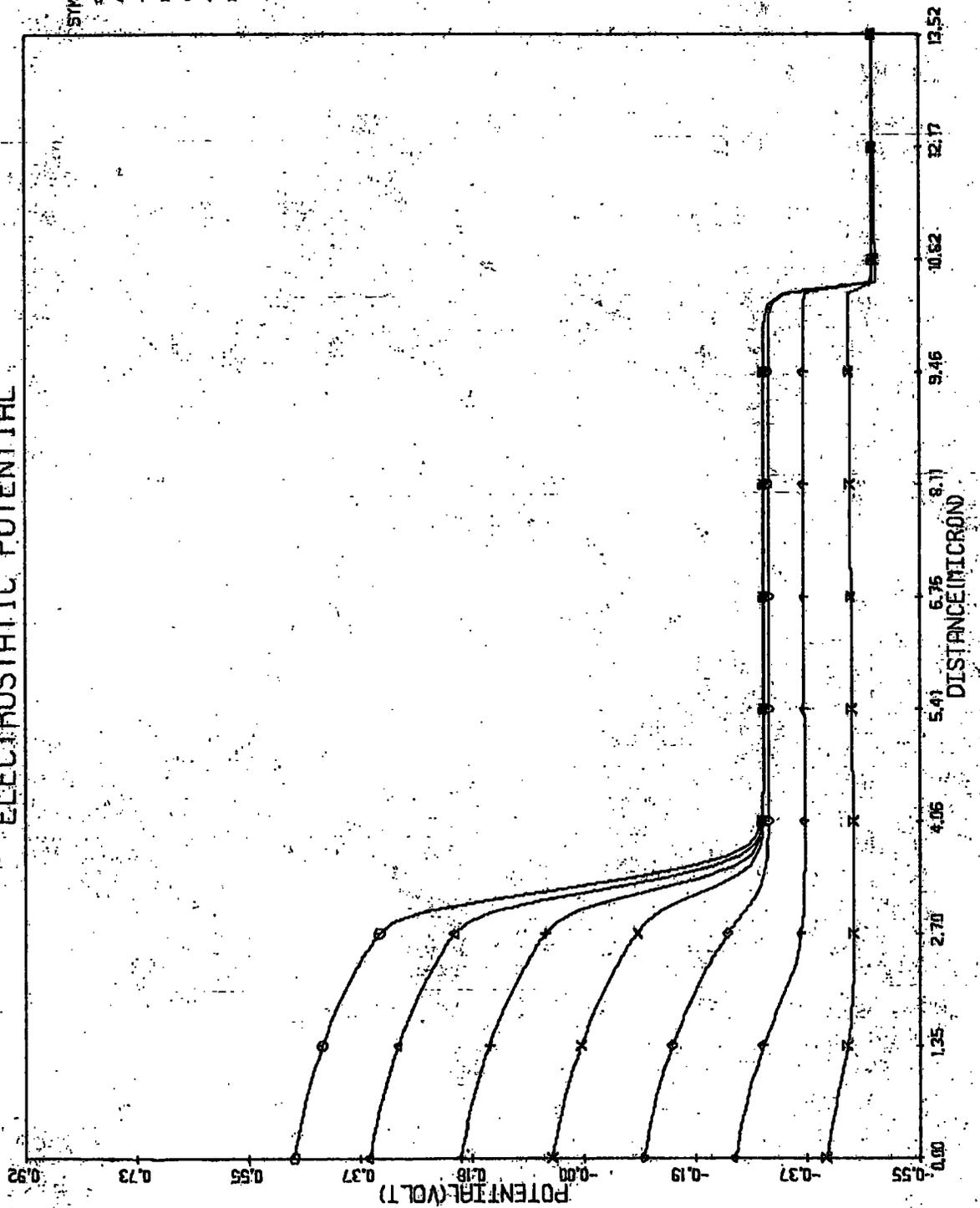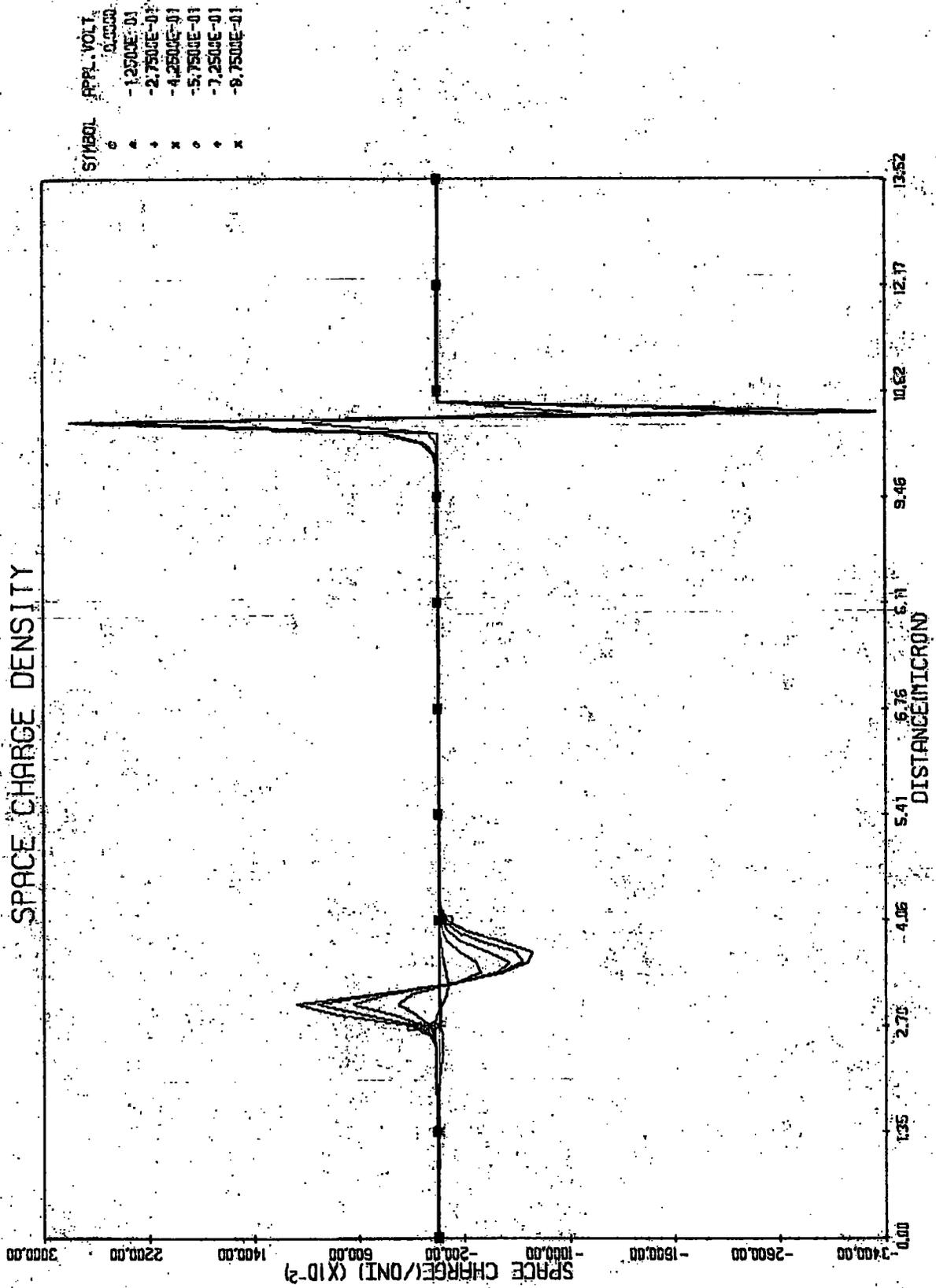
FIGURE (4.3)

SPACE CHARGE DENSITY
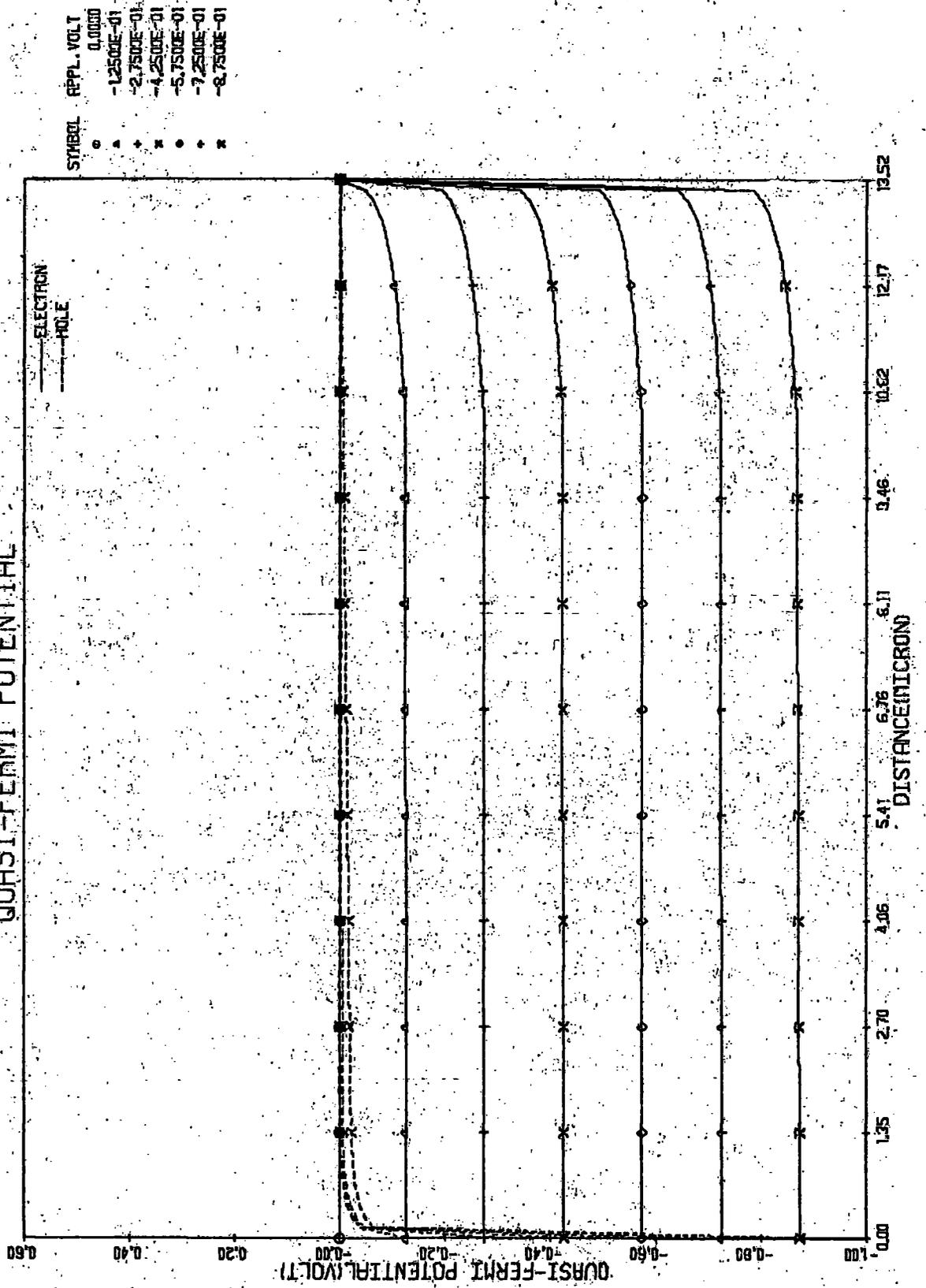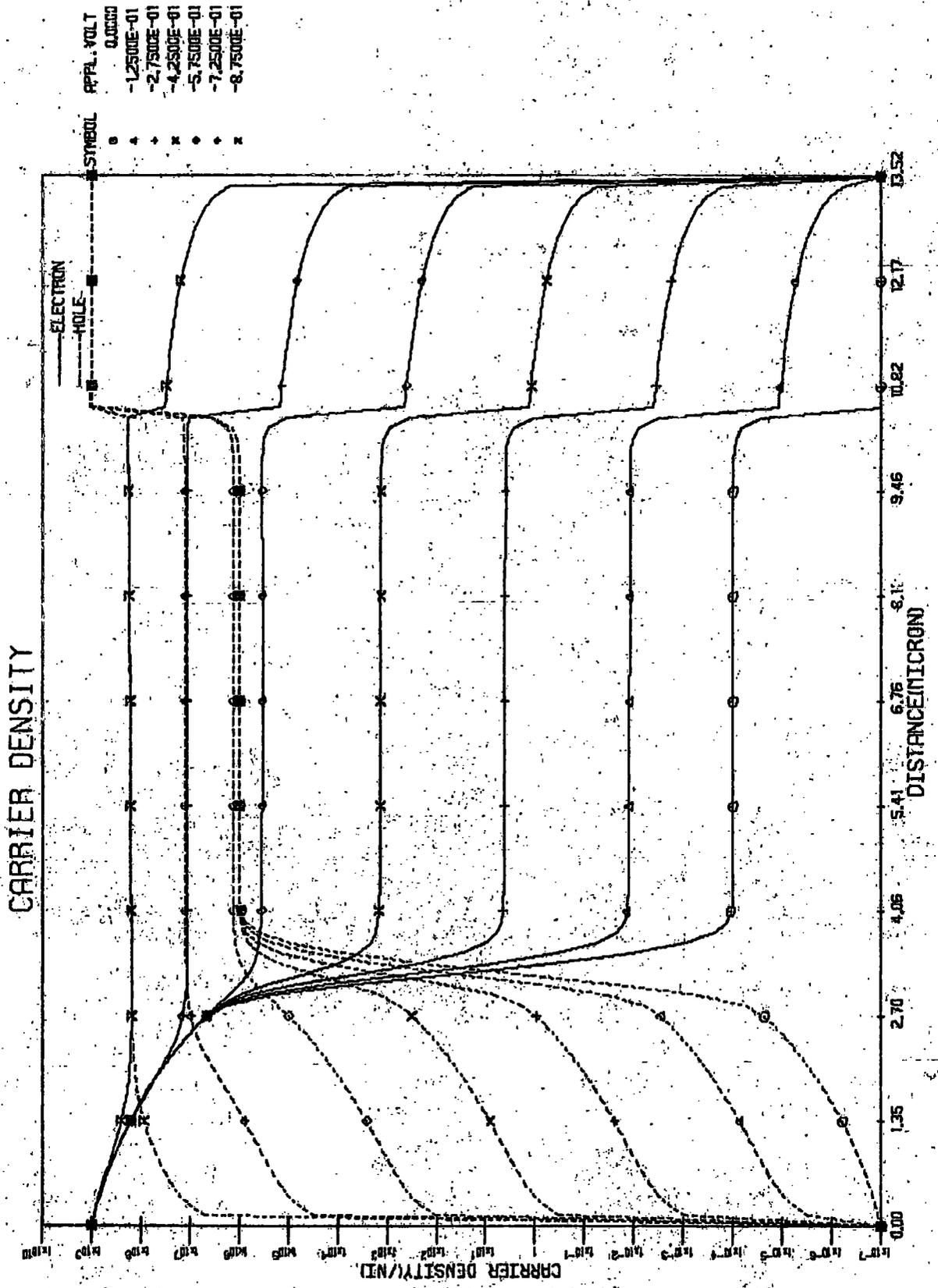
FIGURE (4.4)
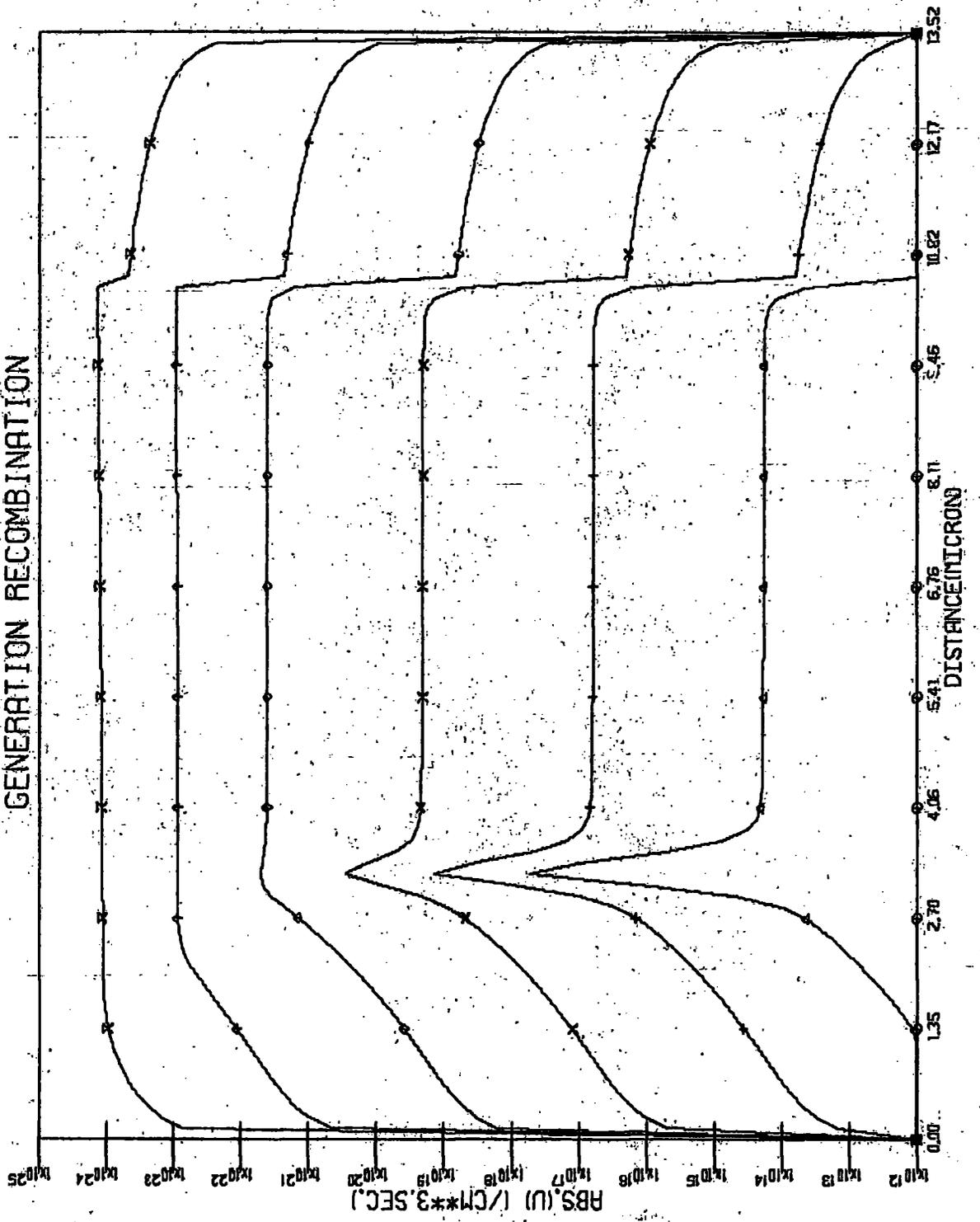
FIGURE (4.5)

FIGURE (4.6)

FIGURE (4.7).

CURRENT DENSITY

FIGURE (4.8)

FIGURE (4.9)

4.6.1.2 Reverse bias conditions.

Contrary to the result obtained for the forward bias condition, Fig. 4.12 shows that the quasi Fermi potentials are no longer constant throughout the device. Instead, they follow the electrostatic potential as equations 4.6, 4.7 implies. Under reverse bias, the electrostatic potential increases with the applied voltage and suppresses the diffusion currents, but the existence of the electric field in the space charge region enables the drift currents to flow. Just as the forward current can be described by the recombination process throughout the device, the reverse current can be accounted for by the generation process. The minority carriers generated near either side of the space charge layer diffuse to the edge of the region where they are swept to the other side of the junction by the strong field. Also carrier generation can take place within the space charge region itself, mainly through the emission process from the traps, and the carriers are swept out of the region before recombination can occur. The first of these processes results in the current flows as depicted in Fig. 4.15 . The effect of the generation current in the space charge region is shown in Fig. 4.16 where the reverse current increases continuously, rather than remaining constant as is the case when the generation current is omitted.

It should also be noted from Fig. 4.13 that the Boltzmann relation is not valid, even for low reverse bias.

FIGURE (4.10)

FIGURE (4.11)

FIGURE (4.12)

FIGURE (4.13)
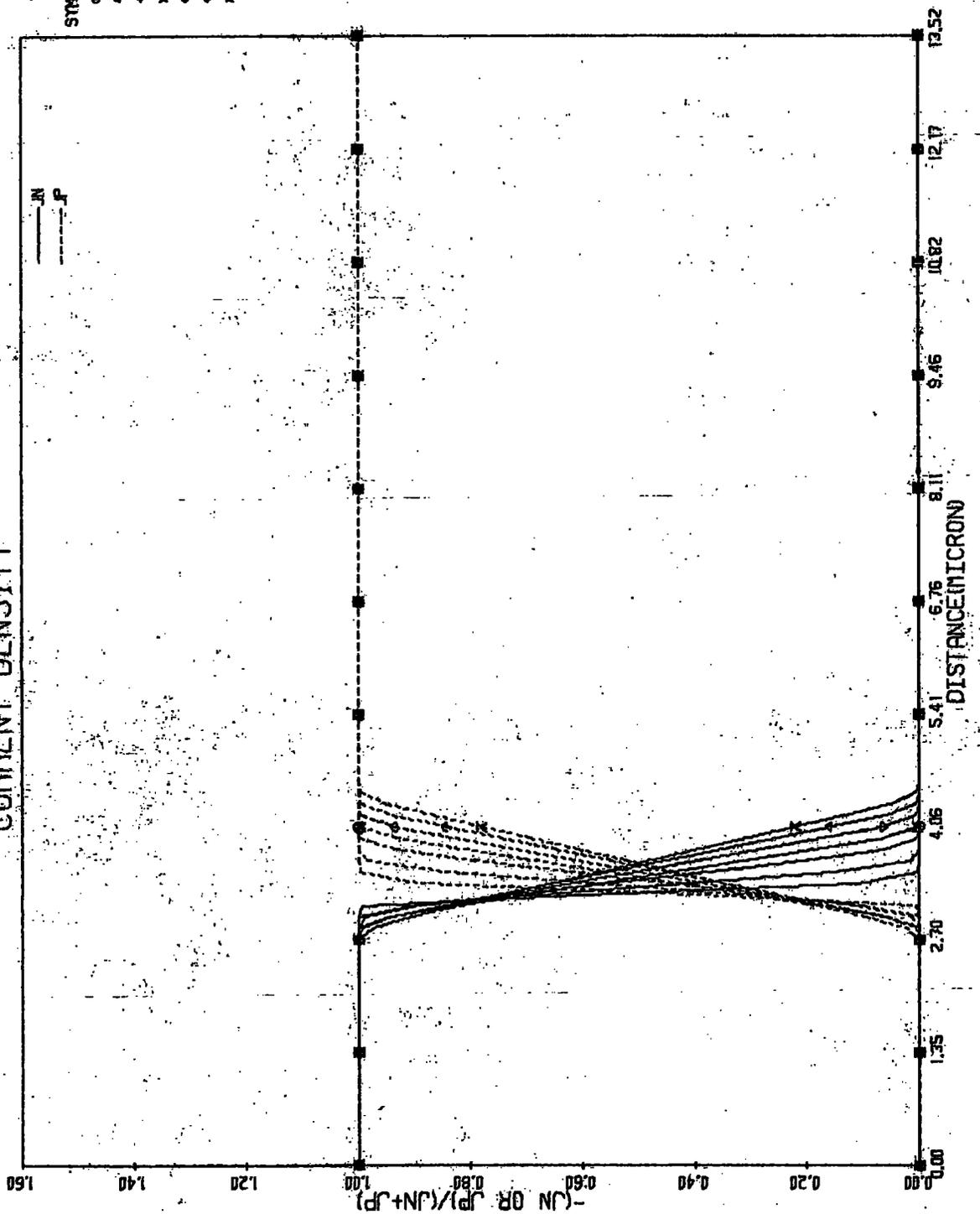
FIGURE (4.14)
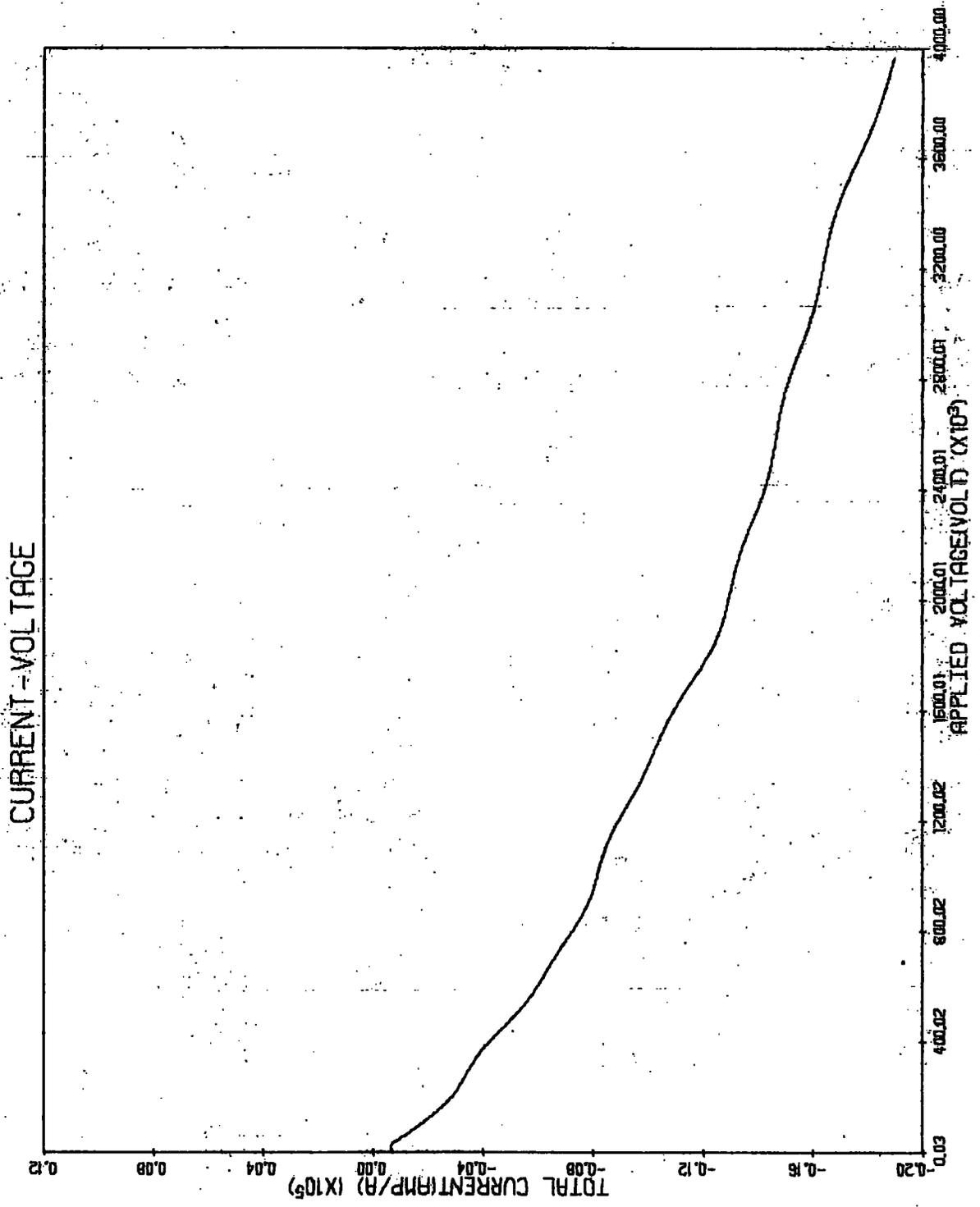
FIGURE (4.15)

FIGURE (4.16)

4.6.2 Terminal characteristics.

The diode profile in Fig. 4.17 is used to investigate the terminal characteristics so that the results can be compared with the dynamic behaviours obtained later in chapter 5.

4.6.2.1 Effect of carrier lifetime on forward characteristics.

The carrier lifetime has a direct influence on the generation recombination rate $U(x)$ and hence on the current flowing through the device, and the voltage drop in the bulk regions. It is therefore a valuable parameter to investigate. In this section we shall consider its effect on the forward current in different diodes.

a) Diodes with the same width.

Fig. 4.18 shows the effect of carriers lifetimes having values from 10 microseconds to 10 nanoseconds on the forward currents of diodes whose widths are fixed at 10 microns. A decrease of carrier lifetime corresponds to an increase in the recombination rate $U(x)$ which results in increasing current. Under low level injection conditions, the currents are small and produce little voltage drop in the bulk regions. At moderate and high injection levels, the voltage drop in the bulk region becomes significant and hence the effective voltage across the space charge region is less than the applied voltage. The current saturates at high bias.

It should be noted that as the lifetime is increasing, there exists an optimum value beyond which there is no further increase in current. This occurs in our case when the lifetime is about 0.1 microsecond. This effect has been described as the existence of a minimum in the voltage drop across the bulk region <44>, but the results obtain in the next section b and c do not support this view.

The result shown in Fig. 4.18 can be useful when designing a high power device where high forward current is required. Rather than attempt to achieve a very long carrier lifetime in a device, there is an optimum value, beyond which any increase is unnecessary.
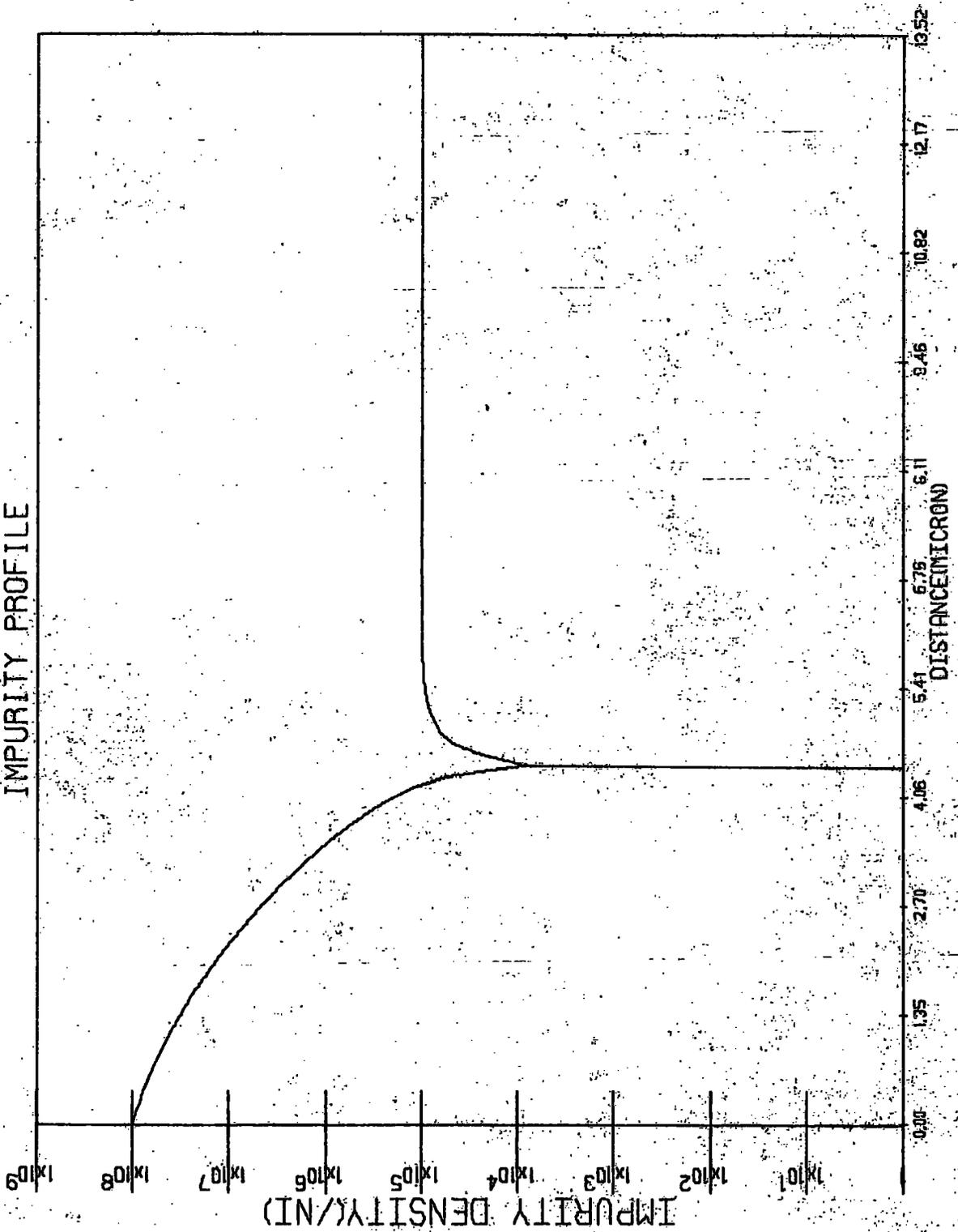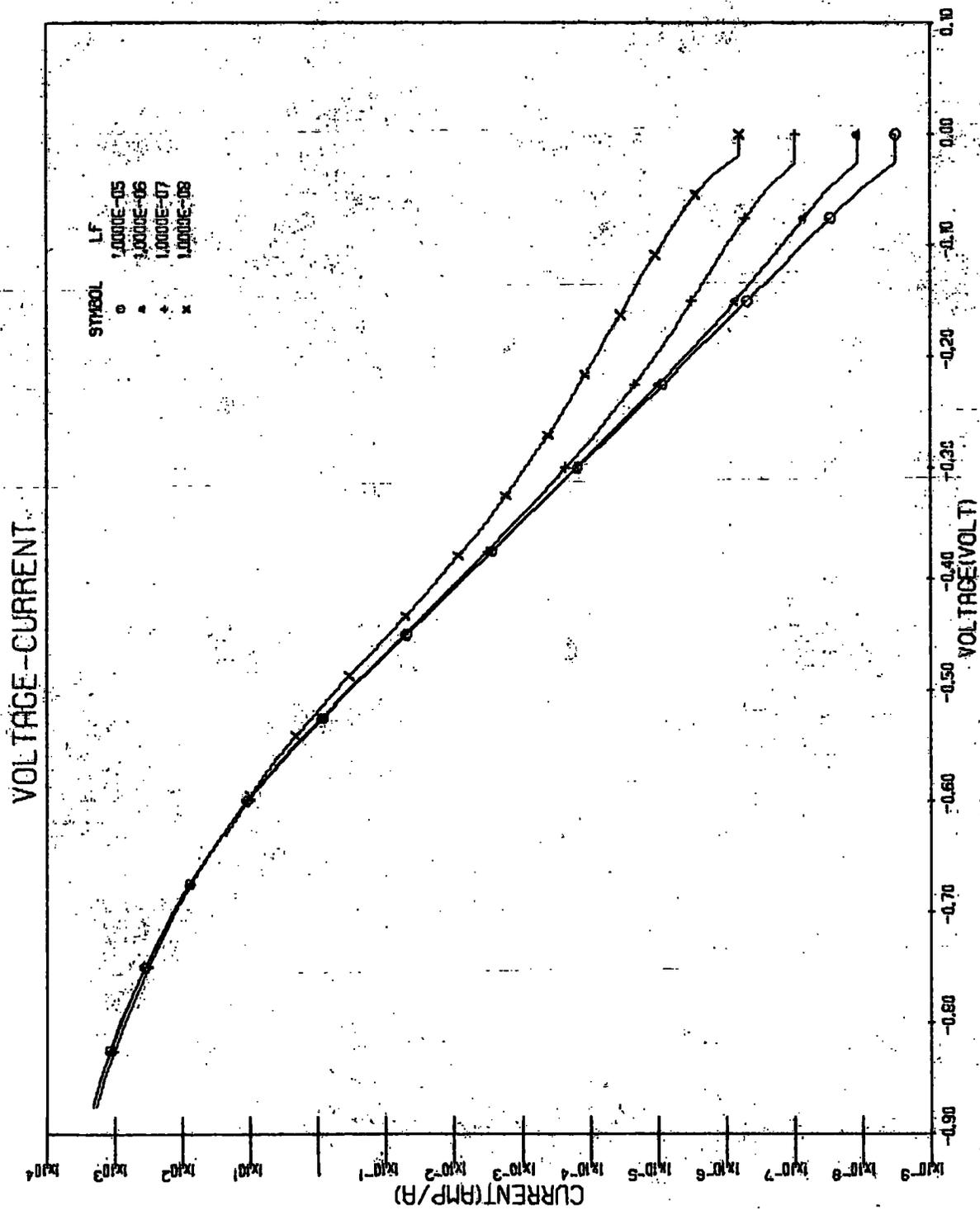
FIGURE (4.17)

FIGURE (4.18)

b) Diodes with the same ratio of W_p/L_n

The preceeding section dealt with the overall effect of the carrier lifetime on diodes of equal length, in which account is taken of differing values of voltage drop in the bulk regions. It is however also worthwhile investigating the cases where all the diodes now have the same recombination criteria i.e, the same normalized width. In this way the effect of voltage drop in the bulk regions of the diodes are neglected, and allows the direct effect of differing lifetimes to be observed. Figs. 4.19 and 4.20 illustrate the solutions for diodes with the ratio of width to diffusion length equal to 1 and 2 respectively. Under moderate and high level injection conditions, the current increases linearly as the lifetime decreases. The increase is relatively higher at low injection level.

The result obtained here however show no saturation effect like that obtained in the previous section.

This may be compared with the analytical solution for the forward current derived from an idealized abrupt p-n junction diode and neglecting the bulk resistance. <46>

$$J = \left\{ \sqrt{\frac{D_n}{T_n}} \cdot \frac{1}{N_A} + \sqrt{\frac{D_p}{T_p}} \cdot \frac{1}{N_D} \right\} qn_i^2 \left[e^{qV/(kT)} - 1 \right] - q \frac{n_i}{2} \cdot \frac{We^{qV/(2kT)}}{T_o}$$

where T_o = an effective lifetime

For medium injection levels where diffusion currents prevail, assuming that $N_D \gg N_A$, we obtain

$$J = \sqrt{\frac{D_n}{\tau_n} \cdot \frac{1}{N_A}} \, q . n_i^2 (e^{qV/(kT)} - 1)$$

The ratio of the currents for a decade decrease of the lifetime can thus be written as

$$\frac{J_2}{J_1} = \sqrt{\frac{10\tau_n}{\tau_n}} = \sqrt{10}$$

Figs. 4.21 and 4.22 show this current ratio on a log scale for the cases of W_p/L_n equal to 1 and 2 respectively. The results give good agreement with that predicted by the analytical formula described above.
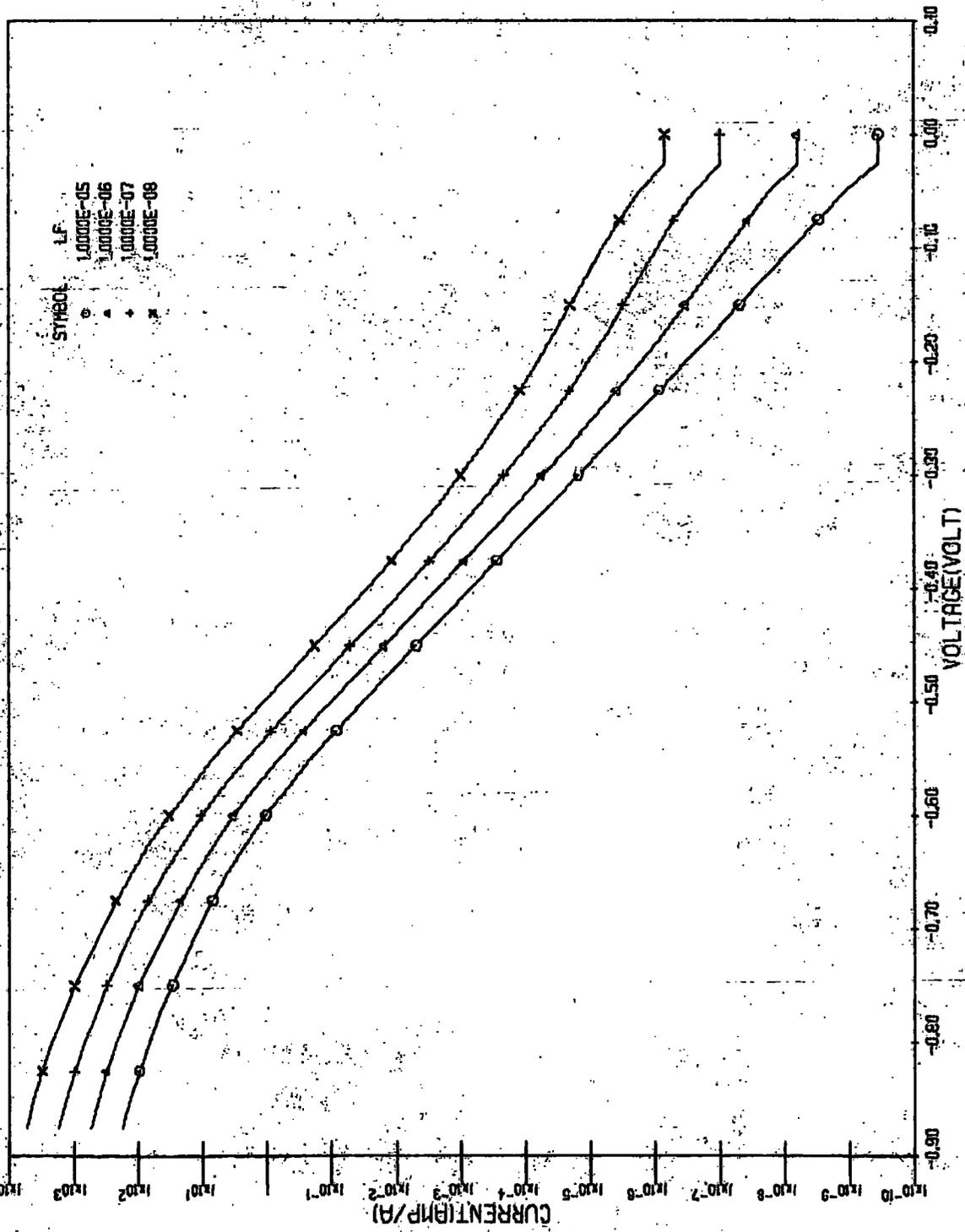
FIGURE (4.19)

VOLTAGE-CURRENT
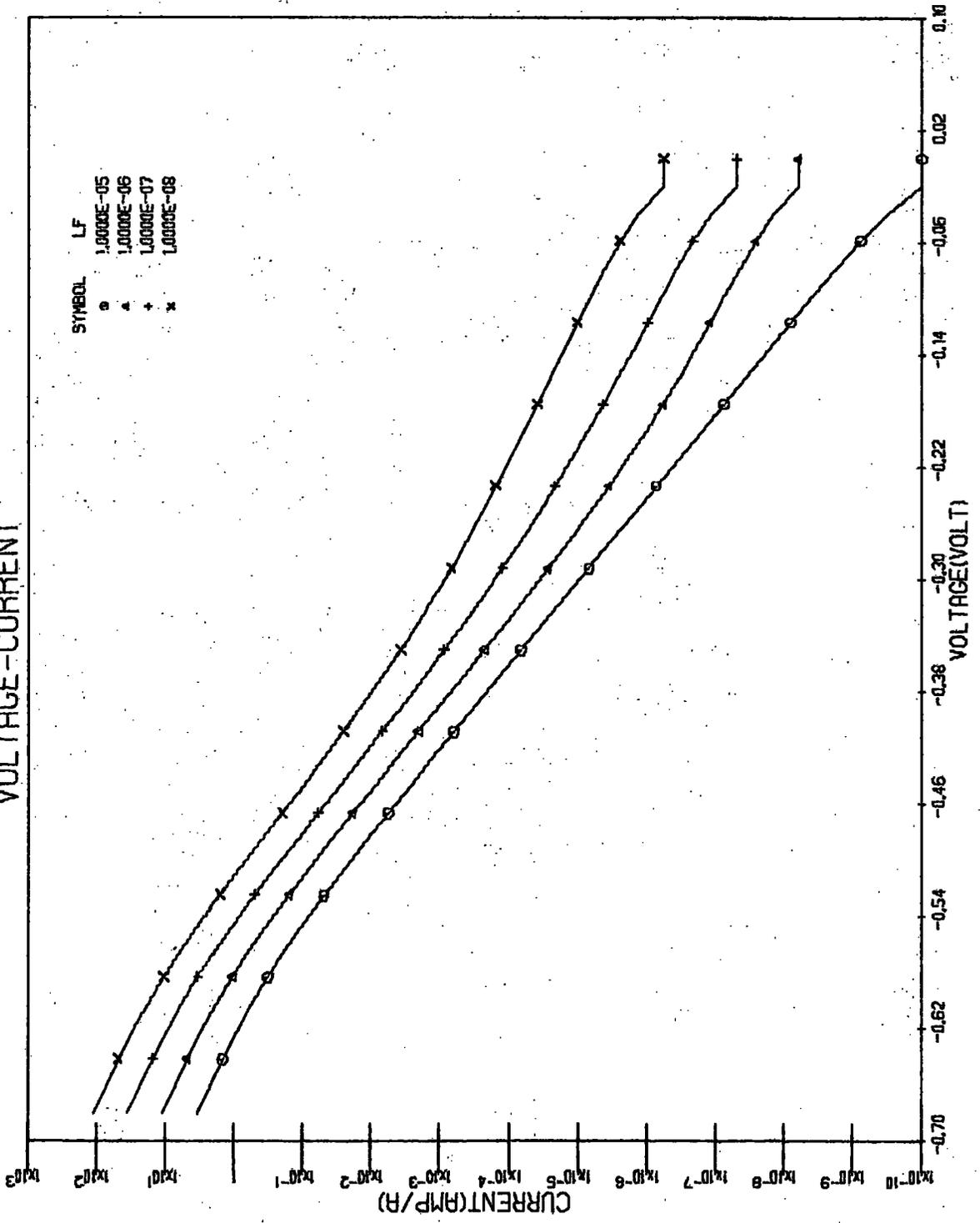
DIODES WITH THE SAME RECOMBINATION CRITERION:NP/LN=2

FIGURE (4.20)
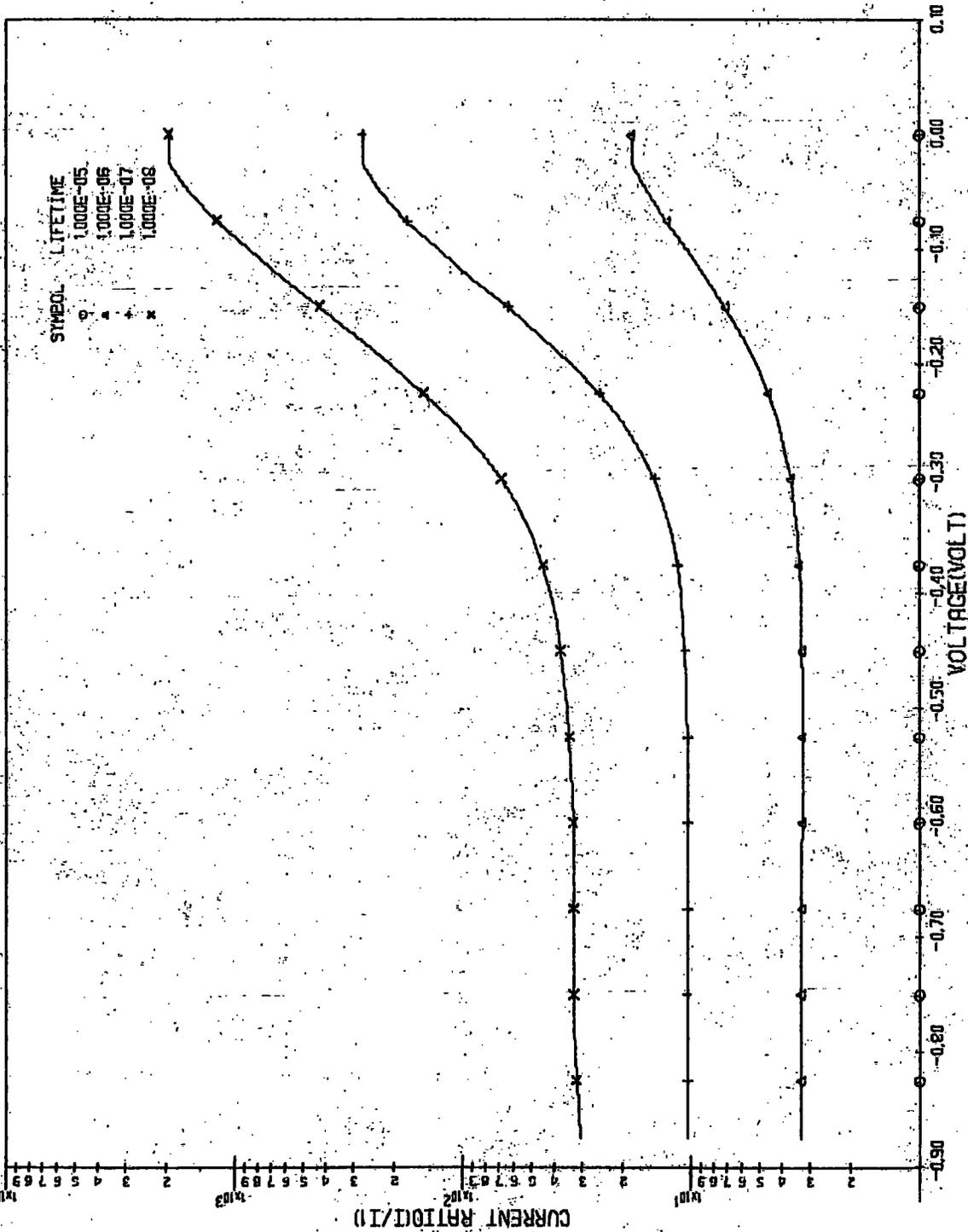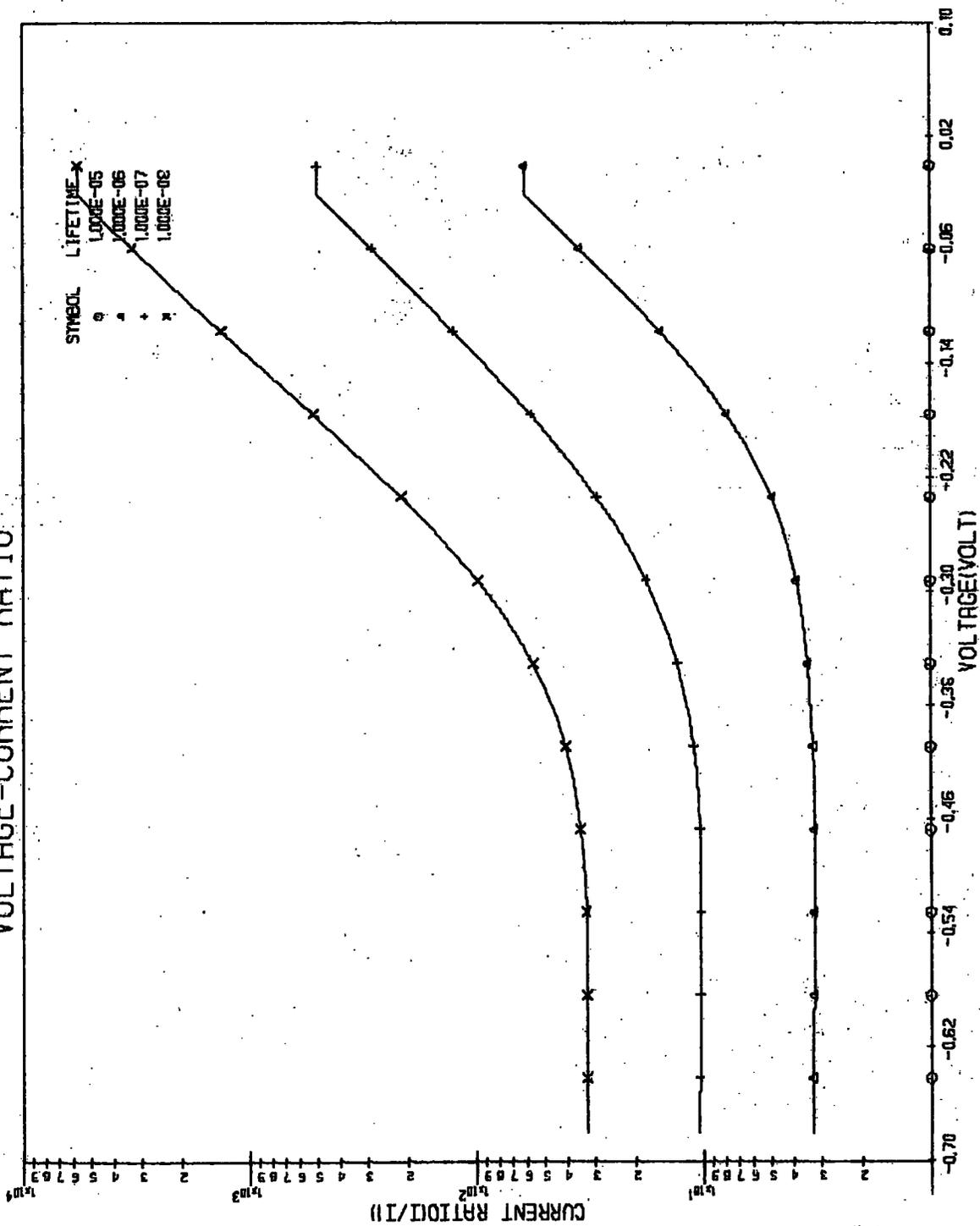
FIGURE (4.21)

FIGURE (4.22)

c) <u>Different sized diodes with a fixed lifetime.</u>

An indirect way to observe the effect of carrier lifetime is to change the width while keep the lifetime constant. Instead of varying only the width of the lightly doped region, which is equivalent to the situation in section a) if the recombination criterion in the heavily doped region is neglected, we shall now vary the overall size of diodes keeping the same proportions of the n and p regions. In order to classify the diodes, the widths are determined by the recombination criterion, i.e, in our case the ratio of p-region width to the electron diffusion length, W_p/L_n

Figs. 4.23 and 4.24 show the forward characteristics of diodes of different sizes with W_p/L_n ranging from 0.1 to 1.0 and 0.5 to 5.0 respectively, for a carrier lifetime of 1 microsecond. In contrast to the case in a) , where both n^+ and p regions are changed, the results in the lower range show no saturation in the current. This effect may also be seen from the simple relation

$$V_{app} = V_j + \int_{\text{bulk region}} (-E)\,dx$$

By using the result of an idealized diode

$$I = I_s(\exp(qV_{app}/kT) - 1)$$

we can write

$$V_{app} = (kT/q)\ln(1+I/I_s) + IR_b \qquad (4.23)$$

where

V_{app} = applied voltage

I_s = saturated current

R_b = bulk resistance

As the diode becomes smaller, voltage drop in the bulk region decreases, thus the first term of the right hand side of equation 4.29 prevails.

On the other hand, in the higher range, Fig. 4.24 show that the bulk resistance become significant, and therefore the situation tend to be the same as in the case a).

Also Figs. 4.25 and 4.26 where the normalized current voltage relations are shown, indicate the nonlinearity of the bulk resistances. The currents are normalized by dividing the currents by the value for W_p/L_n equal to 1.

FIGURE (4.23)
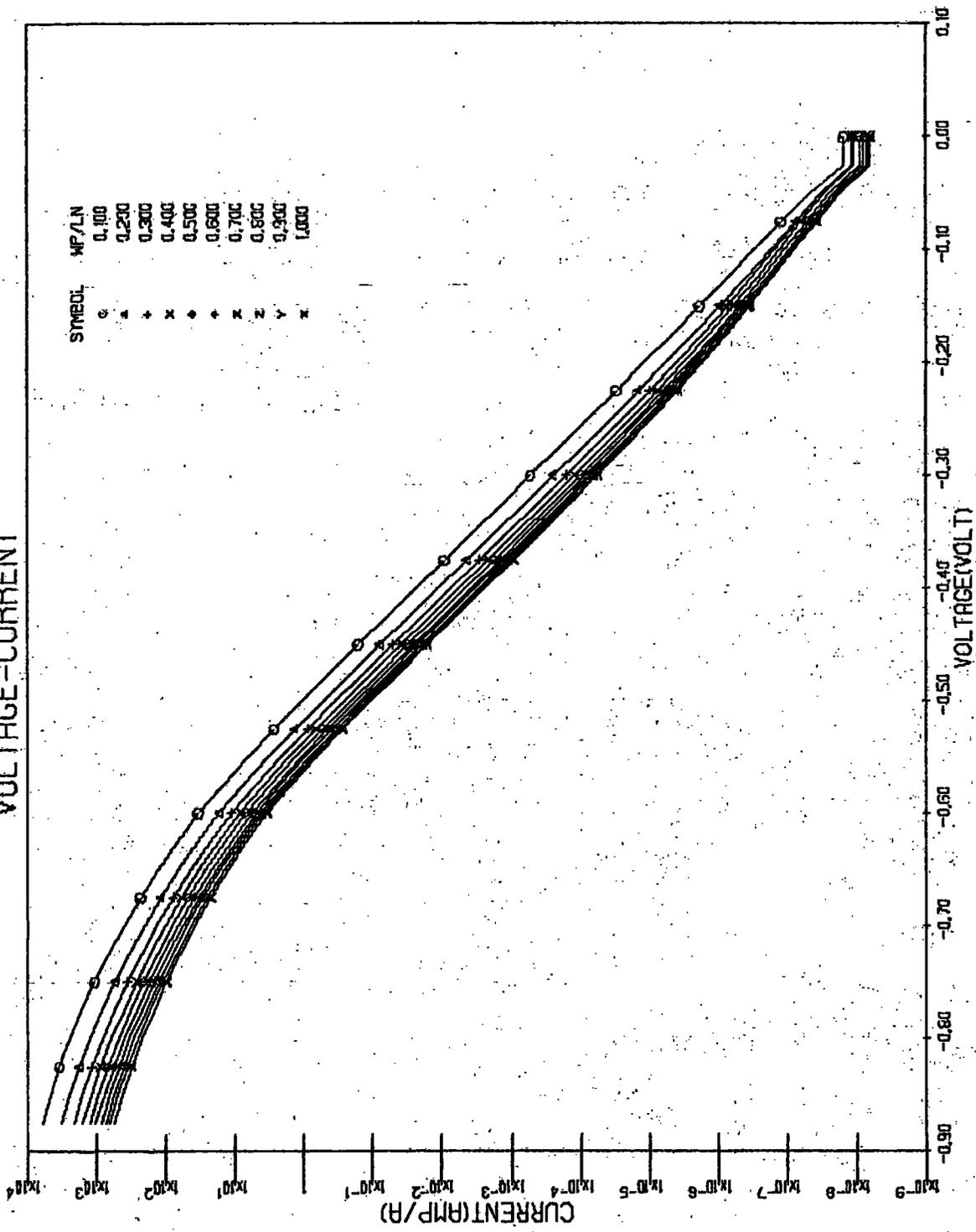
VOLTAGE-CURRENT
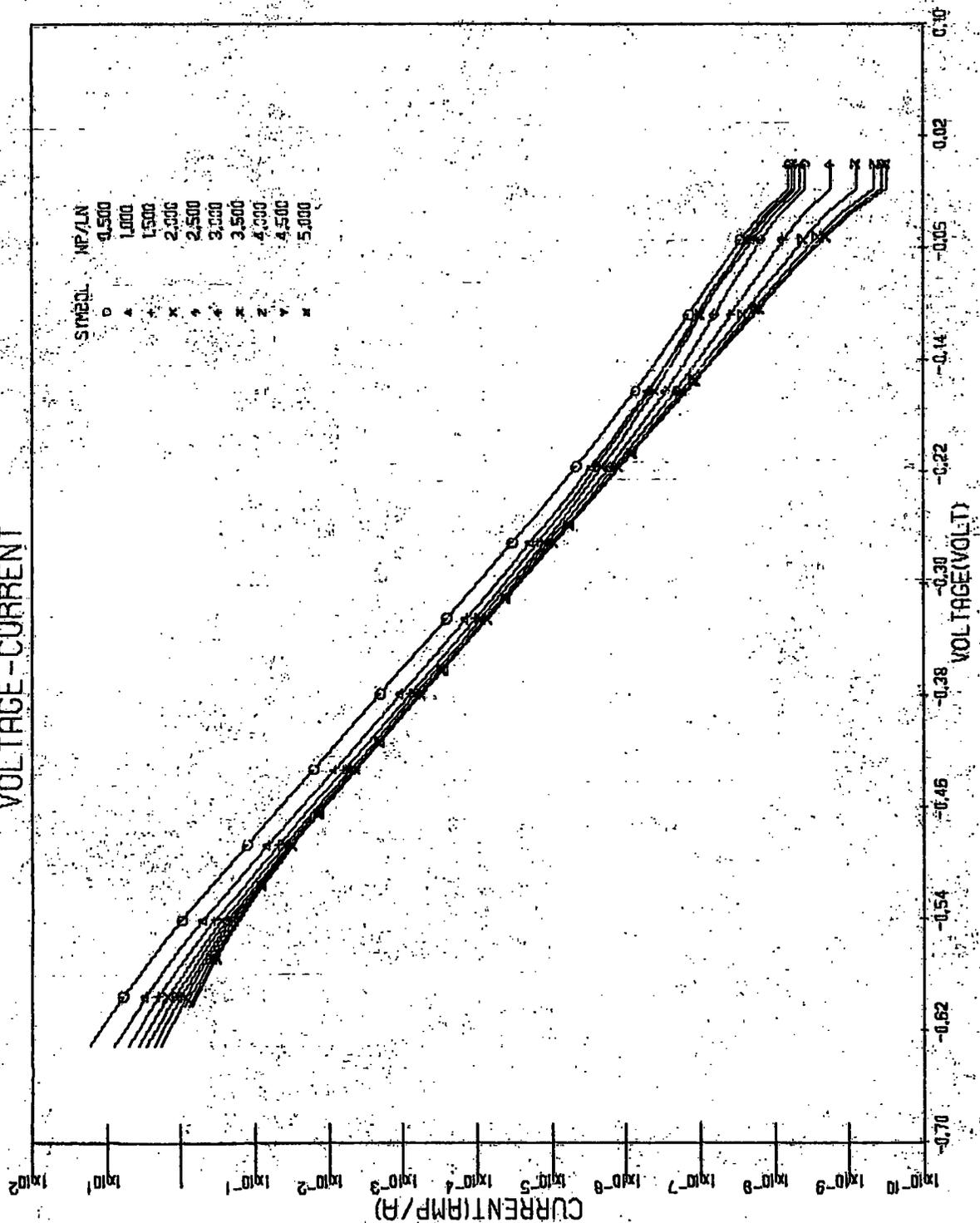
DIODES WITH THE SAME LIFETIME, LF=1E-6

FIGURE (4.24)

VOLTAGE-CURRENT RATIO
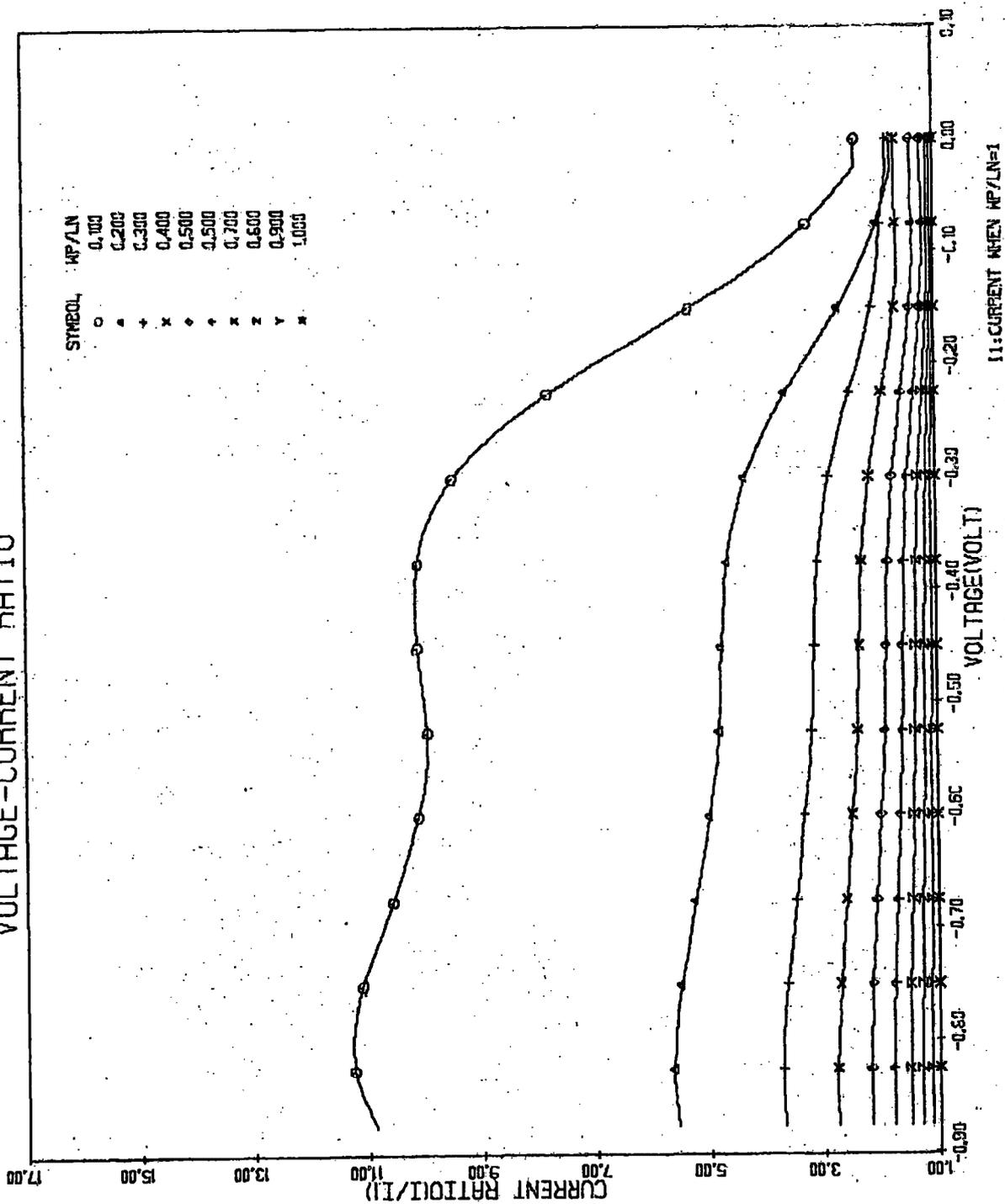
FIGURE (4.25)

VOLTAGE-CURRENT RATIO
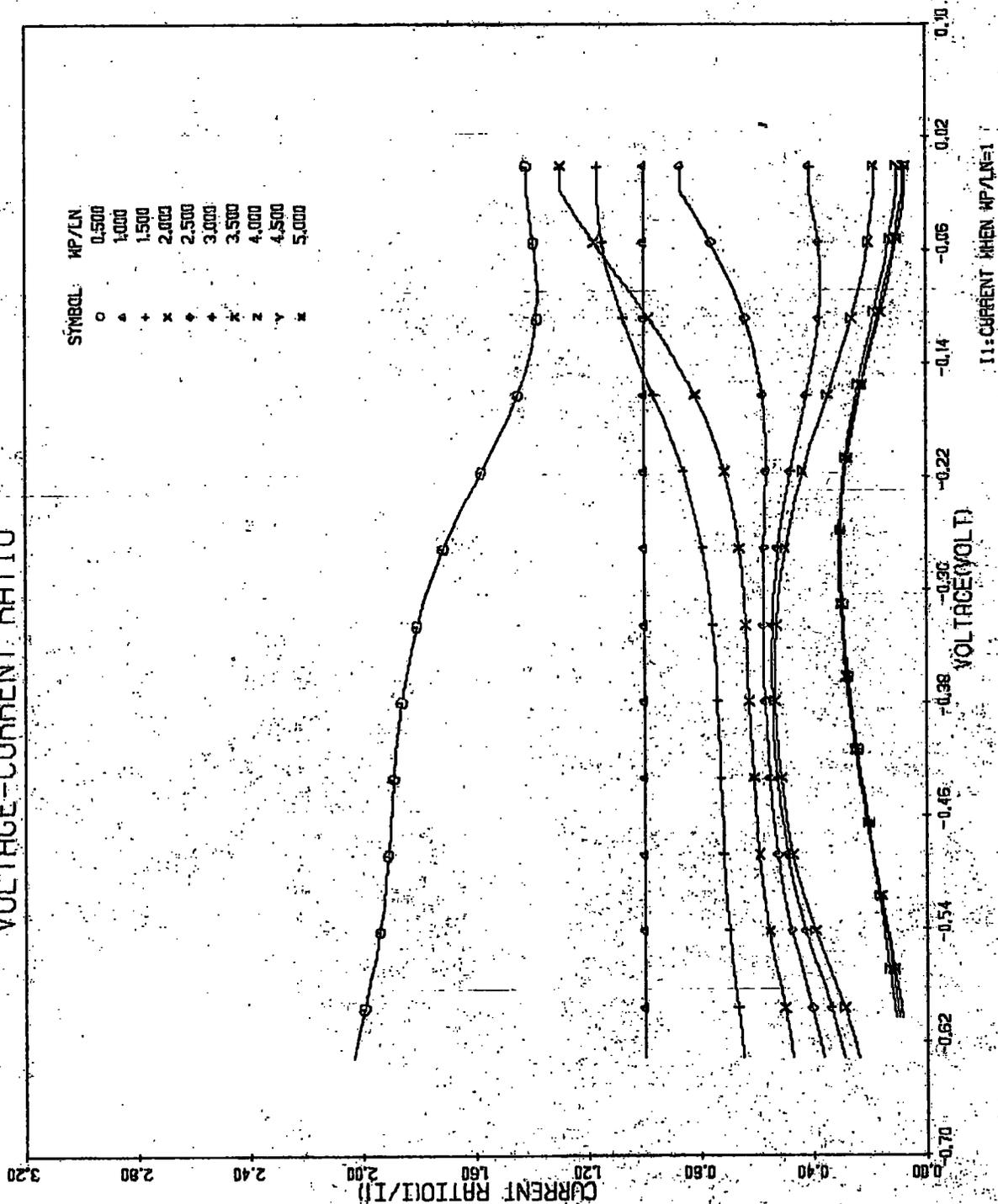
FIGURE (4.26)

4.7 Computational methods for resistor diode circuits.

After having dealt with the physical aspects of p-n junction diodes, we shall complete the modelling by the analysis of a circuit containing the device represented by its static characteristics. This could be done either by employing the optimization technique <22> to fit the results to the circuit model selected and then employing standard circuit analysis, or by solving the equation directly with information obtained from the physical model. Since the latter case requires less extra effort, we will follow this line in the analysis.

Consider the simple diode circuit of Fig. 4.27 operating under large signal condition, where the nonlinear Characteristics of the diode may be represented by

$$i_d = f(v_s) \tag{4.24}$$

and the diode equation is found as

$$i_d - (v_s - v_d)/R = 0 \tag{4.25}$$
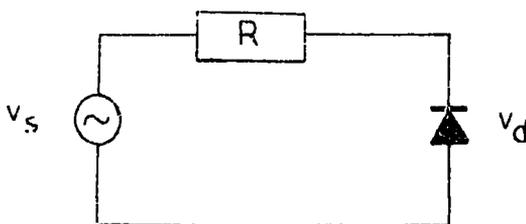
Figure 4.27 A R-D circuit.

Equation 4.25 is a transcendental equation which can only be solved by a successive approximation method. The most widely used method is the Newton Raphson iterative scheme. The nonlinearity can be linearized by expanding

i_d in a truncated Taylor's series about $i_d^{(o)}$,
viz

$$i_d = i_d^{(o)} + \left.\frac{\partial i_d}{\partial v_d}\right|_{v_d^{(o)}} \cdot (v_d - v_d^{(o)})$$

(4 26)

where the subscript o refers to the initial value of current and voltage.

Let, the correction term, after the first iteration
$$\Delta v_d^{(1)} = v_d - v_d^{(o)} \quad,$$

and

$$s = \left.\frac{\partial i_d}{\partial v_d}\right|_{v_d^{(o)}}$$

Equation 4.25 becomes

$$v_d^{(o)} + s \Delta v_d^{(1)} - (v_s - (v_d^{(o)} + \Delta v_d^{(1)}))/R = 0$$

$$\Delta v_d^{(1)} = -(i_d^{(o)} \cdot R + v_d^{(o)} - v_s)/(1+Rs)$$

or, in the general form

$$\Delta v_d^{(k+1)} = -(i_d^{(k)} \cdot R + v_d^{(k)} - v_s)/(1+Rs)$$

(4.27)

Since, the current voltage characteristics obtained from the physical model are in discrete form, which may not coincide with the values required in the iteration, an interpolation scheme is inevitable in evaluating equation 4.27. The first derivative of i_d at each

interpolated points is also required, hence the cubic spline interpolation seems to be an optimum scheme in our case. The details of the cubic spline interpolation used here are given in Appendix B,

The iterative algorithm can be summarized as follows :

1 Estimate an initial value of $v_d^{(o)}$

2 Use the cubic spline interpolation to find i_d and s

3 Calculate Δv_d from equation 4.27, and obtain the better approximation

4 Repeat from step 2 until the absolute value of Δv_d has converged to the accepted accuracy.

The low frequency sinusoidal responses of the circuit of Fig. 4.27 are illustrated in Figs. 4.28 to 4.29 . The forward and reverse i-v characteristics provided for the iteration procedure are obtained from modelling a diode having the profile of Fig. 4.17 . The result show the half-wave rectifying effect which would be expected.
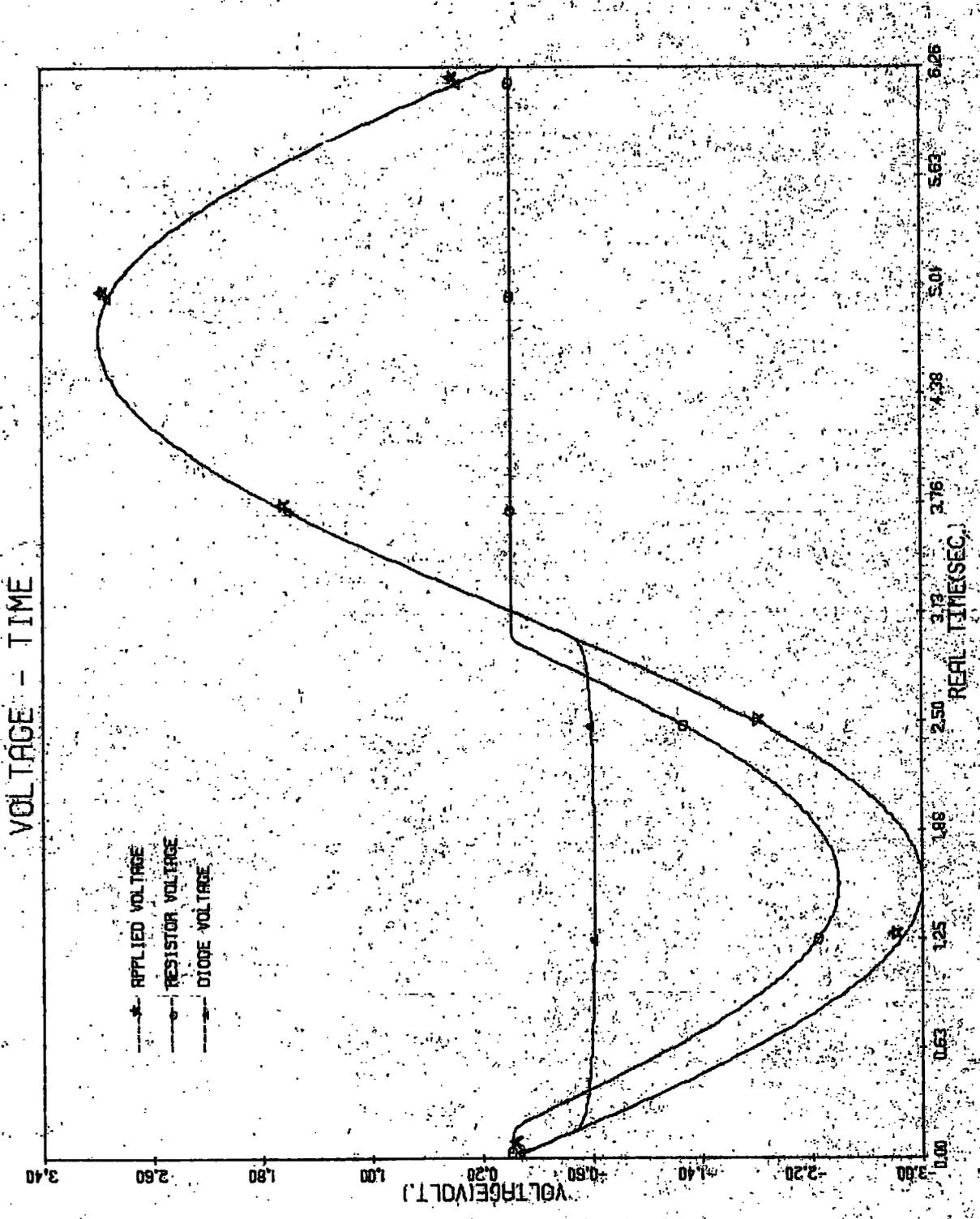
FIGURE (4.28)

CURRENT DENSITY - TIME
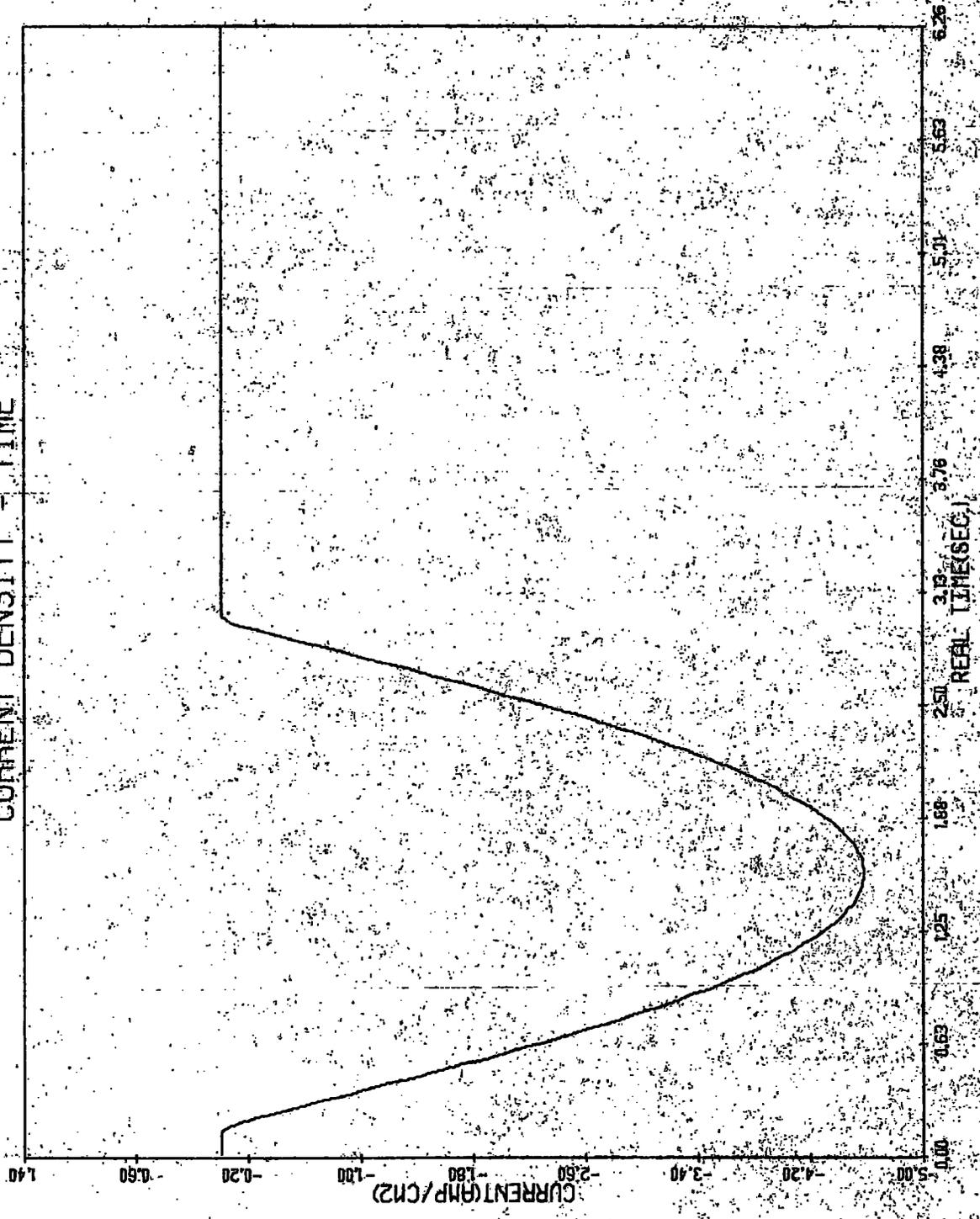
FIGURE (4.29)

The accuracy of the solution may be improved by employing a property of the cubic spline interpolation which also provides the second derivative of a function at each interpolating point. This allows the second order term of the Taylor's series to be included in equation 4.26 , and the algorithm can then proceed in the same manner as above.

Chapter 5.

Time-Dependent Modelling of Junction Devices.

The study of the time-dependent or dynamic behaviour of p-n junction diodes has been the subject of intensive interest due to their widespread applicaton in switching, processing of a-c signals, harmonic analysis, etc. It is well known that the behaviour of a practical diode differs from that predicted from its static characteristic. The only distinction between the static and dynamic operating conditions is the treatment of the time partial derivatives in the system equations, (see chapter 3), which implies the following.

a) The existence of displacement current in the space charge region due to the variation of the field with time.

b) The current densities are not just associated with the recombination or generation of the carriers but also depend on changes in the carrier densities.

The development of an analytical model to represent the dynamic behaviour is somewhat analogous to that of the static case except that some further assumptions and approximations must be made. The devices which can be modelled are then limited to some special ideal cases. On the other hand, a numerical model can be developed by using the algorithm discussed in chapter 3 and developed in chapter 4. However, some modification of the algorithm may be required to ensure convergence and stability.

5.1 Formulation of the system equations.

Since the problem involves time derivatives, the relevant system equations can be chosen from the mathematical model given in chapter 2 as a set of simultaneous nonlinear partial differential equations. These can be rewritten in their normalized forms as follows.

$$\frac{\partial p(x,t)}{\partial t} = -U_p(x,t) - \frac{\partial J_p(x,t)}{\partial x} \tag{5.1}$$

$$\frac{\partial n(x,t)}{\partial t} = -U_n(x,t) + \frac{\partial J_n(x,t)}{\partial x} \tag{5.2}$$

$$\frac{\partial E(x,t)}{\partial t} = J_T(t) - J_p(x,t) - J_n(x,t) \tag{5.3}$$

Where

$$J_p(x,t) = \mu_p(x,t)\left[p(x,t)E(x,t) - \frac{\partial p(x,t)}{\partial x}\right] \tag{5.4}$$

$$J_n(x,t) = \mu_n(x,t)\left[n(x,t)E(x,t) + \frac{\partial n(x,t)}{\partial x}\right] \tag{5.5}$$

The main task here is to solve these equations for the dependent variables. The algorithm discussed in chapter 3 suggests that the equations must be transformed into a set of linear algebraic equations, so that any sucessive approximation method can be applied to obtain the solutions. The transformation can be done by discretization and linearization of the equations respectively.

5.2 Discretization

a) Spatial discretization.

A direct method of discretizing the system equations spatially is to apply the standard difference approximations for the derivative terms in the current density equations 5.4 and 5.5, and substitute these results in equations 5.1 and 5.2 respectively. A numerical instability problem exists as encountered in the dc-steady state case, and so the analytical modification of De Mari's scheme is required. It has been suggested <16> that two set of mesh points should be employed which may ease the stability problem. A set (1,....,i-1,i, i+1,....N) is used to represent meshpoints for p, n, N and V. The other set (1,...,l-1,l,l+1,...N), located midway between the mesh points of the first set, is used to define E, J_p, J_n, J_T and J_D. The discrete domain is depicted in Fig. 5.1 . (Together with the time grid).

Using the same procedure as in chapter 4, but with an integrating factor $\exp(-\int E(x)\,dx)$, we can readily write equation 5.4 for a small interval between a and b as

$$J_p(x,t) = -\mu_p(x,t)\,E(x,t)\left[\frac{\rho(a,t)}{e^{V(b,t)-V(a,t)}-1} + \frac{\rho(b,t)}{e^{-V(b,t)-V(a,t)}-1}\right]$$

At time $j(t_j)$ if a and b correspond to the mesh points i and i+1 respectively and l is located in between, we have

$$E_{lj} = -\frac{V_{i+1,j} - V_{ij}}{h_i}$$
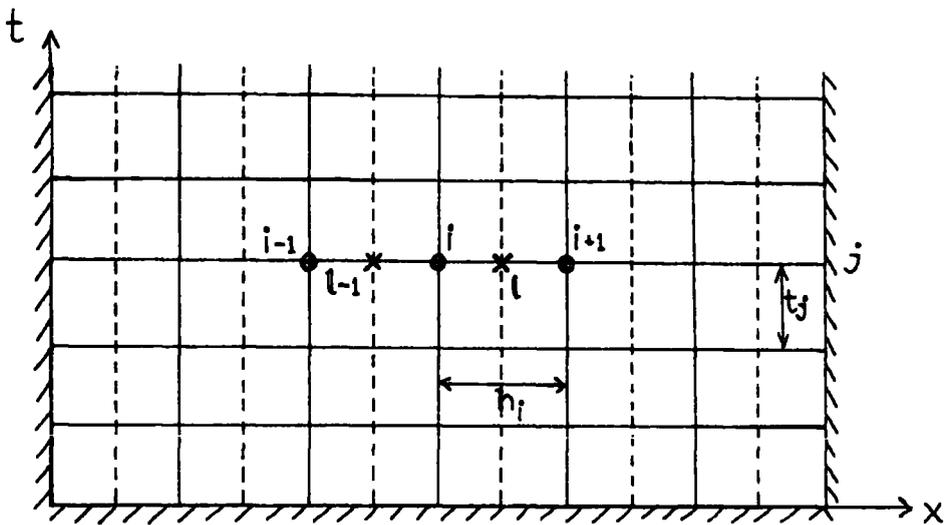
Fig. 5.1 Discrete domain to approximate the system equations.

And the discretized form of equation 5.7 becomes

$$J_{p_{lj}} = -\mu_{p_{lj}} \cdot E_{lj} \left[\frac{p_{ij}}{e^{-E_{lj}h_i} - 1} + \frac{p_{i+1,j}}{e^{E_{lj}h_i} - 1} \right] \qquad (5.8)$$

Similarly, solving 5.5 with an integrating factor $\exp(\int E(x).dx)$ we obtain

$$J_{n_{lj}} = -\mu_{n_{lj}} \cdot E_{lj} \left[\frac{n_{ij}}{e^{E_{lj}h_i} - 1} + \frac{n_{i+1,j}}{e^{-E_{lj}h_i} - 1} \right] \qquad (5.9)$$

We can then apply the difference approximation to the spatial derivative of the current densities in equations 5.1 and 5.2, with the values from equations 5.8 and 5.9 respectively. At time $j(t_j)$ and mesh points i and 1, we finally obtain

$$\frac{\partial p_{ij}}{\partial t} = -U_{p_{ij}} -\frac{1}{h_i} \left\{ -\mu_{p_{1j}} \cdot E_{1j} \left[\frac{p_{ij}}{e^{-E_{1j}h_i} - 1} + \frac{p_{i+1,j}}{e^{E_{1j}h_i} - 1} \right] \right.$$

$$\left. +\mu_{p_{1-1,j}} \cdot E_{1-1,j} \left[\frac{p_{i-1,j}}{e^{-E_{1-1,j}h_i} - 1} + \frac{p_{ij}}{e^{E_{1-1,j}h_i} - 1} \right] \right\} \quad (5\ 10)$$

Similarly we can write

$$\frac{\partial n_{ij}}{\partial t} = -U_{n_{ij}} -\frac{1}{h_i} \left\{ -\mu_{n_{1j}} \cdot E_{1j} \left[\frac{n_{ij}}{e^{E_{1j}h_i} - 1} + \frac{n_{i+1,j}}{e^{-E_{1j}h_i} - 1} \right] \right.$$

$$\left. +u_{n_{1-1\ j}} E_{1-1,j} \left[\frac{n_{i-1,j}}{e^{E_{1-1,j}h_i} - 1} + \frac{n_{ij}}{e^{-E_{1-1,j}h_i} - 1} \right] \right\} \quad (5\ 11)$$

and

$$\frac{\partial E_{1j}}{\partial t} = J_{T_j} \mu_{p_{1j}} \cdot E_{1j} \left[\frac{p_{ij}}{e^{-E_{1j}h_i} - 1} + \frac{p_{i+1,j}}{e^{E_{1j}h_i} - 1} \right]$$

$$+\mu_{n_{1j}} \cdot E_{1j} \left[\frac{n_{ij}}{e^{-E_{1j}h_i} - 1} + \frac{n_{i+1,j}}{e^{E_{1j}h_i} - 1} \right] \quad (5.12)$$

or in the form of functional equations <43>

$$\frac{\partial p_{ij}}{\partial t} = f_p \left[p_{ij}, p_{i-1,j}, p_{i+1,j}, n_{ij}, E_{1j}, E_{1-1,j} \right] \quad (5.13)$$

$$\frac{\partial n}{\partial t}_{ij} = f_n\left[P_{ij}, n_{ij}, n_{i-1,j}, n_{i+1,j}, E_{1j}, E_{1-1,j}\right]$$

(5.14)

$$\frac{\partial E}{\partial t}_{ij} = f_E\left[E_{1j}, \ldots, E_{1j}, \ldots, E_{Nj}, P_{ij}, P_{i+1,j}, n_{ij}, n_{i+1,j}\right]$$

(5.15)

b) Time discretization.

Consider a first order differential equation in time of the form

$$\frac{\partial f}{\partial t} = F(f, \ldots\ldots\ldots\ldots, t)$$

By using the general implicit scheme of finite-difference approximation, the equation can be discretized as

$$\frac{f_{j+1} - f_j}{t_j} = \theta F\bigg|_{t_{j+1}} + (1-\theta)F\bigg|_{t_j}$$

(5.16)

where, in practice, $0 < \theta < 1$, and

$\theta = 0$ gives the explicit scheme,

$\theta = 1/2$ gives the Crank-Nicholson scheme,

$\theta = 1$ gives a fully implicit backward scheme.

Thus, the completed discretized forms of the system equations can be expressed as

$$\frac{P_{i,j+1} - P_{ij}}{t_j} = \theta f_{P_{j+1}} + (1-\theta) f_{P_j}$$

(5.17)

$$\frac{n_{i,j+1} - n_{ij}}{t_j} = \theta f_{n_{j+1}} + (1-\theta) f_{n_j}$$

(5.18)

and

$$\frac{E_{1,j+1} - E_{1j}}{t_j} = \theta f_{E_{j+1}} + (1-\theta) f_{E_j} \qquad (5.19)$$

5.3 Linearization

Since a fast convergence scheme is required for this problem, Newton's method will be employed to linearize the nonlinear algebraic equations. The general form of the R-dimensional Newton's method is given as, (see chapter 3)

$$g_i(\underset{\sim}{x}^{(k)}) + \sum_{r=1}^{R} \frac{\partial g_i}{\partial x_r^{(k)}} s_r^{(k)} = 0$$

$$i = 1,2,\ldots\ldots N$$

and

$$x_r^{(k+1)} = x_r^{(k)} + s_r^{(k)}$$

At time $(j+1)t$, the linearized form of equation 5.17 can therefore be expressed as

$$\left[\frac{p_{i,j+1}^{(k)} - p_{ij}}{t_j} - \theta f_{p_{j+1}}^{(k)} - (1-\theta) f_{p_j}^{(k)} \right]$$

$$+ \left\{ \frac{\partial}{\partial p_{i,j+1}^{(k)}} \left[\frac{p_{i,j+1}^{(k)} - p_{ij}}{t_j} - \theta f_{p_{j+1}}^{(k)} \right] \right\} \left(p_{i,j+1}^{(k+1)} - p_{i,j+1}^{(k)} \right)$$

$$+ \left\{ \frac{\partial}{\partial p_{i-1,j+1}^{(k)}} \left[-\theta f_{p_{j+1}}^{(k)} \right] \right\} \left(p_{i-1,j+1}^{(k+1)} - p_{i-1,j+1}^{(k)} \right)$$

$$+ \left\{ \frac{\partial}{\partial p_{i+1,j+1}^{(k)}} \left[-\theta f_{p_{j+1}}^{(k)} \right] \right\} \left(p_{i+1,j+1}^{(k+1)} - p_{i+1,j+1}^{(k)} \right)$$

$$= 0$$

or

$$\frac{p_{i,j+1}^{(k)}}{t_j} - \frac{p_{ij}}{t_j} - \theta f_{p_{j+1}}^{(k)} - (1-\theta) f_{p_j}^{(k)} - \theta \frac{\partial f_{p_{j+1}}^{(k)}}{\partial p_{i,j+1}^{(k)}} \left(p_{i,j+1}^{(k+1)} - p_{i,j+1}^{(k)} \right)$$

$$- \theta \frac{\partial f_{p_{j+1}}^{(k)}}{\partial p_{i-1,j+1}^{(k)}} \left(p_{i-1,j-1}^{(k+1)} - p_{i-1,j+1}^{(k)} \right)$$

$$- \theta \frac{\partial f_{p_{j+1}}^{(k)}}{\partial p_{i+1,j+1}^{(k)}} \left(p_{i+1,j-1}^{(k+1)} - p_{i+1,j+1}^{(k)} \right)$$

$$= 0$$

which can be rearranged into the form of a tridiagonal
matrix

$$A_{p_i}^{(k)} p_{i-1,j+1}^{(k+1)} + B_{p_i}^{(k)} p_{i,j+1}^{(k+1)} + C_{p_i}^{(k)} p_{i+1,j+1}^{(k+1)} = D_{p_i} \qquad (5\ 21)$$

Similarly, equations 5.18 and 5.19 can be readily written as

$$A_{n_i}^{(k)} n_{i-1,j+1}^{(k+1)} + B_{n_i}^{(k)} n_{i,j+1}^{(k+1)} + C_{n_i}^{(k)} n_{i+1,j+1}^{(k+1)} = D_{n_i} \qquad (5\ 22)$$

and

$$A_{E_l}^{(k)} E_{l-1,j+1}^{(k+1)} + B_{E_l}^{(k)} E_{l,j+1}^{(k+1)} + C_{E_l}^{(k)} E_{l+1,j+1}^{(k+1)} = D_{E_l} \qquad (5\ 23)$$

where

$$A_{p_i}^{(k)} = -\theta \frac{\partial f_{p_{j+1}}^{(k)}}{\partial p_{i-1,j+1}^{(k)}}$$

$$B_{p_i}^{(k)} = \frac{1}{t_j} - \theta \frac{\partial f_{p_{j+1}}^{(k)}}{\partial p_{i,j+1}^{(k)}}$$

$$C_{p_i}^{(k)} = -\theta \frac{\partial f_{p_{j+1}}^{(k)}}{\partial p_{i+1,j+1}^{(k)}}$$

$$D_{p_i}^{(k)} = \frac{p_{ij}}{t_j} + \theta f_{p_{j+1}}^{(k)} + (1-\theta) f_{p_j} - \theta \frac{\partial f_{p_{j+1}}^{(k)}}{\partial p_{i,j+1}^{(k)}} \cdot p_{i,j+1}^{(k)}$$

$$-\theta \frac{\partial f_{p_{j+1}}}{\partial p_{i-1,j-1}^{(k)}} \cdot p_{i-1,j-1}^{(k)} - \theta \frac{\partial f_{p_{j+1}}^{(k)}}{\partial p_{i+1,j+1}^{(k)}} \cdot p_{i+1,j+1}^{(k)}$$

$$A_{n_i}^{(k)} = -\theta \frac{\partial f_{n_{j+1}}^{(k)}}{\partial n_{i-1,j+1}^{(k)}}$$

$$B_{n_i}^{(k)} = \frac{1}{t_j} - \theta \frac{\partial f_{n_{j+1}}^{(k)}}{\partial n_{i,j+1}^{(k)}}$$

$$C_{n_i}^{(k)} = -\theta \frac{\partial f_{n_{j+1}}^{(k)}}{\partial n_{i+1,j+1}^{(k)}}$$

$$D_{n_i}^{(k)} = \frac{n_{ij}}{t_j} + \theta f_{n_{j+1}}^{(k)} + (1-\theta) f_{n_j} - \theta \frac{\partial f_{n_{j+1}}^{(k)}}{\partial n_{i,j+1}^{(k)}} \cdot n_{i,j+1}^{(k)}$$

$$-\theta \frac{\partial f_{n_{j+1}}}{\partial n_{i-1,j-1}^{(k)}} \cdot n_{i-1,j-1}^{(k)} - \theta \frac{\partial f_{n_{j+1}}^{(k)}}{\partial n_{i+1,j+1}^{(k)}} \cdot n_{i+1,j+1}^{(k)}$$

$$A_{E_\ell}^{(k)} = -\theta \, \frac{\partial f_{E_{j+1}}^{(k)}}{\partial E_{\ell-1,j+1}^{(k)}}$$

$$B_{E_\ell}^{(k)} = \frac{1}{t_j} - \theta \, \frac{\partial f_{n_{j+1}}^{(k)}}{\partial E_{\ell,j+1}^{(k)}}$$

$$C_{E_\ell}^{(k)} = -\theta \, \frac{\partial f_{E_{j+1}}^{(k)}}{\partial E_{\ell+1,j+1}^{(k)}}$$

$$D_{E_\ell}^{(k)} = \frac{E_{\ell j}}{t_j} + \theta f_{E_{j+1}}^{(k)} + (1-\theta) f_{E_j} - \theta \, \frac{\partial f_{E_{j+1}}^{(k)}}{\partial E_{\ell,j+1}^{(k)}} \cdot E_{\ell,j+1}^{(k)}$$

$$-\theta \, \frac{\partial f_{E_{j+1}}}{\partial E_{\ell-1,j-1}^{(k)}} \cdot E_{\ell-1,j-1}^{(k)} - \theta \, \frac{\partial f_{E_{j+1}}^{(k)}}{3 E_{\ell+1,j+1}^{(k)}} \cdot E_{\ell+1,j+1}^{(k)}$$

5.4 Computational algorithm.

The linearized algebraic system equations 5.21 to 5.23 with the coefficients in 5.24 are entirely in the same form as equations 4.16, 4.17 and 4.18. The algorithm depicted in Fig.4.1 can therefore be utilized to obtain the solutions. However, some modification involving the time increment must be added. During the computation of the transient behaviour, a test for the steady state condition must be provided to stop computation, but when investigating the sinusoidal response, a time limit can be

set up.   The modified computational algorithm is shown in

Fig. 5.2

The criterion for convergence is obtained from

$$\max_{i} \left| \frac{\left(p_i^{(k+1)} + n_i^{(k+1)}\right) - \left(p_i^{(k)} + n_i^{(k)}\right)}{p_i^{(k)} + n_i^{(k)}} \right| < \epsilon \qquad (5\ 25)$$

where ϵ is the acceptable accuracy.
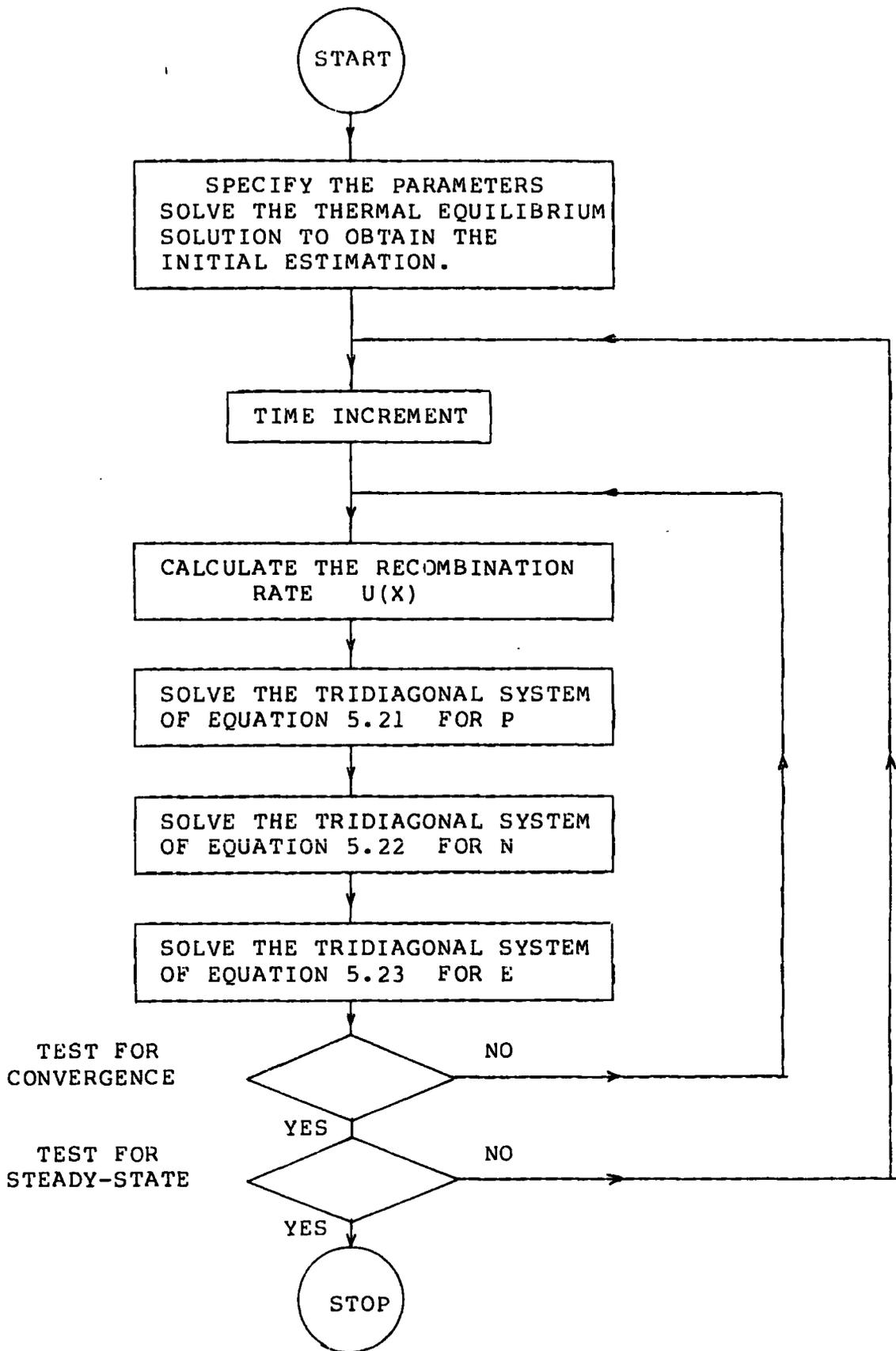
FIGURE 5.2 THE COMPUTATIONAL ALGORITHM.

5.5 Numerical results.

Following the same line of investigation as in the static cases, we shall here consider two problems of diode dynamics which are controlled by the time dependent quantities. The first of these is the internal behaviour involving the response of the diode to large excursions of voltage and current, as in many switching applications. The second is the terminal characteristics which describe the response of the diode to large step and sinusoidal excitations.

A simple resistor diode circuit as in Fig. 5.3 is used to study this behaviour. The diode current in this circuit is given by
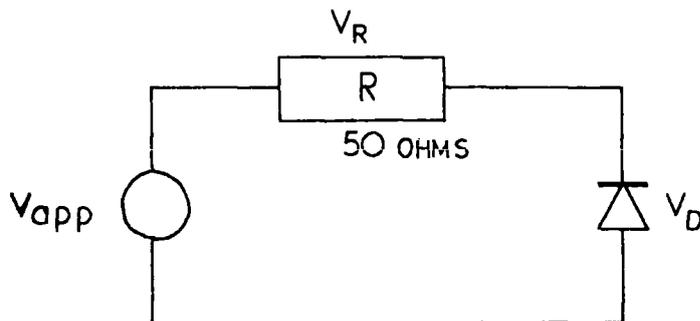
Figure 5.3   A R-D circuit.

$$J_T(t) = (v_{app}(t) - v_D(t))/AR$$

where

$$v_D(t) = v_D(0,t) - v_D(L,t)$$

$$= \int_o^L E(x,t)\,dx - v_{diff}$$

and

$$v_{app}.(t) = \text{applied voltage}$$

$v_D(t)$ = voltage across diode

v_{diff} = diffusion voltage

L = device length

equation 5.26 can be expressed as (in normalized form)

$$V_T(t) = \left[V_{app}(t) - \int_0^L E(x,t)\,dx + V_{diff} \right] V_o L_D / (ARqD_o n_i)$$

(5.27)

The diode under consideration has the same physical parameters as in section(4.6) so that a comparison between the static and dynamic behaviours is possible.

5.5.1 Internal characteristics

Investigation of the dynamic internal behaviour is necessary to provide understanding of the detailed mechanism of the device. We will, in this section, study only the turn-on transient. The turn-off phenomenon can be investigated and explained in a similar fashion when we study the sinusoidal response.

There are two basic phenomena responsible for the behaviour of the device under transient condition. Firstly, there is the relaxation effect involved within a period of the dielectric relaxation time constant , given by

$$T_r = \frac{\epsilon}{q(\mu_p p + \mu_n n)}$$

Secondly, minority carriers take a nonzero time to pass through the base region of the lightly doped region. For narrow base diodes, the transit time T_t, is given by [45]

$$T_t = W_B^2/(2D_B)$$

for low level injection, and

$$T_t = W_B^2/(4D_B)$$

for high level injection.

Where

W_B is the base width, and

D_B is the minority carrier diffusion constant in the base region.

The recombination effects which occurs within the effective lifetime T_{eff} given by <42>

$$T_{eff} = T_{po} = T_{no} \qquad \text{for low level injection, and}$$

$$T_{eff} = T_{po} + T_{no} \qquad \text{for high level injection}$$

may be of interest and can be included as part of the transit effect.

We shall consider a diode having the doping profile shown in Fig. 5.4 . The transient drive applied to the circuit of Fig. 5.3 is a step excitation.

$$V_{app}(t) = \begin{cases} 0 & t<0 \\ -3.0 \text{ Volt} & t>0 \end{cases}$$

in the forward direction. The times of interest are then as follows:

$$T_r = 10^{-14} \text{ second, in highly doped p region}$$

$$T_t = \begin{cases} 4.16 \times 10^{-6} \text{ second, for low level injection} \\ 2.08 \times 10^{-7} \text{ second, for high level injection} \end{cases}$$

Figs 5.5 to 5.9 show the electric field, electrostatic potential, carrier density distributions and the current density distribution respectively at various instants of time. For times less than the dielectric relaxation time constant, the electric field changes drastically without variation of the carrier densities. The displacement current is the dominant component in the total current throughout the interior of the device, whereas the particle currents J_n and J_p remain unchanged from their thermal equilibrium values. The electrostatic potential across the junction also remains unchanged because there is no carrier flow. In other words, this phase of the response is responsible for the build-up of the ohmic voltage drop in the quasi-neutral region.

At later times, within the range of transit time, most of the carriers injected are stored in the transition region charging the transition region capacitance, which results in a reduction of the electric field. The displacement current in the transition region begins to decrease, and hole current flows with the absence of electron current in this region. As time proceeds, the junction voltage build-up and the barrier height falls. The displacement current in the transition region begins to disappear and the carrier currents now become dominent. Diffusion of electrons into the base region reduces the

hole current and any electrons left after crossing the transition region are eventually recombined with holes in the p p^+ region.

An analogous situation for holes also occurs in the n^+ region, but it is a small effect due to the heavy doping.

The displacement currents in the base region as depicted in Fig. 5.9 show an inversion of sign in both interface regions n^+ p and p p^+, The sign inversion at the n^+ p junction occurs at the initial part of the transient (t = 2.0×10^{-10}). This effect has been described by De Mari <15> and Petersen <18> in their analyses, and they suggested that the displacement current is initially positive corresponding to the build-up of the ohmic potential drop in the base region, and decreases as the carrier currents flow into the region. The flow of the carrier currents modulate the conductivity in the base region which results in a decrease of the voltage drop. This effect changes the electric field and consequently reverses the displacement current. A similar explanation applies also for the sign inversion of the displacement current at the p p^+ junction, except that this happens when high level injection conditions occur at later times.
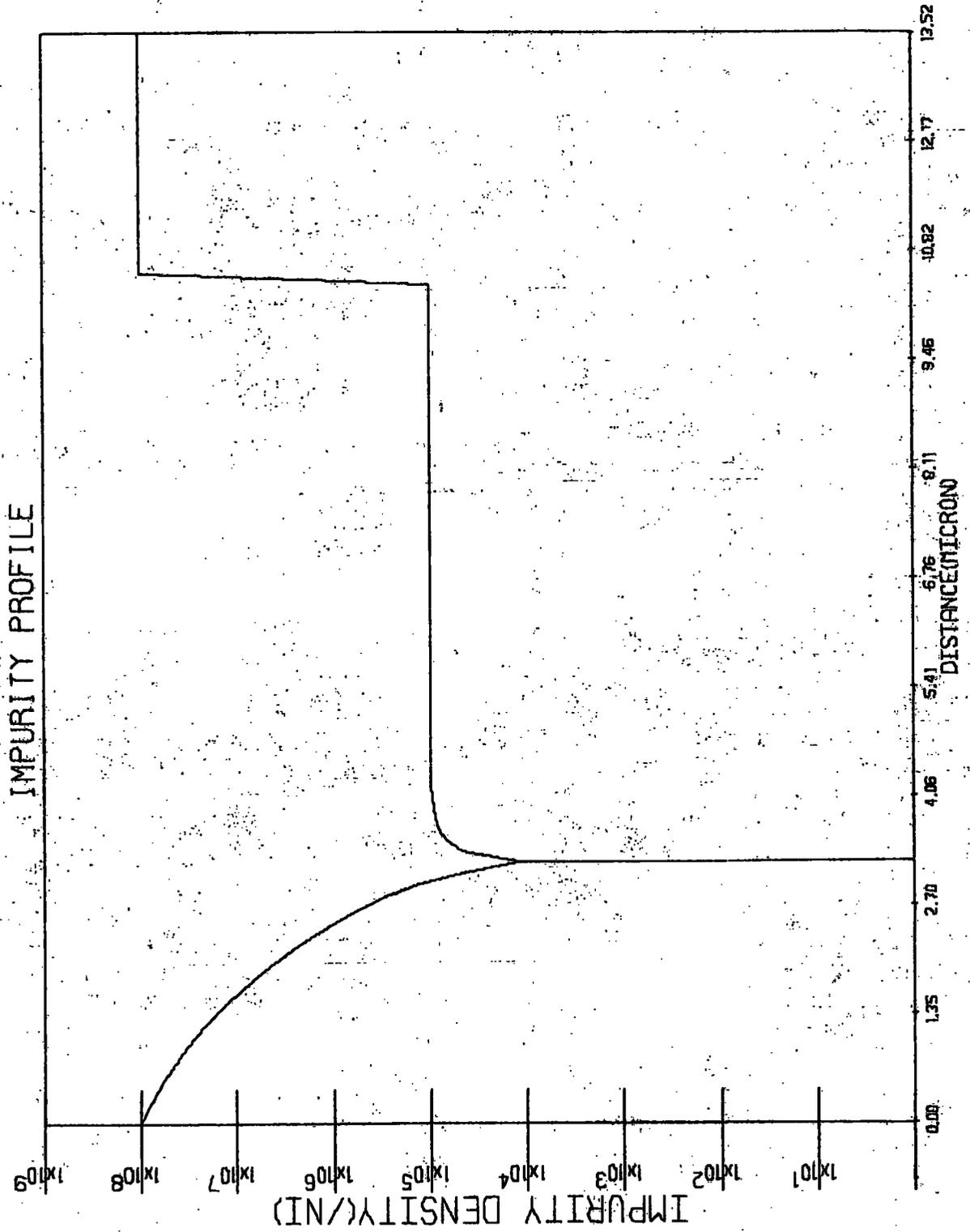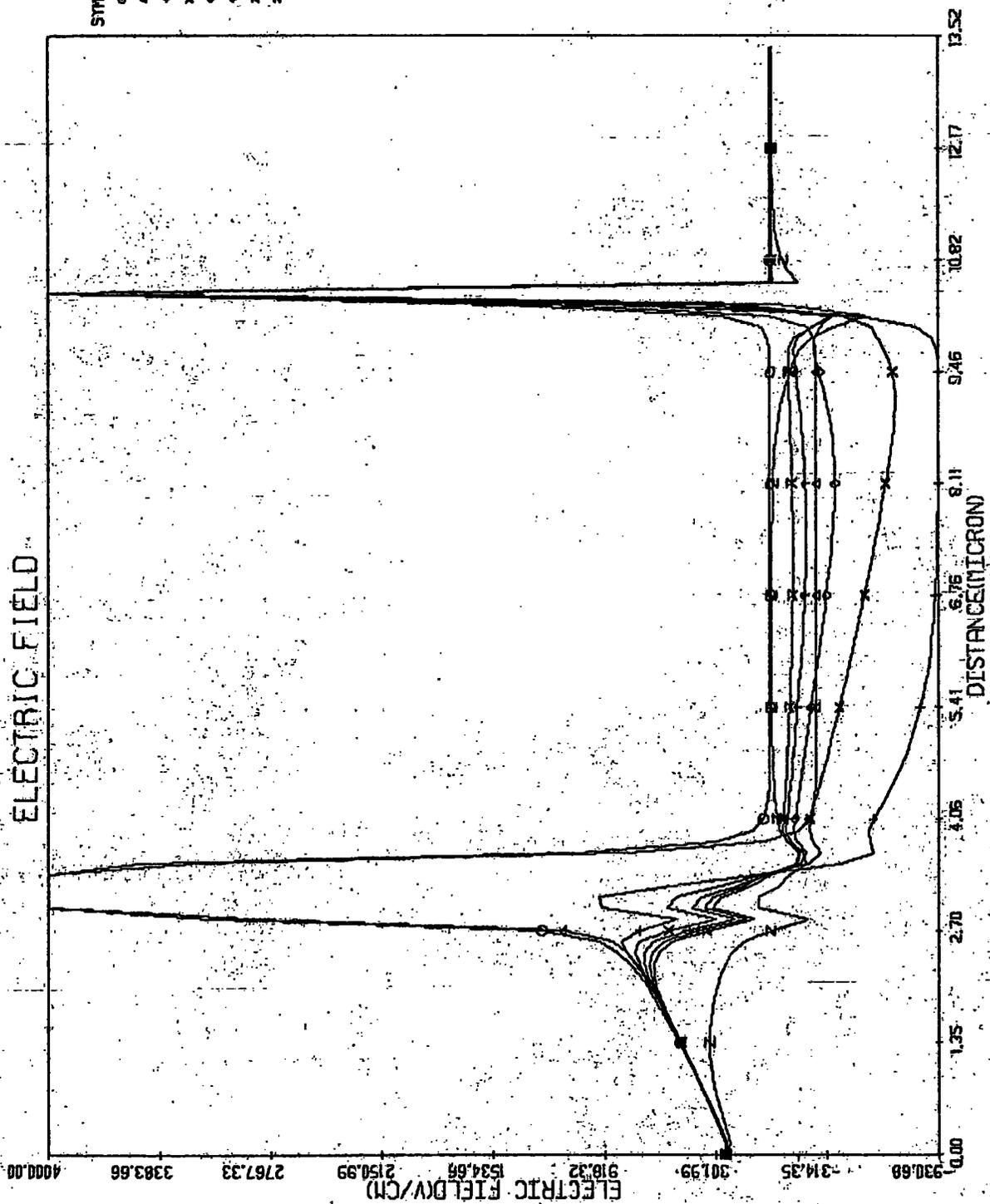
IMPURITY PROFILE

IMPURITY DENSITY(/NI)

DISTANCE(MICRON)

FIGURE (5.4)

FIGURE (5.5)

FIGURE (5.6)

FIGURE (5.7)

CURRENT DENSITY

SYMBOL	TIME (SEC)
⊙	3.6319E-15
△	1.9883E-12
+	2.0675E-10
×	5.1016E-10
✦	1.6292E-09
✚	3.2040E-09
×	4.3944E-09
N	9.3149E-07

JN ------
JP ......

-CURRENT DENSITY(AMP/A)

DISTANCE(MICRON)

FIGURE (5.8)

CURRENT DENSITY

SYMBOL	TIME (SEC)
⊙	9.9919E-15
▲	1.9883E-12
+	2.0673E-10
×	8.1016E-10
◇	1.8092E-09
◆	3.2040E-09
⊠	4.9344E-09
Z	9.9149E-07
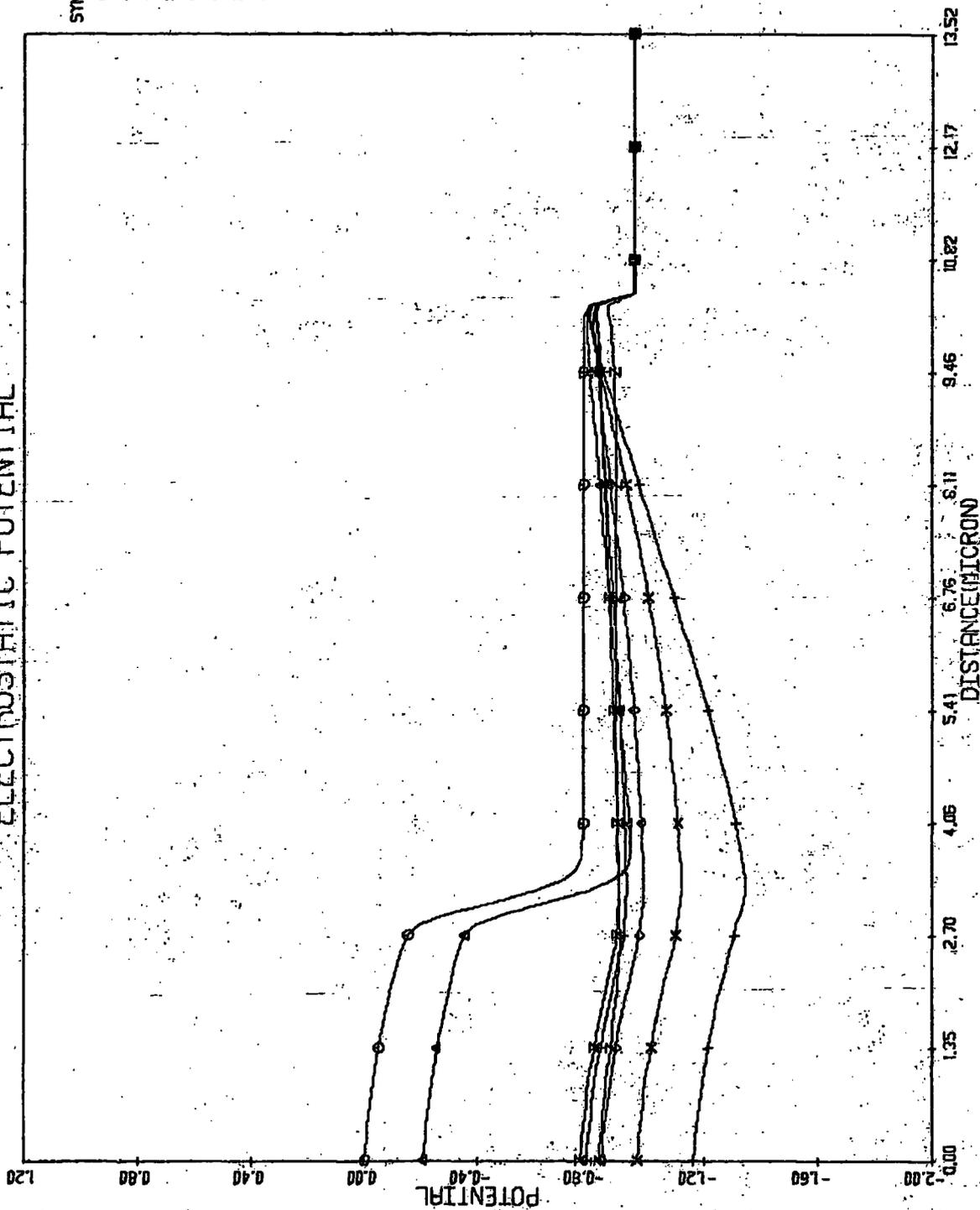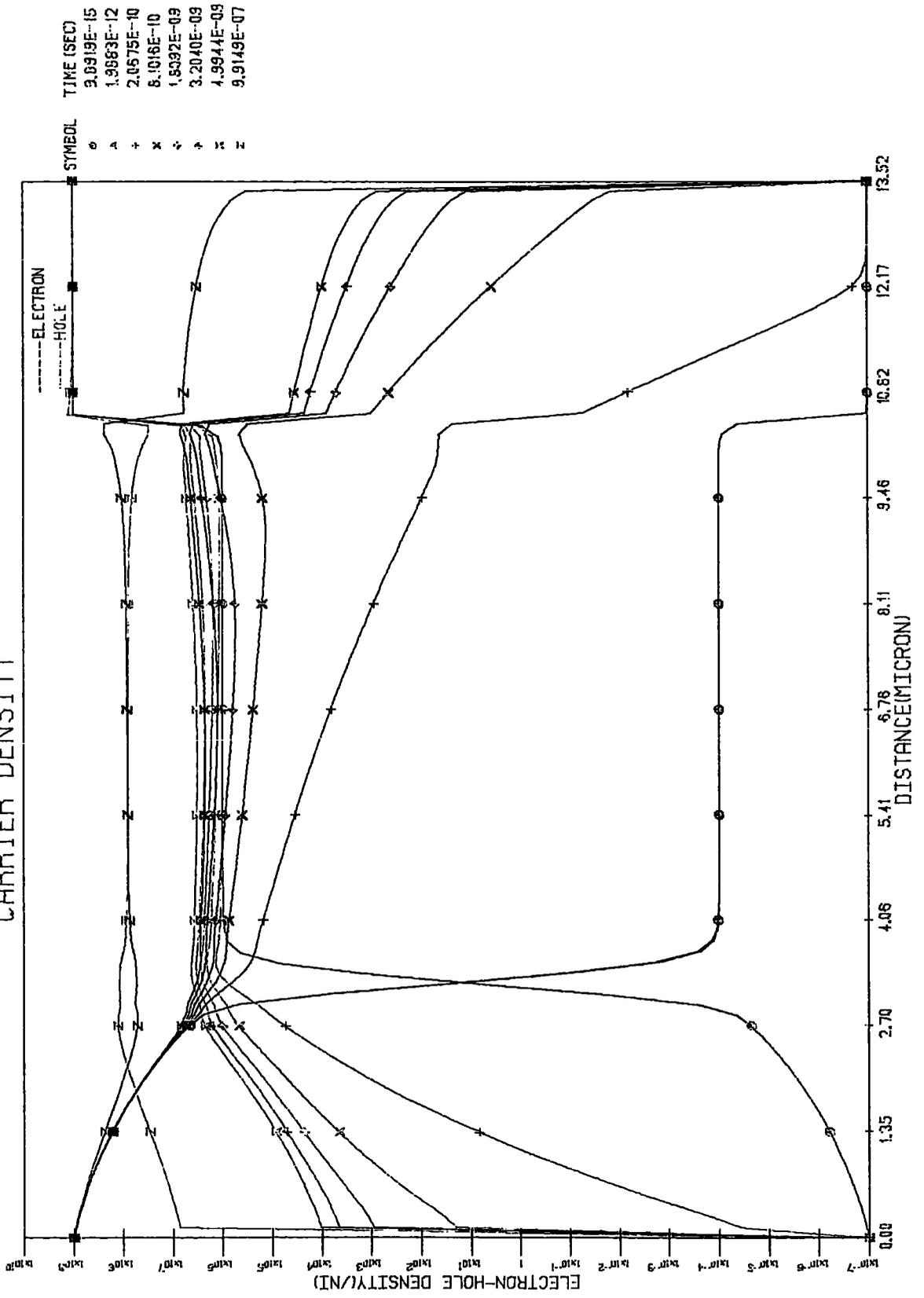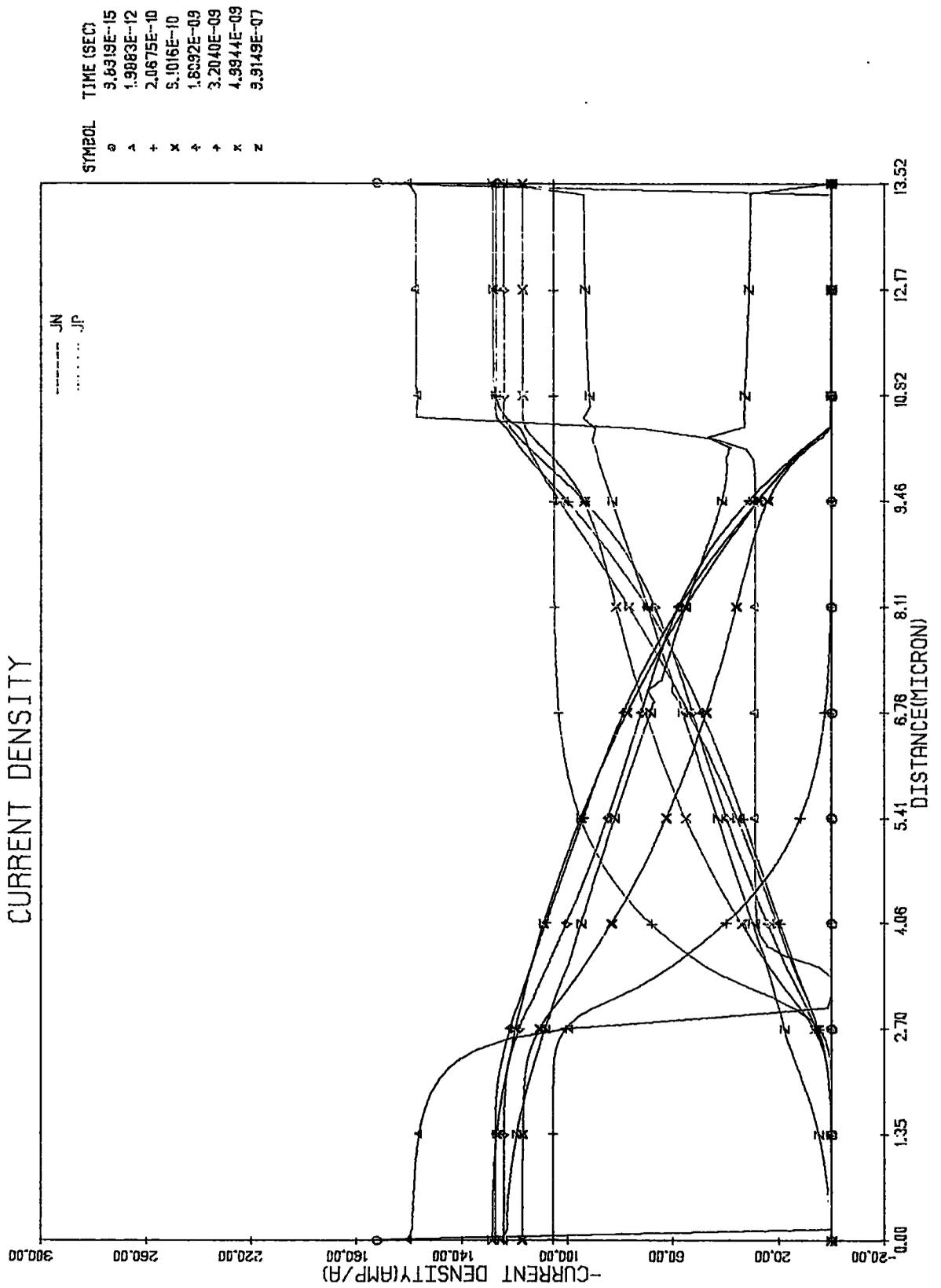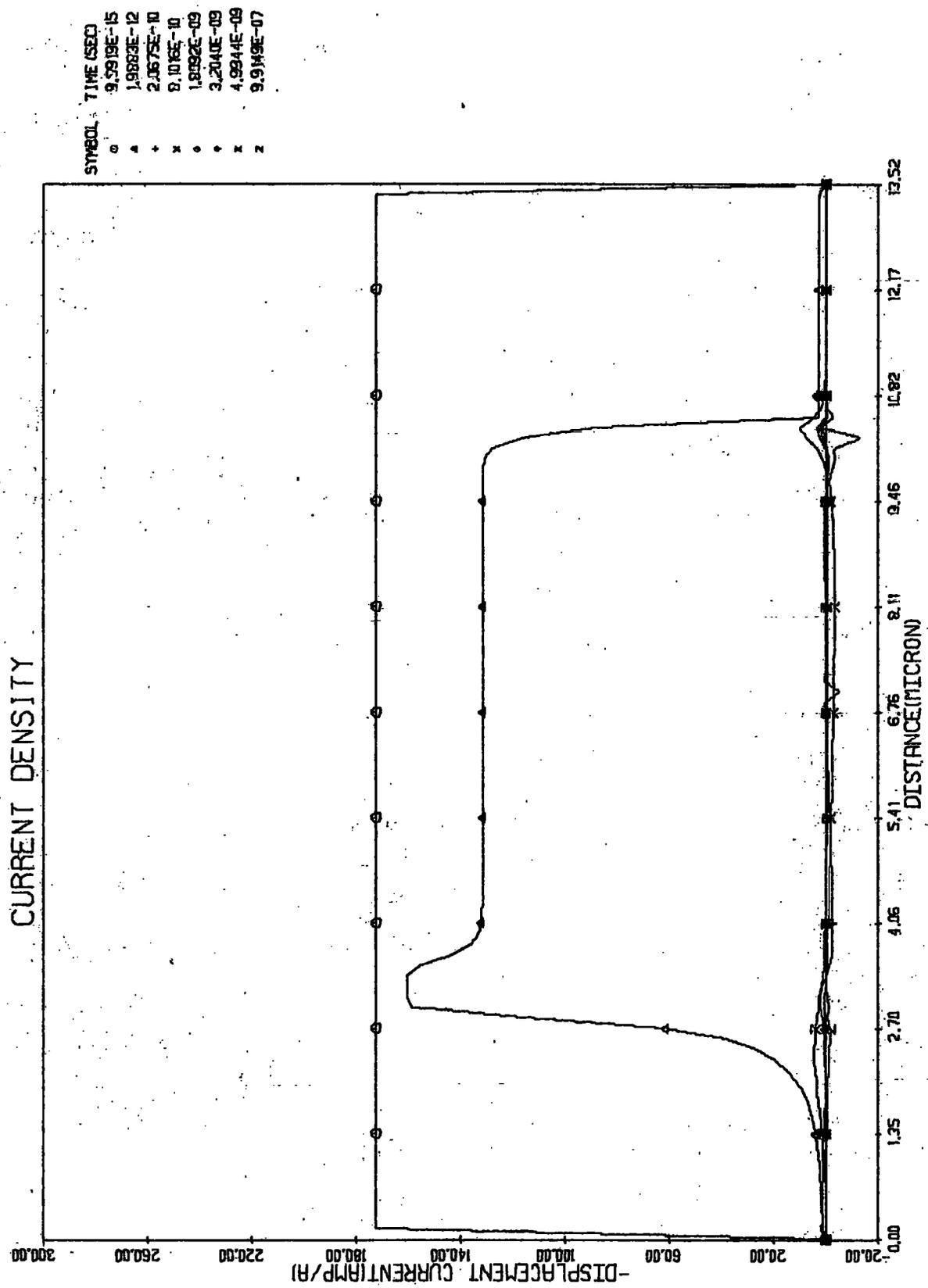
FIGURE (5.9)

5.5.2. Terminal characteristics.

Just as for the static case in chapter 4, the terminal characteristics of the devices will be investigated both under step and sinusoidal excitation, concentrating on a study of conductivity modulation effects and the influence of minority carrier lifetime on the behaviour.

Step response.

Under the same conditions as in the investigation of the internal behaviour, the step response of the diode under different injection level conditions are shown in Figs. 5.10 to 5.12 . The currents vary from low level to high level depending on the value the step voltage applied to the circuit. The terminal voltage of the diode depicted in Fig. 5.11 shows negative overshoot for large currents, but it decreases monotonically for small currents.

This behaviour can be described by the relation derived by Ko <7>, for a step profile n^+ p diode,

$$v_D(t) = \frac{KT}{q} \ln\left[1 + \frac{I_f}{I_S} \mathrm{erf}\sqrt{t/T_n}\right] + I_f R_o \left[1 - \frac{L_n}{w_p} \ln(1 + K \, \mathrm{erf}\sqrt{t/T_n})\right]$$

where

R_o = the intrinsic bulk resistance with no excess carriers

K = a physical constant for the diode material, doping, and geometry, and

I_f, I_S are obtained from the static diode equation

$$I_f = I_S(\exp(qV/kT) - 1)$$

the terminal voltage, $V_D(t)$, is a combination of the junction voltage and the ohmic voltage drop in the bulk region. After the dielectric relaxation time, the injected carrier densities rise from the equilibrium towards their steady-state values, and accordingly there is an increase of the junction voltage. At the same time, the conductivity of the material is increased by the increase of carrier densities. The bulk resistance is therefore reduced, and so the ohmic voltage drops. The junction voltage increases with time, while the ohmic voltage drop decreases with time. Under low level injection conditions, the ohmic voltage drop is small compared with the junction voltage, and so the observed terminal voltage increases with time. At high injection levels, the junction voltage has reached its saturation value, and the ohmic voltage drop is the dominant . In this case, the observed terminal voltage decreases with time.

Figs. 5.13 and 5.15 replot the terminal voltages and currents of the diode on a normalized time scale, t/T. Under low level injection condition, $V_{app} = -0.15$ volt, the result shows that the diode behaves capacitively. If the diode-resistor circuit is modelled as a simple R-C series combination, the response can be approximated with values of 50 ohms and 5 nF. At high-level injection, $V_{app} = -15.0$ volt, it is seen that the diode behaves somewhat inductively. The circuit may be modelled as a R-L series combination. The response can be approximated with values of 50 ohms and 50 nH. More accurate modelling will

require a nonlinear resistance and will not be attempted here.
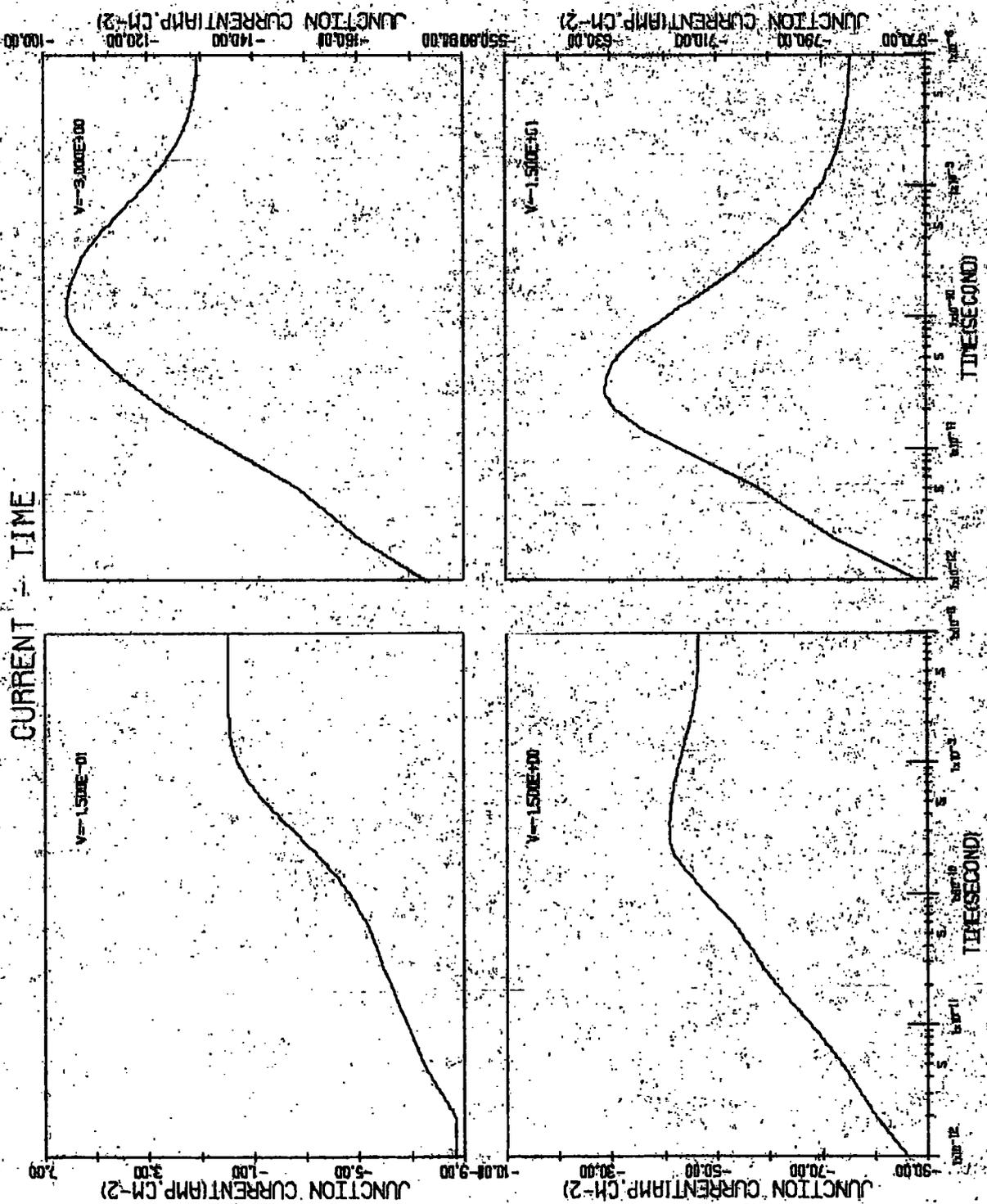
FIGURE (5.10)
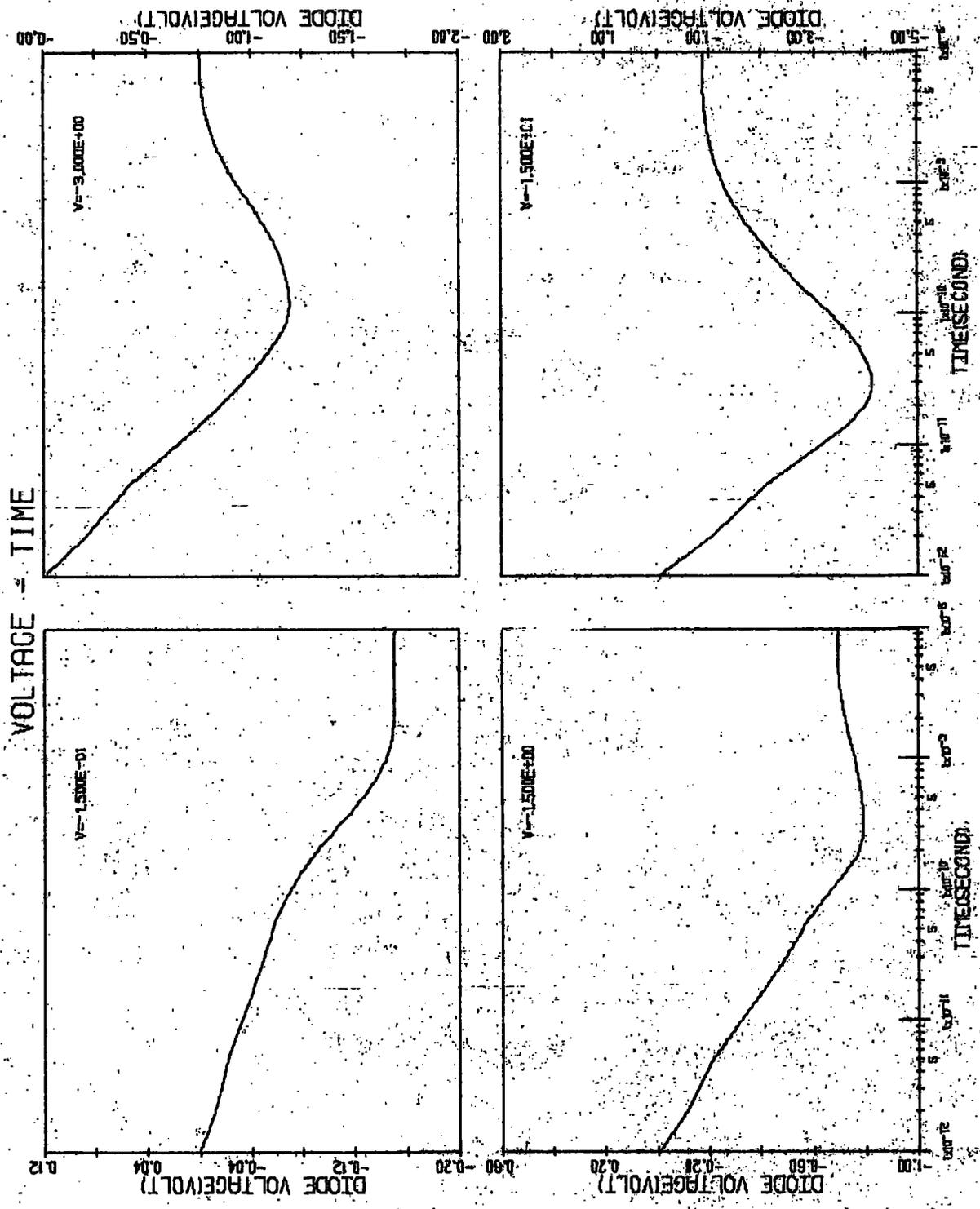
FIGURE (5.11)
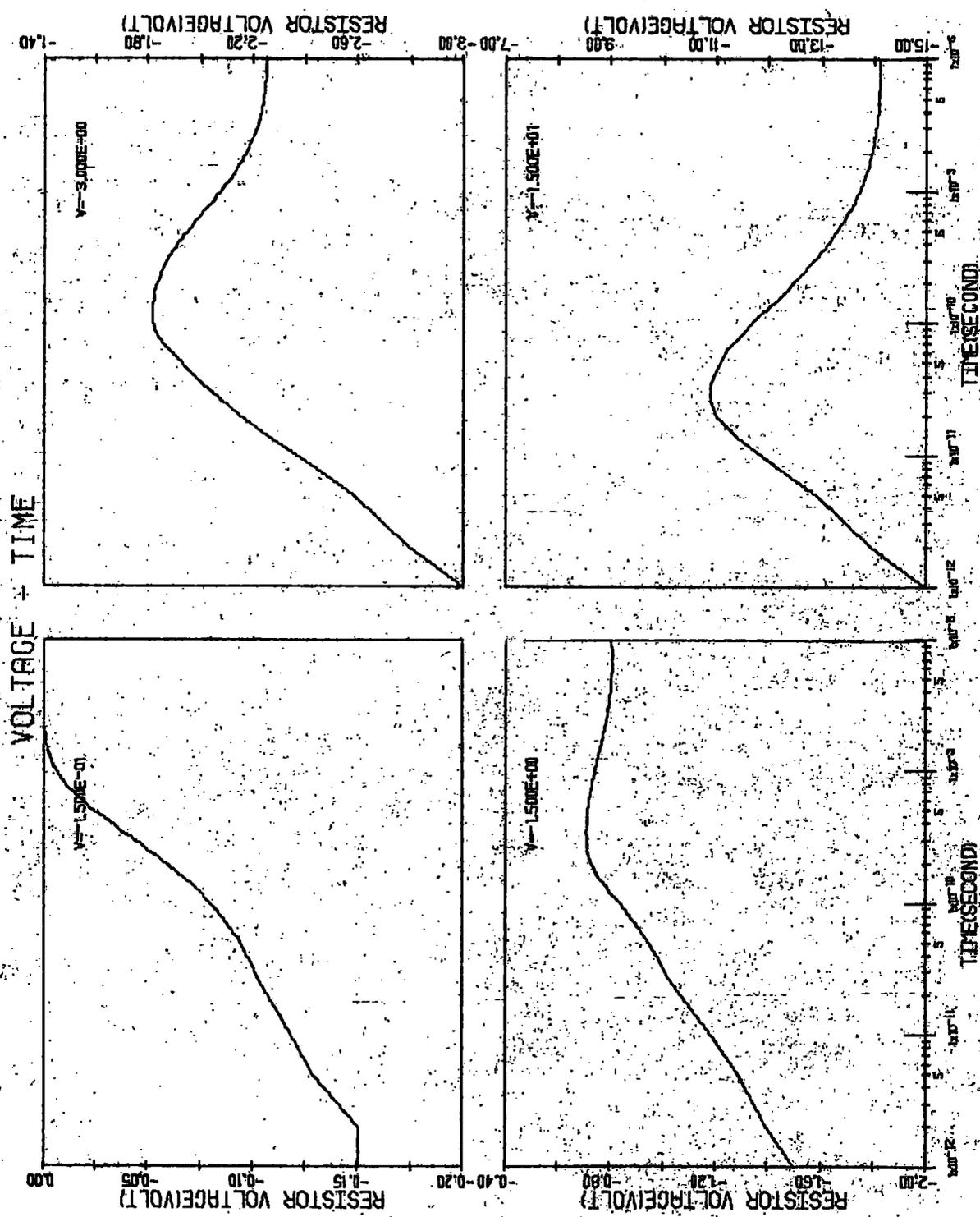
FIGURE (5.12)
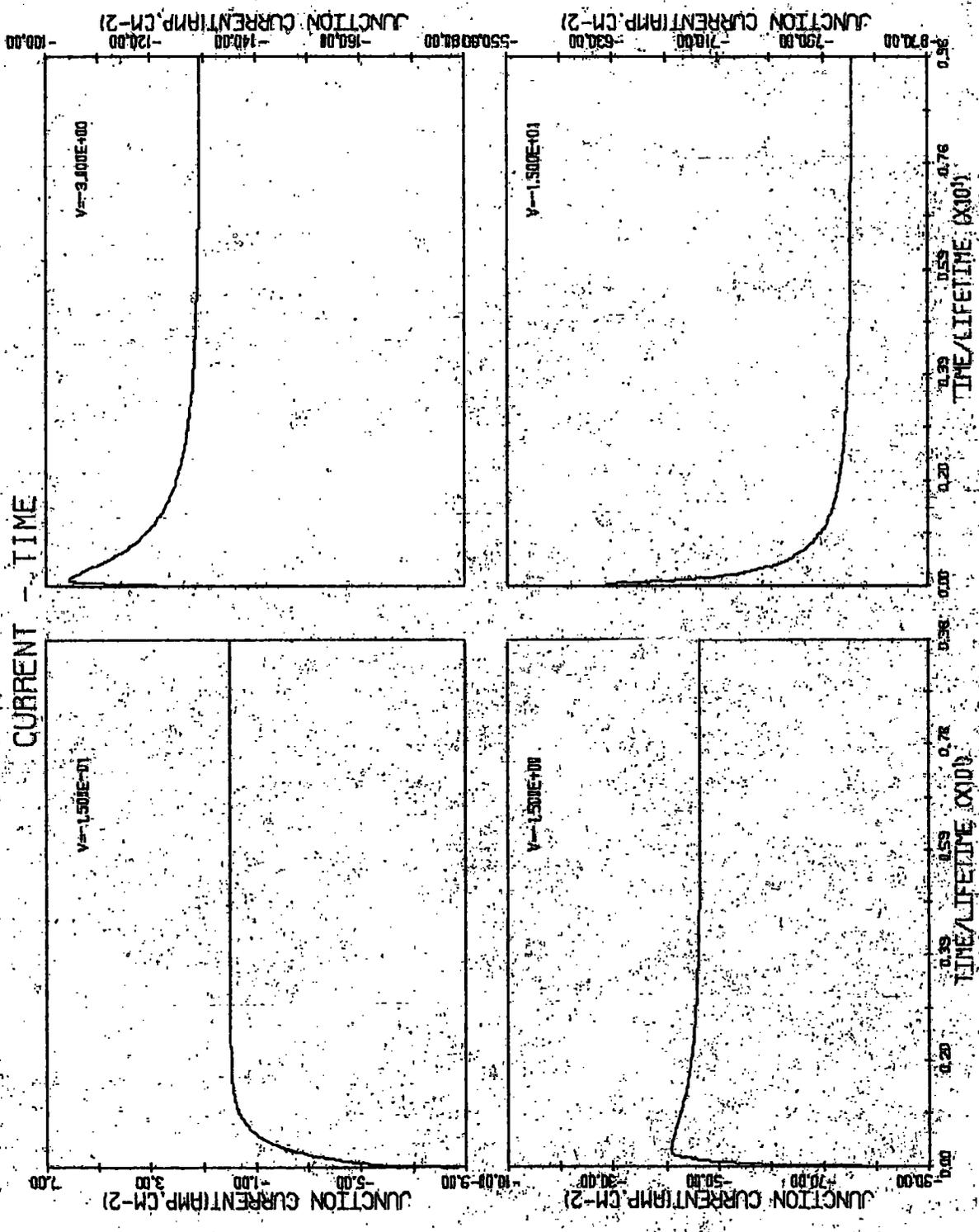
FIGURE (5.13)

VOLTAGE - TIME
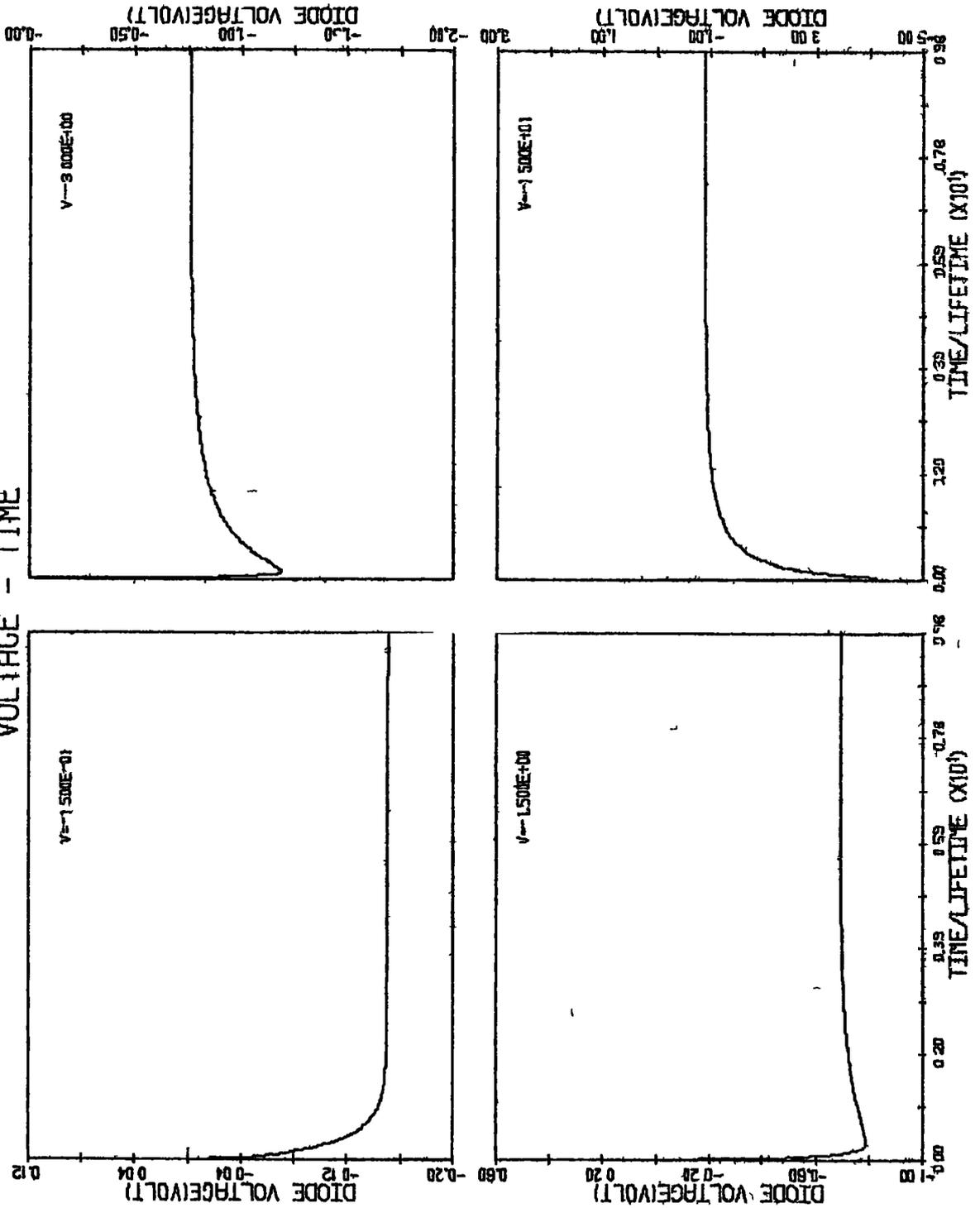
FIGURE (5·14)
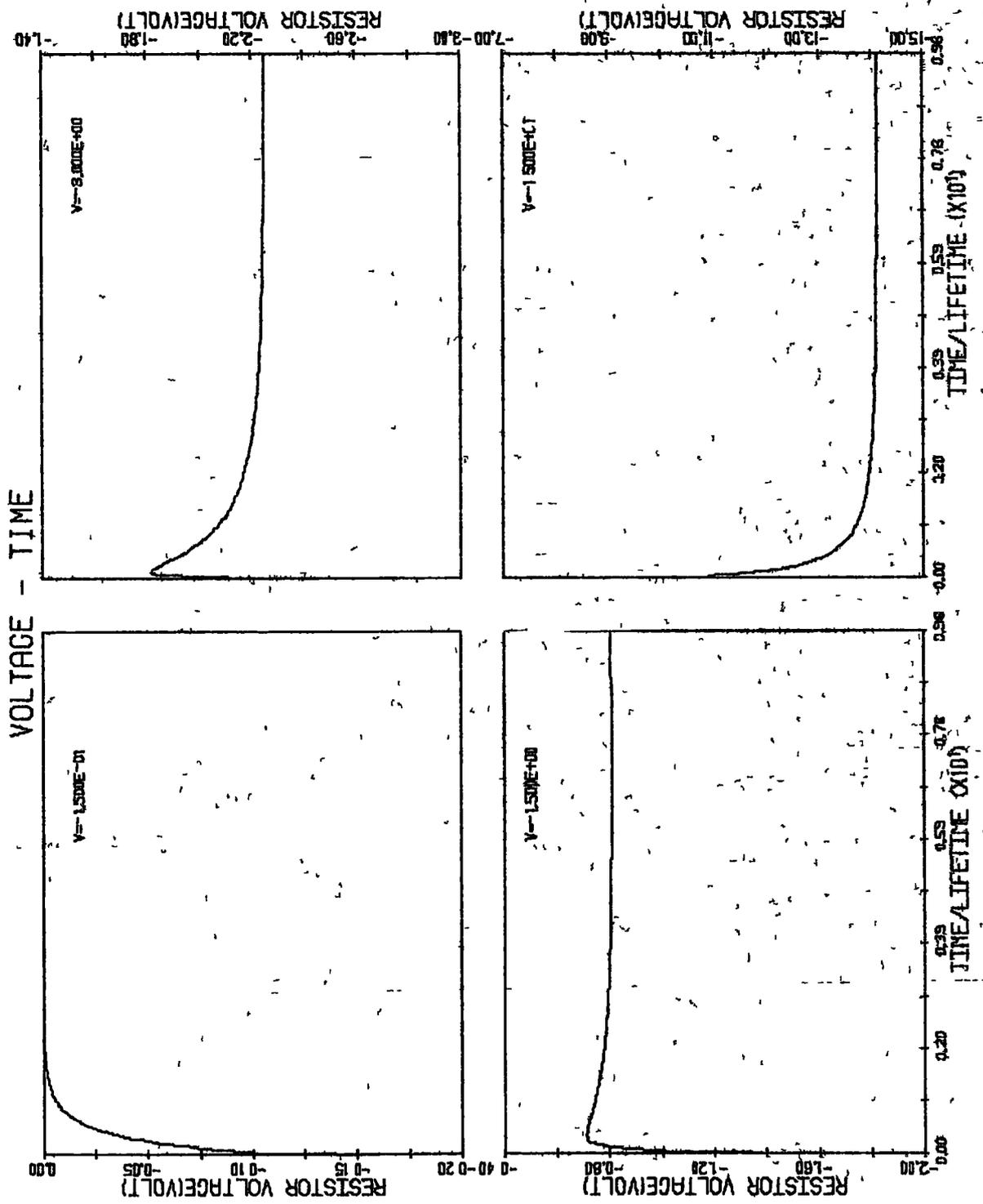
FIGURE (5 15)

' ## Sinusoidal response.

The study of the sinusoidal response of a diode provides an insight into its rectifying effect and the generation of harmonics. For the latter purpose, the steady-state solutions are required, thus the transient effects in the early cycles must be disregarded. This involves more time steps and consequently more computing time. The simpler structure of n^+-p diodes with the doping profile depicted in Fig. 4.17 gives the solutions in about half the time required for n^+-p-p^+ diodes with the doping profile shown in Fig. 5.4 .

For this reason, n^+-p diode with the physical parameters given in section(4.6) will be computed rather than n^+-p-p^+ diodes for the following analyses.

The external excitation is given by

$$V_{app}(t) = -3.0 \ Sin(2\pi ft)$$

where $f = 1$ MHz.

5.5.3 Effect of the minority carrier lifetimes on the terminal characteristics.

a) Diodes with the same ratio of W_p/L_n

The results of chapter 4 suggested that in order to study the influence of the lifetimes, the diodes to be compared should have the same recombination criterion, namely the normalized width W_p/L_n. Figs. 5.16 to 5.18 shown the response of diodes having moderate recombination, for which $W_p/L_n = 1$, but different minority carrier lifetimes varying from 1 microsecond to 10 nanosecond.

During the forward half cycle, the shorter lifetimes gives higher recombination rates, and hence the currents across the junction are larger. This agrees with the results obtained in the static cases.

During the reverse half cycle, the current consists of the generation current and the current due to the stored minority carriers being removed from the transition region. The stored charge results from injection during the forward cycle. Initially the presence of the stored charge causes a large reverse current to flow, and makes the junction voltage change slowly. The junction remains in forward bias, and the diode still conducts. After the so-called storage delay time, the junction becomes reverse biased, and the reverse current starts to decay toward its steady-state value.

Fig. 5.16 confirms that the low recombination rate in the large lifetime diode leads to a large amount of stored

charge and consequently to a considerable overshoot effect and a large storage delay time. On the other hand, a short lifetime diode has little storage charge and makes a good rectifier.

CURRENT - TIME
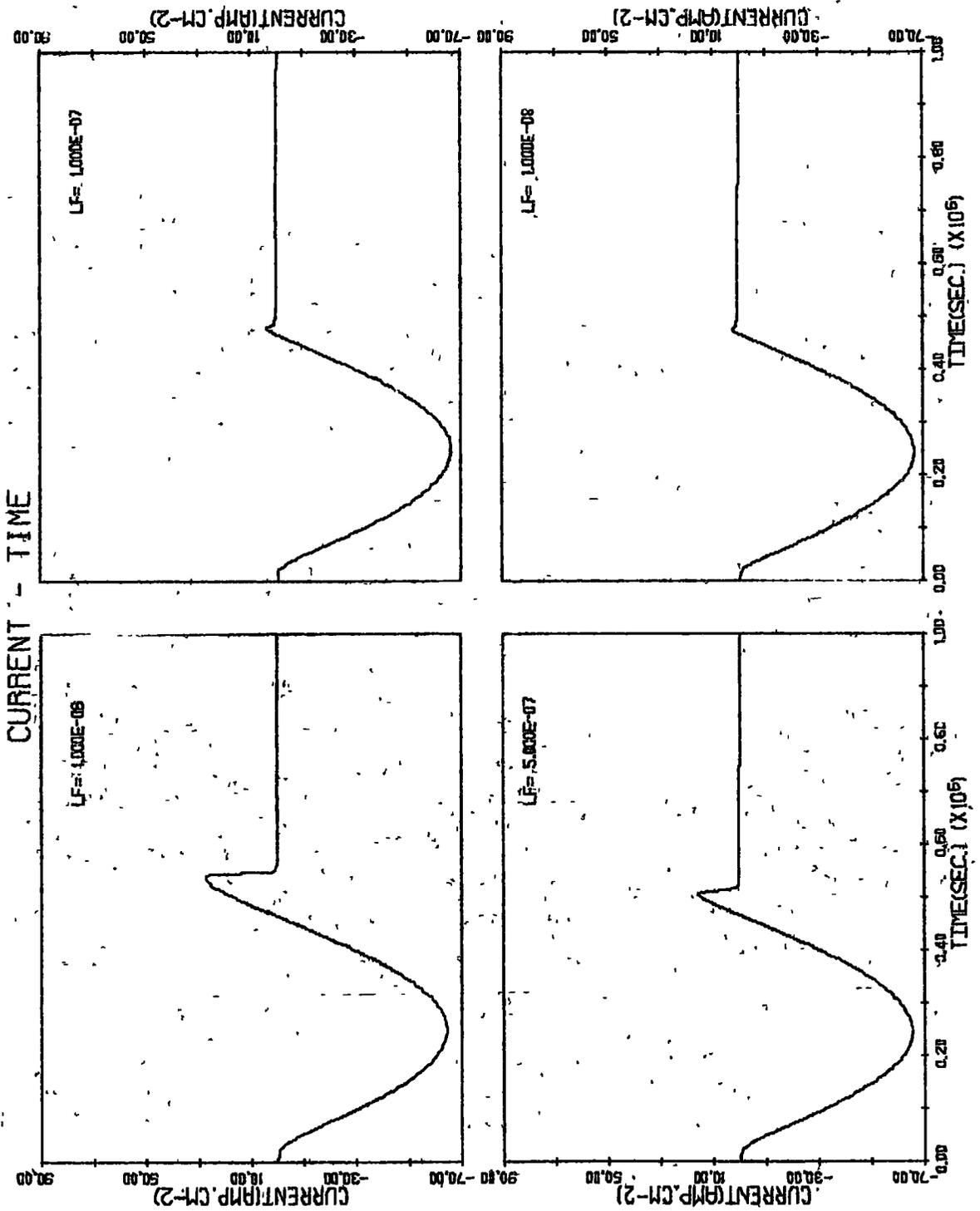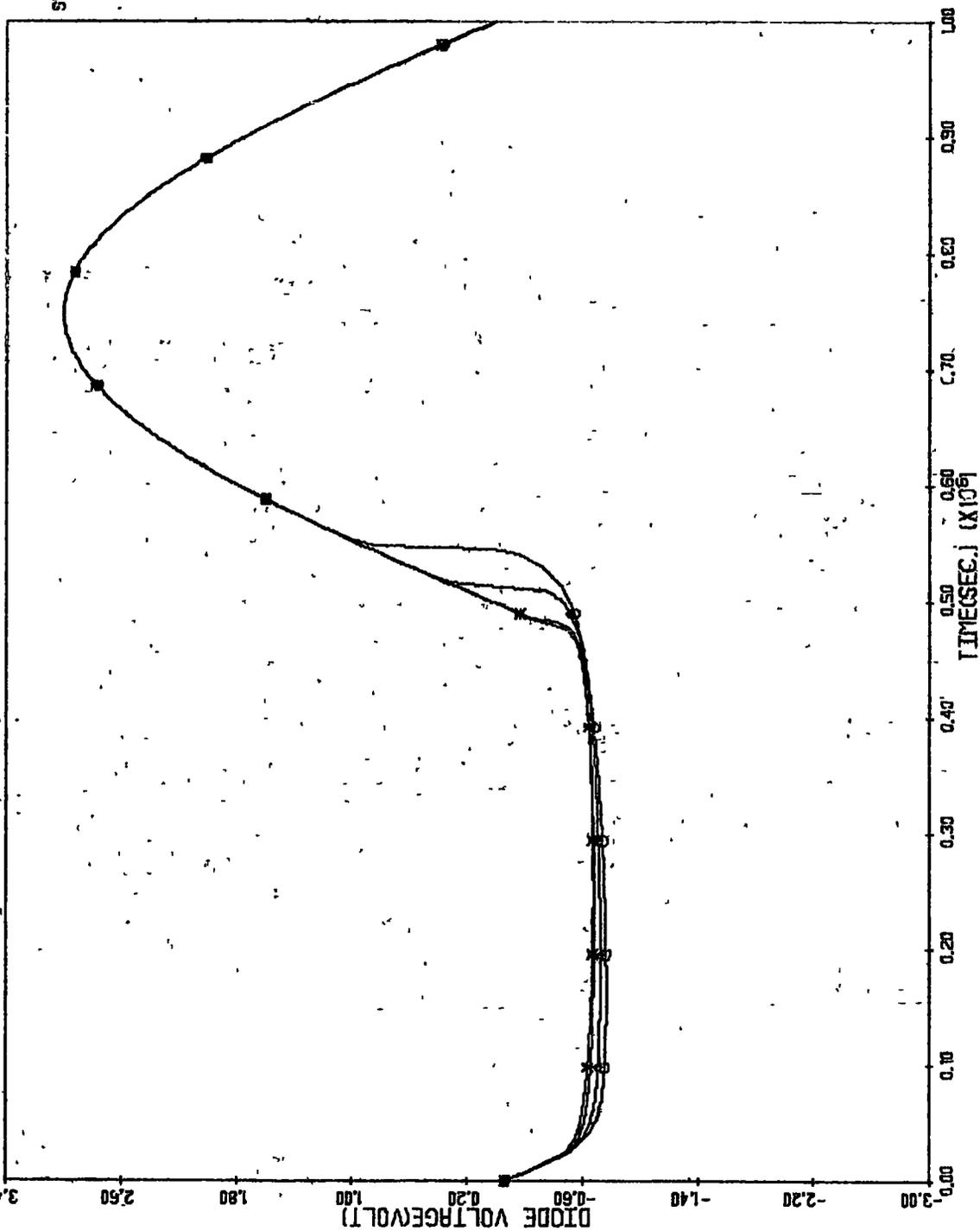
FIGURE (5:16)
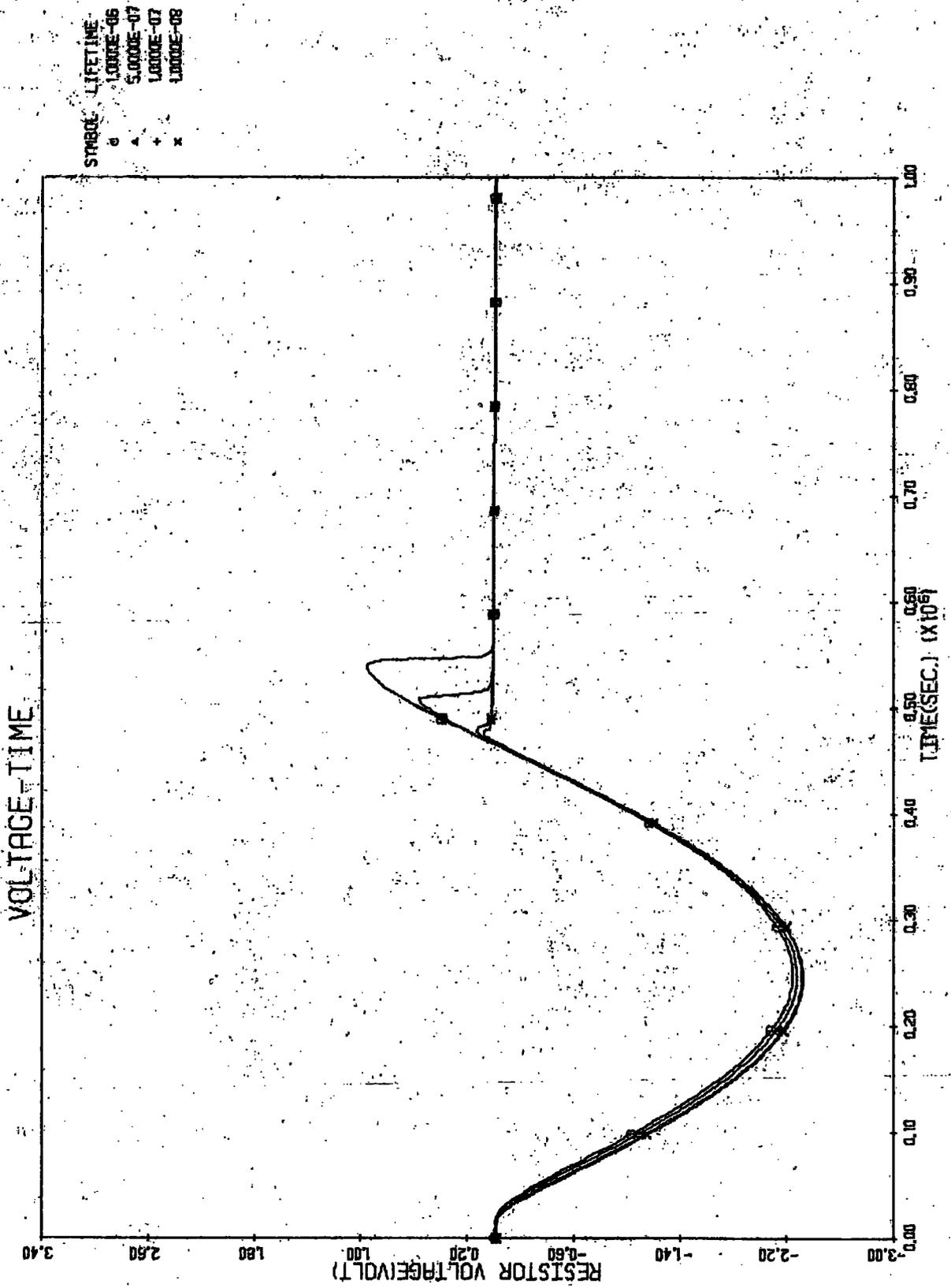
FIGURE (5.17)

FIGURE (5.18)

b) <u>Different sized diodes with a fixed lifetime.</u>

Figs. 5.19 to 5.21 show the responses of diodes of different sizes with normalized width, W_p/L_n, ranging from 0.1 to 1.0, for a carrier lifetime of 1 microsecond

During the forward half cycle, the current continues to increase as the diode is made smaller, or as the bulk resistance becomes lower. This supports the result obtained in chapter 4, and shows that there is no optimum value of the size of the diode.

During the reverse half cycle, the longer diodes have relatively higher storage delay times and larger overshoot effects in comparison with the shorter diodes. This results from the infinite surface recombination velocity assumption at the ohmic contacts. For the shorter diodes, the minority carriers recombine relatively faster than those of the longer diodes. The storage delay time and overshoot effect are therefore much reduced.

CURRENT – TIME
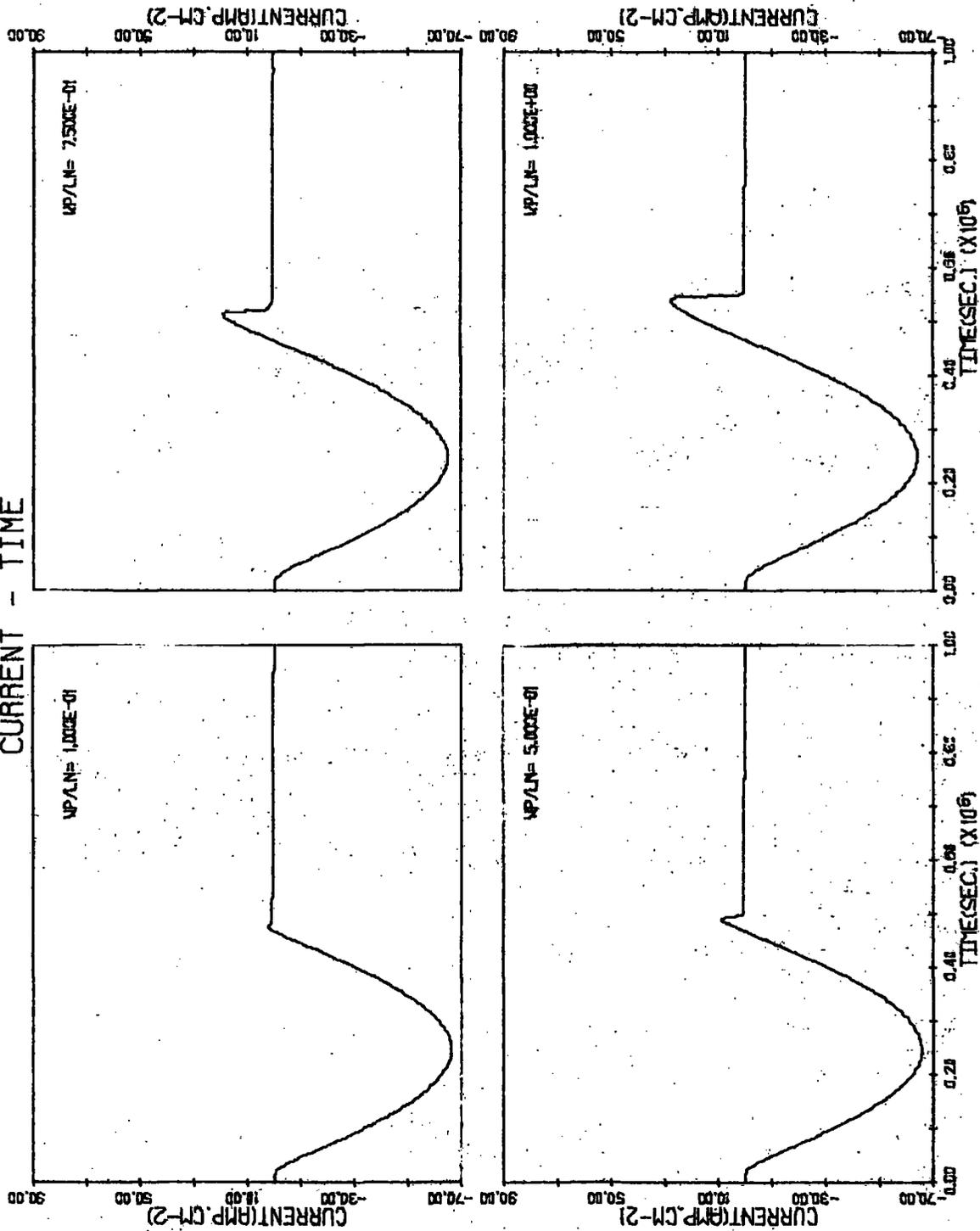
FIGURE (5.19)
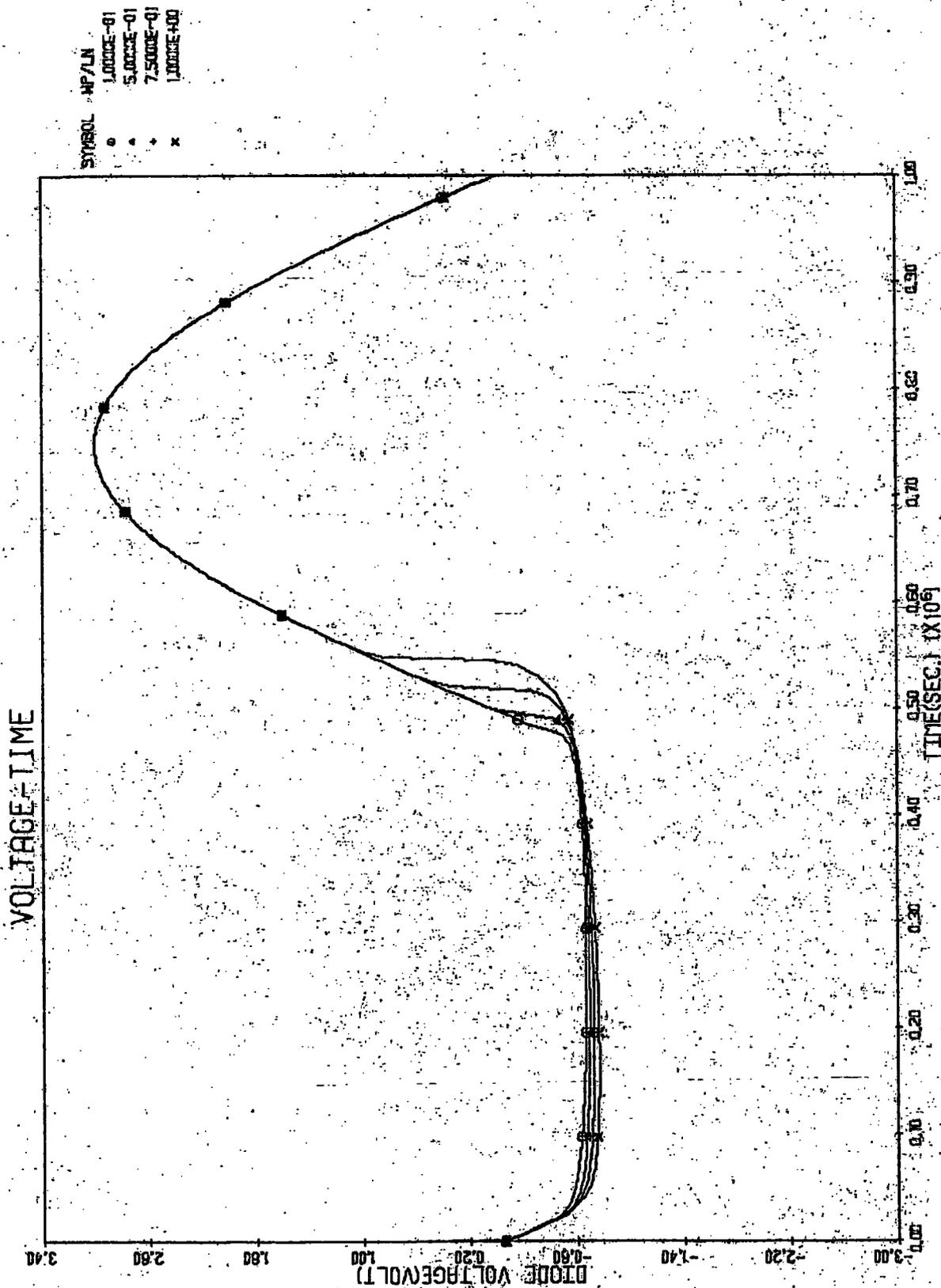
FIGURE (5.20)
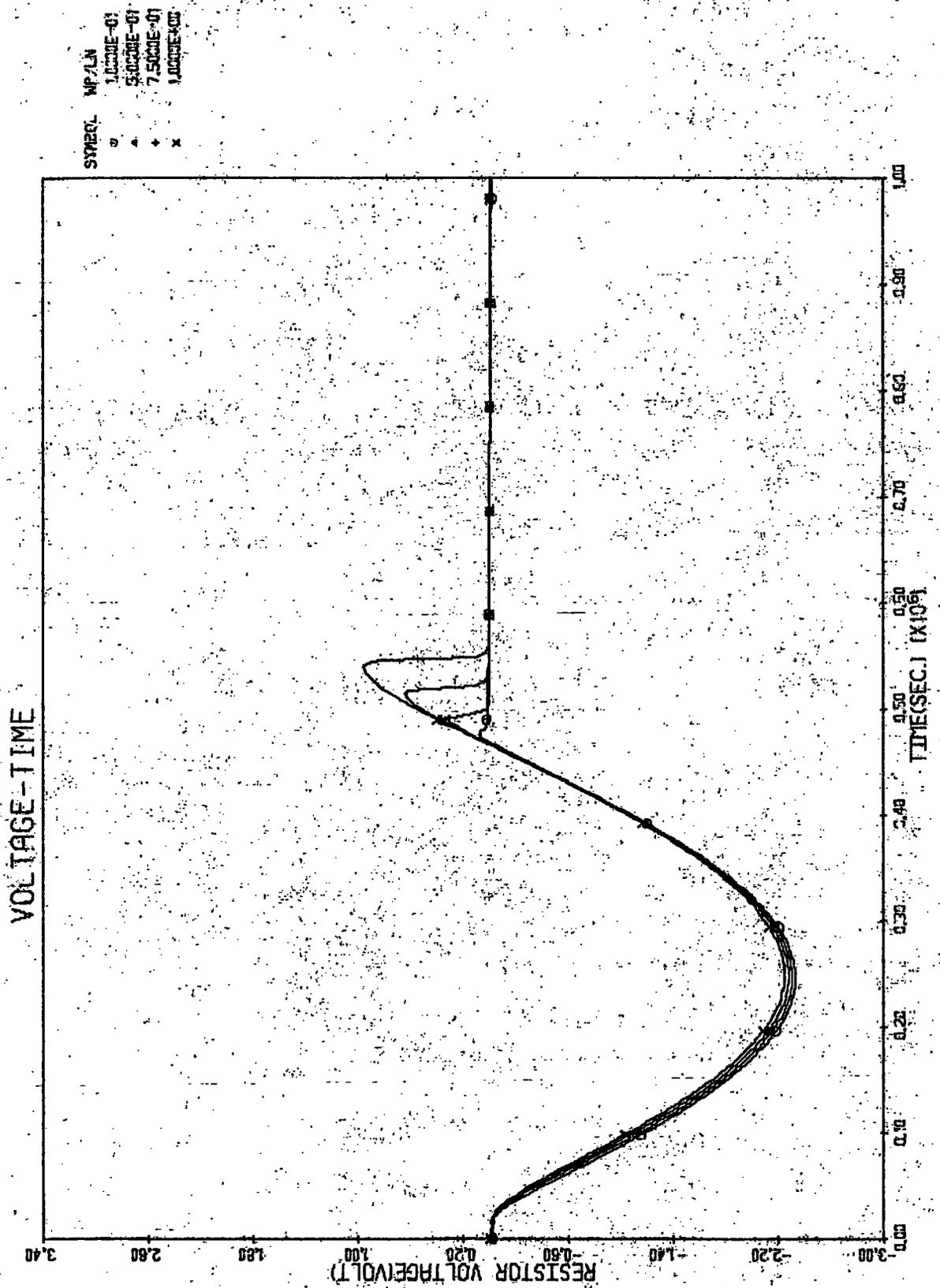
FIGURE (5.21)

c) Diodes with the same width.

Figs. 5.22 to 5.24 show the effect of minority carrier lifetimes having values from 0.1 millisecond to 0.1 nanosecond on the response of the diodes whose widths are fixed at 10 microns.

Under this condition, there are two effects involved: the direct effect of varying the lifetime; and the indirect effect of changing the normalized width, W_p/L_n.
The results in section a) and b) reveal that these effects act in opposite directions. For instance, the increase of the lifetime produces more stored charge, but it subsequently decreases the normalized width which results in the reduction of the stored charge. In this section, the results can therefore be described by the combination of the two effects.

During the reverse half cycle, Fig.(5.22) shows that the storage delay time and overshoot effect are small and nearly constant for the long lifetime diodes. They are relatively smaller and eventually vanish for the shorter lifetime diodes.

During the forward half cycle, the results show that for the long lifetime diodes there exists a maximum current which agree with the results observed in chapter 4. For the shorter lifetime diodes, the current is significantly decreased due to the increase of the bulk resistance.

The responses obtained from the preceeding sinusoidal excitations show good agreement with the results predicted by analytical methods <7><8>, and confirm the intuitive results that in order to achieve a good high speed

switching action, it is necessary to

a) decrease the minority carrier lifetime or

b) reduce the size of the diode.

CURRENT - TIME
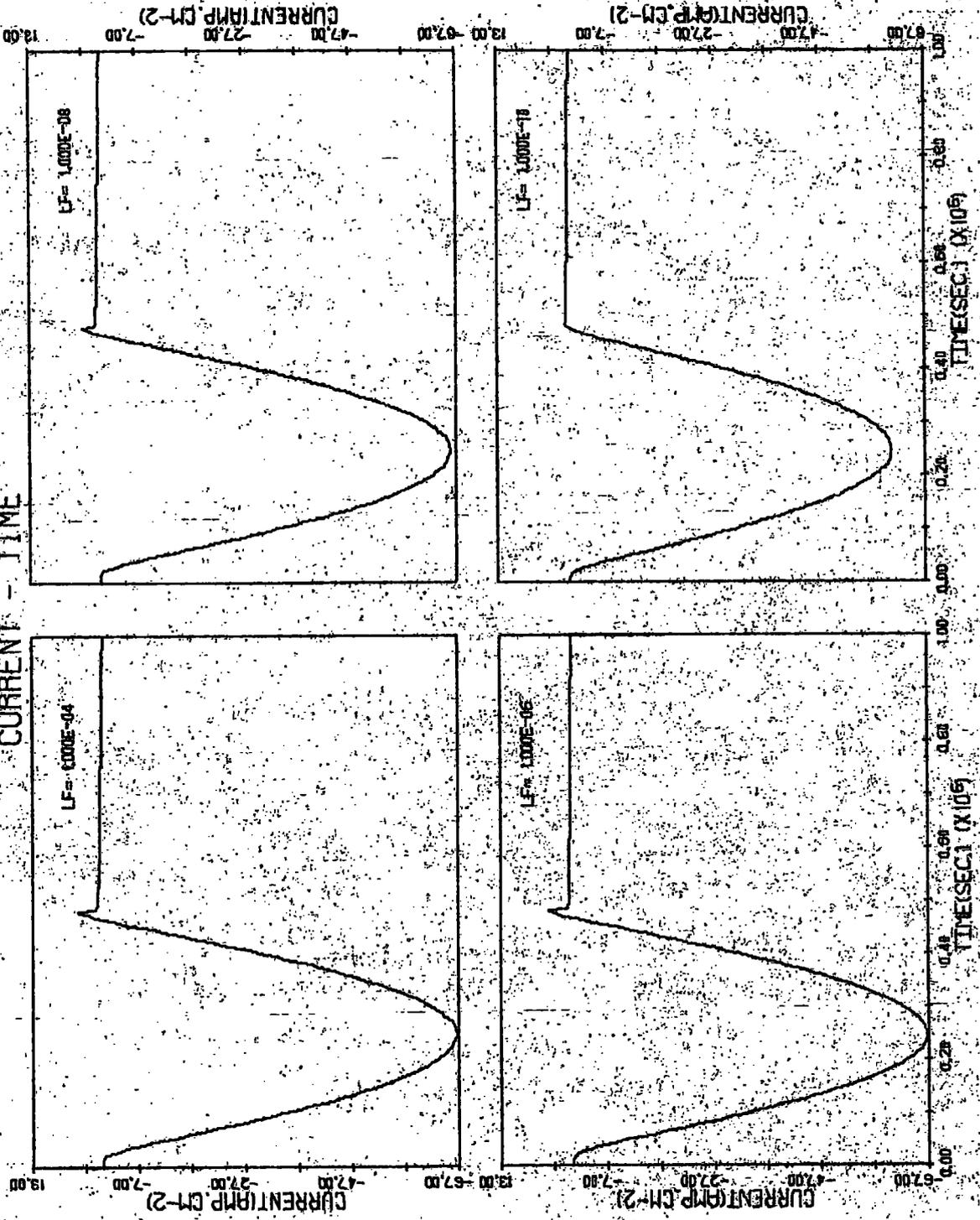
FIGURE (5.22)

FIGURE (5.23)
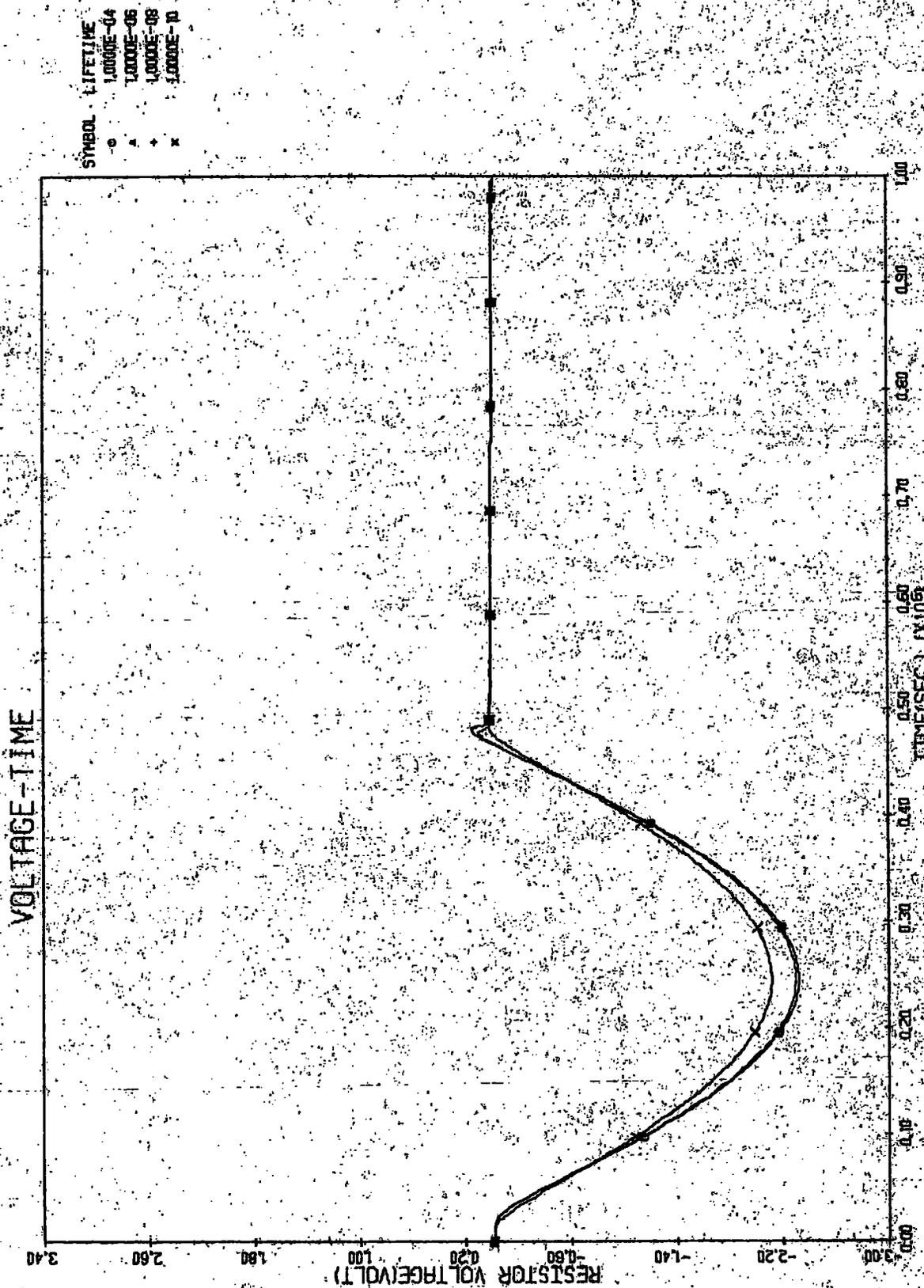
FIGURE (5.24)

Chapter 6.

Harmonic Analysis of p-n Junction Diode.

In principle, the duality between the time and frequency domains makes it possible to study the behaviour of a semiconductor device from either viewpoint. However, some phenomena may be difficult to detect in one domain, but they could be prominent in the other. Also specific information in the frequency domain is required in some applications, for instance, in harmonic generation, distortion measurement, modulation, oscillation, etc.. It is therefore worthwhile investigating the device characteristic in this domain.

Most previous analysis in the frequency domain has relied on certain series representations to denote nonlinearity in the transfer function of the device, and together with the Fourier Transform, the device performance can then be predicted. This approach is limited to slightly nonlinear, i.e., small signal cases <23> , or it depends on an approximation to the characteristic of the devices <27>. However, if an exact response is already available, then the Fourier Transformation can be directly applied to provide a solution in the frequency domain. This approach can preserve the exactness of a solution and is relatively simple to use.

In this chapter, we shall first introduce the Discrete Fourier Transformation and its application in harmonic analysis. This will be applied to the steady-state responses from sinusoidal excitation obtained from chapter

4 and 5 . Finally, the effect of minority carrier lifetime
on harmonic generation is considered.

6.1 Application of the Discrete Fourier Transform in Harmonic Analysis.

To determine the Fourier Transform of a function g(t)
by mean of numerical techniques, it is necessary that the
function to be transformed be represented by discrete
samples usually at equally spaced time intervals T
corresponding to the sampling frequency f_s. The effect
of sampling may add severe distortion to the original
function if the sampling frequency is too low, i.e, less
that twice the highest frequency component of g(t). This
is the so-called aliasing effect in which high frequency
components of g(t) can impersonate low frequencies.

The duality property of the Fourier Transform implies
that sampling in the time domain results in a function
periodic in frequency and sampling in the frequency domain
results in a function periodic in time. Therefore, the
Discrete Fourier Transform requires that both the original
time and frequency functions be modified such that they
become periodic functions in which N time samples and N
frequency values correspond to a period of time and
frequency domain waveform respectively.

For transformation from the time to frequency domain,
this can be done by truncating the sampled function to a
finite interval, and considering the function within this
interval as one period of the periodic function in the time
domain. Therefore, Fourier Transformation is required for

only one period of the function.

The truncation is however equivalent to multiplying the signal by a rectangular window function. If the time period under consideration is equal to T_o seconds, the rectangular window function is defined by

$$w(kT) = \begin{cases} 1 & 0 < kT < T_o \\ 0 & \text{otherwise} \end{cases} \qquad (6.1)$$

the relation between the arguments in the time and frequency domain is given in Fig. 6.1 and the discrete Fourier Transform pair is defined by

$$g(kT) = \frac{1}{N} \sum_{n=0}^{N-1} G(nf) \cdot e^{j2\pi nk/N} \qquad (6.2)$$

d

$$G(nf) = \sum_{k=0}^{N-1} g(kT) \cdot e^{-j2\pi nk/N} \qquad (6.3)$$

where

$k = 0,1,2,\ldots\ldots\ldots,N-1$

$n = 0,1,2,\ldots\ldots\ldots,N-1$

$T_o = NT$

$\frac{1}{T} = f_s$

$f_s = Nf$

$\frac{1}{f} = T_o$
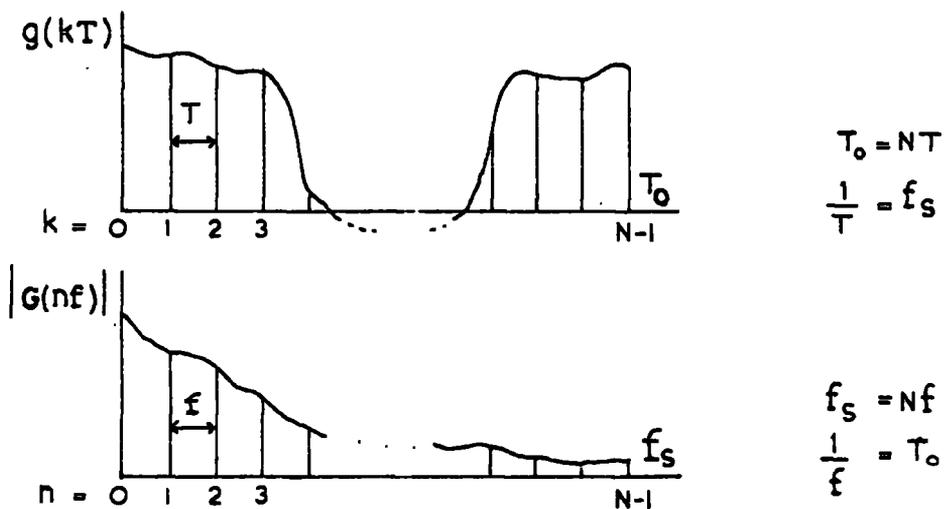
Figure 6.1 Relation between the arguments in the time and frequency domains.

By applying the Discrete Fourier Transform to w(kT) in equation 6.1, we can write

$$W(nf) = \sum_{k=0}^{N-1} e^{-j2\pi nk/N}$$

$$= \frac{1 - e^{-j2\pi nfTN}}{1 - e^{-j2\pi nfT}}$$

$$= e^{-j\pi nfT(N-1)} \cdot \frac{\sin(\pi nfT_o)}{\sin(\pi nfT)} \qquad (6.4)$$

Equation 6.4 indicates that truncation in time domain can introduce a ripple in the frequency domain. This is analogous to the Gibb's phenomenon in the continuous system where truncation introduces a singularlity. This effect can be minimized by employing a non-rectangular window function in order to reduce the singularlity.

However, if the sampled and truncated function is an integral multiple of the period of the function g(t), equation 6.4 shows that the ripple vanishes.

In harmonic analysis, the time domain steady-state solution is normally periodic. If N sample values of this solution represent exactly one complete period, the resulting discrete transform is then ripple-free.

Computation of the transform defined in equations 6.1 and 6.2 requires N^2 mathematical operations on complex quantities which uses considerable computational time and introduce round off error. The use of a Fast Fourier Transform algorithm in which only $2N\log_2 N$ operation are required leads to a substantial reduction of the time and

error. The FFT algorithm can be interpreted in terms of combining the DFTs of the individual data samples in such a way that the occurence times of the samples are taken into account sequentially. These can then applied to the DFTs of progressively larger mutually exclusive subgroups of data samples, which are combined to produce the DFT of the complete set samples. The derivation and computer programming of the FFT algorithm has been widely discussed in the literature and it is available on most main frame computers; for example the NAG package on the NUMAC computer system. Therefore, detailed discussion of this algorithm will be omitted here.

6.2 Harmonic generation in p-n junction diodes.

In chapters 4 and 5, the influences of minority carrier lifetime on the terminal characteristics and responses of. p-n junction diode have been studied intensively. We shall in this chapter consider this effect on harmonic generation in the frequency domain.

For convenience throughout this chapter a response to sinusoidal excitation which is obtained from solving the simple R-D circuit in chapter 4 will be referred to as a "static" response, and a static spectrum denotes its transform pair in the frequency domain. Similarly, the term "dynamic" will be used when dealing with a steady-state response to the sinusoidal excitation as described in chapter 5.

It has been seen that the static response provides nearly ideal half-wave rectification, because of the very

small reverse current in comparison with the forward current. On the other hand, the dynamic response depends not only on the forward characteristic but also on the important effect of stored charge seen in the reverse direction.

Firstly, we shall investigate the dynamic spectrum considering harmonic generation in both forward and reverse directions. Later harmonic generation in each direction will be considered separately. The nonlinear effect in the forward direction can be obtained by subtracting the dynamic response from the associated half-sinusoidal response. On the other hand, the effect in the reverse direction may be obtained by subtracting the static characteristic from the associated dynamic characteristic. This however requires identical environment for each corresponding pair. That is to say the frequency, accuracy etc., must be the same in each case.

In practice, this can not be easily done, because the static response is valid only at very low frequency. The corresponding computer time for a dynamic response at the same frequency is large. However, an alternative method is simply to suppress the forward half cycle of the dynamic response. The remainder is a close approximation to the required effect in the reverse direction, and the suppressed part will be referred to as a quasi-static characteristic.

6.3 Effect of minority carrier lifetimes on harmonic
generation.

a) Diodeswith the same size.

Fig. 6.2   is reproduced from chapter 5 showing the
dynamic response in the time domain of diodes having the
same size (10 microns) , but with lifetime varying from 0.1
nanosecond to 100 microseconds.   Each response was
calculated at 256 points, so that the Fast Fourier
Transform can be directly applied, this results in the
spectra depicted in Fig. 6.3. To aid interpretation, the
odd and even harmonics are separately identified.   These
results confirm the existence of an optimum value of
lifetime as described in chapter 4 and 5. No variation of
the spectra can be seen at longer lifetimes. The harmonic
level becomes relatively smooth for higher orders.   When
the lifetime is very short, 0.1 nanosecond, the higher
harmonics become substantially reduced, and ripples in the
odd and even spectra appear.

Fig. 6.4 shows the associated quasi-static spectra,
the results indicate that the magnitude of the odd
harmonics follow a sinc-like function where a different
sinc-like function holds for the even harmonics. For long
lifetime diodes, the spectrum is less sensitive to the
variation of the lifetime.   However, when the lifetime is
very short, the period of the ripples becomes longer.

For comparison with the results that would have been
obtained if the diode characteristic were linear, Figs. 6.5

and 6.6 show the ideal half-sinusoidal responses and their spectra. These half-sinusoidal responses are simulated with the same amplitude as the quasi-static responses shown in Fig. 6.2. The spectrum reveals the monotonic decrease of both odd and even harmonics, which are evaluated from

$$F(nf) = -\frac{1}{2j} e^{j\pi(fT-n/N)(N/2-1)} \cdot \frac{\sin(\pi(fT_o-n)/2)}{\sin(\pi(fT-n/N))}$$

$$+\frac{1}{2j} e^{-j\pi(fT+n/N)(N/2-1)} \cdot \frac{\sin(\pi(fT_o+n)/2)}{\sin(\pi(fT+n/N))}$$

The results of Figs. 6.4 and 6.6 indicate that the distorted half-sinusoidal waveform due to the nonlinear property of the device is responsible for the ripples seen in the quasi-static spectrum. This nonlinearity is clear from the exponential nature of the current-voltage characteristics. The exact static characteristic obtained in chapter 4 shows multi-exponential behaviour, but in practice, is normally approximated to only single exponential. A question arises then, whether this approximation affects the ripples and the spectrum. Using the algorithm developed in section (4.7), Fig. 6.7 shows the quasi-static spectra obtained from the responses to the sinusoidal excitations applied to the diodes having the exact static characteristic and the approximated single exponential characteristic respectively. For an output current of 11.50 amp/cm^{-2} or 2.44 in the natural log scale, the results reveal that there is a slight variation only in certain harmonic components. The approximation appears to have little influence on the ripple and the

spectrum at low frequency, and this influence may be neglected.

By subtracting the quasi-static responses from the ideal half-sinusoidal responses, the nonlinear effect in the forward direction is shown in Fig. 6.8 for various values of the lifetimes. The influence of the lifetime is obscure in these time domain responses, but it is prominent in the frequency domain spectra given in Fig. 6.9. These spectra also reveal that there is no variation of the spectrum for lifetime values between 1 microsecond and 10 microseconds. As the lifetime decreases further, the even harmonics change relatively faster than the odd harmonics, and eventually become dominant. The higher harmonics of both odd and even components gradually decrease.

To observe the influence of the lifetime in the reverse direction, the quasi-static spectrum is subtracted from its corresponding dynamic spectrum. We then obtain the overshoot effect and its transform pair shown in Figs. 6.10 and 6.11 respectively. For the diodes under consideration, the overshoot is very small, and it begins to disappear as the lifetime is shorten. The spectrum shown in Fig. 6.11 has nearly constant magnitude for most harmonics in each case. When the lifetime is varied the results also show that there is no variation in the spectra for the longer lifetime diodes. However, for a very short lifetime diode, the higher harmonic content becomes very small.

A pseudo 3-dimensional plot of the dynamic spectrum at various values of lifetime from 0.1 nanosecond to 0.1

millisecond is given in Fig. 6.12 in which the variation
of each harmonic component can be observed.

EFFECT OF LIFETIME ON DYNAMIC RESPONSE
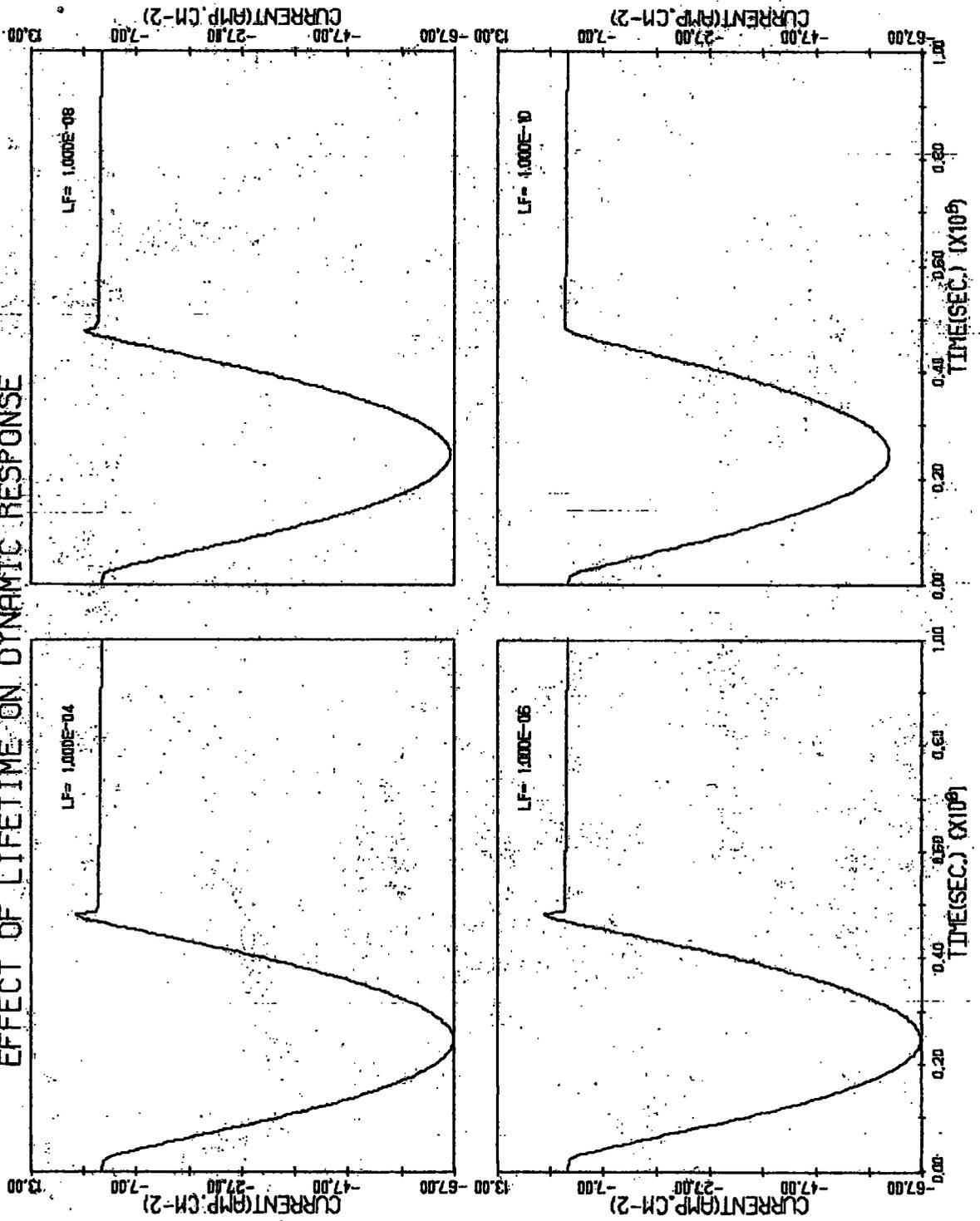
FIGURE (6.2)

FIGURE (6.3)

QUASI-STATIC SPECTRUM
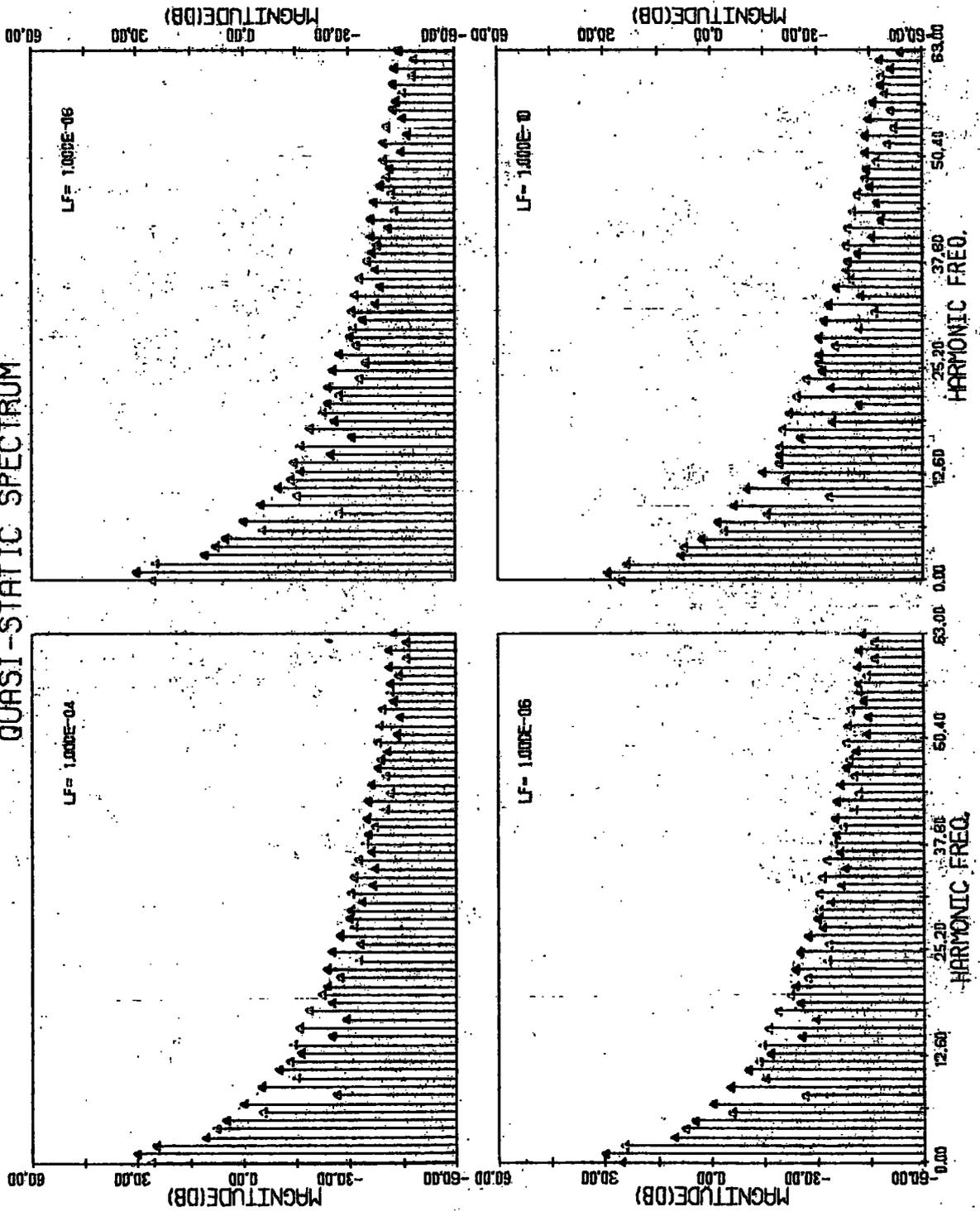
DIODES WITH THE SAME WIDTH OF 10 MICRON

FIGURE (6.4).

HALF-SINUSOIDAL RESPONSE
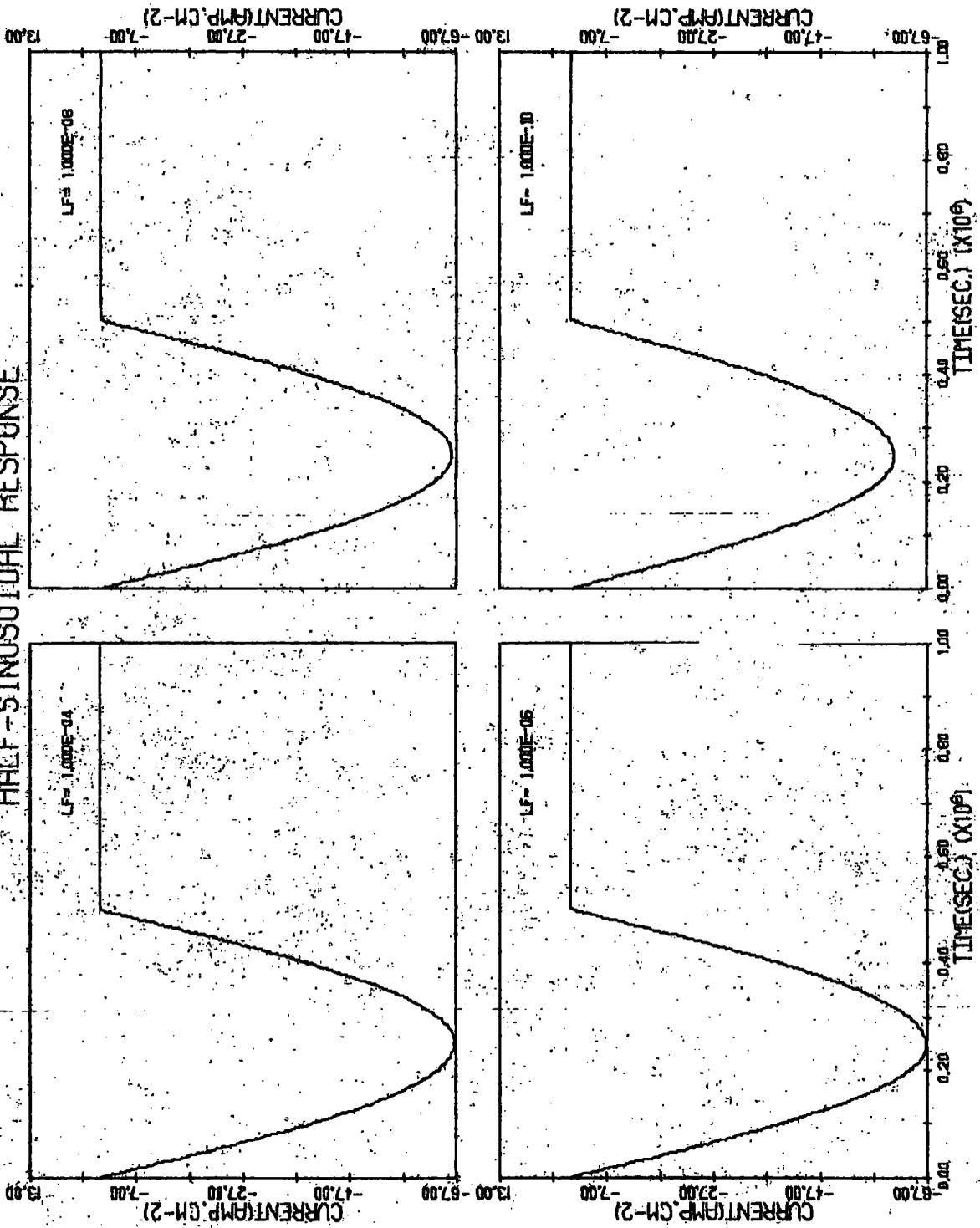
DIODES WITH THE SAME WIDTH OF 10 MICRON

FIGURE (6.5)
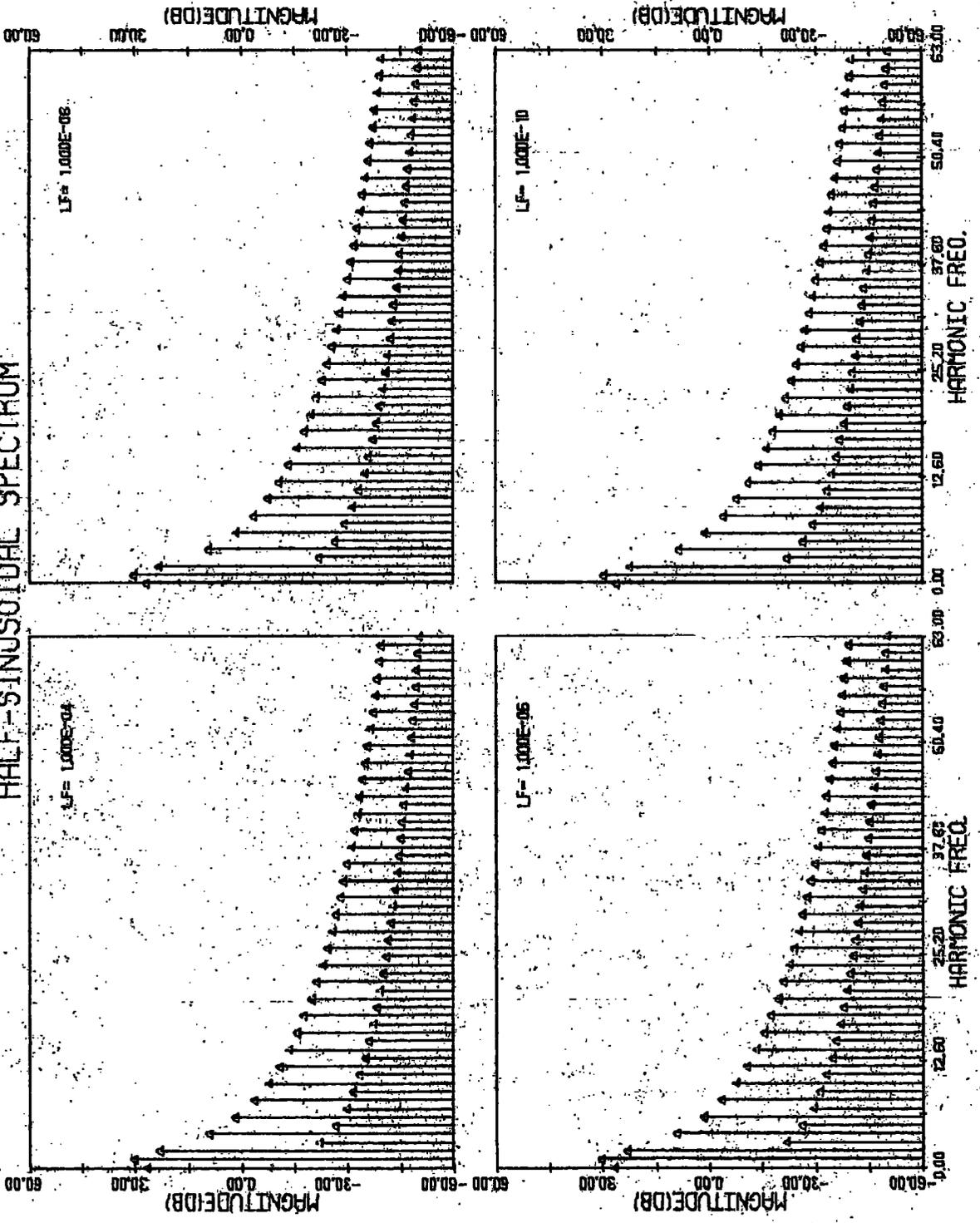
FIGURE (6.6)

STATIC CHARACTERISTIC AND SPECTRUM
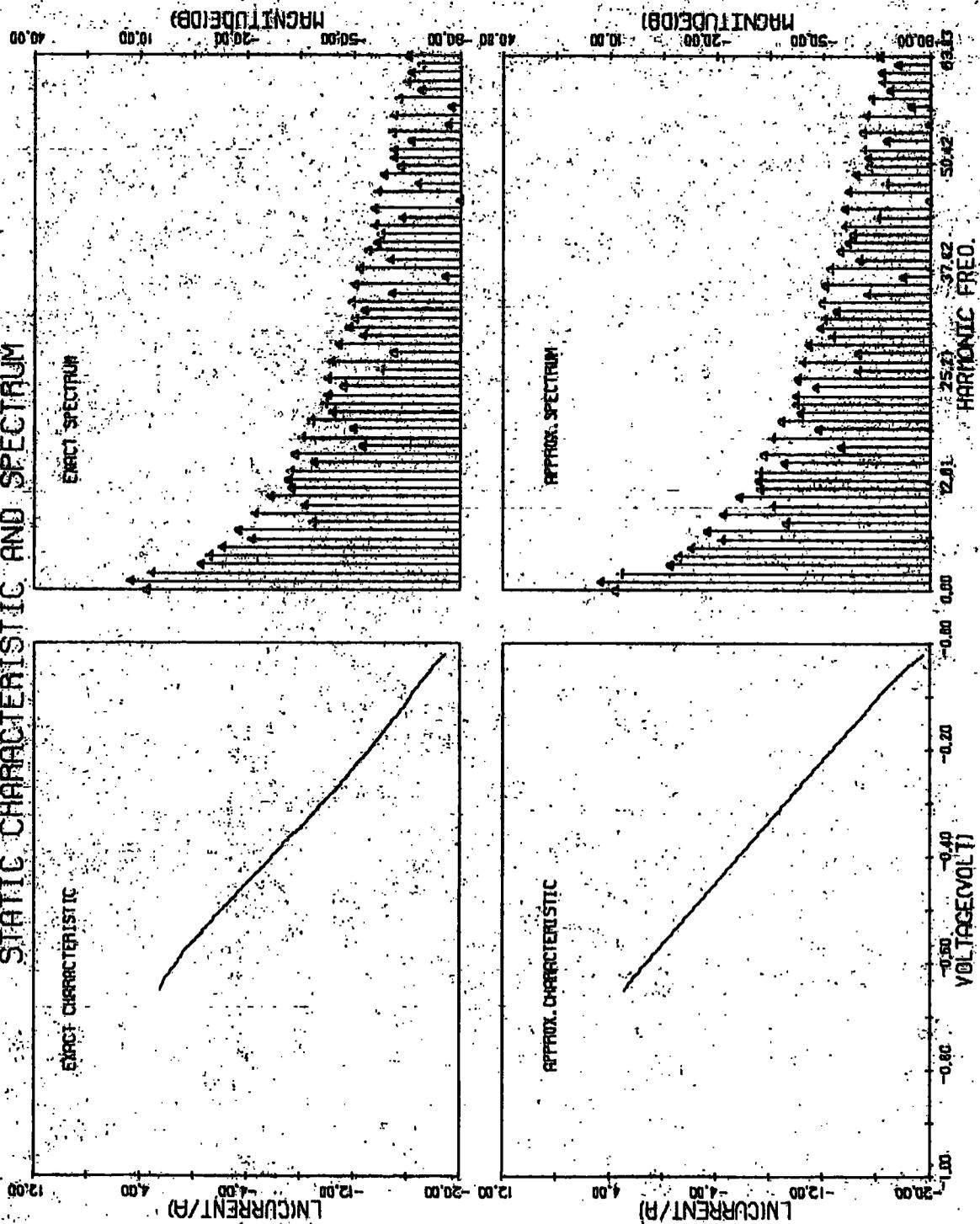
FIGURE (6.7)

EFFECT OF LIFETIME ON FORWARD BIASED RESPONSE
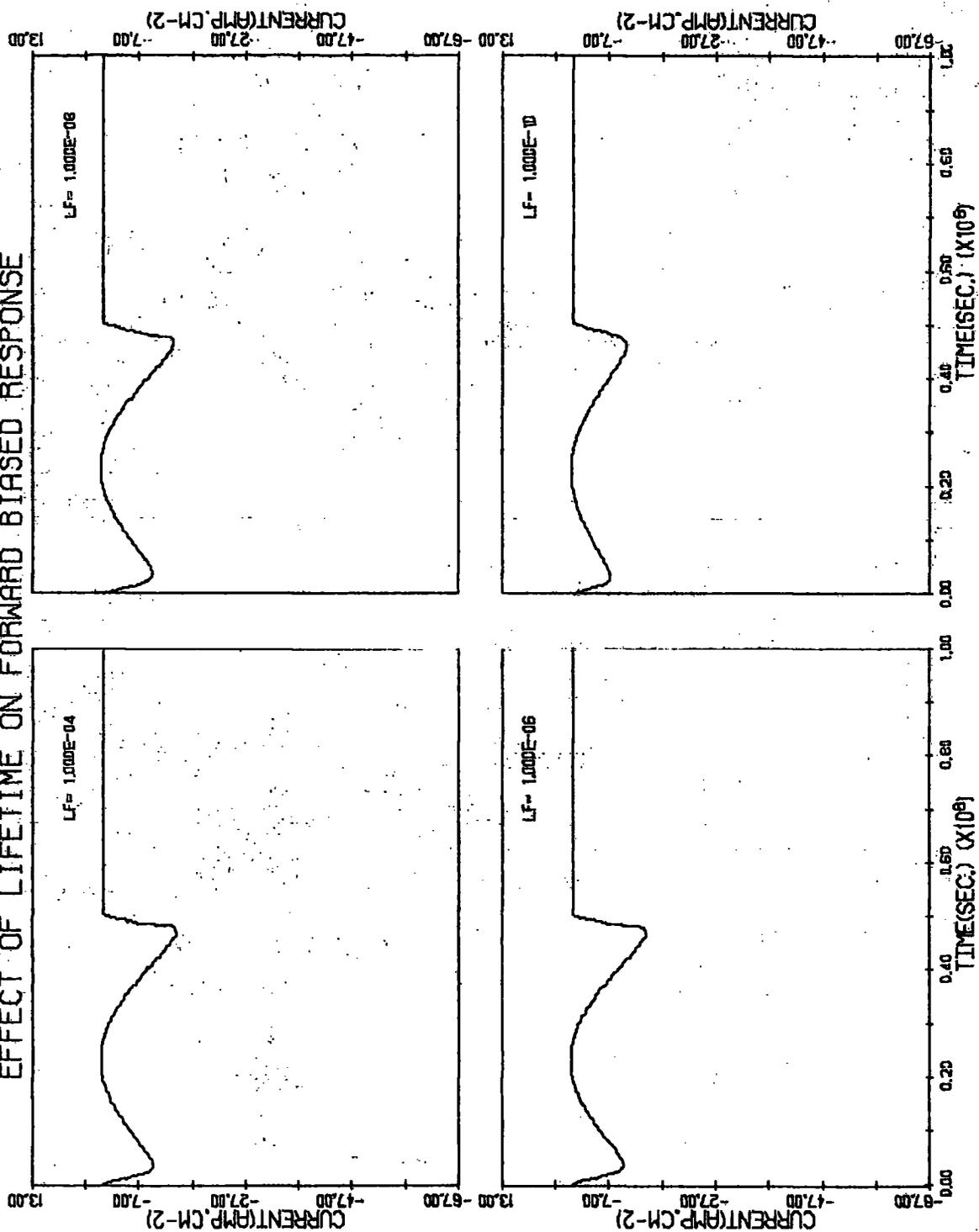
FIGURE (6.8)

EFFECT OF LIFETIME ON FORWARD BIASED SPECTRUM
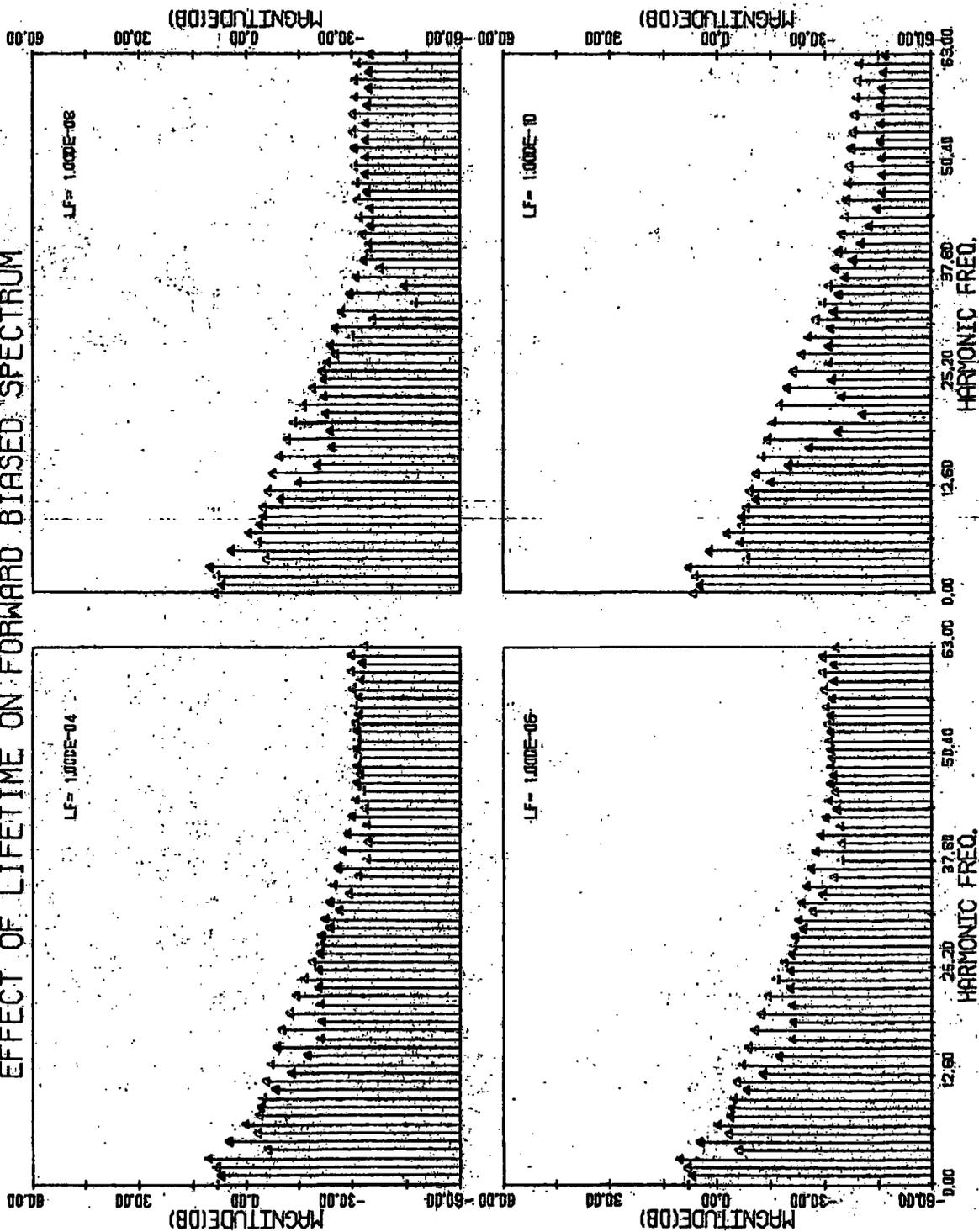
DIODES WITH THE SAME WIDTH OF 10 MICRON

FIGURE (6.9)

EFFECT OF LIFETIME ON REVERSE BIASED RESPONSE
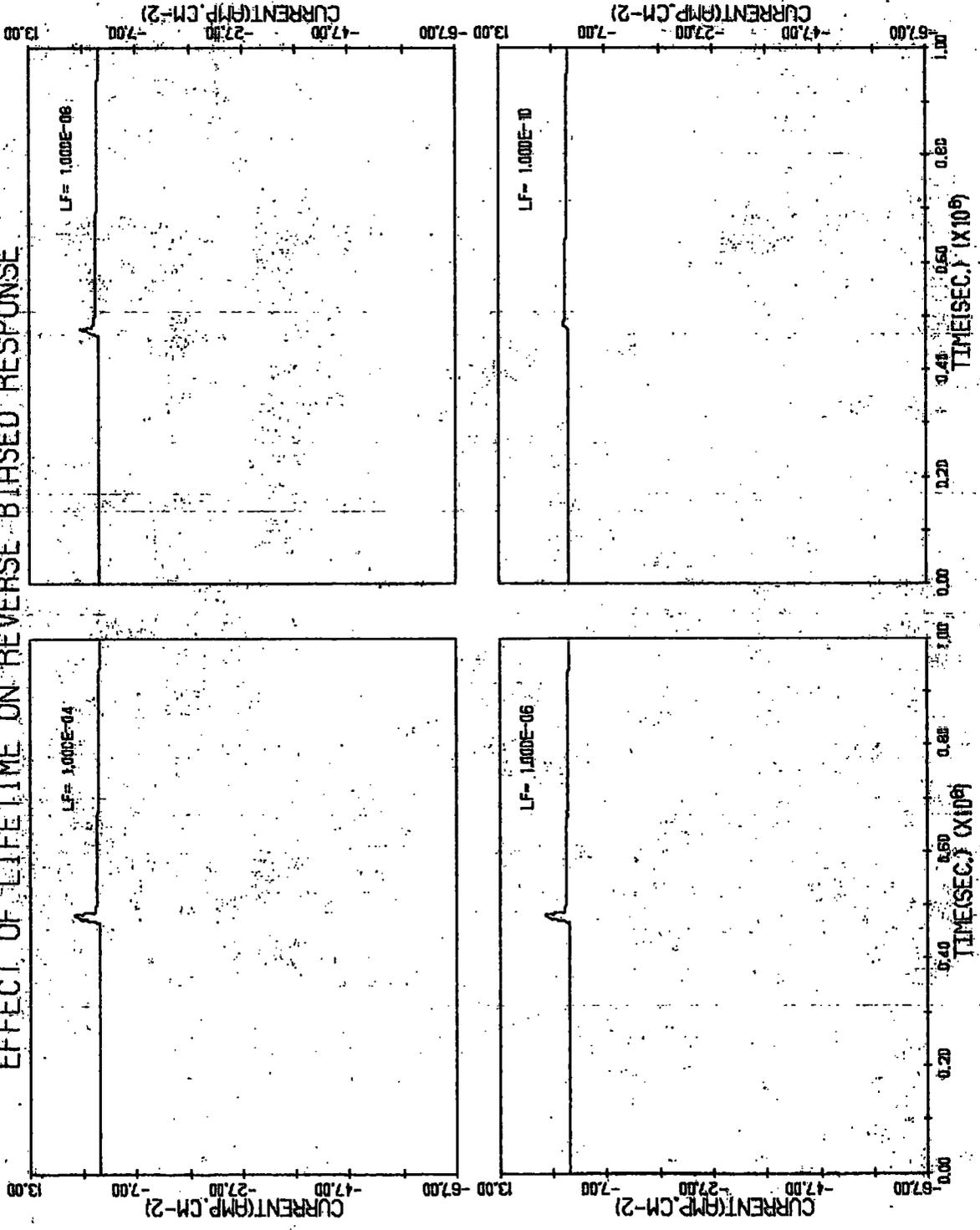
FIGURE (6.10)

EFFECT OF LIFETIME ON REVERSE BIASED SPECTRUM
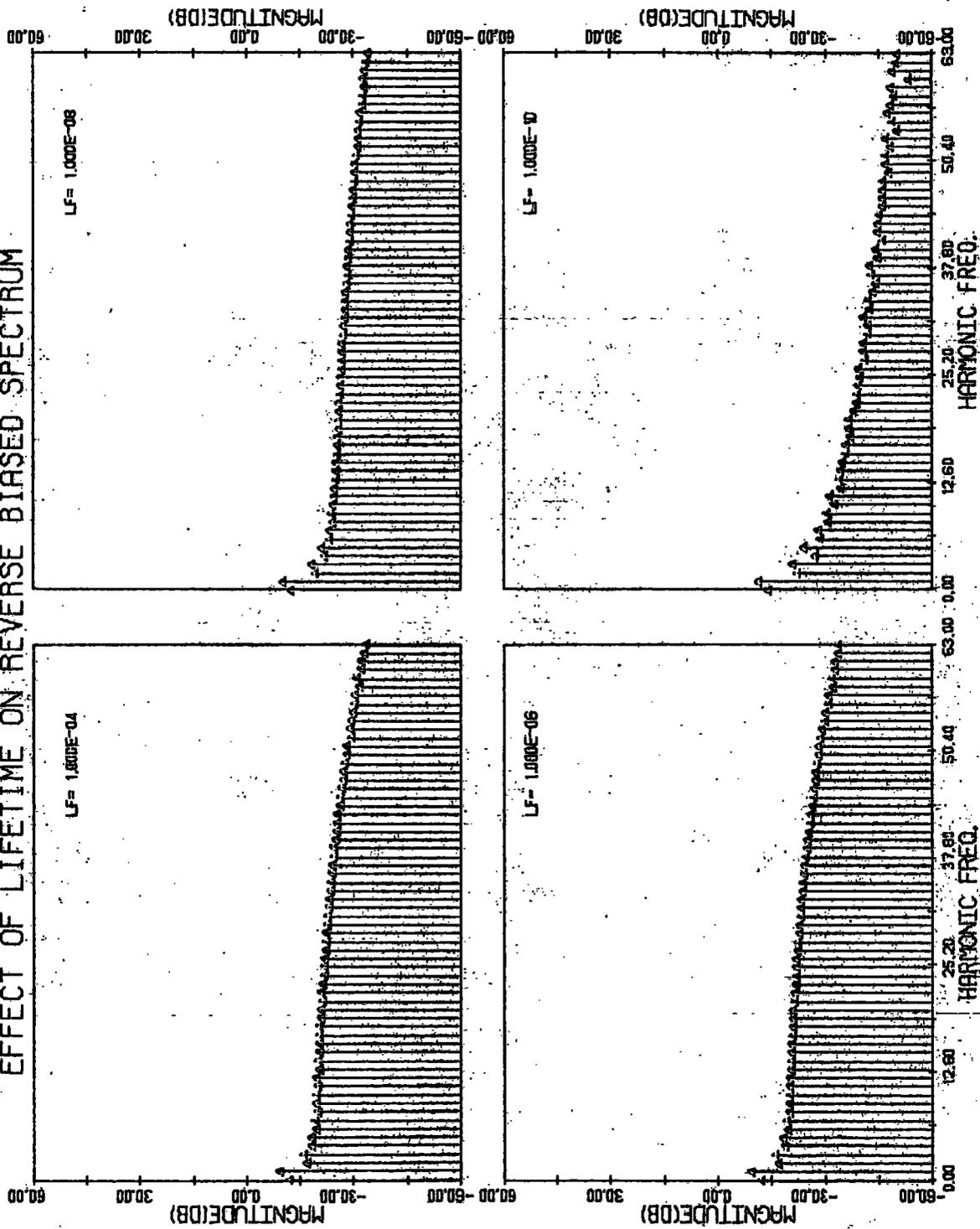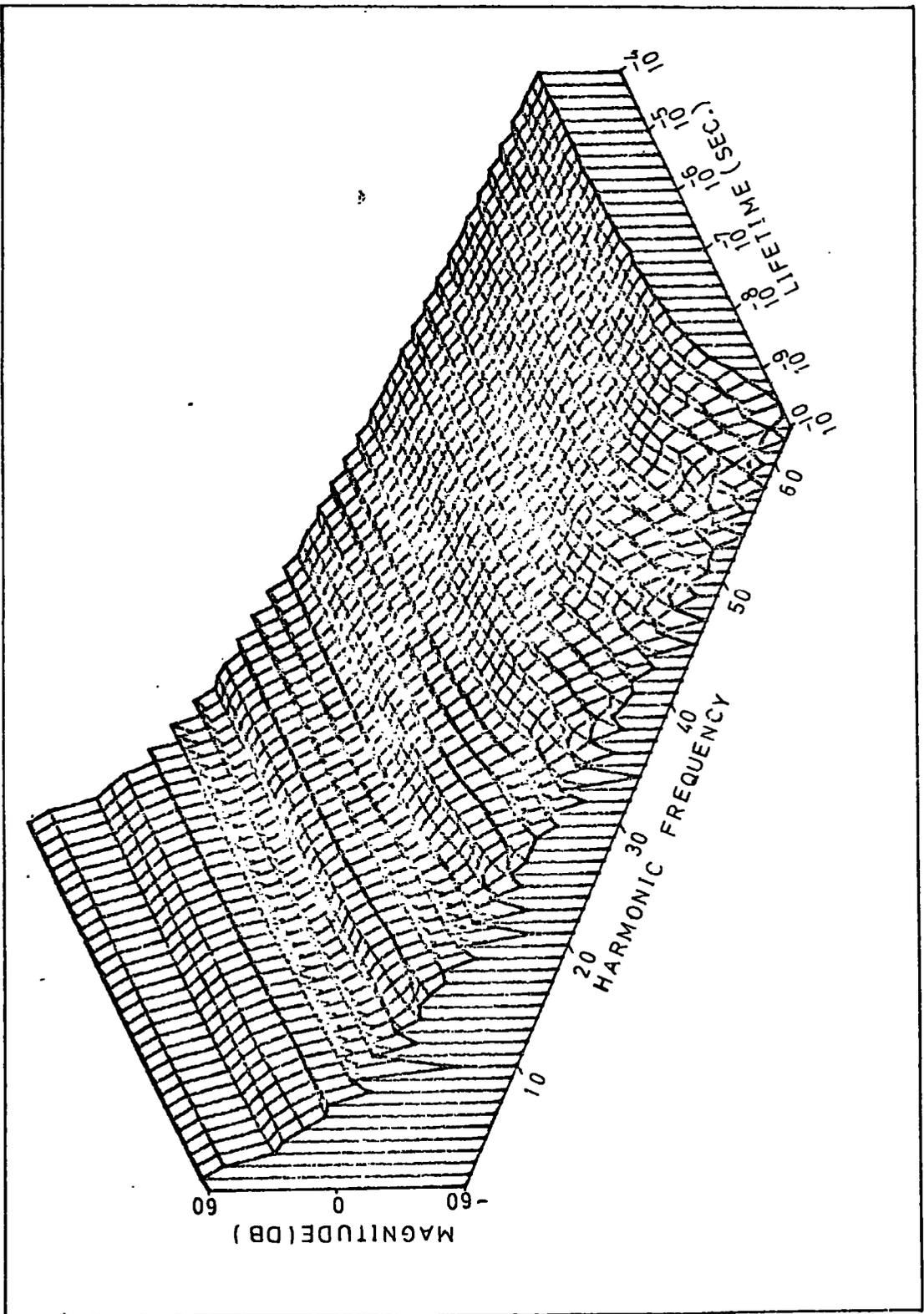
FIGURE (6.11)

FIGURE (6.12)

b) <u>Diodes with the same ratio of</u> W_p/L_n.

Figs. 6.13 and 6.14 show the dynamic responses and their transform pairs of diodes of the same recombination criteria, i.e, the same normalized width, $W_p/L_n=1$. The lifetime varies from 1 microsecond to 10 nanoseconds. The long lifetime diodes with large overshoot give nearly smooth spectra. As the lifetime decreases, the even harmonics are seen to decrease relatively faster than the odd harmonics. Ripples become apparent in the lower harmonics at first, and later are seen in higher order harmonics as well.

The quasi-static spectra given in Fig. 6.5 show the direct effect of lifetime on the distorted half-sinusoidal responses. The shortening of the lifetime seems to reduce the minimum values of the ripples, while the peaks of the ripples remain unchanged.

Figs. 6.16 and 5.17 show the direct influence of the lifetime on the time domain response in the forward direction and its corresponding spectrum respectively. For the long lifetime diodes the decrease of the current in the time domain resulting from the increase of the lifetime, has little effect on the spectrum. However, as the lifetime decreases further, at the value of 0.1 and 0.01 microsecond, the influence of the lifetime becomes prominent. The odd harmonics decrease in magnitude and the even harmonics become dominant.

The direct effect of the lifetime in the reverse direction is shown in Figs. 6.18 and 5.19. The large overshoot of the long lifetime diode produces a spectrum

which is similar to that of an impulse response. The shortening of the lifetime decreases both magnitude and width of the overshoot, which results in a reduction in magnitude of the harmonics and an increase in the period of the ripples.

The results obtained suggest that the direct effect of increasing the lifetime in both forward and reverse directions is to promote the smoothness and relatively stability of the dynamic spectrum. In addition, Fig. 6.20 also provides a pseudo 3-dimensional plot of the dynamic spectrum of the diodes at various lifetimes, from 0.1 nanosecond to 1 microsecond.

EFFECT OF LIFETIME ON DYNAMIC RESPONSE
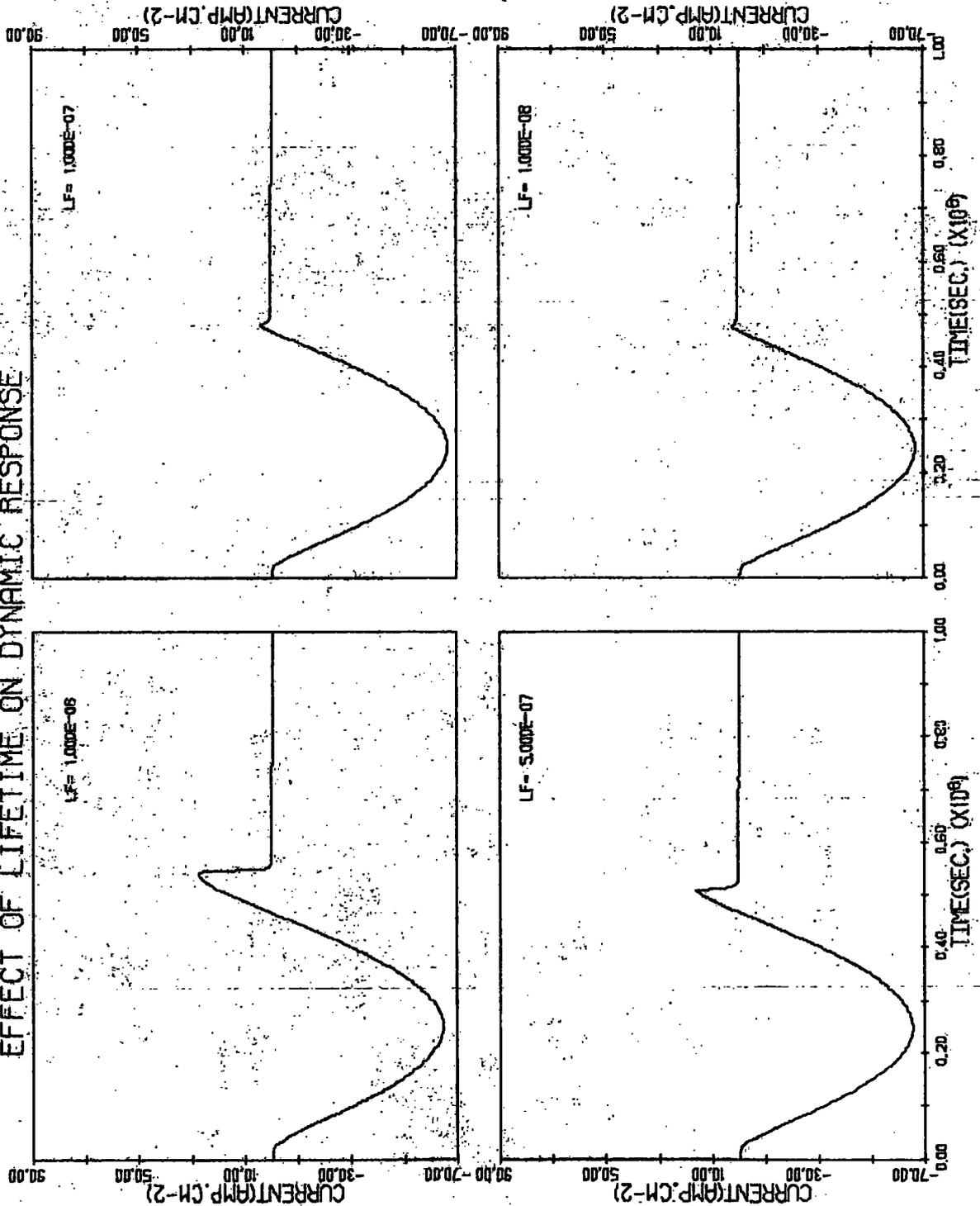
FIGURE (6.13)

DYNAMIC SPECTRUM
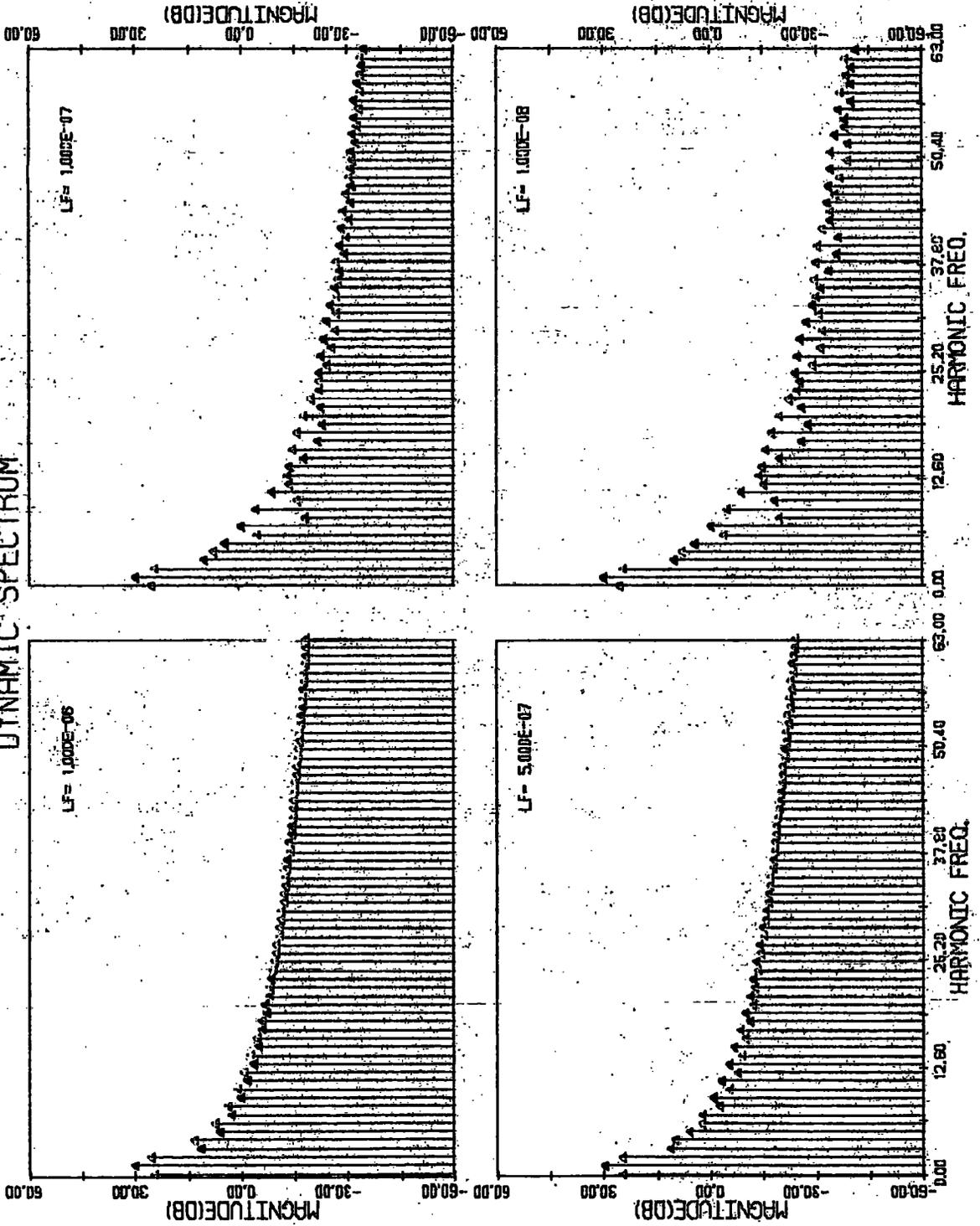
FIGURE (6.14)

QUASI-STATIC SPECTRUM
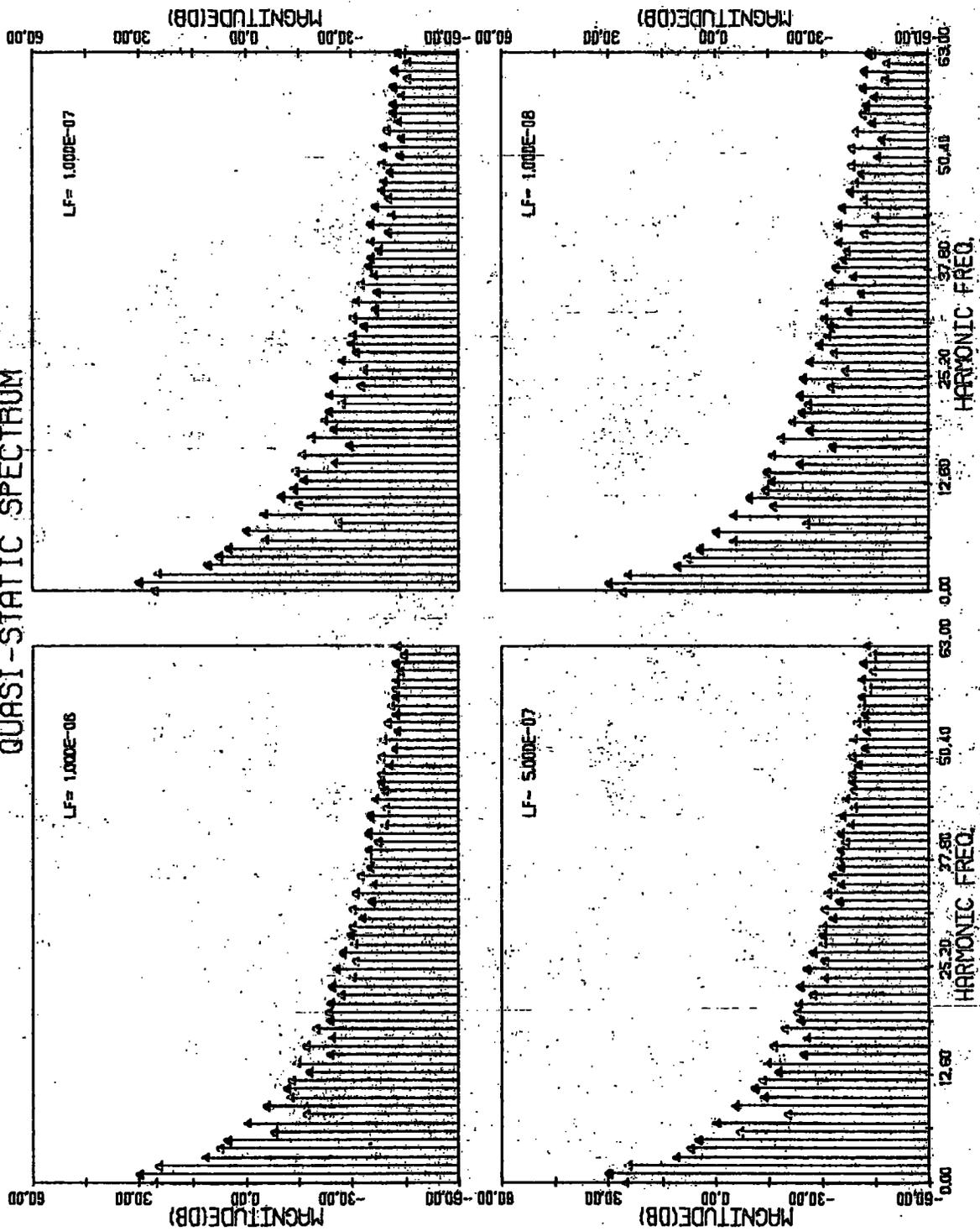
FIGURE (6.15)
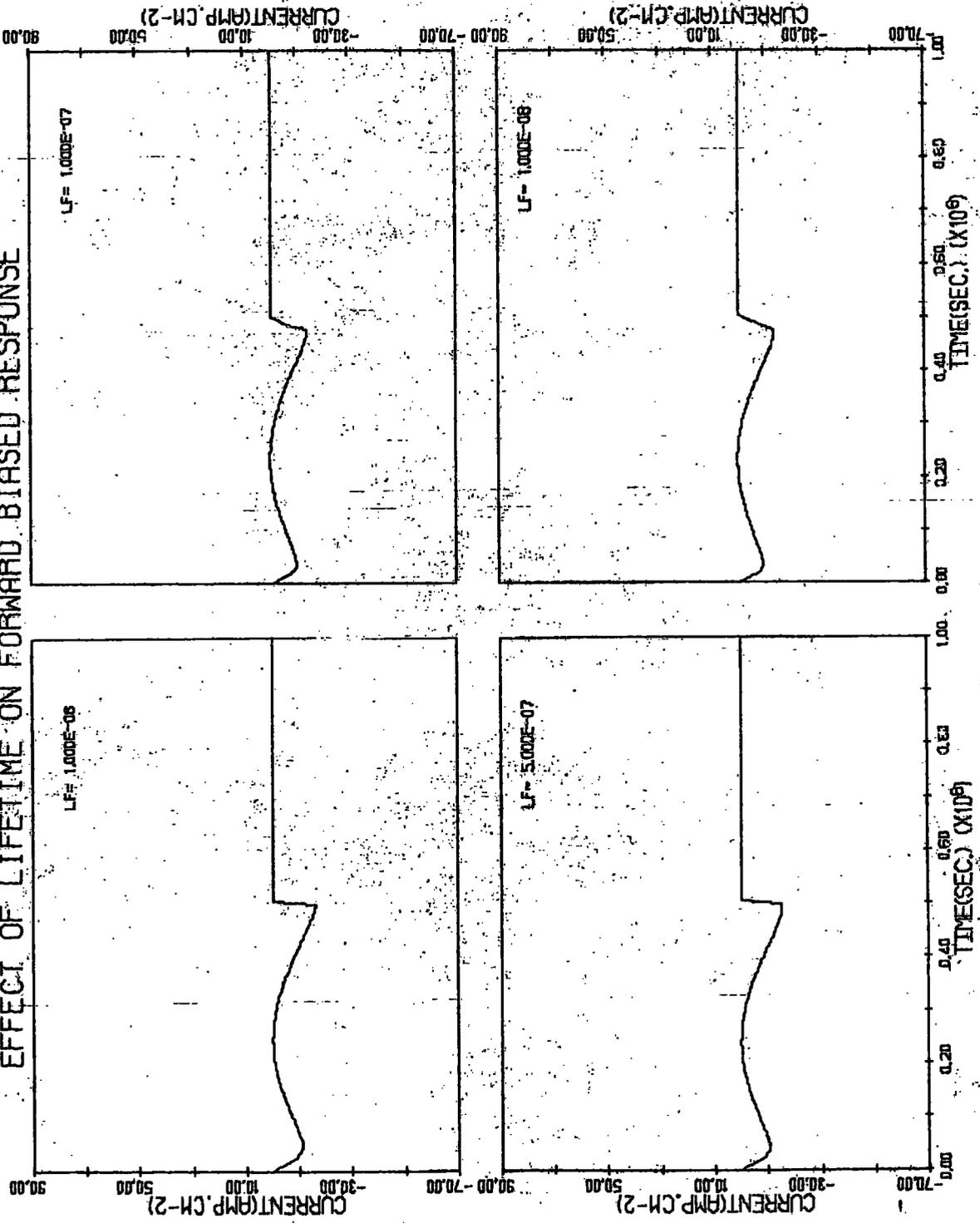
EFFECT OF LIFETIME ON FORWARD BIASED RESPONSE

FIGURE (6.16)

EFFECT OF LIFETIME ON FORWARD BIASED SPECTRUM
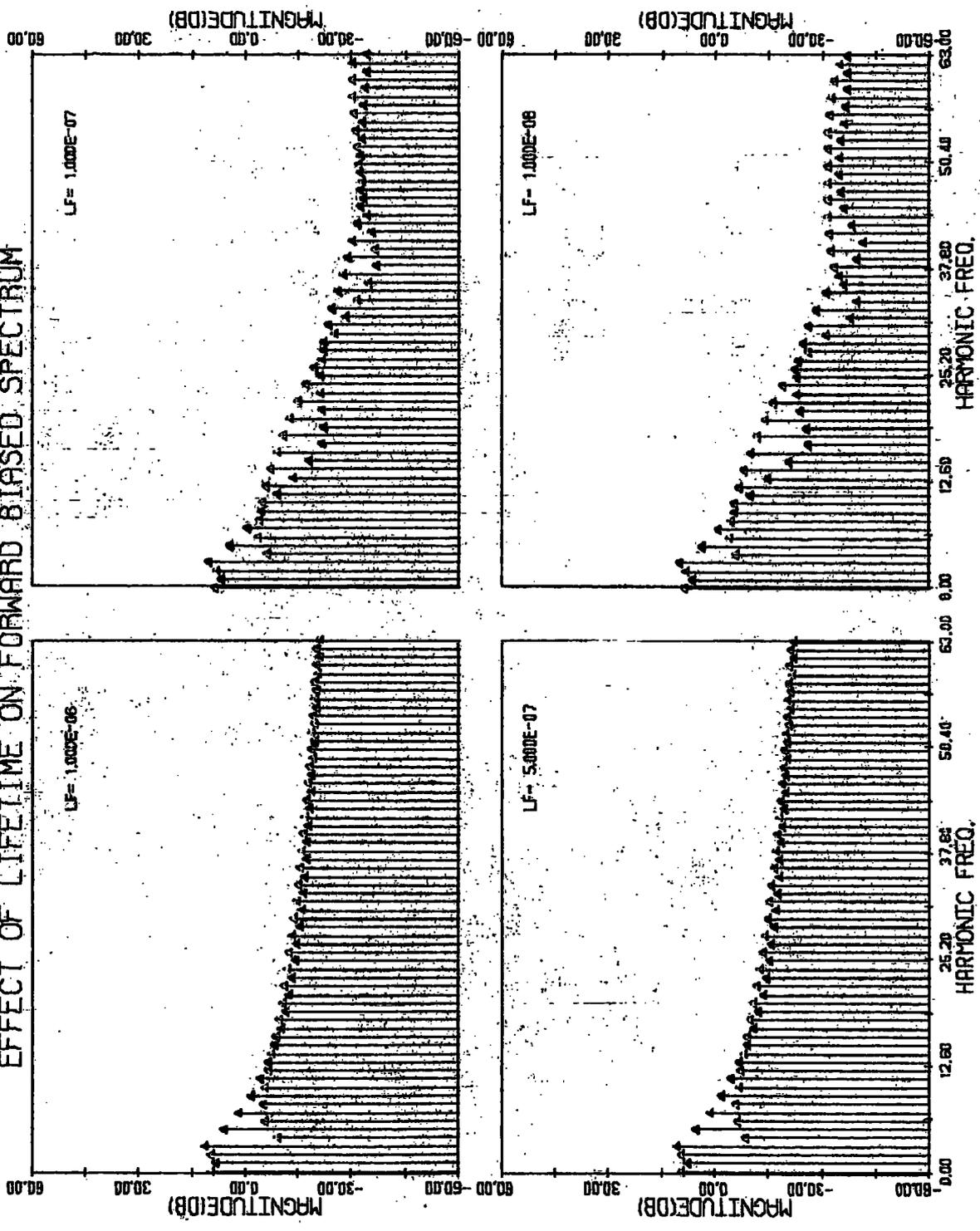
FIGURE (6.17)

EFFECT OF LIFETIME ON REVERSE BIASED RESPONSE
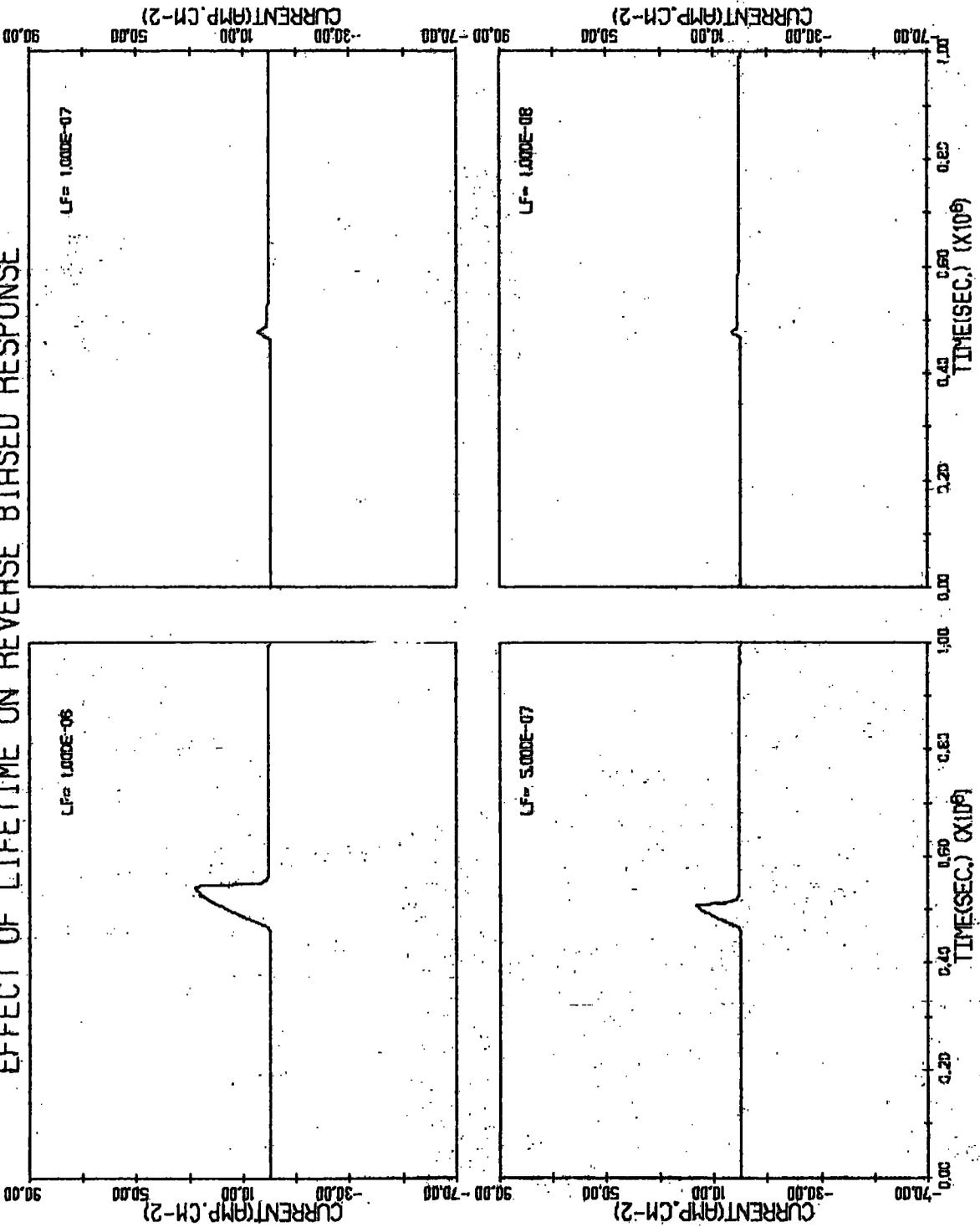
FIGURE (6.18)

EFFECT OF LIFETIME ON REVERSE BIASED SPECTRUM
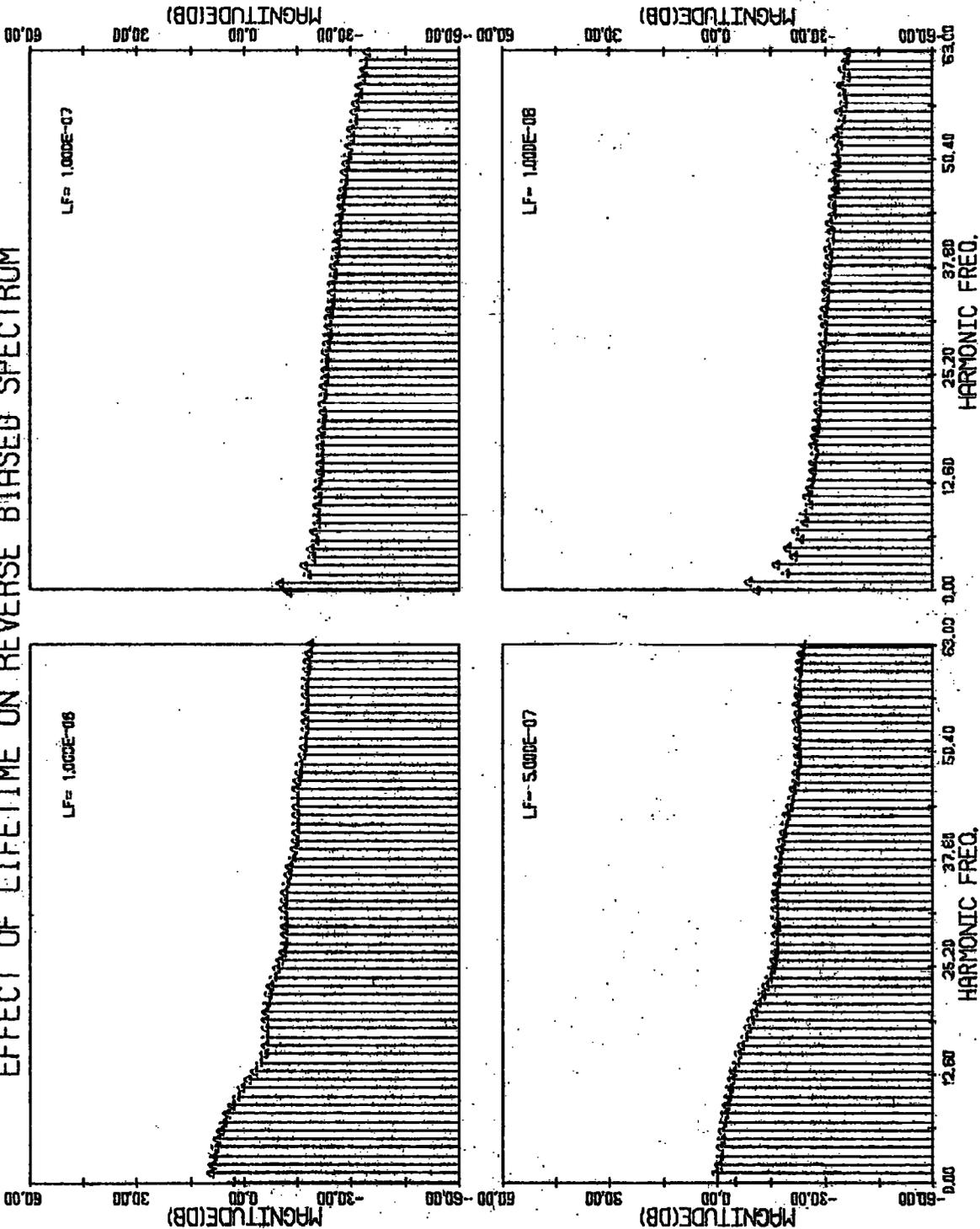
FIGURE (6.19)

DYNAMIC SPECTRUM
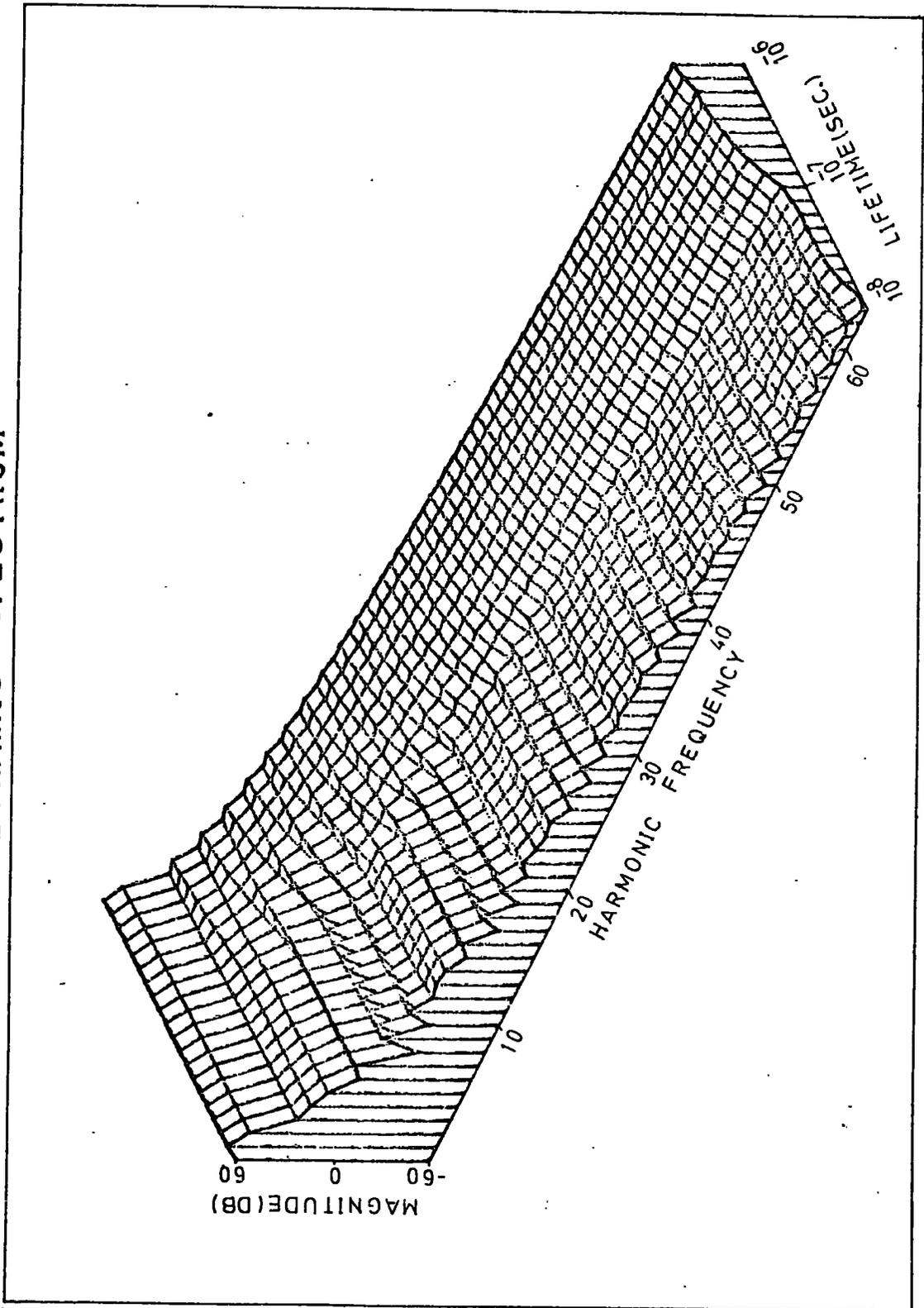
FIGURE (6.20)

c) <u>Different sized diodes with a fixed lifetime</u>.

Figs. 6.21 and 6.22 show the dynamic responses and their spectra of diodes of different sizes with W_p/L_n ranging from 0.1 to 1.0 respectively, for a lifetime of 1 microsecond. The results reveal that a long diode with relatively large overshoot gives a nearly smooth spectrum and a large magnitude of the higher order harmonics. As the size of the diode decreases, the higher order harmonics become smaller, and the ripple effect appears.

Figs. 6.23 to 6.27 show the quasi-static spectrum, and the effect of the length of the diode on the spectrum for the forward and reverse directions respectively. It is seen that the influence of varying the size is equivalent to the direct influence of the lifetime, as considered in section b). Shortening of the diode gives the same effect as reducing the lifetime in both the time and frequency domains, which introduces ripples into the spectrum.

A specific implication of these results suggests that, for some devices such as switching diodes , power diodes, etc., an attempt to control the lifetime may be replaced or assisted by varying the width of the device.

EFFECT OF LIFETIME ON DYNAMIC RESPONSE

FIGURE (6.21)

DYNAMIC SPECTRUM

FIGURE (6.22)

DIODES WITH THE SAME LIFETIME OF 1 MICROSECOND

QUASI-STATIC SPECTRUM

WP/LN= 1.000E-01

WP/LN= 7.500E-01

WP/LN= 5.000E-01

WP/LN= 1.000E+00

HARMONIC FREQ.

HARMONIC FREQ.

MAGNITUDE(DB)

MAGNITUDE(DB)
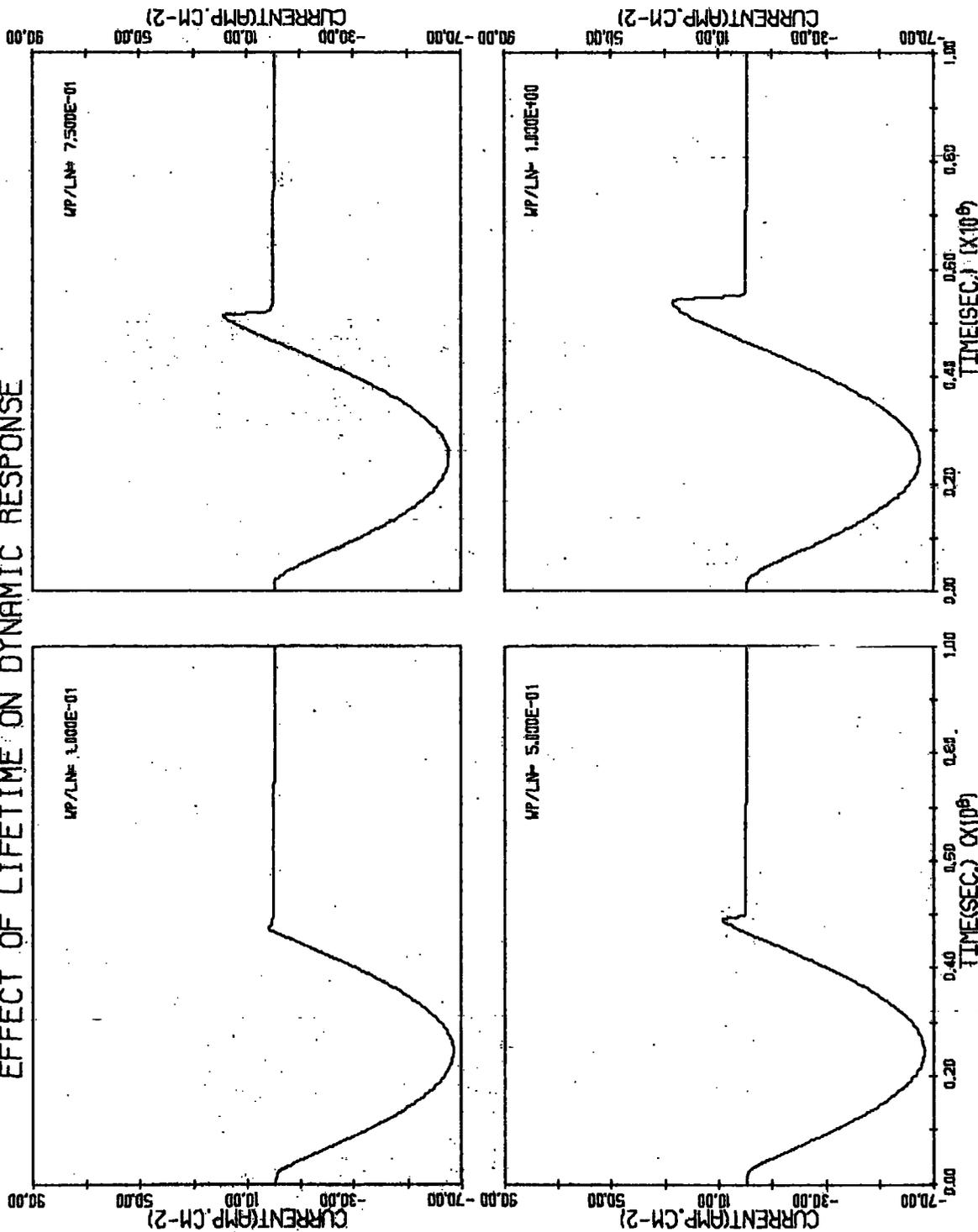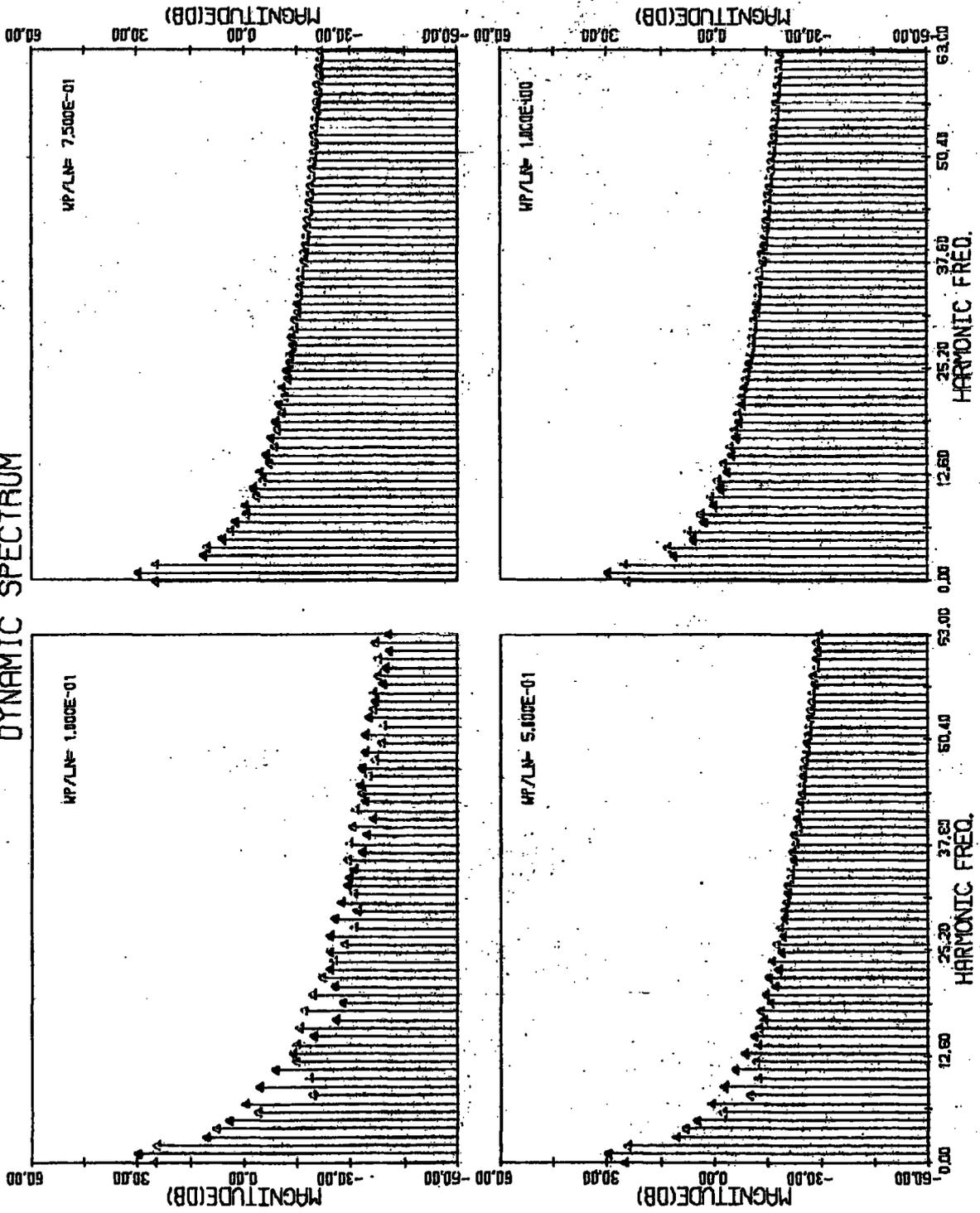
DIODES WITH THE SAME LIFETIME OF 1 MICROSECOND

FIGURE (6.23)

EFFECT OF LIFETIME ON FORWARD BIASED RESPONSE

FIGURE (6.24)

EFFECT OF LIFETIME ON FORWARD BIASED SPECTRUM

FIGURE (6.25)

EFFECT OF LIFETIME ON REVERSE BIASED RESPONSE

FIGURE (6.26)

EFFECT OF LIFETIME ON REVERSE BIASED SPECTRUM.

FIGURE (6.27)

Chapter 7.

Conclusions.

Large signal modelling and analysis of p-n junction diodes have been developed and studied intensively. The behaviour of the devices is described by a system of nonlinear differential equations namely ; the continuity equations, the current density equations and Maxwell's equations. The algorithm for the solutions developed in this study were based on the finite difference technique. The nonlinear system equations can be transformed into a set of linear algebraic equations with the use of the finite difference approximation together with either Newton's method or Picard-like iteration. Therefore, any sucessive approximation method can then be applied for the solutions.

The simulation began with the problem at thermal equilibrium and then under reverse bias conditions in which the current flow was neglected. With these conditions, the system equations reduced to only Poisson equation. This allows a general algorithm to be introduced. In addition, the solution at thermal equilibrium was used as a initial trial solution in the iteration scheme of the later problems.

When current flow was included, the whole set of system equations must be taken into account. Firstly, we considered the time-independent modelling, in which the problem becomes solving a set of nonlinear ordinary differential equations. An algorithm was developed and

used to study the internal and terminal characteristics of some diodes. The algorithm was a modification of the Calzolari's algorithm. It employed the R-dimensional Newton's method in dealing with the Poisson equation, rather than working on the corrected term in one-dimensional Newton method. The calculation of the current densities were based on the De Mari's analytical formulations in order to avoid instability problem. The algorithm was shown to be faster than the original and was also valid over a wide range of operation.

The use of the diodes in a simple R-D circuit under large-signal sinusoidal excitation was investigated. The method employed a cubic spline interpolation and the Newton-Raphson iteration to solve the circuit equation.

Secondly, we studied the time-dependent modelling of the diodes. In this case, the system equations became a set of nonlinear partial differential equations. An algorithm was developed using the R-dimensional Newton method to linearize the equations, and employing the general implicit scheme of finite-difference approximation in the time discretization. Scharfetter's spatial mesh distributions were included to ensure stability. The algorithm was used to investigate the internal and terminal transient characteristics of a diode under turn-on step excitations. The steady-state responses of large-signal sinusoidal excitation were also obtained and studied.

In both cases, the influence of minority carrier lifetime on the terminal characteristics was comprehensively studied. However, the variation of the

lifetime also affects the ratio W_p/L_n. The lifetime and the ratio are inversely related. Therefore, the influence of the lifetime has been considered separately for diodes with the same length, diodes with the same ratios W_p/L_n, and finally diodes with different ratio but the same lifetime.

In the forward direction, the results showed that a decrease of the lifetime resulted in an increase of the current (for the diodes with the same ratio). But an increase of the ratio causes the current to decrease. So the effect of the lifetime on the fixed length diode current was therefore a combination of these two variations. In the reverse direction, the overshoot effect due to stored charge was shown to become larger as the lifetime increases (for the diodes with the same ratio). But decreasing of the ratio was shown to minimize the overshoot effect.

In addition, frequency domain analysis of these diodes has been included, by applying the Fast Fourier Transform directly to the solutions obtained. Following the same line of investigation as in the time domain, we also studied the influence of the lifetime on the harmonic generation of the diodes. For the diodes with the same ratio , an increase of the lifetime tended to smooth the spectrum and raise the higher order harmonics in the forward direction. However, in the reverse direction it introduced ripples in the spectrum and raised the lower order harmonics. Similarly, this effect showed in the diodes when the ratio became higher, i.e, longer diodes.

For the diodes with the same length, the spectrum confirmed that there exists an optimum value of the lifetime at which a saturated current occurs.

To some extent, the results obtained were intuitively obvious and showed good agreement with those described by the classical analytical theory. This confirmed the validity and reliability of the algorithms used. However, for more complicated cases, e.g. arbitrary doping profile diodes, large signal operations, etc. the analytical methods become impractical and only approximated solutions are available. On the other hand, our numerical algorithms provide not only the exact and complete solutions, but also the practical methods to observe certain phenomena such as the harmonic spectrum generated. This work may therefore be useful in a detailed study of semiconductor devices where the influence of physical parameters on the characteristics is of interest. The devices may then be designed to meet exact requirements. The use of the finite-difference technique provides flexibility in that the algorithms can be extended into two-dimensional problems.

It is seen that the basis of the algorithms used in this work is repeated inversion of a tridiagonal matrix until the solution is found. The use of a single processor requires a sequential algorithm for this matrix inversion. This needs a large amount of processing time, particularly when an accurate solution is desired. For two-dimensional cases, this problem becomes critical and uneconomical in practice. However, recent work on parallel numerical

algorithms provides an alternative method to solve this problem. The matrix can be sliced into N sections, and then N-processors may be used in parallel. The processing time is ideally N-time less than a sequential algorithm. For future work, this parallel algorithm may be considered for both one and two dimensional cases, and a hardware simulator could also be developed.

Appendix A.

Tridiagonal system.

The general form of a tridiagonal system is :

$$b_1 X_1 + c_1 X_2 \qquad\qquad = d_1 \qquad\qquad (A.1)$$

$$a_2 X_1 + b_2 X_2 + c_2 X_3 \qquad\qquad = d_2 \qquad\qquad (A.2)$$

$$a_3 X_2 + b_3 X_3 + c_3 X_4 \qquad\qquad = d_3 \qquad\qquad (A.3)$$

$$\cdots\cdots\cdots\cdots \qquad\qquad \cdot$$

$$\cdots\cdots\cdots\cdots\cdots \qquad\qquad \cdot$$

$$a_{N-1} X_{N-2} + b_{N-1} X_{N-1} + c_{N-1} X_N = d_{N-1} \qquad (A.N-1)$$

$$a_N X_{N-1} + b_N X_N = d_N \qquad\qquad (A.N)$$

The equations can be solved by Gaussian elimination, and taking into account the tridiagonal nature of the system.

Multiplying equation A.1 by a_2/b_1 and subtracting from equation A.2 we obtain new equation A.2 as

$$[b_2 - (a_2/b_1) c_1] X_2 + c_2 X_3 = d_2 - (a_2/b_1) d_1$$

or

$$b_2^* X_2 + c_2 X_3 = d_2^* \qquad\qquad\qquad (A.2)$$

Similarly, equation A.3 can be eliminated as

$$[b_3 - (a_3/b_2^*) c_2] X_3 + c_3 X_4 = d_3 - (a_3/b_2^*) d_2^*$$

or

$$b_3^* X_3 + c_3 X_4 = d_3^* \qquad\qquad\qquad (A.3)$$

Thus, in general, by using the recurrence relations

$$b_1^* = b_1$$

$$d_1^* = d_1$$

$$b_i^* = b_i - (a_i/b_{i-1}^*) \ c_{i-1}$$

$$d_i^* = d_i - (a_i/b_{i-1}^*) \ d_{i-1}^*$$

$$i = 2,3,4,\ldots\ldots\ldots,N$$

we can write

$$b_i^* \ X_i + c_i X_{i+1} = d_i^* \tag{A.i}$$

and the last equation becomes

$$b_N^* \ X_N = d_N^* \tag{A.N}$$

By back substitution, the solutions can be determined from

$$X_N = d_N^*/b_N^*$$

and

$$X_i = (d_i^* - c_i X_{i+1})/b_i^*$$

$$i = (N-1),(N-2),\ldots\ldots\ldots,1$$

Appendix B.

Cubic spline interpolation.

A cubic spline $S(x)$ interpolating $f(x)$ at the points

$$x_o < x_1 < x_2 < \ldots \ldots \ldots , < x_n$$

has the following properties :

1) $S(x)$ is a cubic polynomial in $[x_k, x_{k+1}]$

$$k = 0, 1, 2, \ldots \ldots \ldots , n-1$$

2) $S(x) = f(x_k)$

$$k = 0, 1, 2, \ldots \ldots \ldots , n$$

3) $S'(x)$ and $S''(x)$ are continuous in (x_o, x_n)

For $x \in [x_k, x_{k+1}]$, $S(x)$ can be written as

$$S(x) = a_k(x-x_k)^3 + b_k(x-x_k)^2 + c_k(x-x_k) + d_k \qquad \text{(B.1)}$$

By differentiating,

$$S'(x) = 3a_k(x-x_k)^2 + 2b_k(x-x_k) + c_k \qquad \text{(B.2)}$$

and

$$S''(x) = 6a_k(x-x_k) + 2b_k \qquad \text{(B.3)}$$

For simplicity, let

$$S''(x_k) = M_k \qquad \text{(B.4)}$$

Using the second property, for $x \in |x_k, x_{k+1}|$, equation B.1 gives

$$f_k = S(x_k) = d_k \qquad \text{(B.5)}$$

$$f_{k+1} = S(x_{k+1}) = a_k h_k^3 + b_k h_k^2 + c_k h_k + d_k \qquad \text{(B.6)}$$

where

$$h_k = (x_{k+1} - x_k)$$

Similarly, equation B.3 gives

$$M_k = 2b_k$$

and

$$M_{k+1} = 6a_k h_k + 2b_k$$

Thus, we can write

$$b_k = M_k/2 \tag{B.7}$$

$$a_k = (M_{k+1} - M_k)/6M_k \tag{B.8}$$

Substituting a_k, b_k and c_k into equation B.6, we get

$$c_k = \frac{f_{k+1} - f_k}{h_k} - \frac{(2h_k M_k + h_k M_{k+1})}{6} \tag{B.9}$$

From equation B.2, with $x = x_k$, we have

$$S'(x_k) = c_k \tag{B.10}$$

Similarly, in the previous interval $x \in [x_{k-1}, x_k]$, equation B.2 is in the form

$$S'(x) = 3a_{k-1}(x - x_{k-1})^2 + 2b_{k-1}(x - x_{k-1}) + c_{k-1}$$

with $x = x_k$, we have

$$S'(x) = 3a_{k-1}h_{k-1}^2 + 2b_{k-1}h_{k-1} + c_{k-1} \tag{B.11}$$

where

$$h_{k-1} = (x_k - x_{k-1})$$

Using the third property, equation B.10 and B.11 can be equated, and together with the values of a,b,c and d derived above, we finally obtain a tridiagonal system

$$h_{k-1}M_{k-1} + (2h_{k-1} + 2h_k)M_k + h_kM_{k+1} = 6\left[\frac{f_{k+1} - f_k}{h_k} - \frac{f_k - f_{k-1}}{h_{k-1}}\right]$$

$$k = 1,2,\ldots\ldots,n-1$$

(B.12)

This gives (n-2) equations relating the n values of M_k, therefore two additional equations are required. To some extent these end conditions are arbitrary. However, for some specific splines, the following end conditions are given.

1) Natural cubic spline.

$$S'(x_0) = 0 = S''(x_n)$$

or

$$M_0 = 0 = M_n$$

2) Complete cubic spline.

$$S'(x_0) = f'(x_0)$$

and

$$S'(x_n) = f'(x_n)$$

or

$$2M_0 + M_1 = \frac{6}{h_0}\left[\frac{f_1 - f_0}{h_0} - f_0\right]$$

and

$$2M_n + M_{n-1} = \frac{6}{h_{n-1}}\left[f'_n - \frac{f_n - f_{n-1}}{h_{n-1}}\right]$$

Appendix C.

Computer Subroutines.

```
      SUBROUTINE COWELL(N,H,FN,Y,TA,TB,TC,PM,R,IFLAG)
C     SUBROUTINE FOR SOLVING POISSON EQUATION IN  CHAPTER3.
      IMPLICIT REAL *8(A-H,O-Z)
      DIMENSION FN(1),Y(1),TA(1),TB(1),TC(1),PM(1),R(1)
      DATA EPS/1.0D-12/
      W=0.7
      NP1=N+1
      CM=H*H
      DM=-CM
      IFLAG=0
      WK=(1.0-W)/W
      NM1=N-1
      DO 5 J=1,6
      DO 10 I=3,NM1
10    PM(I)=(Y(I-1)-2.0*Y(I)+Y(I+1))*WK
      PM(2)=(-2.0*Y(2)+Y(3))*WK
      PM(N)=(Y(N-1)-2.0*Y(N))*WK
      DO 20 I=2,N
      BMATX=DM*FN(I)
      IF(I.GT.2) GO TO 22
      BMATX=BMATX-Y(1)
      GO TO 21
22    IF(I.LT.N) GO TO 21
      BMATX=BMATX-Y(NP1)
21    FSMALL=CM*DEXP(Y(I))
      FBIG=CM*DEXP(Y(I))
      TA(I)=1.0/W
      TC(I)=1.0/W
      TB(I)=(-2.0-FBIG)/W
20    R(I)=FSMALL+BMATX-FBIG*Y(I)/W+PM(I)
      TA(2)=0.0
      TC(N)=0.0
      CALL TDGNAL(2,N,TA,TB,TC,R)
      DO 25 I=2,N
25    Y(I)=R(I)
5     CONTINUE
```

```
      B2=(1.0/12.0)*(CM*DEXP(Y(1))+DM*FN(1))-Y(1)
      BN=(1.0/12.0)*(CM*DEXP(Y(NP1))+DM*FN(NP1))-Y(NP1)
      K=0
    1 K=K+1
      IF(K.EQ.100) GO TO 990
      DO 27 I=2,N
      FSMALL=CM*DEXP(Y(I))+DM*FN(I)
      FBIG=CM*DEXP(Y(I))
      TC(I)=1.0-(1.0/12.0)*CM*DEXP(Y(I+1))
      TB(I)=-2.0-(10.0/12.0)*FBIG
      PM(I)=FSMALL-FBIG*Y(I)
      IF(I.EQ.2) GO TO 27
      TA(I)=1.0-(1.0/12.0)*CM*DEXP(Y(I-1))
   27 CONTINUE
      TA(2)=0.0
      TC(N)=0.0
      NM1=N-1
      DO 29 I=3,NM1
      R(I)=(PM(I-1)+10.0*PM(I)+PM(I+1))/12.0
   29 CONTINUE
      R(2)=(10.0*PM(2)+PM(3))/12.0+B2
      R(N)=(PM(N-1)+10.0*PM(N))/12.0+BN
      CALL TDGNAL(2,N,TA,TB,TC,R)
      DO 30 I=2,N
      IF(DABS(R(I)-Y(I)).GT.EPS) GO TO 31
   30 CONTINUE
      GO TO 980
   31 DO 32 I=2,N
      Y(I)=R(I)
   32 CONTINUE
      GO TO 1
  980 R(1)=Y(1)
      R(NP1)=Y(NP1)
      WRITE(5,590) K
  590 FORMAT(5X,'NUMBER OF ITERATIONS=',I5)
      GO TO 800
  990 WRITE(6,610) I
```

```
  610 FORMAT(5X,'NO SOLUTION AFTER 100 ITERATIONS. AT I=',I5)
      IFLAG=1
  800 RETURN
      END


      SUBROUTINE GAUSFN(NP1,H,X,FN)
C     THE DOPING FUNCTION IS OF THE GAUSSIAN  FUNCTION.
      IMPLICIT REAL *8(A-H,O-Z)
      DIMENSION X(1),FN(1)
      COMMON /AAA/YEQ1,YEQNP1
      DATA FNMAX,RP,DELRP,FINTR/5.0D16,0.25D-04,0.06D-04,1.5D10/
      DATA XDEBYE/3.31D-03/
      DATA V0,EG/2.58D-02,1.11D00/
C VACUUM WORK  FUNCTION OF GOLD = 4.70 EV.
C VACUUM WORK  FUNCTION OF SILICON = 5.15 EV.
C THE METAL-SEMICONDUCTOR WORK-FUNCTION DIFF.(VMS) IS DEFINED AS,
C VMS=VM-VS
      DATA VM,VS/4.70D00,5.15D00/
      VMS=VM-VS
      RP=RP/XDEBYE
      DELRP=DELRP/XDEBYE
      DO 1 I=1,NP1
      X(I)=(I-1)*H
      FN(I)=1.0D14+FNMAX*DEXP(-0.5*((X(I)-RP)/DELRP)**2)
      FN(I)=FN(I)/FINTR
    1 CONTINUE
C SET THE BOUNDARY VALUES.(=+  FOR N-TYPE; =-  FOR  P-TYPE)
      YEQNP1=DLOG(DABS(FN(NP1)/2.)+DSQRT(1.+(FN(NP1)/2.)**2))
C INCLUDE THE METAL-SEMICONDUCTOR WORK FUNCTION, VMS.
      YEQ1=(VMS+(EG/2.0))/V0
      RETURN
      END
```

```
C
      SUBROUTINE STATIC(N,H,FN,Y,TA,TB,TC,TD,P,EN,DEL,X,IFLAG,U)
      SUBROUTINE FOR TIME-INDEPENDENT MODELLING IN CHAPTER4.
      IMPLICIT REAL *8(A-H,O-Z)
      DIMENSION FN(1),Y(1),TA(1),TB(1),TC(1),TD(1),P(1),EN(1),DEL(1)
      DIMENSION H(1),X(1),U(1),UN(900),UP(900)
      COMMON /AAA/YEQ1,YEQNP1
      COMMON /LFMOB/TAUN,TAUP,UN,UP
      DATA EPS/1.00D-05/
      NP1=N+1
      IFLAG=0
      P(1)=DEXP(-YEQ1)
      P(NP1)=DEXP(-YEQNP1)
      EN(1)=DEXP(YEQ1)
      EN(NP1)=DEXP(YEQNP1)
      K=0
    1 K=K+1
      IF(K.EQ.100) GO TO 990
      DO 17 I=1,NP1
   17 U(I)=(P(I)*EN(I)-1.)/(TAUP*(EN(I)+1.)+TAUN*(P(I)+1.))
      DO 20 I=2,N
      UPPLS=0.50*(UP(I)+UP(I+1))
      UPMNS=0.50*(UP(I)+UP(I-1))
      TA(I)=(UPMNS/H(I-1))*DEXP((Y(I-1)-Y(I))/2.0)
      TC(I)=(UPPLS/H(I))*DEXP((Y(I+1)-Y(I))/2.0)
      TB(I)=-(UPMNS/H(I-1))*DEXP((Y(I)-Y(I-1))/2.)
      TB(I)=TB(I)-(UPPLS/H(I))*DEXP((Y(I)-Y(I+1))/2.)
      TD(I)=U(I)*((H(I)+H(I-1))/2.0)
      IF(I.EQ.2) TD(2)=TD(2)-TA(2)*P(1)
      IF(I.EQ.N) TD(N)=TD(N)-TC(N)*P(NP1)
   20 CONTINUE
      CALL TDGNAL(2,N,TA,TB,TC,TD)
      DO 25 I=2,N
   25 P(I)=TD(I)
      DO 30 I=2,N
      UNPLS=0.50*(UN(I)+UN(I+1))
      UNMNS=0.50*(UN(I)+UN(I-1))
```

```
      TA(I)=(UNMNS/H(I-1))*DEXP((Y(I)-Y(I-1))/2.0)
      TC(I)=(UNPLS/H(I))*DEXP((Y(I)-Y(I+1))/2.0)
      TB(I)=-(UNMNS/H(I-1))*DEXP((Y(I-1)-Y(I))/2.)
      TB(I)=TB(I)-(UNPLS/H(I))*DEXP((Y(I+1)-Y(I))/2.)
      TD(I)=U(I)*((H(I)+H(I-1))/2.0)
      IF(I.EQ.2) TD(2)=TD(2)-TA(2)*EN(1)
      IF(I.EQ.N) TD(N)=TD(N)-TC(N)*EN(NP1)
   30 CONTINUE
      CALL TDGNAL(2,N,TA,TB,TC,TD)
      DO 35 I=2,N
   35 EN(I)=TD(I)
      DO 40 I=2,N
      BETA=0.5D00*(H(I)+H(I-1))
      AI=1.0/H(I-1)
      CI=1.0/H(I)
      BI=-AI-CI
      TA(I)=AI
      TC(I)=CI
      TB(I)=BI-(EN(I)+P(I))*BETA
      TD(I)=EN(I)-P(I)-FN(I)-(EN(I)+P(I))*Y(I)
      TD(I)=TD(I)*BETA
      IF(I.EQ.2) TD(2)=TD(2)-TA(2)*Y(1)
      IF(I.EQ.N) TD(N)=TD(N)-TC(N)*Y(NP1)
   40 CONTINUE
      CALL TDGNAL(2,N,TA,TB,TC,TD)
      DO 50 I=2,N
      IF(DABS(TD(I)-Y(I)).GT.EPS) GO TO 61
   60 CONTINUE
      GO TO 680
    1 DO 62 I=2,N
      Y(I)=TD(I)
   62 CONTINUE
      GO TO 1
  580 WRITE(6,590) K
  590 FORMAT(5X,'NUMBER OF ITERATIONS=',I5)
      GO TO 800
  990 WRITE(6,610) I
```

```fortran
  610 FORMAT(5X,'NO SOLUTION AFTER 100 ITERATIONS. AT I=',I5)
      IFLAG=1
  800 RETURN
      END

C     SUBROUTINE EQVM(N,H,FN,Y,TA,TB,TC,TD,P,EN,DEL,X,IFLAG)
      SUBROUTINE FOR SOLVING EQUILIBRIUM SOLUTION REQUIRED IN STATIC CASE.
      IMPLICIT REAL *8(A-H,O-Z)
      DIMENSION FN(1),Y(1),TA(1),TB(1),TC(1),TD(1),P(1),EN(1),DEL(1)
      DIMENSION H(1),X(1)
      COMMON /AAA/YEQ1,YEQNP1
      DATA EPS,W0/1.0D-05,0.3D00/
      NP1=N+1
      IFLAG=0
      DEL(1)=0.0
      DEL(NP1)=0.0
    1 K=K+1
      IF(K.EQ.100) GO TO 990
      DO 40 I=2,N
      TA(I)=1.0/H(I-1)
      TC(I)=1.0/H(I)
      TB(I)=-TA(I)-TC(I)-(H(I)+H(I-1))*DCOSH(Y(I))
      TD(I)=(H(I)+H(I-1))*(2.0*DSINH(Y(I))-FN(I))
      TD(I)=TD(I)-(TA(I)*Y(I-1)+(-TA(I)-TC(I))*Y(I)+TC(I)*Y(I+1))
      IF(I.EQ.2) TD(2)=TD(2)-TA(2)*DEL(1)
      IF(I.EQ.N) TD(N)=TD(N)-TC(N)*DEL(NP1)
   40 CONTINUE
      CALL TDGNAL(2,N,TA,TB,TC,TD)
      DO 45 I=2,N
   45 DEL(I)=TD(I)
      W=W0+0.01*K
      DO 50 I=2,N
   50 Y(I)=Y(I)+W*DEL(I)
      DO 60 I=2,N
      IF(DEL(I).GT.EPS) GO TO 1
   60 CONTINUE
```

```
      DO 65 I=2,N
      P(I)=DEXP(-Y(I))
      EN(I)=DEXP(Y(I))
 65   CONTINUE
      P(1)=DEXP(-YEQ1)
      P(NP1)=DEXP(-YEQNP1)
      EN(1)=DEXP(YEQ1)
      EN(NP1)=DEXP(YEQNP1)
      WRITE(6,590) K
 590  FORMAT(5X,'NUMBER OF ITERATIONS=',I5)
      WRITE(6,510)(Y(I),EN(I),P(I),FN(I),X(I),I=1,NP1)
 510  FORMAT(/,'COMPUTED POTENTIAL',5X,'ELECTRON DENSITY',7X,'HOLE DENSI
     *TY',9X,'DOPING DENSITY',8X,'DISTANCE X.',//,(5(E15.7,7X)))
      GO TO 800
 990  WRITE(6,610) I
 610  FORMAT(5X,'NO SOLUTION AFTER 100 ITERATIONS. AT I=',I5)
      IFLAG=1
 800  RETURN
      END

C
      SUBROUTINE CRTDEN(N,P,EDEN,HOLCUR,ELECUR,H,Y,U)
      SUBROUTINE FOR CALCULATION OF HOLE AND ELECTRON CURRENT DENSITIES.
      IMPLICIT REAL *8(A-H,O-Z)
      DIMENSION P(1),EDEN(1),HOLCUR(1),ELECUR(1),H(1),Y(1),U(1)
      DIMENSION UN(900),UP(900),RUN(900),RUP(900)
      DIMENSION FU(900),RJP(900),RJN(900)
      COMMON /CCC/ISTEPS,IPLOT
      COMMON /LFMOB/TAUN,TAUP,UN,UP
      NP1=N+1
      DO 90 I=1,N
      RUN(I)=1.0D00/UN(I)
 90   RUP(I)=1.0D00/UP(I)
      RUN(NP1)=RUN(N)
      RUP(NP1)=RUP(N)
      FU(1)=0.0
      DO 100 I=1,N
```

```
      FU(I+1)=FU(I)+(H(I)/2.)*(U(I)+U(I+1))
100   CONTINUE
      EPFU=0.0
      DO 200 I=1,N
      EPFU=EPFU+(H(I)/2.)*(RUP(I)*DEXP(Y(I))*FU(I)+RUP(I+1)*DEXP(Y(I+1))
     $*FU(I+1))
200   CONTINUE
      DVP=0.0
      DO 300 I=1,N
      DVP=DVP+(H(I)/2.)*(RUP(I)*DEXP(Y(I))+RUP(I+1)*DEXP(Y(I+1)))
300   CONTINUE
      ENFU=0.0
      DO 400 I=1,N
      ENFU=ENFU+(H(I)/2.)*(RUN(I)*DEXP(-Y(I))*FU(I)+RUN(I+1)*DEXP(-Y(I+1
     $))*FU(I+1))
400   CONTINUE
      DVN=0.0
      DO 500 I=1,N
      DVN=DVN+(H(I)/2.)*(RUN(I)*DEXP(-Y(I))+RUN(I+1)*DEXP(-Y(I+1)))
500   CONTINUE
      CONSTP=(P(NP1)*DEXP(Y(NP1))-P(1)*DEXP(Y(1))-EPFU)/DVP
      CONSTN=(EDEN(1)*DEXP(-Y(1))-EDEN(NP1)*DEXP(-Y(NP1))+ENFU)/DVN
      DO 600 I=1,NP1
      HOLCUR(I)=FU(I)+CONSTP
      ELECUR(I)=-FU(I)+CONSTN
      TC=HOLCUR(I)+ELECUR(I)
      RJP(I)=HOLCUR(I)/TC
      RJN(I)=ELECUR(I)/TC
600   CONTINUE
      IF(ISTEPS.EQ.1) GO TO 887
      IF(IPLOT.NE.5) GO TO 888
887   WRITE(6,677) EPFU,ENFU,DVP,DVN,CONSTP,CONSTN
677   FORMAT('INTEGRATION FROM 0 TO L OF EXP(Y(X))*FU(X).DX =',E15.7,
     */,'INTEGRATION FROM 0 TO L OF EXP(-Y(X))*FU(X).DX =',E15.7,
     */,'INTEGRATION FROM 0 TO L OF EXP(Y(X)).DX =',E15.7,
     */,'INTEGRATION FROM 0 TO L OF EXP(-Y(X)).DX =',E15.7,
     */,'CONSTANT-P =',E15.7,/,'CONSTANT-N =',E15.7,//)
```

```
      WRITE(6,678)(Y(I),EDEN(I),P(I),FU(I),U(I),ELECUR(I),
     *HOLCUR(I),RJN(I),RJP(I),I=1,NP1)
  578 FORMAT(2X,'POTENTIAL',4X,'ELE.DENS.',4X,'HOLE DENS.',3X,
     *'INT.U(X)',8X,'U(X)',10X,'JN',11X,'JP',11X,'JN/J',9X,'JP/J',
     *//,(9(E13.5)))
  888 RETURN
      END


C     SUBROUTINE ERFCPS(NP1,H,X,FN)
      THE DOPING FUNCTION IS OF THE ERROR   FUNCTION,FOR N-P-P+ S/C.
      IMPLICIT REAL *8(A-H,O-Z)
      DIMENSION X(1),FN(1),H(1)
      COMMON /AAA/YEQ1,YEQNP1
      COMMON /BBB/XLLMAX
      DO 1 I=1,NP1
      IF(I.GT.1) GO TO 11
      X(1)=0.0
      GO TO 111
   11 X(I)=X(I-1)+H(I-1)
  111 XCHG=0.77D00*XLLMAX
      IF(X(I).GT.XCHG) GO TO 112
      FN(I)=1.0D08*DERFC(9.8*X(I)/XLLMAX)-1.0D05
      GO TO 1
  112 FN(I)=1.0D08*DERFC(9.8*X(I)/XLLMAX)-1.0D08
    1 CONTINUE
      YEQ1=DLOG(DABS(FN(1)/2.)+DSQRT(1.+(FN(1)/2.)**2))
      YEQNP1=-1.0*DLOG(DABS(FN(NP1)/2.)+DSQRT(1.+(FN(NP1)/2.)**2))
      RETURN
      END


      SUBROUTINE FIXM1(H,N)
      IMPLICIT REAL*8(A-H,O-Z)
      DIMENSION H(1)
      COMMON /BBB/XLLMAX
      N=100
```

```
      DO 1  I=1,N
      H(I)=XLLMAX/DFLOAT(N)
    1 CONTINUE
      RETURN
      END

      SUBROUTINE LINVAP(NSTEPS,VMAX,VINCRE)
      IMPLICIT REAL*8(A-H,O-Z)
      VINCRE=VMAX/DFLOAT(NSTEPS)
      RETURN
      END


C     SUBROUTINE DYNAMC
C     SUBROUTINE FOR TIME-DEPENDENT MODELLING IN  CHAPTER5.
      IMPLICIT REAL*8(A-H,O-Z)
      DIMENSION H(310),E(310),DELTAT(12000),RPDELT(12000),VAPP(12000)
      DIMENSION EXPLUS(310),EXMNUS(310),EDEPLS(310),EDEMNS(310)
      DIMENSION DJPDP1(310),DJPDP2(310),DJNDN1(310),DJNDN2(310)
      DIMENSION DJPDE(310),DJNDE(310),DJTDE(310),P(310),EN(310)
      DIMENSION HOLCUR(310),ELECUR(310),FN(310),DY(310),Y(310)
      DIMENSION FS(310),GS(310),HS(310),ES(310),FSTK(310),GSTK(310)
      DIMENSION HSTK(310),PTK(310),ENTK(310),ETK(310),PNS(310)
      DIMENSION TA(310),TB(310),TC(310),TD(310),UP(310),UN(310),X(310)
      DIMENSION DVU(310),U(310),DUDP(310),DUDN(310)
      COMMON /QCHK/DVU,U,DUDP,DUDN,EXPLUS,EXMNUS,EDEPLS,EDEMNS
      COMMON /QCHK2/DJPDP1,DJPDP2,DJNDN1,DJNDN2,DJPDE,DJNDE,DJTDE,VDIFF
      COMMON /AAA/YEQ1,YEQNP1
      COMMON /QAAB/TAUN,TAUP,UN,UP,FACNOR,ZETA,DY,XDEBYE,X,Y,HS,FNINTR
      COMMON /QABB/I,IFLAG,ISTEDY,J,K,N,NP1
      COMMON /QBBB/E,EN,P,FN,DELTAT,RPDELT,VAPP,ELECUR,HOLCUR,TOTCUR
      COMMON /TABC/TA,TB,TC,TD
      COMMON /QEPS/EPS,EPSPOI,EPST
      DATA EZERO,ELIMIT/1.0D-10,1.74D02/
      IFLAG=0
```

```
      KFINIS=0
      ISTEDY=0
      K=0
    5 K=K+1
      IF(K.EQ.100) GO TO 990
      SUMEDX=0.0
      DO 15 L=1,NP1
   15 SUMEDX=SUMEDX+E(L)*H(L)
      TOTCUR=(VAPP(J)-(SUMEDX-VDIFF))/FACNOR
      DO 10 I=1,N
     _VU(I)=TAUN*(P(I)+1.)+TAUP*(EN(I)+1.)
      U(I)=(P(I)*EN(I)-1.0)/DVU(I)
      DUDP(I)=(EN(I)-U(I)*TAUN)/DVU(I)
      DUDN(I)=(P(I)-U(I)*TAUP)/DVU(I)
      EDX=E(I)*H(I)
      ETEST=DABS(EDX)
      IF(ETEST.LT.EZERO) GO TO 9
      IF(EDX.LT.(-ELIMIT))  EDX=-ELIMIT
      IF(EDX.GT.ELIMIT)  EDX=ELIMIT
      EXPLUS(I)=DEXP(EDX)-1.0
      EXMNUS(I)=DEXP(-EDX)-1.0
      EDEPLS(I)=E(I)/EXPLUS(I)
      EDEMNS(I)=E(I)/EXMNUS(I)
      DJPDP1(I)=-UP(I)*EDEMNS(I)
      DJPDP2(I)=-UP(I)*EDEPLS(I)
      DJNDN1(I)=-UN(I)*EDEPLS(I)
      DJNDN2(I)=-UN(I)*EDEMNS(I)
      DJPDE(I)=-UP(I)*(P(I)*(1.0-EDEPLS(I)*H(I))/EXMNUS(I)
     $+P(I+1)*(1.0+EDEMNS(I)*H(I))/EXPLUS(I))
      DJNDE(I)=-UN(I)*(EN(I)*(1.0+EDEMNS(I)*H(I))/EXPLUS(I)
     $+EN(I+1)*(1.0-EDEPLS(I)*H(I))/EXMNUS(I))
      DJTDE(I)=-H(I)/FACNOR
      GO TO 8
    9 DJPDP1(I)=UP(I)/H(I)
      DJPDP2(I)=-UP(I)/H(I)
      DJNDN1(I)=-UN(I)/H(I)
      DJNDN2(I)=UN(I)/H(I)
```

```
      DJPDE(I)=0.0
      DJNDE(I)=0.0
      DJTDE(I)=-H(I)/FACNOR
    8 HOLCUR(I)=P(I)*DJPDP1(I)+P(I+1)*DJPDP2(I)
      ELECUR(I)=EN(I)*DJNDN1(I)+EN(I+1)*DJNDN2(I)
   10 CONTINUE
      ELECUR(1)=TOTCUR
      HOLCUR(NP1)=TOTCUR
      HOLCUR(1)=0.0D00
      ELECUR(NP1)=0.0D00
      DO 12 I=1,NP1
      IF(I.GT.1) GO TO 11
      FS(1)=-U(1)
      GS(1)=-U(1)
      GO TO 13
   11 FS(I)=-U(I)-(HOLCUR(I)-HOLCUR(I-1))/H(I)
      GS(I)=-U(I)+(ELECUR(I)-ELECUR(I-1))/H(I)
   13 HS(I)=TOTCUR-HOLCUR(I)-ELECUR(I)
   12 CONTINUE
      IF(J.GT.1) GO TO 16
      DO 17 I=1,NP1
      PTK(I)=P(I)
      ENTK(I)=EN(I)
      PNS(I)=P(I)+EN(I)
      ETK(I)=E(I)
      FSTK(I)=FS(I)
      GSTK(I)=GS(I)
   17 HSTK(I)=HS(I)
   16 DO 20 I=2,N
      DFDPNM=DJPDP1(I-1)/H(I)
      DFDPN=-DUDP(I)+(-DJPDP1(I)+DJPDP2(I-1))/H(I)
      DFDPNP=-DJPDP2(I)/H(I)
      TA(I)=-ZETA*DFDPNM
      TB(I)=RPDELT(J)-ZETA*DFDPN
      TC(I)=-ZETA*DFDPNP
      TD(I)=(PTK(I)*RPDELT(J))+(1.0-ZETA)*FSTK(I)+ZETA*(FS(I)
     $-DFDPN*P(I)-DFDPNM*P(I-1)-DFDPNP*P(I+1))
```

```
20 CONTINUE
   TD(2)=TD(2)-TA(2)*P(1)
   TD(N)=TD(N)-TC(N)*P(NP1)
   CALL TDGNAL(2,N,TA,TB,TC,TD)
   DO 25 I=2,N
25 P(I)=TD(I)
   DO 30 I=2,N
   DGDNNM=-DJNDN1(I-1)/H(I)
   DGDNN=-DUDN(I)+(DJNDN1(I)-DJNDN2(I-1))/H(I)
   DGDNNP=DJNDN2(I)/H(I)
   TA(I)=-ZETA*DGDNNM
   TB(I)=RPDELT(J)-ZETA*DGDNN
   TC(I)=-ZETA*DGDNNP
   TD(I)=(ENTK(I)*RPDELT(J))+(1.0-ZETA)*GSTK(I)+ZETA*(GS(I)
  $-DGDNN*EN(I)-DGDNNM*EN(I-1)-DGDNNP*EN(I+1))
30 CONTINUE
   TD(2)=TD(2)-TA(2)*EN(1)
   TD(N)=TD(N)-TC(N)*EN(NP1)
   CALL TDGNAL(2,N,TA,TB,TC,TD)
   DO 35 I=2,N
35 EN(I)=TD(I)
   DJTDE(NP1)=DJTDE(N)
   DO 40 I =2,N
   DHDEMM=DJTDE(I-1)
   DHDEM=DJTDE(I)-DJPDE(I)-DJNDE(I)
   DHDEMP=DJTDE(I+1)
   TA(I)=-ZETA*DHDEMM
   TB(I)=RPDELT(J)-ZETA*DHDEM
   TC(I)=-ZETA*DHDEMP
   TD(I)=(ETK(I)*RPDELT(J))+(1.0-ZETA)*HSTK(I)+ZETA*(HS(I)
  $-DHDEM*E(I)-DHDEMM*E(I-1)-DHDEMP*E(I+1))
40 CONTINUE
   TD(2)=TD(2)-TA(2)*E(1)
   TD(N)=TD(N)-TC(N)*E(NP1)
   CALL TDGNAL(2,N,TA,TB,TC,TD)
   DO 45 I=2,N
45 E(I)=TD(I)
```

```
      ERRMAX=0.0
      DO 50 I=2,N
      PNSP1=P(I)+EN(I)
      ERROR=(PNSP1-PNS(I))/PNS(I)
      ERROR=DABS(ERROR)
      ERRMAX=DMAX1(ERRMAX,ERROR)
   50 CONTINUE
      IF(ERRMAX.GT.EPS) GO TO 883
      KFINIS=1
      DO 55 I=2,N
      ERROR=DABS(E(I)-ETK(I))
      IF(ERROR.GT.EPST) ISTEDY=1
   55 CONTINUE
      WRITE(6,590) J,K
  590 FORMAT(5X,'J =',I5,5X,'NUMBER OF ITERATIONS =',I5)
      DO 70 I=2,N
      PTK(I)=P(I)
      ENTK(I)=EN(I)
      ETK(I)=E(I)
      FSTK(I)=FS(I)
      GSTK(I)=GS(I)
   70 HSTK(I)=HS(I)
  883 DO 60 I=2,N
      PNS(I)=P(I)+EN(I)
      ES(I)=E(I)
   60 CONTINUE
      IF(KFINIS.NE.1) GO TO 5
      GO TO 800
  990 WRITE(5,610) I
  610 FORMAT(5X,'NO SOLUTIONS AFTER 100 ITERATIONS AT I=',I5)
      IFLAG=1
  800 RETURN
      END
```

```fortran
      SUBROUTINE EQILBM
C     SUBROUTINE FOR SOLVING EQUILIBRIUM SOLUTION REQUIRED IN DYNAMIC CASE.;
      IMPLICIT REAL *8 (A-H,O-Z)
      DIMENSION H(310),E(310),DELTAT(12000),RPDELT(12000),VAPP(12000)
      DIMENSION HOLCUR(310),ELECUR(310),FN(310),HS(310),P(310),EN(310)
      DIMENSION TA(310),TB(310),TC(310),TD(310),UP(310),UN(310),X(310)
      DIMENSION DVU(310),U(310),DUDP(310),DUDN(310),DY(310),DEL(310)
      DIMENSION Y(310)
      COMMON /AAA/YEQ1,YEQNP1
      COMMON /QAAB/TAUN,TAUP,UN,UP,FACNOR,ZETA,DY,XDEBYE,X,Y,HS,FNINTR
      COMMON /QABB/I,IFLAG,ISTEDY,J,K,N,NP1
      COMMON /QBBB/E,EN,P,FN,H,DELTAT,RPDELT,VAPP,ELECUR,HOLCUR,TOTCUR
      COMMON /TABC/TA,TB,TC,TD
      COMMON /QEPS/EPS,EPSPOI,EPST
      DATA W0/0.3D00/
      IFLAG=0
      DEL(1)=0.0
      DEL(NP1)=0.0
      DO 10 I=2,N
      IF(FN(I).GE.EPS) SIGN=1.0
      IF(FN(I).LT.EPS) SIGN=-1.0
      Y(I)=SIGN*DLOG(DABS(FN(I)/2.)+DSQRT(1.+(FN(I)/2.)**2.))
   10 CONTINUE
      K=0
    1 K=K+1
      IF(K.EQ.100) GO TO 990
      DO 40 I=2,N
      TA(I)=1.0/H(I-1)
      TC(I)=1.0/H(I)
      TB(I)=-TA(I)-TC(I)-(H(I)+H(I-1))*DCOSH(Y(I))
      TD(I)=(H(I)+H(I-1))*(2.0*DSINH(Y(I))-FN(I))
      TD(I)=TD(I)-(TA(I)*Y(I-1)+(-TA(I)-TC(I))*Y(I)+TC(I)*Y(I+1))
      IF(I.EQ.2) TD(2)=TD(2)-TA(2)*DEL(1)
      IF(I.EQ.N) TD(N)=TD(N)-TC(N)*DEL(NP1)
   40 CONTINUE
      CALL TDGNAL(2,N,TA,TB,TC,TD)
```

```
      DO 45 I=2,N
45    DEL(I)=TD(I)
      W=W0+0.01*K
      DO 50 I=2,N
50    Y(I)=Y(I)+W*DEL(I)
      DO 60 I=2,N
      IF(DEL(I).GT.(1.0D-07)) GO TO 1
60    CONTINUE
      DO 65 I=1,N
      P(I)=DEXP(-Y(I))
      EN(I)=DEXP(Y(I))
65    CONTINUE
      (NP1)=H(N)
      DO 70 I=2,N
      DY(I)=(H(I)+H(I-1))/2.0
70    E(I)=-(Y(I+1)-Y(I))/H(I)
      E(1)=E(2)
      E(NP1)=E(N)
      DY(1)=DY(2)
      DY(NP1)=DY(N)
      P(1)=DEXP(-YEQ1)
      P(NP1)=DEXP(-YEQNP1)
      EN(1)=DEXP(YEQ1)
      EN(NP1)=DEXP(YEQNP1)
      WRITE(5,590) K
590   FORMAT(5X,'NUMBER OF ITERATIONS=',I5)
      WRITE(6,510)(Y(I),E(I),EN(I),P(I),FN(I),X(I),I=1,NP1)
510   FORMAT(3X,'POTENTIAL',5X,'ELEC. FIELD',4X,'ELECTRON DENS.',
     *2X,'HOLE DENSITY',2X,'DOPING DENSITY',4X,'DISTANCE X.',
     *//,(6(E15.7)))
      GO TO 800
990   WRITE(6,610) I
610   FORMAT(5X,'NO SOLUTION AFTER 100 ITERATIONS. AT I=',I5)
      IFLAG=1
800   RETURN
      END
```

```
      SUBROUTINE MOBIL(FN,UP,UN,N,FNINTR,FMUNOR)
C     SUBROUTINE FOR CALCULATION OF THE NORMALIZED MOBILITIES.
      IMPLICIT REAL*8(A-H,O-Z)
      DIMENSION FN(1),UP(1),UN(1)
      NP1=N+1
      DO 1 I=1,N
      REALDP=(DABS((FN(I)+FN(I+1))/2.0))*FNINTR
      RPMP=1.0+(81.0*REALDP)/(REALDP+3.24E18)
      RPMP=DSQRT(RPMP)
      RPMP=RPMP*FMUNOR/480.0
      UP(I)=1.0/RPMP
      RPPN=1.0+(350.0*REALDP)/(REALDP+1.05E19)
      RPPN=DSQRT(RPPN)
      RPPN=RPPN*FMUNOR/1400.0
    1 UN(I)=1.0/RPPN
      UP(NP1)=UP(N)
      UN(NP1)=UN(N)
      RETURN
      END


      SUBROUTINE VAPPY1(VTH,VAPP,TIME,J,NT)
      IMPLICIT  REAL*8(A-H,O-Z)
      DIMENSION VAPP(1),TIME(1)
      VAPP(J)=VTH
      RETURN
      END


      SUBROUTINE TSPAC1(TRELAX,DELTAT,RPDELT,NT)
      IMPLICIT  REAL*8(A-H,O-Z)
      DIMENSION DELTAT(1),RPDELT(1)
      DELT=TRELAX/2.0
      DELTAT(1)=DELT
      RPDELT(1)=1.0/DELT
      DO 100 I=2,NT
```

```
      IF(I.LE.(NT/2)) DELTAT(I)=I*100.0*DELT
      IF(I.GT.(NT/2)) DELTAT(I)=1.5*DELTAT(I-1)
100   RPDELT(I)=1.0/DELTAT(I)
      RETURN
      END

      SUBROUTINE DRSPY(ISPY,VS,VD,CURENT,IFAIL)
C     SUBROUTINE FOR CALCULATION OF THE QUASI-STATIC RESPONSE§IN SECTION 4.7
      IMPLICIT REAL*8 (A-H,O-Z)
      DIMENSION X(300),Y(300),XTEMP(300),YTEMP(300),FM(300)
      COMMON /SPY/FM
      COMMON /SPYDR/X,Y
      COMMON /RESIS/ R
      DATA AREA/3.48D-04/
      DATA GUESS,EPS,NCONV/0.60D+00,1.0D-06,200/
      IF(ISPY.GT.1) GO TO 49
      R=750.0
      EAD(5) NDATA,(X(I),Y(I),I=1,NDATA)
      DO 3 I=1,NDATA
      Y(I)=Y(I)*AREA
C CHANGE VOLTAGE POLARITY,I.E POSITIVE FOR FORWARD.
3     X(I)=0.0-X(I)
      IF(X(3)-X(2)) 48,49,49
C FOR X(3) < X(2). REARRANGE SO THAT X(I) < X(I+1) < X(I+2) < ........
48    DO 4 I=1,NDATA
      YTEMP(I)=Y(I)
4     XTEMP(I)=X(I)
      DO 54 I=1,NDATA
      IJ=NDATA+1-I
      Y(IJ)=YTEMP(I)
54    X(IJ)=XTEMP(I)
49    VD=GUESS
      M=0
1     M=M+1
      IF(M.GE.NCONV) GO TO 988
      CALL SPLINE(ISPY,NDATA,X,Y,VD,SLOPE,CURENT)
```

```
      ISPY=2
      DELVD=-(R*CURENT+VD-VS)/(1.0+R*SLOPE)
      IF(DABS(DELVD).LE.EPS) GO TO 55
      VD=VD+DELVD
      IF(VD.LT.X(1)) VD=X(1)+1.00D-05
      IF(VD.GT.X(NDATA)) VD=X(NDATA)-1.00D-05
      GO TO 1
988   IFAIL=1
55    RETURN
      END

      SUBROUTINE TDGNAL(IF,L,A,B,C,D)
C     SUBROUTINE FOR SOLVING A TRIDIAGONAL MATRIX SYSTEM.
      IMPLICIT REAL*8(A-H,O-Z)
      DIMENSION A(1),B(1),C(1),D(1)
      IFP1=IF+1
      DO 1 I=IFP1,L
      RR=A(I)/B(I-1)
      B(I)=B(I)-RR*C(I-1)
1     D(I)=D(I)-RR*D(I-1)
      D(L)=D(L)/B(L)
      LAST=L-IF
      DO 2 K=1,LAST
      I=L-K
2     D(I)=(D(I)-C(I)*D(I+1))/B(I)
      RETURN
      END

      SUBROUTINE SPLINE(IS,NDATA,X,Y,XINT,DSDX,SX)
C     SUBROUTINE FOR A CUBIC SPLINE INTERPOLATION.
      IMPLICIT REAL *8(A-H,O-Z)
      DIMENSION X(1),Y(1),TA(300),TB(300),TC(300),TD(300),FM(300)
      COMMON /SPY/FM
      N=NDATA-1
      SPACE=X(3)-X(2)
```

```
      RSP2=6.0/(SPACE**2)
      IF(IS.GT.1) GO TO 995
      DO 10 I=2,N
      TA(I)=1.00D00
      TB(I)=4.00D00
      TC(I)=1.00D00
      TD(I)=RSP2*(Y(I+1)-2.0*Y(I)+Y(I-1))
   10 CONTINUE
      CALL TDGNAL(2,N,TA,TB,TC,TD)
      DO 20 I=2,N
      FM(I)=TD(I)
   20 FM(1)=0.0D00
      FM(NDATA)=0.0D00
  995 DO 30 I=1,NDATA
      IF(X(I)-XINT) 30,40,40
   30 CONTINUE
   40 K=I
      RL=1.0/SPACE
      RL2=1.0/(2.0*SPACE)
      RL6=1.0/(6.0*SPACE)
      SX=FM(K-1)*RL6*((X(K)-XINT)**3)+FM(K)*RL6*((XINT-X(K-1))**3)
      SX=SX+(Y(K)/SPACE-(1.0/5.0)*FM(K)*SPACE)*(XINT-X(K-1))
      SX=SX+(Y(K-1)/SPACE-(1.0/6.0)*FM(K-1)*SPACE)*(X(K)-XINT)
      DSDX=-FM(K-1)*RL2*((X(K)-XINT)**2)+FM(K)*RL2*((XINT-X(K-1))**2)
      DSDX=DSDX+(Y(K)-Y(K-1))/SPACE-(SPACE/5.0)*(FM(K)-FM(K-1))
      RETURN
      END
```

```fortran
C     AN EXAMPLE OF THE MAIN PROGRAMME FOR TIME-INDEPENDENT MODELLING.
      IMPLICIT REAL *8 (A-H,O-Z)
      DIMENSION Y(310),TA(310),TB(310),TC(310),U(310),
     *TD(310),P(310),X(310),EDEN(310),FN(310),COMMT(10)
      DIMENSION DEL(310),H(310),FNPLOT(310),HOLCUR(310),ELECUR(310)
      DIMENSION DFEN(310),DFFP(310),DRTN(310),DRTP(310)
      DIMENSION VOLT(200),TOTALJ(200),UN(900),UP(900),VWRITE(60)
      DIMENSION PLTVT(11,310),PLTEN(11,310),PLTHO(11,310),PLTU(11,310)
      DIMENSION PLTJN(11,310),PLTJP(11,310),PLTX(11,310),PLTX1D(310)
      DIMENSION PLTQSN(11,310),PLTQSP(11,310)
      DIMENSION PLTSPC(11,310)
      COMMON /AAA/YEQ1,YEQNP1
      COMMON /BBB/XLLMAX
      COMMON /CCC/ISTEPS,IPLOT
      COMMON /LFMOB/TAUN,TAUP,UN,UP
      DATA FMUNOR,FJNOR,V0/3.87D01,-7.25D-07,2.58D-02/
      DATA XDEBYE,EPS/3.31D-03,1.0D-06/
      FNINTR=1.50D10
      UNORM=FNINTR/(XDEBYE**2)
C     READ-IN MAXIMUM VOLTAGE(VOLT),AT X=0,AND THE DISTANCE(MICRON).
      READ(5,101)(COMMT(L),L=1,9)
      READ(5,102) VMAX,FLONG,TAU
  101 FORMAT(9A8)
  102 FORMAT(F10.2,/,F10.2,/,E10.3)
C     NORMALIZE THE PARAMETERS
      XLLMAX=FLONG*1.0D-04/XDEBYE
      TNORM=XDEBYE**2
      VMAX=VMAX/V0
      TAUN=TAU/TNORM
      TAUP=TAU/TNORM
C     CALL SUBROUTINE FOR MESH DISTRIBUTION.
      CALL FIXM1(H,N)
      NP1=N+1
      NM1=N-1
      WRITE(5,300)(COMMT(L),L=1,9)
  300 FORMAT(9A8)
```

```
        WRITE(6,400) N,XLLMAX
400 FORMAT('NUMBER OF GRIDS=',I6,/,
   *'MAXIMUM LENGTH IN UNIT OF DEBYE LENGTH.=',E12.5)
C CALL DOPING FUNTION
        CALL ERFCPS(NP1,H,X,FN)
C CALL SUBROUTINE FOR A NORMALIZED DOPING-DEPENDENT MOBILITIES.
        CALL MOBIL(FN,UP,UN,N,FNINTR,FMUNOR)
        DO 2 I=1,NP1
        IF(FN(I).LT.EPS) GO TO 3
2 CONTINUE
3 JUNCTN=I
C USE POTENTIAL AT X=L AS REFERENCE.
        Y(NP1)=YEQNP1
        XMIN=0.0
        F=FLONG/10.0
C SCALE FOR FORWARD BIAS.
        IF(VMAX.GT.EPS) GO TO 6
        VPMAX=0.001
        VMIN=VMAX
        YMTEST=VMAX+YEQ1
        IF(YMTEST.LT.YEQNP1) YMIN=YMTEST-3.0
        IF(YMTEST.GT.YEQNP1) YMIN=YEQNP1-3.0
        YF=((YEQ1+10.0)-YMIN)/7.0
        GO TO 7
C FOR REVERSE BIAS UP TO 120 VT.
6 VPMAX=VMAX
        VMIN=0.001
        YMIN=YEQNP1-3.0
        YF=(DABS(VMAX)+DABS(YEQ1)+DABS(Y(NP1)))/7.0
7 VX=(VPMAX-VMIN)/10.0
8 IF(VMAX.GT.EPS) NSTEPS=120
        IF(VMAX.LT.EPS) NSTEPS=36
        IF(VMAX.GT.EPS) IPO=NSTEPS/5
        IF(VMAX.LT.EPS) IPO=NSTEPS/5
        NSTP1=NSTEPS+1
        Y(1)=YEQ1
        IPLOT=0
```

```
      LP=0
      DO 4 ISTEPS=1,NSTP1
      IF(ISTEPS.EQ.1) GO TO 444
C CALL SUBROUTINE FOR INCREMENTAL APPLIED VOLTAGE.
      CALL LINVAP(NSTEPS,VMAX,VINCRE)
      Y(1)=Y(1)+VINCRE
  444 VOLT(ISTEPS)=Y(1)-YEQ1
      IF(IPLOT.EQ.IPO) IPLOT=0
      IPLOT=IPLOT+1
      WRITE(6,500) Y(1),Y(NP1)
  500 FORMAT('THE BOUNDARY VALUES',/,'Y(1)=',E12.5,10X,'Y(N+1)=',E12.5)
C CALCULATE THE TRIAL POTENTIAL.
      IF(ISTEPS.GT.1) GO TO 11
      DO 10 I=2,N
      IF(FN(I).GE.EPS)  SIGN=1.0
      IF(FN(I).LT.EPS)  SIGN=-1.0
      Y(I)=SIGN*DLOG(DABS(FN(I)/2.)+DSQRT(1.+(FN(I)/2.)**2))
   10 CONTINUE
C DETERMINE THE EQUILIBRIUM SOLUTION BY USING S/R EQVM.
      CALL EQVM(N,H,FN,Y,TA,TB,TC,TD,P,EDEN,DEL,X,IFLAG)
      IF(IFLAG.EQ.1) GO TO 999
   11 CALL STATIC(N,H,FN,Y,TA,TB,TC,TD,P,EDEN,DEL,X,IFLAG,U)
      IF(IFLAG.EQ.1) GO TO 999
C CALL SUBROUTINE FOR CURRENT DENSITIES.
   12 CALL CRTDEN(N,P,EDEN,HOLCUR,ELECUR,H,Y,U)
      TOTALJ(ISTEPS)=ELECUR(JUNCTN)+HOLCUR(JUNCTN)
C DENORMALIZE BY MULTIPLY BY -1.
      TOTALJ(ISTEPS)=-FJNOR*TOTALJ(ISTEPS)
      VOLT(ISTEPS)=VOLT(ISTEPS)*V0
      IF(ISTEPS.GT.1) GO TO 52
      CALL PLTXMX(160.0)
      CALL PLTSIZ(0.7)
      FLIMIT=1.0D00
      IF(VMAX.GT.EPS)  YLGMIN=DLOG10(P(1)*1.0D-03)
      IF(VMAX.LE.EPS)  YLGMIN=DLOG10(P(1))
      YLGMAX=FN(1)*1.0D01
      DO 50 I=1,NP1
```

```
      FNPLOT(I)=FN(I)
      IF(FN(I).LT.FLIMIT) FNPLOT(I)=FLIMIT
      IF(FN(I).LT.(-FLIMIT)) FNPLOT(I)=DABS(FN(I))
      IF(FN(I).GT.YLGMAX) YLGMAX=FN(I)
   50 CONTINUE
      YLGMAX=DLOG10(YLGMAX)
      SY=(YLGMAX-YLGMIN)/8.0
      FMIN=DLOG10(FLIMIT)
      FSCALE=(YLGMAX-FMIN)/8.0
   52 IF(ISTEPS.EQ.1) GO TO 54
      IF(IPLOT.NE.IPO) GO TO 4
   54 LP=LP+1
      DO 61 I=1,NP1
      CR=HOLCUR(I)+ELECUR(I)
      PLTVT(LP,I)=Y(I)*V0
      PLTEN(LP,I)=EDEN(I)
      PLTHO(LP,I)=P(I)
      PLTJN(LP,I)=ELECUR(I)/CR
      PLTJP(LP,I)=HOLCUR(I)/CR
      PLTX(LP,I)=X(I)*XDEBYE*1.0D+04
      PLTU(LP,I)=U(I)*UNORM
      PLTSPC(LP,I)=P(I)-EDEN(I)+FN(I)
      PLTQSN(LP,I)=PLTVT(LP,I)-V0*DLOG(EDEN(I))
      PLTQSP(LP,I)=PLTVT(LP,I)+V0*DLOG(P(I))
   61 CONTINUE
      VWRITE(LP)=VOLT(ISTEPS)
    4 CONTINUE
      KSYM=0
      YOR=1.50
      PK=YOR+7.50
      CALL LOG1D2('DISTANCE(MICRON)',16,'CARRIER DENSITY(/NI)',
     *20,XMIN,XF,YLGMIN,SY,PLTX,PLTEN,PLTHO,2,1,NP1,KSYM,PK,LP,1,
     *VWRITE,'CARRIER DENSITY',15,4.0,YOR,'APPL.VOLT',9,11)
      CALL PSYMB(12.,(YOR+7.8),-0.1,'------ELECTRON',0.0,14)
      CALL PSYMB(12.,(YOR+7.6),-0.1,'------HOLE',0.0,10)
      CALL PSYMB(2.5,5.5,-0.2,'FIGURE (4.6)',270.0,12)
      CALL PLTEND
```

```
      KSYM=0
      YOR=1.50
      PK=YOR+7.50
      CALL PSCALE(8.,1.,CURMIN,CURSF,PLTJN(1,2),NM1,22,PLTJN(LP,2),
     *NM1,22,PLTJP(1,2),NM1,22,PLTJP(LP,2),NM1,22)
      CALL LNPLT2('DISTANCE(MICRON)',16,'-(JN OR JP)/(JN+JP)',19,
     *XMIN,XF,CURMIN,CURSF,PLTX,PLTJN,PLTJP,2,1,NP1,KSYM,PK,LP,1,VWRITE,
     *'CURRENT DENSITY',15,4.0,YOR,'APPL.VOLT',9,11)
      CALL PSYMB(12.,(YOR+7.8),-0.1,'-----JN',0.0,8)
      CALL PSYMB(12.,(YOR+7.6),-0.1,'-----JP',0.0,8)
      CALL PSYMB(2.5,6.5,-0.2,'FIGURE (4.8)',270.0,12)
      CALL PLTEND
      KSYM=0
      YOR=1.50
      PK=YOR+7.50
      IF(VMAX.GT.EPS) GO TO 74
      ULOW=1.0D12
      UMAX=1.0D25
      GO TO 75
   74 ULOW=1.0D15
      UMAX=1.0D17
   75 DO 78 IL=1,LP
      DO 77 JL=1,NP1
      PLTU(IL,JL)=DABS(PLTU(IL,JL))
      IF(PLTU(IL,JL).LT.ULOW) PLTU(IL,JL)=ULOW
   77 CONTINUE
   78 CONTINUE
      ULGMIN=DLOG10(ULOW)
      ULGMAX=DLOG10(UMAX)
      ULGX=(ULGMAX-ULGMIN)/8.0
      CALL PLTLOG(1)
      CALL PLTOFS(XMIN,XF,ULGMIN,ULGX,4.0,YOR)
      DO 76 II=1,LP
      KSYM=KSYM+1
      CALL PLINE(PLTX(II,1),PLTU(II,1),NP1,22,10,KSYM,1.0)
   76 CONTINUE
      CALL PLGAXS(4.0,YOR,'ABS.(U) (/CM**3.SEC.)',21,8.,90.,ULGMIN,ULGX)
```

```
      CALL PLTREC
      CALL PAXIS(4.,YOR,'DISTANCE(MICRON)',-16,10.,0.,XMIN,XF,1.0)
      CALL PENUP(4.0,9.5)
      CALL PENDN(14.0,9.5)
      CALL PENDN(14.0,1.5)
      CALL PSYMB(7.,9.6,-.2,'GENERATION RECOMBINATION',0.,24)
      CALL PSYMB(2.5,6.5,-0.2,'FIGURE (4.7)',270.0,12)
      CALL PLTEND
  999 TOTALJ(1)=TOTALJ(2)
      VMIN=VMIN*V0
      VX=VX*V0
      CALL PLTREC
      CALL PSCALE(8.,1.,TJMIN,TJX,TOTALJ(1),NSTEPS,2)
      CALL PLTOFS(VMIN,VX,TJMIN,TJX,4.0,1.5)
      CALL PFLINE(VOLT(1),TOTALJ(1),NSTEPS,2,1.0)
      CALL PAXIS(4.,1.5,'APPLIED VOLTAGE(VOLT)',-21,10.,0.,
     +  SNGL(VMIN),SNGL(VX),1.0)
      CALL PAXIS(4.,1.5,'TOTAL CURRENT(AMP/A)',20,8.,90.,TJMIN,TJX,1.)
      CALL PSYMB(7.,9.6,-0.2,'CURRENT-VOLTAGE',0.0,15,0)
      CALL PENUP(4.0,9.5)
      CALL PENDN(14.0,9.5)
      IF(VMAX.LT.EPS) GO TO 71
      CALL PENDN(14.0,1.5)
      GO TO 72
   71 TLGMIN=DABS(TJMIN)
      DO 70 I=1,NSTEPS
      TOTALJ(I)=DABS(TOTALJ(I))
   70 IF(TOTALJ(I).LT.TLGMIN) TOTALJ(I)=TLGMIN
      NM1STP=NSTEPS-1
      CALL PLTLOG(1)
      CALL PLGSCL(8.0,TLGMIN,TGX,TOTALJ(2),NM1STP,2)
      CALL PLTOFS(VMIN,VX,TLGMIN,TGX,4.0,1.5)
      CALL PDSHLN(VOLT(2),TOTALJ(2),NM1STP,2,0.04,1.0)
      CALL PLGAXS(14.,1.5,'TOTAL CURRENT(AMP/A)',-20,8.,90.,TLGMIN,TGX)
   72 CALL PLTREC
      CALL PSYMB(2.5,6.5,-0.2,'FIGURE (4.9)',270.0,12)
      CALL PLTEND
```

```fortran
      KSYM=0
      YOR=1.50
      PK=YOR+7.5
      CALL PSCALE(8.,1.,QSMIN,QSX,PLTQSN(1,1),NP1,22,PLTQSN(LP,1),NP1,
     *22,PLTQSP(1,1),NP1,22,PLTQSP(LP,1),NP1,22)
      CALL LNPLT2('DISTANCE(MICRON)',16,'QUASI-FERMI POTENTIAL(VOLT)',
     *27,XMIN,XF,QSMIN,QSX,PLTX,PLTQSN,PLTQSP,2,1,NP1,KSYM,PK,LP,1,
     *VWRITE,'QUASI-FERMI POTENTIAL',21,4.0,YOR,'APPL.VOLT',9,11)
      CALL PSYMB(12.,(YOR+7.8),-0.1,'------ELECTRON',0.0,14)
      CALL PSYMB(12.,(YOR+7.6),-0.1,'------HOLE',0.0,10)
      CALL PSYMB(2.5,6.5,-0.2,'FIGURE (4.5)',270.0,12)
      CALL PLTEND
      WRITE(7) NSTEPS,(VOLT(ISTEPS),TOTALJ(ISTEPS),ISTEPS=1,NSTEPS)
      CALL SETDSN(9,'-DPLOT')
      KSYM=0
      YOR=1.50
      PK=YOR+7.50
      YMIN=YMIN*V0
      YF=YF*V0
      CALL LNPLT2('DISTANCE(MICRON)',16,'POTENTIAL(VOLT)',15,
     *XMIN,XF,YMIN,YF,PLTX,PLTVT,0.0,1,1,NP1,KSYM,PK,LP,1,VWRITE,
     *'ELECTROSTATIC POTENTIAL',23,4.0,YOR,'APPL.VOLT',9,11)
      CALL PSYMB(2.5,6.5,-0.2,'FIGURE (4.3)',270.0,12)
      CALL PLTEND
      KSYM=0
      YOR=1.50
      PK=YOR+7.50
      CALL PSCALE(8.,1.,SPCMIN,SPCSF,PLTSPC(1,1),NP1,22,PLTSPC(LP,1),
     *NP1,22)
      CALL LNPLT2('DISTANCE(MICRON)',16,'SPACE CHARGE(/QNI)',
     *18,XMIN,XF,SPCMIN,SPCSF,PLTX,PLTSPC,0.0,1,1,NP1,KSYM,PK,LP,1,
     *VWRITE,'SPACE CHARGE DENSITY',20,4.0,YOR,'APPL.VOLT',9,11)
      CALL PSYMB(2.5,6.5,-0.2,'FIGURE (4.4)',270.0,12)
      CALL PLTEND
      DO 79 I=1,NP1
   79 PLTX1D(I)=PLTX(1,I)
      KSYM=0
```

154

```
      YOR=1.5
      PK=YOR+7.50
      CALL LOG1D1('DISTANCE(MICRON)',16,'IMPURITY DENSITY(/NI)',21,
     *XMIN,XF,FMIN,FSCALE,PLTX1D,FNPLOT,0.0,1,1,NP1,0,
     *'IMPURITY PROFILE',16,4.,YOR)
      CALL PSYMB(2.5,6.5,-0.2,'FIGURE (4.2)',270.0,12)
      CALL PLTEND
      STOP
      END


C     AN  EXAMPLE  OF  THE  MAIN  PROGRAMME  FOR  TIME-DEPENDENT  MODELLING.
      IMPLICIT REAL *8 (A-H,O-Z)
      DIMENSION H(310),E(310),DELTAT(12000),RPDELT(12000),VAPP(12000)
      DIMENSION HOLCUR(310),ELECUR(310),FN(310),HS(310),VTOTAL(260)
      DIMENSION TA(310),TB(310),TC(310),TD(310),UP(310),UN(310),X(310)
      DIMENSION P(310),EN(310),DY(310),TWRITE(260),COMMT(10),TREAL(260)
      DIMENSION DVU(310),U(310),DUDP(310),DUDN(310),CONCUR(310)
      DIMENSION EXPLUS(310),EXMNUS(310),EDEPLS(310),EDEMNS(310)
      DIMENSION DJPDP1(310),DJPDP2(310),DJNDN1(310),DJNDN2(310)
      DIMENSION DJPDE(310),DJNDE(310),DJTDE(310),DIFUEN(310),Y(310)
      DIMENSION DNPLOT(310),DRIFHO(310),DRIFEN(310),DIFUHO(310)
      DIMENSION REALJP(310),REALJN(310),REALJD(310),REALJC(260)
      DIMENSION EPLOT(310),VTERM(260),VDIODE(260),VXPLOT(310),VJ(310)
      DIMENSION PLTVT(11,310),PLTEF(11,310),PLTEN(11,310),PLTHO(11,310)
      DIMENSION PLTJN(11,310),PLTJP(11,310),PLTJD(11,310),PLTDRN(11,310)
      DIMENSION PLTDRH(11,310),PLTDFN(11,310),PLTDFH(11,310)
      DIMENSION PLTX(11,310),PLTX1D(310),PLTU(11,310)
      COMMON /QCHK/DVU,U,DUDP,DUDN,EXPLUS,EXMNUS,EDEPLS,EDEMNS
      COMMON /QCHK2/DJPDP1,DJPDP2,DJNDN1,DJNDN2,DJPDE,DJNDE,DJTDE,VDIFF
      COMMON /AAA/YEQ1,YEQNP1
      COMMON /BBB/XLLMAX
      COMMON /QAAB/TAUN,TAUP,UN,UP,FACNOR,ZETA,DY,XDEBYE,X,Y,HS,FNINTR
      COMMON /QABB/I,IFLAG,ISTEDY,J,K,N,NP1
      COMMON /QBBB/E,EN,P,FN,H,DELTAT,RPDELT,VAPP,ELECUR,HOLCUR,TOTCUR
      COMMON /TABC/TA,TB,TC,TD
      COMMON /QEPS/EPS,EPSPOI,EPST
```

```
      DATA EMUNOR,EJNOR,V0/3.87D01,7.25D-07,2.58D-02/
      DATA AREA,ZTH/3.48D-04,5.00D01/
      EPS=1.00D-04
      EPSPOI=1.00D-02
      EPST=1.00E-02
      FNINTR=1.50D10
      XDEBYE=3.31D-03
      ZETA=1.0
      TAUN=1.00D-07
      TAUP=1.00D-07
      TNORM=XDEBYE**2
      ENORM=V0/XDEBYE
      UNORM=FNINTR/(XDEBYE**2)
C READ-IN MAX.VOLTAGE(VOLT),AT X=0.,THE REAL DISTANCE(MICRON),
C THE NUMBER OF TIME STEPS,AND THE PLOTTING SPACE.
      READ(5,101)(COMMT(L),L=1,9)
      READ(5,102) VMAX,FLONG,NT,IPSPAC
  101 FORMAT(9A8)
  102 FORMAT(F15.7,/,F15.7,/,I3,/,I2)
C NORMALIZE THE PARAMETERS.
      VTH=VMAX/V0
      XLLMAX=FLONG*1.0D-04/XDEBYE
      TAUN=TAUN/TNORM
      TAUP=TAUP/TNORM
      FACNOR=AREA*ZTH*FJNOR/V0
C CALL SUBROUTINE FOR MESH DISTRIBUTION.
      CALL FIXM1(H,N)
      NP1=N+1
      NM1=N-1
      WRITE(6,300)(COMMT(L),L=1,9)
  300 FORMAT(9A8)
      WRITE(6,400) N,XLLMAX
  400 FORMAT('NUMBER  OF GRIDS=',I6,/,
     *'MAXIMUM LENGTH IN UNIT OF DEBYE LENGTH.=',E12.5)
C CALL A NORMALIZED DOPING FUNTION
      CALL ERFCPS(NP1,H,X,FN)
C CALL SUBROUTINE FOR A NORMALIZED DOPING MOBILITIES.
```

```
      CALL MOBIL(FN,UP,UN,N,FNINTR,FMUNOR)
      DO 2 I=1,NP1
      IF(FN(I).LT.EPS) GO TO 13
    2 CONTINUE
   13 JUNCTN=I
C USE POTENTIAL AT X=L AS REFERENCE.
      Y(1)=YEQ1
      Y(NP1)=YEQNP1
      CALL EQILBM
      IF(IFLAG.EQ.1) GO TO 999
      VDIFF=YEQ1-YEQNP1
      DO 21 I=1,N
      IF(I.EQ.1) TRELAX=1.0/(UP(1)*P(1)+UN(1)*EN(1))
      RELAX=1.0/(UP(I)*P(I)+UN(I)*EN(I))
   21 TRELAX=DMIN1(TRELAX,RELAX)
      PRELAX=TRELAX*TNORM
      WRITE(6,211) PRELAX
  211 FORMAT(5X,'MINIMUM DIELECTRIC RELAXATION TIME CONSTANT=',E15.7)
C CALL  SUBROUTINE FOR THE TIME SPACE.
      CALL TSPAC1(TRELAX,DELTAT,RPDELT,NT)
      FILMAX=4.0D03
      CLIMIT=1.0D-07
      DLIMIT=1.0D00
      DLGMIN=DLOG10(DLIMIT)
      DLGMAX=FN(1)*1.0D01
      DO 31 I=1,NP1
      DNPLOT(I)=FN(I)
      IF(FN(I).LT.DLIMIT) DNPLOT(I)=DLIMIT
      IF(FN(I).LT.(-DLIMIT)) DNPLOT(I)=DABS(FN(I))
      IF(FN(I).GT.DLGMAX) DLGMAX=FN(I)
   31 CONTINUE
      DLGMAX=DLOG10(DLGMAX)
      DOPSF=(DLGMAX-DLGMIN)/8.0
      LP=0
      IPLOT=0
      TBEGIN=0.0
      TTEMP=TBEGIN/TNORM
```

```
      DO 4 J=1,NT
      TTEMP=TTEMP+DELTAT(J)
      TLAST=TTEMP*TNORM
      TSPACE=DELTAT(J)*TNORM
      TREAL(J)=TTEMP*TNORM
C CALL SUBROUTINE FOR THE EXCITATION VOLTAGE.
      CALL VAPPY1(VTH,VAPP,TREAL,J)
      IF(IPLOT.EQ.IPSPAC) IPLOT=0
      IPLOT=IPLOT+1
      INDEXT=J
      WRITE(6,500)TREAL(J),TSPACE ,Y(1),Y(NP1)
500   FORMAT(3X,'REAL TIME =',E12.5,/,3X,'REAL TIME SPACE =',E12.5,
     */,'THE BOUNDARY VALUES',/,'Y(1)=',E12.5,10X,'Y(N+1)=',E12.5)
      CALL DYNAMC
      IF(IFLAG.EQ.1) GO TO 999
      EPLOT(1)=E(1)*ENORM
      DO 405 I=1,N
      DRIFHO(I)=UP(I)*P(I)*E(I)*FJNOR
      DRIFEN(I)=UN(I)*EN(I)*E(I)*FJNOR
      DIFUHO(I)=-((P(I+1)-P(I))/H(I))*FJNOR
      DIFUEN(I)=((EN(I+1)-EN(I))/H(I))*FJNOR
405   CONTINUE
      DRIFHO(NP1)=DRIFHO(N)
      DRIFEN(NP1)=DRIFEN(N)
      DIFUHO(NP1)=DIFUHO(N)
      DIFUEN(NP1)=DIFUEN(N)
      DO 408 I=1,NP1
C CALCULATE REAL CURRENT .
      REALJP(I)=HOLCUR(I)*FJNOR
      REALJN(I)=ELECUR(I)*FJNOR
      REALJD(I)=HS(I)*FJNOR
      CONCUR(I)=REALJP(I)+REALJN(I)+REALJD(I)
408   EPLOT(I)=E(I)*ENORM
      REALJC(J)=REALJP(JUNCTN)+REALJN(JUNCTN)+REALJD(JUNCTN)
      VJUNC=0.0
      DO 409 I=1,NP1
409   VJUNC=VJUNC+E(I)*H(I)
```

```
      VDIODE(J)=-(VDIFF-VJUNC)*V0
      VTERM(J)=REALJC(J)*AREA*ZTH
      VTOTAL(J)=VTERM(J)+VDIODE(J)
      VJ(1)=VDIFF-VJUNC
      DO 411 I=2,NP1
      VJ(I)=VJ(I-1)+E(I)*H(I)
411   VXPLOT(I)=-VJ(I)*V0
      VXPLOT(1)=-VJ(1)*V0
      IF(IPLOT.EQ.IPSPAC)   WRITE(6,555)(EPLOT(I),VXPLOT(I),DRIFHO(I),
     *DIFUHO(I),REALJP(I),DRIFEN(I),DIFUEN(I),REALJN(I),REALJD(I),
     *CONCUR(I),I=1,NP1)
555   FORMAT(2X,'ELEC.FIELD',2X,'DIODE VOLT',2X,'DRIFT JP',4X,
     *'DIFFUSE JP',2X,'REAL JP',5X,'DRIFT JN',4X,'DIFFUSE JN',2X,
     *'REAL JN',5X,'REAL JD',5X,'JP+JN+JD',//,(10E12.4))
      IF(J.EQ.1) GO TO 44
      IF(J.EQ.2) GO TO 44
      IF(J.EQ.NT) GO TO 44
      IF(IPLOT.NE.IPSPAC) GO TO 4
44    LP=LP+1
      IF(LP.EQ.1) FILMIN=EPLOT(1)
      DO 450 I=1,NP1
      PLTU(LP,I)=U(I)*UNORM
      PLTVT(LP,I)=VXPLOT(I)
      PLTEF(LP,I)=EPLOT(I)
      IF(PLTEF(LP,I).GT.FILMAX) PLTEF(LP,I)=FILMAX
      FILMIN=DMIN1(FILMIN,PLTEF(LP,I))
      PLTEN(LP,I)=EN(I)
      PLTHO(LP,I)=P(I)
C FOR PLOTTING PURPOSE,MULTIPLY THE CURRENT BY -1
      PLTJN(LP,I)=-REALJN(I)
      PLTJP(LP,I)=-REALJP(I)
      PLTJD(LP,I)=-REALJD(I)
      PLTDRN(LP,I)=-DRIFEN(I)
      PLTDRH(LP,I)=-DRIFHO(I)
      PLTDFN(LP,I)=-DIFUEN(I)
      PLTDFH(LP,I)=-DIFUHO(I)
      PLTX(LP,I)=X(I)*XDEBYE*1.0D+04
```

```
450   CONTINUE
      TWRITE(LP)=TREAL(J)
      IF(LP.EQ.8) GO TO 999
   4  CONTINUE
 999  XMIN=0.0
      XF=FLONG/10.0
      CALL PLTXMX(160.0)
      CALL PLTSIZ(0.7)
      CHGMAX=DMAX1(P(1),P(NP1),EN(1),EN(NP1))
      CHGMIN=DMIN1(P(1),P(NP1),EN(1),EN(NP1))
      CHGMAX=DLOG10(CHGMAX*1.0D01)
      CHGMIN=DLOG10(CHGMIN)
      CHGSF=(CHGMAX-CHGMIN)/8.0
      KSYM=0
      YOR=1.50
      PK=YOR+7.50
      CALL LOG1D2('DISTANCE(MICRON)',16,'ELECTRON-HOLE DENSITY(/NI)',
     *26,XMIN,XF,CHGMIN,CHGSF,PLTX,PLTEN,PLTHO,2,1,NP1,KSYM,PK,LP,1,
     *TWRITE,'CARRIER DENSITY',15,4.0,YOR,'TIME(SEC)',9,11)
      CALL PSYMB(12.,(YOR+7.8),-0.1,'----- ELECTRON',0.0,14)
      CALL PSYMB(12.,(YOR+7.6),-0.1,'----- HOLE',0.0,10)
      CALL PSYMB(2.5,6.5,-0.2,'FIGURE (       )',270.0,13)
      CALL PLTEND
      KSYM=0
      YOR=1.50
      PK=YOR+7.50
      CALL PSCALE(8.,1.,CURMIN,CURSF,PLTJN(1,2),NM1,22,PLTJN(LP,2),
     *NM1,22,PLTJP(1,2),NM1,22,PLTJP(LP,2),NM1,22,PLTJD(1,2),NM1,22,
     *PLTJD(LP,2),NM1,22)
      CALL LNPLT2('DISTANCE(MICRON)',16,'-CURRENT DENSITY(AMP/A)',23,
     *XMIN,XF,CURMIN,CURSF,PLTX,PLTJN,PLTJP,2,1,NP1,KSYM,PK,LP,1,TWRITE,
     *'CURRENT DENSITY',15,4.0,YOR,'TIME(SEC)',9,11)
      CALL PSYMB(12.,(YOR+7.8),-0.1,'----- JN',0.0,9)
      CALL PSYMB(12.,(YOR+7.5),-0.1,'----- JP',0.0,9)
      CALL PSYMB(2.5,6.5,-0.2,'FIGURE (       )',270.0,13)
      CALL PLTEND
      IF(IFLAG.EQ.1) INDEXT=INDEXT-1
```

```
      WRITE(5,611)(REALJC(I),VDIODE(I),VTERM(I),VTOTAL(I),I=1,INDEXT)
611   FORMAT(6X,'REAL JC.',5X,'DIODE VOLT.',5X,'TERM.VOLT.',5X,
     *'TOTAL VOLT.',//,(4E15.6))
      WRITE(7) INDEXT,(TREAL(I),REALJC(I),VDIODE(I),VTERM(I),VTOTAL(I),
     *I=1,INDEXT)
      NTM1=INDEXT-1
      TMIN=DLOG10(TREAL(2))
      TF=(DLOG10(TLAST)-TMIN)/10.0
      CALL PSCALE(8.,1.,CZMIN,CZSF,REALJC(2),NTM1,2)
      CALL PSCALE(8.,1.,VTMIN,VF,VDIODE(2),NTM1,2,VTERM(2),NTM1,2)
      YOR=1.50
      CALL LOG2D1('TIME(SEC.)',10,'VOLTAGE(VOLT)',13,TMIN,TF,VTMIN,
     *VF,TREAL,VDIODE,VTERM,2,2,NTM1,0,'VOLTAGE - TIME',14,4.,YOR)
      CALL PSYMB(12.,(YOR+7.8),-0.1,'------ DIODE VOLTAGE',0.0,20)
      CALL PSYMB(12.3,(YOR+7.8),-0.1,0,0.0,-3)
      CALL PSYMB(12.,(YOR+7.6),-0.1,'------ RESISTOR VOLTAGE',0.0,23)
      CALL PSYMB(12.3,(YOR+7.6),-0.1,1,0.0,-3)
      CALL PSYMB(2.5,6.5,-0.2,'FIGURE (        )',270.0,13)
      CALL PLTEND
      CALL SETDSN(9,'-DPLOT')
      KSYM=0
      YOR=1.50
      PK=YOR+7.50
      FILSF=(FILMAX-FILMIN)/8.0
      CALL LNPLT2('DISTANCE(MICRON)',16,'ELECTRIC FIELD(V/CM)',20,XMIN,
     *XF,FILMIN,FILSF,PLTX,PLTEF,0.0,1,1,N,KSYM,PK,LP,1,TWRITE,
     *'ELECTRIC FIELD',14,4.0,YOR,'TIME(SEC)',9,11)
      CALL PSYMB(2.5,6.5,-0.2,'FIGURE (        )',270.0,13)
      CALL PLTEND
      KSYM=0
      YOR=1.50
      PK=YOR+7.50
      CALL PSCALE(8.,1.,VMIN,VF,PLTVT(1,1),NP1,22,PLTVT(LP,1),NP1,
     *22,PLTVT(2,1),NP1,22,PLTVT(3,1),NP1,22,PLTVT(4,1),NP1,22,
     *PLTVT(5,1),NP1,22)
      CALL LNPLT2('DISTANCE(MICRON)',16,'POTENTIAL',9,XMIN,XF,VMIN,
     *VF,PLTX,PLTVT,0.0,1,1,NP1,KSYM,PK,LP,1,TWRITE,
```

```
      * 'ELECTROSTATIC POTENTIAL',23,4.0,YOR,'TIME(SEC)',9,11)
        CALL PSYMB(2.5,6.5,-0.2,'FIGURE (    )',270.0,13)
        CALL PLTEND
        KSYM=0
        YOR=1.50
        PK=YOR+7.50
        CALL LNPLT2('DISTANCE(MICRON)',16,'-DISPLACEMENT CURRENT(AMP/A)',
      *28,XMIN,XF,CURMIN,CURSF,PLTX,PLTJD,0.0,1,1,NP1,KSYM,PK,LP,1,
      *'CURRENT DENSITY',15,4.0,YOR,'TIME(SEC)',9,11)
        CALL PSYMB(2.5,6.5,-0.2,'FIGURE (    )',270.0,13)
        CALL PLTEND
        YOR=1.50
        DO 79 I=1,NP1
     79 PLTX1D(I)=PLTX(1,I)
        CALL LOG1D1('DISTANCE(MICRON)',16,'IMPURITY DENSITY(/NI)',21,
      *XMIN,XF,DLGMIN,DOPSF,PLTX1D,DNPLOT,0.0,1,1,NP1,0,
      *'IMPURITY PROFILE',16,4.,YOR)
        CALL PSYMB(2.5,6.5,-0.2,'FIGURE (    )',270.0,13)
        CALL PLTEND
        STOP
        END
```

References.

<1> Shockley W, "The Theory of p-n Junction in Semiconductors and p-n Junction transistors", Bell Sys.Tech.J., PP 435-489, 1949

<2> Cornu J, "Analytical Model for p-n Junctions under High-Injection Conditions", Electron.lett. Vol.7, No.18, PP 509-510, 1971

<3> Choo S.C, "Analytical Approximations for an Abrupt p-n Junction under High-level Conditions", Solid State Electron. Vol.16, PP 793-799, 1973.

<4> Gray P.E,et al, "Physical Electronics and Circuit Models of Transistors.", Wiley, 1964

<5> Barna A.A and Horelick D, "A Simple Diode Model including Conductivity Modulation", IEEE Trans. on Circuit Theory. Vol.CT-18, PP 233-240, 1971.

<6> Wang P.P and Branin F.H.Jr, "Multi-Section Network Modeling of Junction Diodes", Proc.4th Ann.Pittsburg Conf.on Modeling and Simulation, Pittsburg, Penn., 1973.

<7> Ko W.H, "The Forward Transient Behaviour of Semiconductor Junction Diodes", Solid State Electron. Vol.3, PP 59-69, 1961.

<8> Ko W.H, "The Reverse Transient Behaviour of Semiconductor Junction Diodes", IRE.Trans.Electron Devices, Vol.ED-8, PP 123-131, 1961.

<9> Chua L.O And Tseng C.W, "A Memristive Circuit Model for p-n Junction Diodes", Circuit Theory and Applications, Vol.2, PP 367-389, 1974.

<10> Gummel H.K, "A Self Consistent Scheme for One-Dimensional Steady-State Transistor Calculations", IEEE Trans. on Electron. Devices. Vol.ED-11, PP 455-465, 1964.

<11> De Mari A, "An Accurate Numerical Steady-State One-Dimensional Solution of the p-n Junction", Solid State Electron. Vol.11, PP 33-58, 1968.

<12> Arandjelovic V, "Accurate Numerical Steady-State Solution for a Diffused One-Dimensional Junction Diode", Solid State Electron. Vol.13, PP 865-871, 1970.

<13> Calzolari P.U,Graffi S and Pierini G, "A New Program for the DC One-Dimensional Analysis of Semiconductor devices", Alta Frequenza, Vol.8, PP 226e-233e, 1972.

<14> Seidman T and Choo S.C, "Iterative Scheme for Computer Simulation of Semiconductor Devices", Solid State Electron. Vol.15, PP 1229-1235, 1972.

<15> De Mari A, "An Accurate Numerical One-Dimensional Solution of the p-n Junction under Arbitrary Transient Conditons", Solid State Electron. Vol.11, PP 1021-1053, 1968.

<16> Scharfetter D.L and Gummel H.K, "Large Signal Analysis of a Silicon Read Diode Oscillation", IEEE Trans. on Electron. Devices. Vol.ED-16, No.1, PP 64-77, 1969.

<17> Caughey P.M, "Simulation of UHF Transistor Small-Signal Behaviour to 10 GHz for Circuit Modeling", Proc.2nd Biennial Cornwell Elec.Eng. Conf on Computerized Electron, Ithaca, N.Y, 1969.

<18> Petersen O.G,Risoski R.A and Cowles W.W, "Numerical method for the Solution of the Transient Behaviour of Bipolar Semiconductor Devices", Solid State Electron. Vol.16, PP 239-251, 1973.

<19> Hachtel G.D,Richard C.J and Cooley J.W, "A New Efficient One-Dimensional Analysis Program for Junction Device Modeling", Proc.IEEE, Vol.16, No.1, PP 86-98, 1972.

<20> Collins T.W and Churchill J.N, "Exact Modeling of the Transient Response of an MOS Capacitor", IEEE Trans. on Electron. Devices. Vol.ED-22, PP 90-101, 1975.

<21> Fortino A.G and Nadan J.S, "An Efficient Numerical Method for the Small-Signal AC Analysis of MOS Capacitors", IEEE Trans. on Electron. Devices. Vol.ED-24, PP 1137-1147, 1977.

<22> Wilson C.L, "Data Acquisition and Reduction Techniques for Device Modeling", in Semiconductor Device Modeling for Computer-aided Design, Herskowitz and Schilling (Editors), Mcgraw-hill, 1972.

<23> Narayanan S, "Transistor Distortion Analysis using Volterra Series Representation", Bell Sys.Tech.J., Vol.46, No.5, PP 991-1024, 1967.

<24> George D.A, "Continuous Nonlinear Systems", Technical Report 355, Research Lab of Electronics, MIT, 1959.

<25> Kulesza B.L.J and Katib M, "Harmonic Generation in Exponential Resistive Diodes", Report No.23, Dept.of Applied Physics and Electronics, Univ.of Durham, 1977.

<26> Albrecht C and Jansen A.K, "Numerical Analysis of Nonlinear Small-Signal Distortion in p-n Structures", IEEE Trans. on Electron. Devices. Vol.ED-24, No.2, PP 91-98, 1977.

<27> Doi T, "On Large Signal Frequency Domain Analysis of Circuits Containing Junction Diodes and Bipolar Transistors", IEEE Trans. on Circuits and Systems. Vol.CAS-24, No.6, PP 329-341, 1977.

<28> Sze S.M, "Physics of Semiconductor Devices", Wiley, 1969.

<29> Issacson E and Keller H.B, " Analysis of Numerical Methods", Wiley, 1966.

<30> Gear C.W, "Numerical Initial Value Problems in Ordinary Differential Equations", Prentice-Hall, 1971.

<31> Keller H.B, "Numerical Methods for Two-Point Boundary-Value Problems", Blisdell, 1968.

<32> Morrisson D.D, Riley J.D and Zancanaro J.F, "Multiple Shooting Method for Two-Point Boundary-Value Problems", Comm.ACM, Vol.5, PP 613-614, 1962.

<33> Holt J.F, "Numerical Solution of Nonlinear Two-Point Boundary-Value Problems by Finite Difference Methods", Comm.ACM, Vol.7, PP 366-373, 1964.

<34> Peaceman D.W and Rachford H.H.Jr, "The Numerical Solution of Parabolic and Elliptic Differential Equations", J.Soc. Indust. Appl. Math., Vol.3, PP 28-41, 1955.

<35> Ames W.F, "Numerical Methods for Partial Differential Equations", 2nd Ed., Nelson, 1977.

<36> Henrici P, "Discrete Variable Methods in Ordinary Differential Equations", Wiley, 1962.

<37> Klopfenstein R.W and Wu C.P, "Computer Solutions of One-Dimensional Poisson's Equation", IEEE Trans. on Electron. Devices. Vol.ED-22, No.6, PP 329-333, 1975.

<38> Wu C.P,Douglas E.C and Mueller C.W, "Limitations of the CV Technique for Ion-Implanted Profiles", ibid, PP 319-329.

<39> Haselgrove C.B, "The Solution of Nonlinear Equations and of Differential Equations with Two-Point Boundary Conditions", Comp.J., Vol.4, PP 255-259, 1961.

<40> Bellman R,Juncosa M.L and Kalaba R, "Some Numerical Experiments using Newton's Method for Nonlinear Parabolic and Elliptic Boundary-Value Problems", Comm. ACM., Vol.4, PP 187-191, 1961.

<41> Bellman R and kalaba R, "Quasilinearization and Nonlinear Boundary-Value Problems", Elsevier, 1965.

<42> Sah C.T,Noyce R.N and Shockley W, "Carrier Generation and Recombination in p-n Junctions and p-n Junction Characteristics", Proc. IRE., Vol.45, PP 1228-1243, 1957.

<43> Yu S.P and Tantraporn W, "A Computer Simulation Scheme for Various Solid-State Devices", IEEE Trans. on Electron. Devices. Vol.ED-22, No.8, PP 515-522, 1975.

<44> Choo S.C, "Effect of Carrier Lifetime on the Forward Characteristics of High-Power Devices", IEEE Trans. on Electron. Devices. Vol.ED-17, No.9, PP 647-652, 1970.

<45> Ghandhi S.K, "Semiconductor Power Devices", Wiley, 1977.

<46> Grove A.S, "Physics and Technology of Semiconductor Devices", Wiley, 1967.

<47> Brigham E.O, "The Fast Fourier Transform", Prentice-Hall, 1974.

<48> Rabiner L.R and Rader C.M (Editors), "Digital Signal Processing", IEEE Press, 1972.